The Effect of Human Rhinovirus-16 on Thermo-TRP Channels, Hypotonic Activation and ATP Release

Samantha Kimberley Atkinson, BSc. (Hons) (University of Hull)

Thesis submitted for the Degree of Doctor of Philosophy (PhD)

The University of Hull and The University of York

Hull York Medical School

January 2019

Abstract

Human rhinovirus (RV-16) infections are major cause of upper respiratory tract infections (URTI) and are associated with acute exacerbations of asthma and COPD. URTIs are associated with excessive production of mucus within the airway, particularly in sufferers of chronic respiratory conditions. This mucus may lead to altered osmolarity within the airway and contribute to hypotonic stimulation of the airway epithelium and airway hypersensitivity leading to cough. Hypotonic stimulation has previously been shown to activate transient receptor potential (TRP) vanilloid 4 (TRPV4) ultimately leading to ATP release via pannexin-1. RV-16 has been previously shown to cause upregulation of TRP channel expression in the airway, however, the mechanism of common cold cough is unknown. We hypothesise that infection with RV-16 causes increased ATP release in the airway leading to airway hypersensitivity and increased cough frequency.

Infection of airway epithelial (A549) and transfected astrocytoma (1321N1) cell lines with synthetic viral stimulus poly(I:C) failed to cause any change in expression or function of TRPA1, V1, V4 or P2X3 when monitored using RT-PCR, western blot analysis or intracellular calcium signalling. However, infection with RV-16 led to reduced function of thermo-TRP channels without concurrent reduction in expression although function was restored to basal levels by late infection.

The role of hypotonic stimulation on A549 cells was investigated with the aim of further delineating the mechanism of ATP release following hypotonic stimulation. Calcium-calmodulin kinase was identified to play an integral role in downstream ATP release, and that blockade of calcium-calmodulin kinase or pannexin-1 significantly reduced ATP release following hypotonic stimulation. Furthermore, immunofluorescent analysis identified a distinct distribution pattern of pannexin-1 prior to and post hypotonic stimulation, which could be effectively abolished through inhibition of pannexin-1, or significantly reduced following inhibition of calcium-calmodulin kinase, TRPV4 or MLC phosphorylation.

Finally, RV-16 infection led to increased ATP release from 72 hours through 168 hours post infection, independent of further stimulus at a time point which coincides with the

development of viral cough *in vivo*. Furthermore, RV-16 infection led to a glycolytic shift in cell metabolism without any increase in cell death.

In summary, RV-16 induced ATP release, mediated by calcium-calmodulin kinase, and through TRPV4 and pannexin-1 activation, may underpin the development of a viral cough during an upper respiratory tract infection.

Table of Contents

Figures

Tables

Equations

Abbreviations

1321N1	Human astrocytoma cells, subcloned from 1181N1
2-DG	2-deoxy-D-glucose
A23187	Calcium ionophore
A549	Type II alveolar basal epithelial adenocarcinoma cells
ABS	Absorbance
ABU	Arbitrary units
AITC	Allyl isothiocyanate
ALU	Arbitrary light units
ANOVA	Analysis of variance
APS	Ammonium persulphate
ASM	Airway smooth muscle
ATP	Adenosine triphosphate
AUC	Area under curve
BSA	Bovine serum albumin
Caps	Capsaicin
CBX	Carbenoxolone
CCD	Cytochalasin D
CD	Cluster of differentiation
cDNA	Complementary deoxyribonucleic acid
CGRP	Calcitonin gene related peptide
COPD	Chronic obstructive pulmonary disease
CTCF	Corrected total cellular fluorescence

DAG	Diacyl glycerol
DAMPs	Damage-associated molecular patterns
DMEM	Dulbecco's modified eagle medium
DMSO	Dimethyl sulfoxide
dNTP	deoxyribonucleotide triphosphate
dsRNA	Double stranded ribonucleic acid
DTT	Dithiothreitol
E. coli	*Escherichia coli*
EC_{50}	Half maximal effective concentration
ECAR	Extracellular acidification rate
ECL	Enhanced chemiluminescence
ECM	Extracellular matrix
EDTA	Ethylenediaminotetraactic acid
EGFR	Epidermal growth factor receptor
ELISA	Enzyme linked immunosorbent assay
ER	Endoplasmic reticulum
ETC	Electron transport chain
FACS	Fluorescence-activated cell sorting
FCCP	Carbonyl cyanide-4-(trifluoromethoxy)phenylhydrazone
FCS	Foetal calf serum
FILT	Filtered
GFP	Green fluorescent protein
GSK101	GSK1016790A

GTP	Guanosine-5’-triphosphate
HBSE	HEPES buffered saline-EDTA
HBSS	Hanks balanced salt solution
HBSS+	Hanks balanced salt solution-added HEPES
HC06	HC067047 (TRPV4 inhibitor)
HEK	Human embryonic kidney cells
HEK293-V4	Human embryonic kidney cells overexpression TRPV4 transfected cell line
HeLa Ohio	Ohio human cervix carcinoma – derivative of parental cell line HeLa
HEPES	4-(2-hydroxyethyl)-1-piperazineethanesulfonic acid
hpi	Hours post infection
HRP	Horseradish peroxidase
HRS	Hours
HT	Hypotonic
kDa	kilo Daltons
ICAM-1	Intracellular adhesion molecule-1
IFN	Interferon
IL	Interleukin
ISO	Isotonic
LDL-R	Low-density lipoprotein receptor
MAPK	Mitogen activated protein kinase
MK-7624	P2X3 antagonist (formally known as AF-219)
MLC	Myosin light chain
MLCK	Myosin light chain kinase

Phospho-MLC	Phosphorylated myosin light chain
MOI	Multiplicity of infection
mOsm	Milliosmole
mOsm/L	milliosmoles per litre
MUC5AC	Mucin-5AC
NFkB	Kappa light chain enhancer of activated B cells
NGF	Nerve growth factor
NLRX-1	Leucine-rich-repeat protein X-1
NOX-1	Nicotinamide adenine dinucleotide phosphate (NADPH) oxidase 1
NRT	No reverse transcriptase
NT	No treatment/unstimulated
OCR	Oxygen consumption rate
osmol/kg	Osmoles per kg
P2X	Purinergic receptors
P2X2	Purinergic receptor X2
P2X3	Purinergic receptor X3
P2X7	Purinergic receptor X7
PAGE	Polyacrylamide gel electrophoresis
PAMP	Pathogen-associated molecular patterns
PBS	Phosphate buffered saline
PBS-T	Phosphate buffered saline-Tween20
pcDNA 3	HEK cell line containing empty vector ‘pcDNA 3’
pCMV	Vector used for A549 transfection of GFP-tagged TRPV4 receptor

PCR	Polymerase chain reaction
PIP_2	Phosphatidylinositol 4,5-biphosphate
PKA	Protein kinase A
PKC	Protein kinase C
PKR	Protein Kinase R
PLC	Phospholipase C
PMSF	Phenylmethyl sulfonyl fluoride
PNX-1	Pannexin-1
Poly(I:C)	Polyinosinic:polycytidylic acid
PVDF	Polyvinylidene fluoride
qPCR	Quantitative real time polymerase chain reaction
RARs	Rapidly adapting receptors
RFU	Relative fluorescence units
RhoA	Ras homolog gene family, member A
RIPA	Radioimmunoprecipitation assay buffer
RO31	RO31-8220 (pan PKC inhibitor)
ROCK	Rho-associated protein kinase
ROS	Reactive oxygen species
Rot/A	Rotenone/antimycin A
RT	Room temperature
RTI	Respiratory tract infection
RT-PCR	Reverse transcription polymerase chain reaction
RV	Human rhinovirus

RV-16	Human rhinovirus-serotype 16
RVD	Regulatory volume decrease
SD	Standard deviation
SDS	Sodium dodecyl sulphate
SEM	Standard error of the mean
Ser19	Serine 19
SPDEF	Sterile-alpha-motif (SAM)-pointed domain ETS-factor
SRB	Sulforhodamine B
ssRNA	Single stranded ribonucleic acid
TBS	Tris buffered saline
TBS-T	Tris buffered saline- Tween 20
TCA	Trichloroacetic acid
TCID[50]	Tissue culture infective dose-50%
TEMED	Tetramethylethylenediamine
TGF-β	Tumour growth factor beta
TLR	Toll-like receptor
TNF	Tumour necrosis factor
TRP	Transient receptor potential channels
TRPA	Transient receptor potential Ankyrin
TRPA1	Transient receptor potential channel ankyrin receptor 1
TRPM	Transient receptor potential Melastatin
TRPV	Transient receptor potential Vanilloid
TRPV1	Transient receptor potential channel vanilloid receptor 1

TRPV4	Transient receptor potential channel vanilloid receptor 4
URTI	Upper respiratory tract infection
UV	Ultraviolet
Vaco	Vehicle
VH	Vehicle
WT	Wild type
ZO-1	Zonula occludens-1

Publications

Papers

Atkinson, S. A., Sadofsky, L. R., and Morice, A. H. (2016). How does rhinovirus cause the common cold cough? *BMJ Open Resp. Res.* **3:** e000118. Doi:10.1136/bmjresp-2015-000118.

Conference Abstracts

Atkinson. S. A., Morice, A. H., and Sadofsky, L. R. (2015). What causes the common cold cough? Allam Conference 2015, Hull.

Atkinson. S. A., Morice, A. H., and Sadofsky, L. R. (2016) Synthetic double stranded viral RNA stimulus causes upregulation of cough receptors. Allam Conference 2016, Hull.

Atkinson. S. A., Morice, A. H., and Sadofsky, L. R. (2016) Polyinosinic:polycytidylic acid causes upregulation of thermo-TRP channels and P2X3 receptor. HYMS Conference 2016, York.

Atkinson. S. A., Morice, A. H., and Sadofsky, L. R. (2018). Synthetic viral stimulus, polyinosinic:polycytidylic acid increased expression of cough receptors but human rhinovirus-16 causes reduced cough receptor function. Allam Conference 2018, Hull.

Atkinson. S. A., Morice, A. H., and Sadofsky, L. R. (2018). Effect of synthetic viral stimulus, polyinosinic:polycytidylic acid, and human rhinovirus-16 on expression and function of thermo-TRP channels and P2X3 receptor in the airway. HYMS Conference 2018, Hull.

Atkinson. S. A., Morice, A. H., and Sadofsky, L. R. (2018). Synthetic viral stimulus poly(I:C) increased expression of TRP channels but human rhinovirus-16 reduced cough receptor function. British Association of Lung Research (BALR), Birmingham.

Atkinson. S. A., Morice, A. H., and Sadofsky, L. R. (2018). Exploring the effect of human rhinovirus-16 on expression of pannexin-1 in alveolar cells. British Thoracic Society (BTS), London. Thorax, 73, supplement IV.

Acknowledgements

I would like to thank my supervisors Dr. Laura Sadofsky and Professor Alyn Morice for all their support, encouragement and guidance over the past four years. I am grateful to have had the opportunity to work with you both. I would like to say a special thank you to Laura for everything you've done and all that time we spent in your office, you've shown me inexplicable kindness and support far beyond that of a supervisor. Thank you.

I would like to thank everyone in the respiratory research group past and present for making my time here so wonderful, especially Jonathan Knaggs and Simon Fraser for his help with ELISA experiments, and both for their crucial input.

Most importantly, I am so grateful to my husband Lloyd for his unwavering support and encouragement, and all his time spent talking through ideas with me, and a special thank you to my son Callan for making the last few years so special. I couldn't have done this without you both.

This thesis is dedicated to my husband and son,

Lloyd and Callan

Declaration

I confirm that this work is original and that if any passage(s) or diagrams(s) have been copied from academic papers, books, the internet or any other sources these are clearly identified by the use of quotation marks and the reference(s) is fully cited. I certify that, other than where indicated, this is my own work and does not breach the regulation of HYMS, the University of Hull or the University of York regarding plagiarism or academic conduct in examinations. I have read the HYMS Code of Practice on Academic Misconduct, and state that this piece of work is my own and does not contain any unacknowledged work from any other sources'.

Chapter 1

General Introduction

1.1 Cough

Cough is a protective mechanism that occurs through the stimulation of a reflex arc to prevent aspiration and can be triggered by a multitude of stimuli. It aids in the clearance of harmful particulate matter, irritants and pathogens. It is the most common respiratory symptom for which people seek medical help (Morice *et al.*, 2007). In 2014 £98.7 million (Birring *et al.*, 2017) was spent on over the counter (OTC) cough remedies, despite findings of a systematic review that stated OTC preparation were no more effective than a placebo in the treatment of cough (Schroeder & Fahey, 2002).

The most common cause of acute cough (<3 weeks in duration) is respiratory tract infection (RTI) (Irwin *et al.*, 2018). These are illnesses caused by acute infection from bacteria, fungi and most frequently, viruses. Other conditions most likely to cause acute and chronic cough include asthma, gastro-oesophageal disease (GORD)/reflux, rhinitis, post-nasal drip syndrome and sinusitis (Palombini *et al.*, 1999). Whilst rarer causes include ACE-inhibitor induced cough, cardiovascular related conditions such as pulmonary embolism, hypertension and heart failure, lung cancers and post-viral cough, which whilst a rarer cause of cough has no treatment. Post-viral cough will be discussed in further detail later.

Cough causes a plethora of complications affecting the cardiovascular, gastrointestinal and respiratory system with far reaching psychological, neurological and musculoskeletal effects (Morice *et al.*, 2007; Irwin *et al.*, 2006; McGarvey & Morice, 2006).

1.1.1 Cough reflex

The cough reflex arc is composed of the afferent, central and efferent pathway, connected through a series of action potentials that ultimately results in the stimulation of the cough action (Irwin, Madison & Fraire, 2000). The cough response can be initiated both unconsciously, through the stimulation of sensory receptors, activated by a wide range of stimuli including chemical, mechanical, pH, temperature and osmolarity and consciously (Irwin, Madison & Fraire, 2000; Karlsson & Fuller, 1999; Widdicombe, 1954, 1995). The initiation of cough requires a high enough stimulus of receptors and channels present in the

airways at a sustained frequency to potentiate activation of afferent nerves to create an 'urge-to-cough' response (Dicpinigaitis *et al.*, 2014; Canning & Mori, 2011). The exact mechanism of cough is not completely understood, whereby it is unclear precisely which afferent nerves mediate the cough response.

There are three types of afferent nerve which are distinguished by their sensitivities to mechanical or chemical stimuli and further differentiated by their speed of adaption, myelination conduction velocities and site of termination (Karlsson & Fuller, 1999; Irwin, Madison & Fraire, 2000). Myelinated rapidly adapting receptors (RARs)/A-delta mediate cough by mechanical and chemical stimulation (Irwin, Madison & Fraire, 2000; Widdicombe, 1995). Myelinated slowly adapting receptor (SARS), do not respond to irritants but are crucial in making a cough more forceful (Hanácek, Davies & Widdicombe, 1984). The third type are unmyelinated C-fibres, which can be found within both pulmonary and bronchial branches of the airway (Karlsson & Fuller, 1999). Unmyelinated C-fibres constitute the majority of innervating nerves in the airways and are the most likely candidate for cough due to their location, distribution, expression of tussive receptors and response to tussive agent capsaicin (Winning *et al.*, 1986).

The cough reflex is essentially composed of a series of three major events (Fig. 1.1). Firstly, sensory nerves are activated through the stimulation of tussive receptors in the airways. This activation induces membrane depolarization and production of action potentials along the vagus nerve (Canning, Mori & Mazzone, 2006) to the 'cough centre' in the nucleus of solitary tract (NTS) of the brain. This is followed by relay of signals along the efferent nerves from the spinal cord to respiratory muscles to initiate the cough action. Finally, the actual cough event is a sequence of muscle contractions to forcibly remove air and secretions from the larynx, trachea and bronchi (Karlsson & Fuller, 1999). Under innervation from the phrenic and intercostal nerves, the diaphragm and external intercostal muscles contract creating a negative pressure in the lungs causing a deep inspiration. To equalise the intra-thoracic pressure, the glottis closes, abdominal and internal intercostal muscles contract, and the diaphragm relaxes. This facilitates the reopening of the glottis, and a vast and rapid exhalation of air producing the characteristics cough sound.

Receptors present in the airways, including transient receptor potential (TRP) channels which detect noxious stimuli, such as citric acid and capsaicin (Dicpinigaitis & Alva, 2005), leading to the initial activation of sensory nerves in the airways resulting in a cough response are of pharmacological interest to target. The association between several subsets of TRP channels, found on vagal sensory nerves, and the cough reflex/sensitivity have been extensively researched but despite the application of antagonists, the cough reflex cannot be fully inhibited (Khalid *et al.*, 2014) implying there may be cross-talk with other receptors or channels to precipitate the reflex. Purinergic receptors (P2XR), which are activated by ATP a known cough stimulant, are becoming of significant interest in the search to finally elucidate the mechanism of cough, especially the perpetuation of chronic cough (Fowles *et al.*, 2017; Bonvini *et al.*, 2016; Abdulqawi *et al.*, 2015). Recent lines of enquiry have focused their attention on the cross talk between TRP and P2X receptors. Whilst there is a strong correlation between TRP channels and cough, data surrounding the role of P2X receptors is sparse which pose an exciting new area of research.

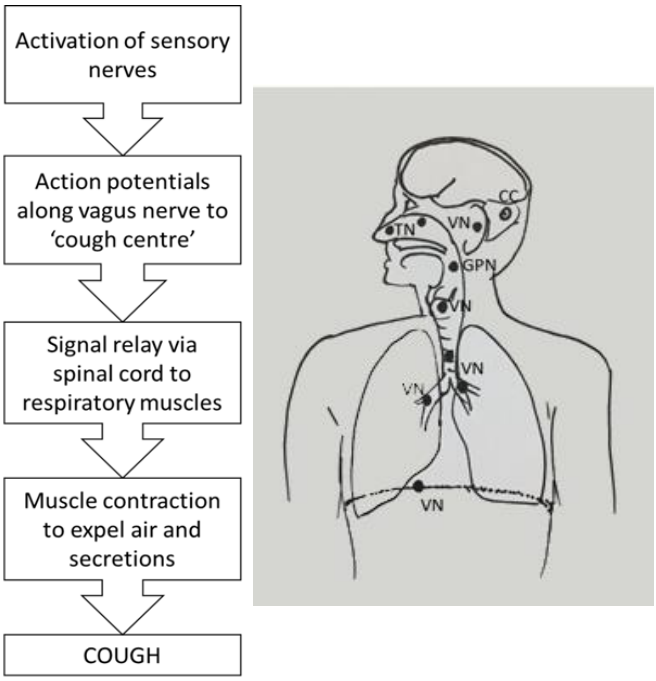

Figure 1.1. ***Cough reflex arc.*** *Schematic diagram of respiratory tract airway with neuronal innervation and simplified steps of the cough reflex arc. Specific nerve innervation of the brain, upper and lower respiratory tract is labelled; Trigeminal nerve – TN; vagus nerve – VN; cough centre – CC; glossopharyngeal nerve – GPN.*

1.2 TRP Channels

TRP channels are transient receptor potential channels whose namesake arose from research carried out by Cosens & Manning (1969) on mutant *Drosophila* fruit flies. Using mutant flies, electroretinogram responses identified a lack of calcium entry causing only transient light-induced current opposed to the expected sustained current seen in wild type *Drosophila*. This work was expanded upon by Minke, Wu & Pak (1975) who identified mutant *trp*. As a consequence of these findings a new interest in TRP channels was sparked and thanks to rapidly advancing technological progress in cloning and molecular biology a new field began to emerge. The *trp* gene was first isolated, sequenced and cloned in 1989 by Montell & Rubin from *Drosophila* flies. Analysis of the protein sequence facilitated the identification of the protein function, which was determined to be a non-specific calcium permeable influx channel. This had major implications in the field of biology due to the significance of calcium as a signalling molecule. This led research of TRP channels into mammalian homologs and the identification of the first recognised mammalian TRP channel, TRPC1 and the establishment of the TRPC family (Wes *et al.*, 1995).

To date, 7 families of TRP channels have been identified, including TRP ankyrin (TRPA), TRP canonical (TRPC), TRP melastatin (TRPM), TRP melastatin-like (TRPML), TRP no mechanoreceptor potential C (NOMPC) (TRPN), TRP polycystic (TRPP) and TRP vanilloid (TRPV) (Montell, 2005). These families contain 28 members in total with orthologs in a multitude of species including *Drosophila*, *Mus musculus*, *Caenorhabditis elegans* and humans (Vannier *et al.*, 1999; Okada *et al.*, 1999; Petersen *et al.*, 1995; Cosens & Manning, 1969) (for a comprehensive review see Montell, 2005; Ramsey, Delling & Clapham, 2006). Unlike other protein channel families, TRP channel families are categorised according to amino acid sequence homology. They are highly conserved with a common ancestral point branching back approximately 500 million years (Nilius, Appendino & Owsianik, 2012) (Fig. 1.2).

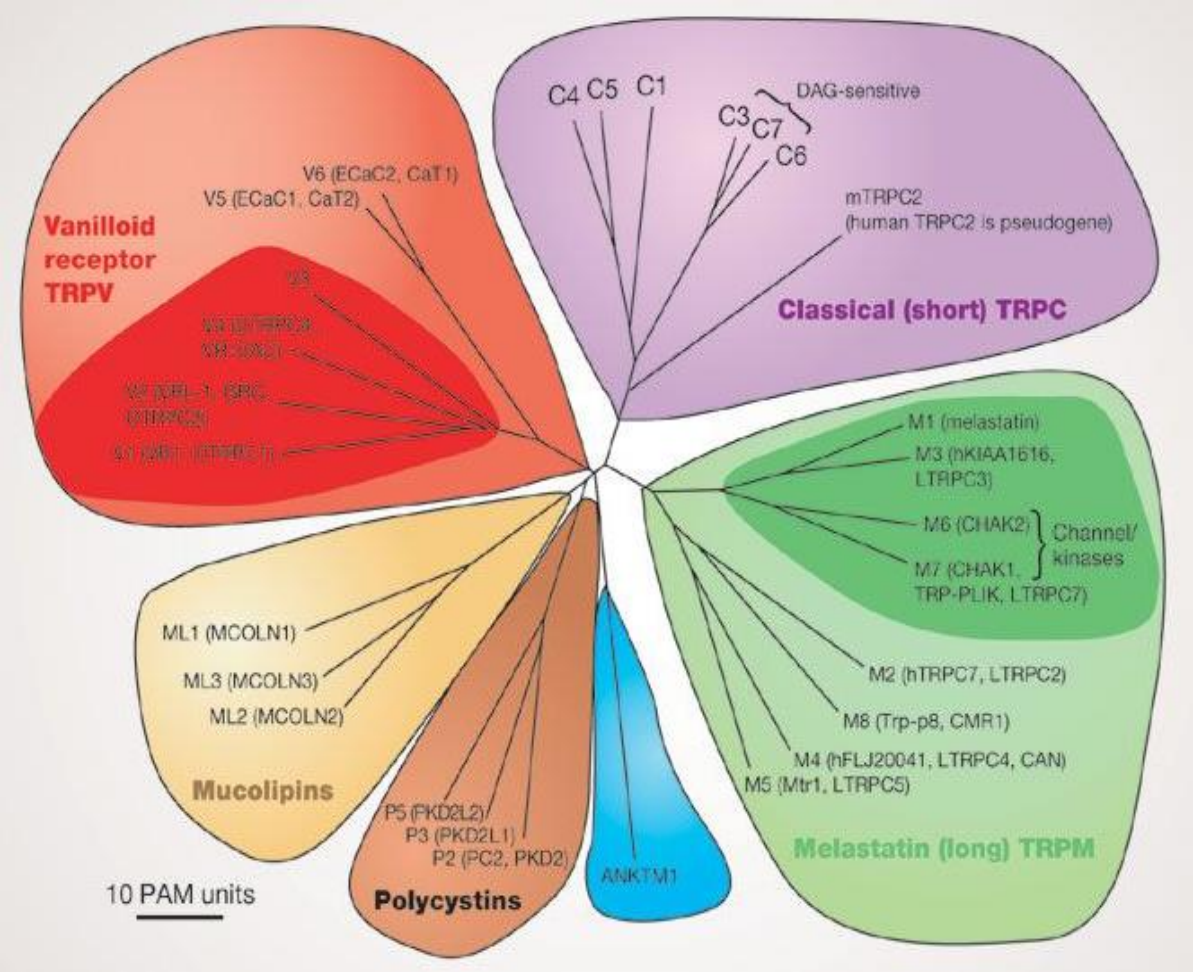

Figure 1.2. ***TRP channel evolution tree.*** *The evolutionary distance is shown by the total branch lengths in point accepted mutations (PAM) units, which is the mean number of substitutions per 100 residues. Diacylglycerol – DAG. [*Figure taken from (Clapham, 2003*]].*

TRP channels all share a similar architecture composing six transmembrane (TM) spanning domains, a hydrophobic loop between domain 5 and 6, referred to as a P-loop, and form heteromeric or homomeric structures (Hellwig *et al.*, 2005; Murakami *et al.*, 2003; Strübing *et al.*, 2003; Kedei *et al.*, 2001; Kuzhikandathil *et al.*, 2001; García-Martínez *et al.*, 2000).

A subcategory of TRP channels composes thermo-TRP channels including TRPV1-4, TRPA1 and TRPM8; with TRPV1, TRPV4 and TRPA1 the primary focus of this project. Identified through extensive cloning and characterisation, these channels were identified to be thermally sensitive (Fig. 1.3) and heavily involved in nociception (Lee *et al.*, 2005a; Moqrich *et al.*, 2005;

Todaka *et al.*, 2004; Suzuki *et al.*, 2003; McKemy, Neuhausser & Julius, 2002; Peier *et al.*, 2002; Smith *et al.*, 2002; Caterina *et al.*, 2000, 1999).

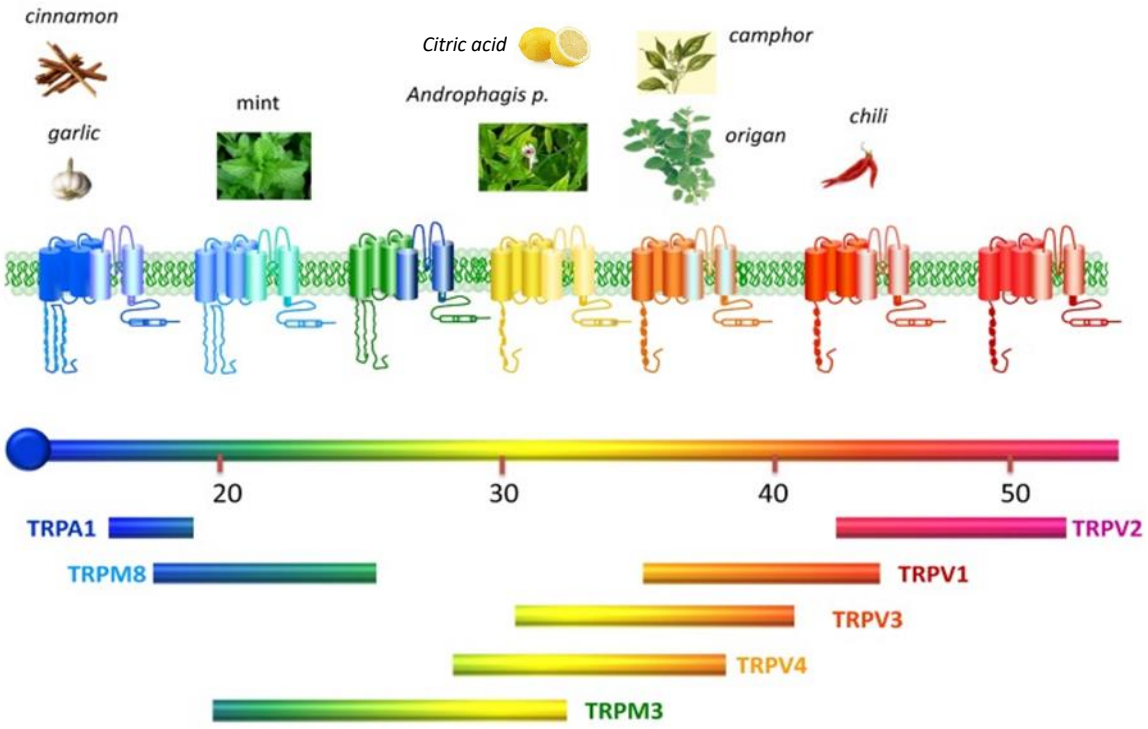

Figure 1.3. ***Structures and thermo-sensitive ranges of thermo-transient receptor potential (TRP) channels showing common natural product agonists.*** *Thermo-TRP channels are tetramers composed of six transmembrane domains (S1-S6), a hydrophobic pore loop linking transmembrane units S5 and S6, a cytoplasmic N- and C-terminals. TRPA1 displays noxious cold sensing tendencies whilst TRPV2 displays harmful hot sensing properties. [modified from (Ferrandiz-Huertas et al., 2014) adapted from (Latorre, Zaelzer & Brauchi, 2009).*

1.2.1 TRPA1

TRPA1 has been the most recently discovered TRP channel and previously referred to as ANKTM1 (Story *et al.*, 2003). Genetic analysis of predicted gene sequences unearthed a sequence with ankyrin repeats, and transmembrane domains indicative of a putative TRPA1 sequence. The mRNA was cloned from sensory neurons DRG and found to also possess thermosensitive properties like TRPV1, but instead responsive to noxious cold temperatures <18^{o}C (Story *et al.*, 2003). Following a generic TRP structure, TRPA1 possesses a distinctive structural difference with the presence of multiple (14-18) ankyrin repeats, referred to as an ankyrin repeat domain (ARD), on the cytosolic amino (N)-terminal (Fig. 1.4) (Paulsen *et al.*, 2015; Cvetkov *et al.*, 2011), believed to be the site of covalent modification (Macpherson *et al.*, 2007; Hinman *et al.*, 2006). Originally thought to be essential for membrane expression, the N-terminal has been since shown to be dispensable (Moparthi *et al.*, 2014). A series of mutagenic experiments of key residues within the EF motif, found within the ARD, displayed significantly diminished responsiveness to calcium and activation by calcium (Bessac & Jordt, 2008; Doerner *et al.*, 2007; Zurborg *et al.*, 2007). This work has since been disputed by Wang *et al.* (2008), who claimed under the same experimental conditions the EF motif was not essential for TRPA1 activation ultimately leaving their role as potentiator ambiguous. Like other TRP channels, TRPA1 is a non-specific flux channel to physiological cellular ions but recognised for its calcium permeability (Story *et al.*, 2003).

There is a lot of conflicting data surrounding the role of endogenous ligand and plasma membrane component phosphatidylinositol 4,5-biphosphate (PIP_2) on TRPA1 channels. In some TRP channels, such as TRPV1 it functions in an inhibitory capacity (Prescott & Julius, 2003) whilst in other channels including TRPV5 and TRPM8 it is stimulatory (Lee *et al.*, 2005b; Liu & Qin, 2005; Rohács *et al.*, 2005). An interesting observation given TRPV1, TRPM8 and TRPA1 all have similar structures in comparison to other members of the larger TRP family. Research by Karashima *et al.* (2008) believed to have finally elucidated that PIP_2 is an activator of TRPA1 and regulates the effect of desensitisation of agonists, albeit to a lesser extent than other TRP channels such as TRPV1. However, Kim, Cavanaugh & Simkin (2008) found PIP_2 inhibits TRPA1 and leads to reduced sensitivity of some agonists. It is quite clear that the role of PIP_2 is complex and many variables affect the function *in vitro*,

however, it is not surprising to think that PIP_2 may play a role of modulation of the channel given the close interaction of PIP_2, calmodulin and calcium in the phospholipase C cellular signalling pathway (Putney & Tomita, 2012).

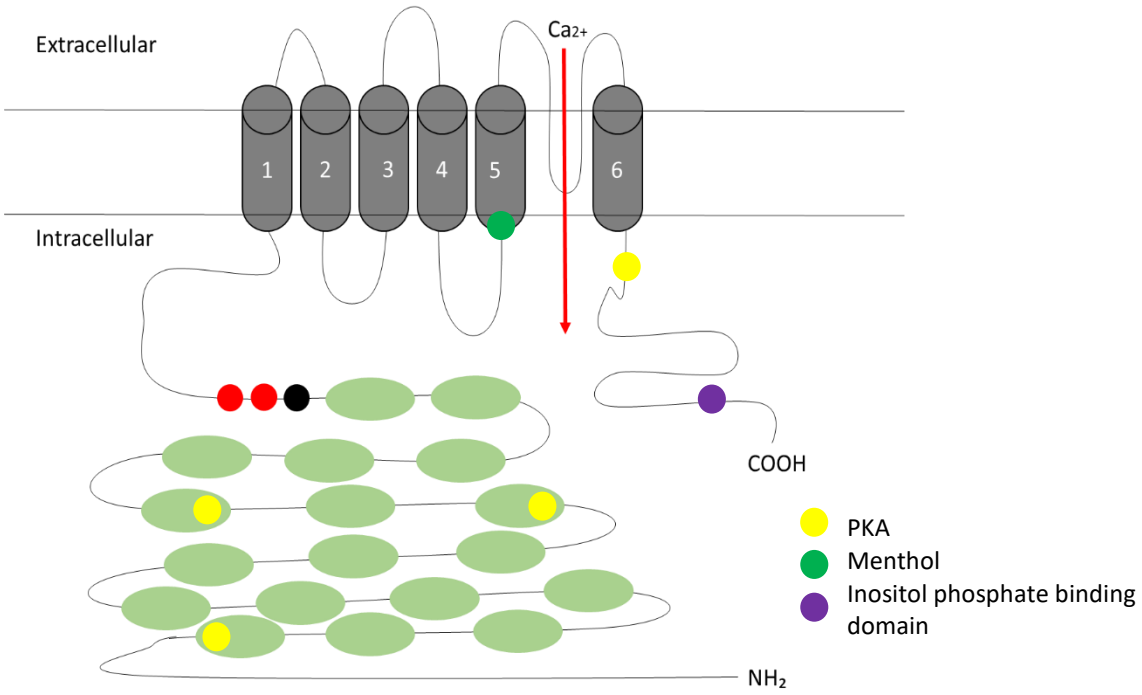

Figure 1.4. ***TRPA1 structure.*** *Transmembrane domains are 1-6 are grey columns labelled 1-6. Pore structure between transmembrane domains 5 and 6 indicated with a red arrow demonstrating calcium flux capability. Intracellular N- and C- terminals are indicated with NH_2 and COOH. Green ovals represent ankyrin repeats on N-terminal tail. Coloured circles indicate cysteine residues essential for covalent activation of TRPA1; red are human specific, black are essential for both mouse and human. Yellow circles indicate PKA binding sites; dark green circle indicate menthol binding site; purple circle indicates inositol phosphate binding site. [Adapted from* (Macpherson *et al.*, 2007; Hinman *et al.*, 2006; Meents, Fischer & McNaughton, 2017; Jardín *et al.*, 2017)*].*

TRPA1 has three modes of activation – direct, such as temperature and mechanical stimuli; ligand, and receptor based, including G protein coupled receptors (Story *et al.*, 2003; Kwan & Corey, 2009; Kerstein *et al.*, 2009; Bandell *et al.*, 2004). They are also renowned for their promiscuous binding. This behaviour facilitates their activation by a variety of ligands, including allyl isothiocyanates, an electrophilic activator found in mustard oil; cinnamaldehyde, the unsaturated aldehyde found in cinnamon; allicin, the agent responsible for the aroma of garlic; and acrolein, a major component of tear gas and

precursor to cinnamaldehyde synthesis (Bandell *et al.*, 2004; Bautista *et al.*, 2006; Jordt *et al.*, 2004; Macpherson *et al.*, 2005). The relaxed binding capabilities of TRPA1 have been attributed to their highly reactive N-terminal cysteine residues (McAlexander & Taylor-Clark, 2011; Hinman *et al.*, 2006). These enable the channel to bind and activate via the formation of a covalent bond between reactive thiol groups and electrophilic molecules, such as endogenous signalling molecules prostaglandin and reactive oxygen species (ROS) (Hu *et al.*, 2010). These electrophilic molecules are able to bind through covalent modification in two distinct ways. Either direct or conjugate addition, however, molecules show a preference to bind via direct addition despite possessing the ability to bind either way (Sadofsky *et al.*, 2011; Macpherson *et al.*, 2007). Covalent modification of cysteine residues are not readily reversible and as a result display a sustained response time (Macpherson *et al.*, 2007). In spite of this, signal transduced modulation has been suggested to be controlled by negatively charged carboxyl (C)-terminal due to the presence of a series of basic residues (Sura *et al.*, 2012; Samad *et al.*, 2011). The C-terminal of TRPA1 has also been shown to be involved in voltage-dependent activation of the channel, identified through mutagenesis of intracellular α-helices, whereby the channel lost the voltage-sensing abilities (Samad *et al.*, 2011). Despite their efforts, the mechanism of exactly how TRPA1 senses voltage and changes in voltage has yet to be fully elucidated.

TRPA1 channels are also open to non-electrophilic modification, which show a tendency to form non-covalent modifications. Most non-covalent modulators function bimodaly (Karashima *et al.*, 2007), for example they may activate at a low concentration whilst displaying an inhibitory function at a higher concentration. Such reactions are reversible and tend to produce a more transient response.

Until recently TRPA1 was functionally confirmed as a noxious cold detector (McAlexander & Taylor-Clark, 2011) with activation at temperatures as low as 17^{o}C (Story *et al.*, 2003) but controversy now surrounds this. Discrepancies found in cold detection have been attributed to differences in species (Chen *et al.*, 2013). A single residue difference has been identified between rodent and human TRPA1 genes within the S5 transmembrane domain, whereby rodent (mouse and rat) displayed activation at temperatures from 16^{o}C, primate (rhesus monkey and human) did not illicit such a response.

TRPA1 also functions in a mechanosensory capacity. This role was identified in a TRPA1 mutant in *C.elegans* that displayed a defective response to touch (Kindt *et al.*, 2007). TRPA1 has also been implicated to function in a mechanosensory role in pathophysiological conditions including inflammatory hypersensitivity whereby skin afferent nerves displayed a lower threshold of activation and increased expression of TRPA1 (Dunham, Kelly & Donaldson, 2008). Furthermore, *in vivo* studies which have used HC030031 to study the effect of antagonism of TRPA1 in afferent terminal sensory neurons showed a significantly reduced response to formalin in rat studies (McNamara *et al.*, 2007). This was further supported in TRPA1 deficient rodents, which also showed no response to noxious stimuli upon the application of formalin (Kerstein *et al.*, 2009). Evidence from the *Drosophila* gene *painless*, found within the heart, functions to adjust cardiac muscle activity and mediates mechanotranduction. Mutations isolated corresponding to a pressure induced response caused arrhythmias and cardiac arrest (Sénatore *et al.*, 2010). TRPA1 is also expressed in all sensory epithelia hair cells of the inner ear (Minke, 2006) and disruption in these channels causes defects in hearing (Montell, 2005). However, contrary to previous findings, TRPA1 deficient mice displayed normal hearing reflexes (Bautista *et al.*, 2006; Kwan *et al.*, 2006). These mechanotransduction functions have been attributed to TRPA1's distinct characteristic ankyrin repeats, akin to a spring, a common feature to NOMPC, another TRP channel (Howard & Bechstedt, 2004; Sotomayor, Corey & Schulten, 2005), which functions as bristle and hair cell mechanoreceptor in flies and zebrafish, respectively (Nagata *et al.*, 2005). Recently, the structure of TRPA1 was finally elucidated by Cvetkov *et al.* (2011) (Fig. 1.5) which may shed light onto the conflicting data surrounding the exact role of TRPA1 in hearing, although more evidence in support of its role exists over opposing research.

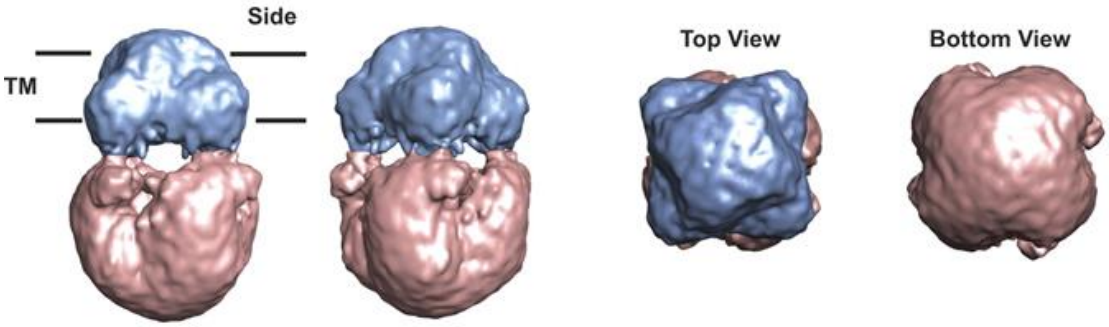

Figure 1.5. ***3D reconstruction of TRPA1*** *is presented at a threshold corresponding to a molecular mass of 525 kDa. The proposed transmembrane domain (TM, blue) and cytoplasmic domain (CP, pink) are indicated. Side, top and bottom views of the reconstruction are shown. Reconstruction carried out using Segger and visualised with Chimera software. [Adapted from (Cvetkov et al 2011)].*

1.2.2 TRPV

There are six currently identified members of the vanilloid TRP family. They all show some degree of response to temperature and vanilloids. The vanilloid TRP subfamily is roughly divided in to two further subgroups, TRPV1-4 displays moderate calcium selectivity and high temperature dependence and thereby referred to as thermo-TRPs, and TRPV5 and V6 display high calcium selectivity and low temperature dependence (Watanabe *et al.*, 2002a, 2002c; Liedtke *et al.*, 2000; Strotmann *et al.*, 2000; Caterina *et al.*, 1999, 1997; Voets *et al.*, 2002). Like other TRP channels, the TRPV family forms multimeric structures within the plasma membrane. The utilisation of coimmunoprecipitation and FRET analysis determined TRPV1-4 show a tendency to form homomeric structure over heteromeric (Hellwig *et al.*, 2005). The focus of this review are thermo-TRP channels V1 and V4.

1.2.2.1 TRPV1

TRPV1 was the first discovered thermal TRPV channel, previously known as VR1. It was identified through a series of novel and ground breaking cloning experiments carried out by Caterina *et al.* (1997). It was discovered to possess a vanilloid moiety, was activated by hydrophobic lipid capsaicin and sensitive to noxious temperature suggestive of its role in transduction of pain signals (Caterina *et al.*, 1997). Following this, a human orthologue was isolated and cloned possessing 92% homology to the rat clone previously identified (Hayes *et al.*, 2000). In accordance with previous findings, TRPV1 was found heavily expressed in

the DRG and neuronal pathway, but mRNA expression could also be found in the global periphery (Hayes *et al.*, 2000) through the use of sensitive quantitative-PCR measurements.

TRPV1 undergoes multimerisation forming homo- and heterotetramers (Garcia-Sanz *et al.*, 2004; Kedei *et al.*, 2001). After years of speculation, recent advancements in electron cryo-microscopy and 3D modelling have allowed us to definitively determine that TRPV1 forms a tetramer structure in the plasma membrane (Liao *et al.*, 2013; Moiseenkova-Bell *et al.*, 2008; Kedei *et al.*, 2001; Kuzhikandathil *et al.*, 2001) (Fig. 1.6). Like other TRP channels, TRPV1 has cytosolic N- and C-terminals, a highly conserved TRP domain on the C-terminal, and three ankyrin repeats on the N-terminal thought to provide rigidity and involved in protein interactions (Mosavi *et al.*, 2004; Gorina & Pavletich, 1996). Protein mutagenesis has allowed the identification of many amino acids essential for specific functions such as binding and activation, modulation, permeability, phosphorylation, desensitisation and multimerisation (Kedei *et al.*, 2001) (Fig. 1.7). Figure. 1.7 details the amino acid binding and modulating sites of many of TRPV1 agonists and interacting proteins, including capsaicin, protons, calmodulin, A-kinase anchoring protein (AKAP), protein kinases and lipoxygenase product (Jung *et al.*, 1999; Jordt, Tominaga & Julius, 2000; Rosenbaum *et al.*, 2004; Numazaki *et al.*, 2003; Zhang, Li & McNaughton, 2008; Mohapatra & Nau, 2003; Bhave *et al.*, 2002, 2003; Numazaki *et al.*, 2002; Jung *et al.*, 2004).

The primary function of TRPV1 is detection and regulation of temperature. As it is mainly expressed in the nervous system (Hayes *et al.*, 2000), TRPV1 is involved in the transmission and modulation of nociception (Caterina *et al.*, 2000). The most well-known and potent agonist of TRPV1 is capsaicin, which possesses a vanillyl moiety. Interestingly, repeated and continuous exposure with capsaicin causes TRPV1 receptor desensitisation, which paradoxically in the body this leads to alleviation of pain (Jancsó, Jancsó-Gábor & Szolcsányi, 1967). Bladder epithelium, keratinocytes and epithelial cells of the gastrointestinal system have also been shown to express functional TRPV1 (Hayes *et al.*, 2000; Southall *et al.*, 2003; Inoue *et al.*, 2002). TRPV1 is expressed within the airways (Watanabe *et al.*, 2006) and activation by air pollutants and particulate matter (Deering-Rice *et al.*, 2012) have been shown to lead to apoptosis and inflammation which further potentiate TRPV1 channel activation (Agopyan *et al.*, 2004). TRPV1 is thought to play a major role in the mechanism of cough, however despite attempts to block the receptor,

cough still persists upon application of nebulised capsaicin in chronic cough (Khalid *et al.*, 2014). The role of TRPV1 in the airway is discussed further in section 1.2.3.

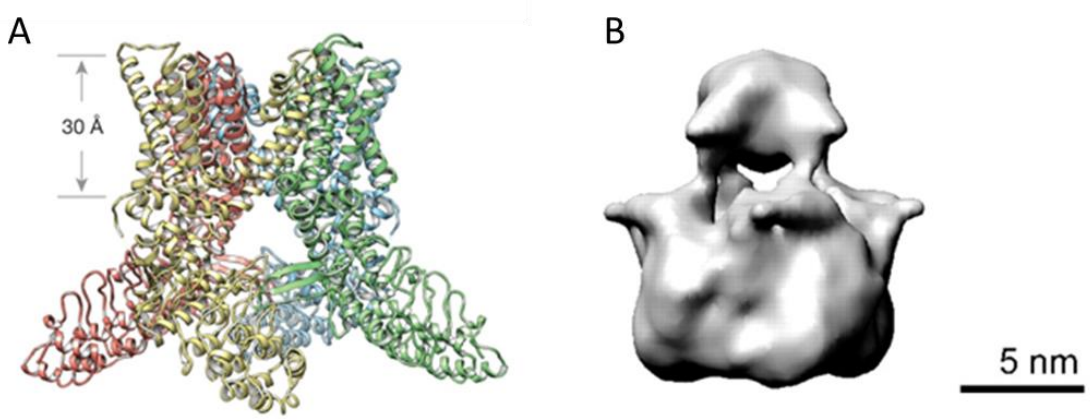

Figure 1.6. ***Structure of TRPV1*** *as determined by electron cyromicroscopy. A) Ribbon diagram of tetramer TRPV1 atomic model composed of four identical subunits (red, yellow, blue and green). B) 3D isosurface representation of single particle electron microscopy of TRPV1 corresponding to mass of 500 kDa. [A and B adapted from* Liao *et al.*, 2013 and Moiseenkova-Bell *et al.*, 2008*, respectively.]*

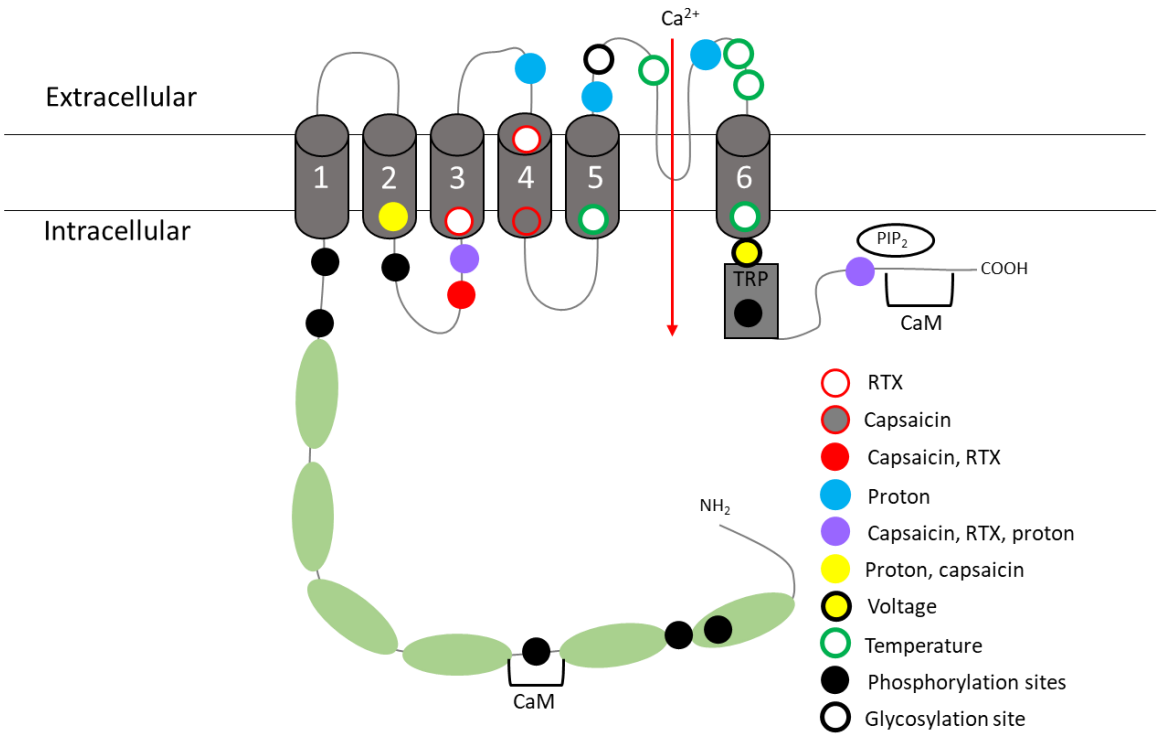

Figure 1.7. ***TRPV1 structure and binding sites.*** *Transient receptor potential vanilloid type 1 (TRPV1) channel topology with highlighted key residues and amino acids involved in gating function evoked by different stimuli are indicated. Phosphatidylinositol 4, 5-bispohsphate – PIP_2; phosphorylation sites involved in sensitising actions of protein kinase C and protein kinase A – black circles; calcium-calmodulin binding sites – CaM; ankyrin repeats – green ovals.*

1.2.2.2 TRPV4

The discovery and genetic analysis of *C.elegans* osmosensory channel protein OSM-9 identified a structure reminiscent of previously discovered TRP proteins from *Drosophila* containing six hydrophobic membrane spanning regions, cytoplasmic N- and C-terminals, ankyrin consensus motif and a highly conserved region specific to the TRP channel family (Colbert, Smith & Bargmann, 1997). Further analysis of the cloning and sequencing experiments from the discovery of TRPV1 (Caterina *et al.*, 1997), identified a section of nucleotide sequence found to belong to TRPV4, a vertebrate homolog of OSM-9, possessing strong homology with TRPV1-V3 with minimal sequence difference between human, murine and rodent (Liedtke *et al.*, 2000; Strotmann *et al.*, 2000). Together these studies identified that TRPV4 was related to TRPV1 and possessed osmosensory properties, with the threshold of activation by hypotonicity as little as 1% decrease in tonicity.

Also referred to as TRP12, OTRPC4 and VR-OAC, confirmation of human TRPV4 osmosensing properties came from findings of Liedtke *et al.* (2000), Strotmann *et al.* (2000) and Nilius *et al.* (2001). They not only discovered TRPV4 senses and regulates cellular responses to osmotic changes but that extensive mRNA analysis displayed the highest expression in the lung, airway and kidneys (Liedtke *et al.*, 2000; Strotmann *et al.*, 2000; Wissenbach *et al.*, 2000). It is also found within DRG, bladder, vascular endothelium and skin to name a few (Delany *et al.*, 2001; Birder *et al.*, 2007). Further work has since revealed TRPV4 sensitive to other modes of activation including, moderately warm temperature, shear stress, acidic pH, phorbol ester lipids including phorbol 12-myristate 13-acetate (PMA) and 4α-phorbol 12,13-didecanoate (4αPDD) and arachidonic acid (AA) metabolites such as 5,6-epoxyeicosatrienoic acid (Nilius *et al.*, 2004; Vriens *et al.*, 2004; Suzuki *et al.*, 2003; Watanabe *et al.*, 2003, 2002a, 2002b).

Whilst TRPV4 only shares approximately 40% homology to TRPV1 and TRPV2 (Liedtke *et al.*, 2000; Strotmann *et al.*, 2000) cyro-electromicroscopy revealed a similar quaternary structure (Shigematsu *et al.*, 2010). TRPV4 possess both PKA non-modifying and PKC modifying phosphorylation sites (Gao, Wu & O'Neil, 2003; Xu, Satoh & Iijima, 2003; Watanabe *et al.*, 2002a), tyrosine kinase phosphorylation site, an N-terminal ARD, calcium-calmodulin binding site and a glycosylation site to close the pore (Xu *et al.*, 2003) (Fig. 1.8).

The amino-terminal ARD, which contains a minimum of 3 ankyrin repeats, was found to be important for mechano- and thermo- sensation, whereby ankyrin knockouts in *C.elegans* caused a delayed response to mechanical stimuli (Liedtke *et al.*, 2000). These repeats have also been suggested to be important for cellular trafficking and may aid in cytoskeletal anchoring (Shigematsu *et al.*, 2010; Suzuki, Hirao & Mizuno, 2003) and also provide a lipid-binding domain for PIP_2 interaction and channel activity modulation (Takahashi *et al.*, 2014). Further mutagenesis of *C.elegans* identified the C-terminal of TRPV4 was also important for mechanosensation (Liedtke *et al.*, 2003). TRPV4 is also thought to undergo phosphorylation by Lyn, a Src family tyrosine kinase, (Xu *et al.*, 2003) following activation by hypotonicity but evidence has been found to the contradictory (Vriens *et al.*, 2004) instead suggesting phospholipase A2 (PLA_2) is the signal transducer in cellular swelling. Previous electrophysiological studies had identified that hypotonic activation of TRPV4 was dependent on PLA_2 (Basavappa *et al.*, 1998) where these currents were blocked using PLA_2 specific inhibitors (Vriens *et al.*, 2004; Watanabe *et al.*, 2003).

Like other TRP channels TRPV4 is capable of functional coupling and regulatory interactions to other proteins, an example of which are aquaporins (AQP). Aquaporins are integral water channels essential for water transport between cells (Verkman, 2013). Several of these proteins have been found to closely interact with TRPV4. Cellular swelling under hypotonic conditions is caused by the flux of water through AQP. Within the lung, TRPV4 directly downregulates the membrane expression of AQP5 when exposed to hypotonic conditions (Sidhaye *et al.*, 2006). TRPV4 not only regulates the expression of proteins involved in hypotonic induced changes but can also regulate itself. Cystic fibrosis transmembrane conductance regulator (CFTR) is thought to regulate TRPV4 expression, as when defective, in the case of cystic fibrosis, cells are unable to undergo regulatory volume decrease (RVD) (Arniges *et al.*, 2004), a compensatory mechanism during hypotonic exposure. This was also found in healthy airway when TRPV4 was knocked down with antisense oligonucleotides (Arniges *et al.*, 2004).

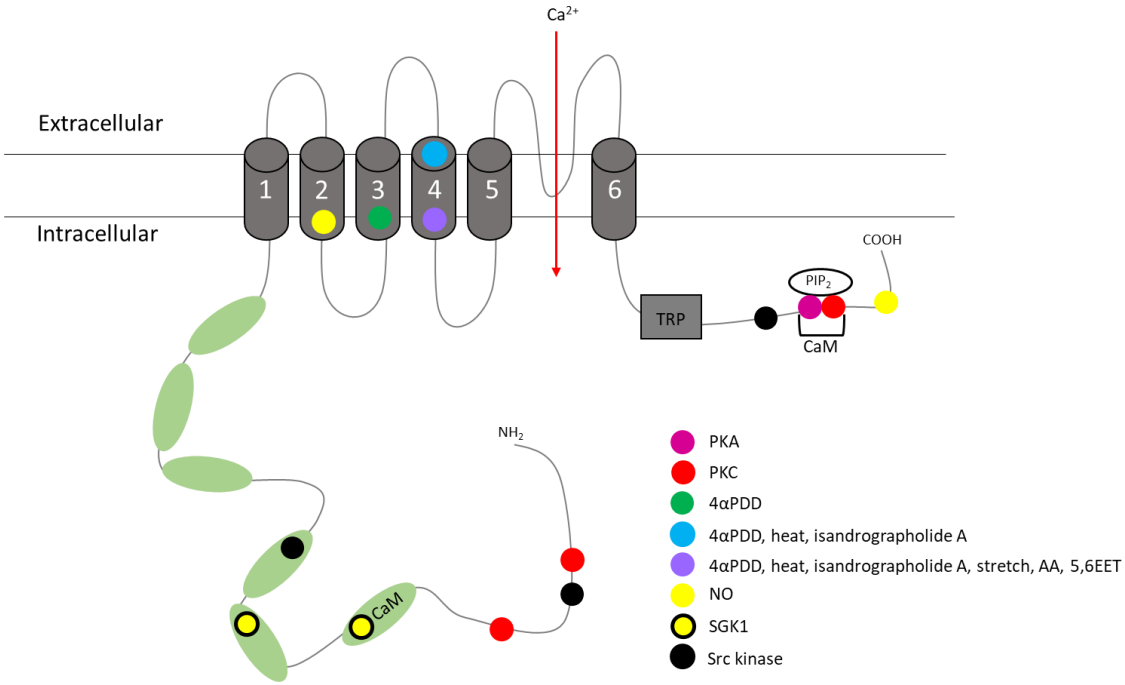

Figure 1.8. ***TRPV4 structure and binding sites.*** *Transient receptor potential vanilloid type 4 (TRPV4) channel topology with highlighted key residues and amino acids involved in gating function evoked by different stimuli are indicated. Phosphatidylinositol 4, 5-bispohsphate – PIP_2; phosphorylation sites involved in sensitising actions of protein kinase A (PKA), and protein kinase C (PKC) – pink and red circles, respectively; calcium-calmodulin binding sites – CaM, 4α-Phorbol 12,13-didecanoate (4αPDD) – green, blue and purple circles; arachidonic acid (AA) – purple circles; epoxyeicosatrienoic acid (5,6 EET) – purple circles; nitric oxide (NO) – yellow circles; serine/threonine-protein kinase Sgk1 (SGK1) – yellow and black circle; TRP box motif (TRP); ankyrin repeats – green ovals.*

1.2.3 Role of TRPA1, V1 and V4 in the airway

TRP channels are increasing associated with respiratory diseases including asthma, COPD, idiopathic pulmonary fibrosis and idiopathic cough (Grace *et al.*, 2012; Zhu *et al.*, 2009a; Nilius *et al.*, 2007). Both TRPA1 and TRPV1 may be responsible for the production of cough seen in asthmatics due to the increased levels of TRP agonists and inflammatory molecules including PGE2 and bradykinin (Grace *et al.*, 2014, 2012; Maher, Birrell & Belvisi, 2009; Choudry, Fuller & Pride, 1989). This was further supported by data which suggested TRPV1 mRNA is increased in emphysema sufferers (Grace *et al.*, 2014) and that SNP variations in TRPV1 genes are associated with increased cough symptoms, however this was not seen with TRPA1 (Smit *et al.*, 2012). Smokers have been found to have an increased incidence of cough (Gerrard *et al.*, 1980). Likely a result of the presence of toxic compounds, including

acrolein and crotonaldehyde, found within cigarette smoke that are potent agonists to TRPA1 (Shapiro *et al.*, 2013; Birrell *et al.*, 2009; Bautista *et al.*, 2006, 2005). This suggests that TRPA1 may play some form of role in the detection and permission of cough through smoking, which is a key driver in the pathogenesis of COPD (Andrè *et al.*, 2008). Oxidative stress is a common harmful by-product of cigarette smoke, present in vast quantities in the lungs of COPD sufferers. As TRPA1 functions as a sensor of oxidative stress, it is thought to play an important role in the pathogenesis of COPD, possibly through a non-neuronal inflammatory response (Nassini *et al.*, 2012).

TRP channels are also increasingly thought to play a role in the cough reflex during RTI. Cell line *in vitro* neuronal and airway models showed that stimulation with human rhinovirus, the major causative agent of the common cold and respiratory syncytial virus, a virus that causes severe RTI, caused upregulation of TRPA1 and TRPV1 as early as 2-4 hours post infection and as late as 12 hours (Omar *et al.*, 2017; Abdullah *et al.*, 2014). Furthermore, treatment with potent TRPV1 inhibitor capsazepine prevented viral induced upregulation of TRPV1 (Omar *et al.*, 2017). Unfortunately, attempts to inhibit cough through blockade of TRPV1 have been unsuccessful (Khalid *et al.*, 2014). As a result, research efforts have shifted to TRPV4 and its effect on the cough reflex. TRPV4 is expressed in the lung airway epithelium and smooth muscle cells (Delany *et al.*, 2001; Jia *et al.*, 2004). Previous data have shown TRPV4 may play a role in the pathophysiology of asthma and cystic fibrosis (Arniges *et al.*, 2004; Jia *et al.*, 2004) due to their distribution and the fact that airway is constantly exposed to mechanical stress and frequently to hypotonic stress, two potent activation routes. A potential activation pathway following hypotonic stimulation was identified by Seminario-Vidal *et al.*, (2011) which found TRPV4 activation lead to ATP release in the airway. The importance of which was highlighted by *ex vivo* guinea pig primary nodose ganglions whereby P2X3 antagonism blocked TRPV4 induced cough (Bonvini *et al.*, 2016). Whilst P2X3 antagonism has been used to treat chronic cough in humans very effectively (Abdulqawi *et al.*, 2015), further research is required to determine if TRPV4 plays a role in the cough reflex during RTI and if it contributes to airway hypersensitivity seen in RTI and post-virally.

1.3 P2X Receptors

P2X receptors (P2XR) are part of a larger family of receptors known as purinergic receptors (purinoceptors). Purinoceptors are ATP activated cation permeable, membrane-spanning receptors (Brake, Wagenbach & Julius, 1994; Valera *et al.*, 1994; Rassendren *et al.*, 1997). There are three distinct classes of receptor, P1 and P2Y are metabotropic receptors activated via a G-protein coupled receptor and signal via second messenger systems (Webb *et al.*, 1993), both of which function similarly. The third type, P2XR are ionotropic ligand gated ion channels (Valera *et al.*, 1994) and consist of seven subtypes (North, 2002) denoted P2X1-P2X7. P2XR subunits co-assemble trimerically to form pore structures (Barrera *et al.*, 2005; Nicke *et al.*, 1998) from which these structures form homo- and heteromultimers (Jiang *et al.*, 2003; Nakazawa *et al.*, 2005).

P2XR are a distinct set of receptors, structurally resembling sodium channels (Surprenant, Buell & North, 1995). P2XR are extensively expressed throughout the nervous, vascular, digestive and pulmonary systems, and are also found in the bladder, bone and haematopoietic cells (Cockayne *et al.*, 2000; Collo *et al.*, 1996; Rubio & Soto, 2001; Ma *et al.*, 1999; Maruo *et al.*, 2006; Falzoni *et al.*, 1995; Chiozzi *et al.*, 1997). P2XR play a key role in sensory and neuronal innervation as such the receptor distribution within the airway are of particular interest. They have been identified as having roles in the cough reflex, the inflammatory responses to pathogens, and paracrine functions (Placido *et al.*, 2006; Kamei *et al.*, 2005; Hede *et al.*, 1999; Hazama, Hayashi & Okada, 1998; Li *et al.*, 1991). The main agonist of P2XR is ATP (Egan & Khakh, 2004). These receptors have relatively low affinity to ATP but vary in their re-sensitisation speed. Furthermore, sensitivities to ATP can be modulated by alteration of extracellular pH and heavy metal exposure including zinc, cadmium and copper (Acuña-Castillo *et al.*, 2007; Ma *et al.*, 2006; Virginio, North & Surprenant, 1998). Zinc in particular, potentiates ATP currents through P2X2, P2X3 and P2X4 whilst it inhibits through P2X1 and P2X7 by allosteric modulation of extracellular histidine residues to alter channel opening (Nagaya *et al.*, 2005; North, 2002). Whilst these receptors are generally cation specific, their permeabilities can be modulated by duration of ATP application. For example, prolonged ATP application causes reversible pore dilation to the extent that allows permeation of N-methyl-D-glucamine (NMDG) and propidium dye (YO-PRO-1) (Khakh *et al.*, 1999; Virginio *et al.*, 1999) a significantly larger organic molecule.

There are data consistent with the idea that a cation-binding site is present within the pore region (Ding & Sachs, 1999), and further supported by the fact that permeability can be altered, it suggests that it may also possess a selectively filter that favour some cations over another. For example, P2X5 is chloride permeable (Bo *et al.*, 2003) whilst P2X2 and P2X3 tend to favour calcium based on their relative permeabilities values (Collo *et al.*, 1996; Koshimizu, Koshimizu & Stojilkovic, 1999; Virginio, North & Surprenant, 1998).

Receptor P2X3 is the primary focus of this work and will be discussed in further detail.

1.3.1 P2X3 Receptor

P2X3 was first discovered in 1995 when cDNA was isolated from a subset of rat DRG sensory neurons (Chen *et al.*, 1995). When *Xenopus* oocytes were transfected with a P2X3 expressing plasmid, the receptor showed ATP-dependent calcium flux in a multimeric manner. P2X3R exhibits the same generic topology as other P2XRs with two hydrophobic membrane-spanning extracellular regions and cytosolic N- and C-terminals (Mansoor *et al.*, 2016; Brake, Wagenbach & Julius, 1994; Chen *et al.*, 1995; Valera *et al.*, 1994). Recent advancements in X-ray crystallography allowed the crystallisation of human P2X3R in its resting state, activated and inhibited states (Fig. 1.9) (Mansoor *et al.*, 2016). In a resting state P2X3R has a closed pore region but when activated, by ATP and analogues, the pore region opens. However, when desensitised, the receptor retains the agonist within the pore region but closes its pore region (Mansoor *et al.*, 2016).

During the initial investigation into P2X3R, further analysis of the rat DRG identified that P2X3R was expressed by capsaicin-sensitive neurons (Chen *et al.*, 1995), indicative of sensory neurons co-expressing TRPV1 and P2X3R. More recent findings utilising more sensitive fluorescent labelling techniques have confirmed the co-localisation of TRPV1 and P2X3 in rat vagal afferent nerves (Hermes, Andresen & Aicher, 2016). Electrophysiological experiments to assess the functional protein response of P2X3R in sensory nerves found expression of P2X3R on small-diameter nociceptive sensory neurons (Chen *et al.*, 1995). Although expression has been found on epithelial cells and enteric neurons (Poole *et al.*, 2002; Sun & Chai, 2004) P2X3 is found almost exclusively on small to medium diameter C and Aδ fibres sensory neurons from the nodose and jugular ganglia.

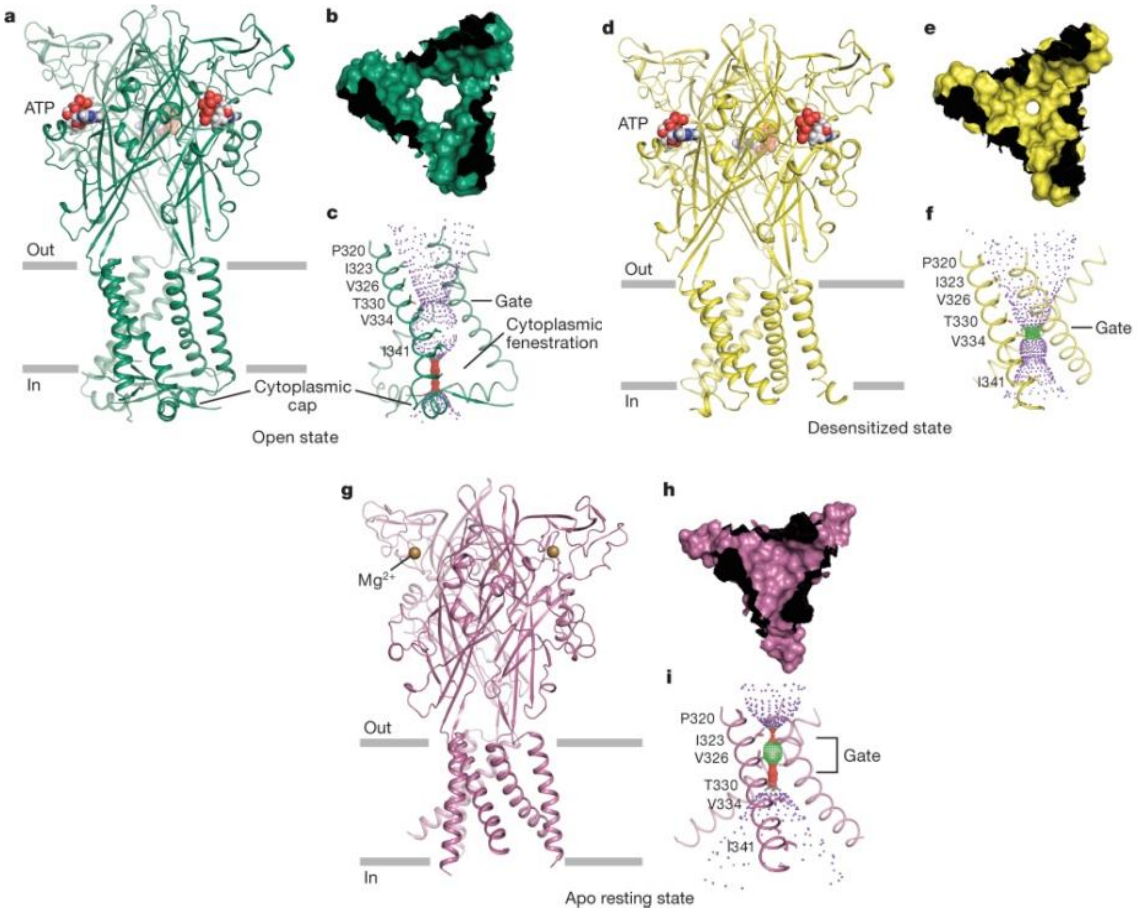

Figure 1.9. ***P2X3 structure.*** *Cartoon representation of each hP2X3 structure shown parallel to the membrane as a side view, perpendicular to the membrane from the extracellular side as a surface representation, and the ion permeation pathway, respectively, are drawn for open state (a-c) coloured green, desensitised state (d-f) coloured yellow, and apo state (g-i) coloured red-purple. For the pore size plots, different colours represent different radii, as calculated by the program HOLE: red <1.15A, green 1.15-2.30 A, and purple >2.30A. [Adapted from (*(Mansoor *et al.*, 2016)*]*

1.3.2 Role of P2X3 in the airway

P2X3 receptors have gained significant interest as modulators of cough in recent years. These receptors are highly responsive which makes them finely tuned for neural transmission, particularly within the airways. The signal transduction involved in cough is complex and there appears to be a missing link between perceived stimuli and the production of a cough response. Whilst it is widely recognised that TRP channels are responsible for sensing a cough stimulus, it is now thought that P2X3 receptors bridge the gap between these events (Abdulqawi *et al.*, 2015; Bonvini *et al.*, 2016).

TRPV1 was initially thought to play a role in idiopathic chronic cough, whereby sufferers have an enhanced cough reflex arising from abnormal neuronal pathways, supported by the fact that cough response to capsaicin was doubled in conditions of idiopathic chronic cough (Belvisi *et al.*, 2016), however, antagonism failed to produce significant reduction in chronic cough when compared to placebo (Khalid *et al.*, 2014). A clinical trial with a novel P2X3 antagonist, MK-7264 (formerly AF-219), was undertaken on patients with chronic refractory cough, which found a striking 75% reduction in daytime cough frequency (Abdulqawi *et al.*, 2015). This was the first antagonist to target the afferent portion of the cough reflex with significant efficacy at reducing cough. These patients generally had a heightened response to ATP in cough challenge (Lommatzsch *et al.*, 2010) which suggests they may have a lowered threshold for activation through a centralised sensitisation; however, no one to date has managed to delineate the signal transductions in its entirety. Furthermore, ATP has been previously shown to cause cough and bronchoconstriction in asthmatics, smokers and COPD sufferers (Basoglu *et al.*, 2015, 2005). This therefore suggests that P2X3 may play an important role in the cough reflex, or at least conclusively in the cases of idiopathic occurrence.

1.4 RhoA

Guanosine triphosphate(GTP)-ase proteins are hydrolase enzymes capable of binding to and hydrolysing GTP via a highly conserved domain (Bourne, Sanders & McCormick, 1990; Diekmann *et al.*, 1991; Garrett *et al.*, 1989; Hiraoka *et al.*, 1992). These proteins play important roles in transport, translocation, cellular control, protein synthesis and signal transduction (Ridley *et al.*, 1992; Ridley & Hall, 1992; Kahn *et al.*, 1991; Serafini *et al.*, 1991; Trahey & McCormick, 1987). A subfamily of GTPases are small GTPases. The Ras subfamily GTPases are the most widely studied small GTPases, made up of 167 proteins and categorised into five further families including: Ras, Ras-related nuclear protein (Ran), Rab, adenosine diphosphate (ADP) ribosylation factors (Arf) and Ras homolog (Rho) GTPases (Etienne-Manneville & Hall, 2002; Rojas *et al.*, 2012). From here on in, we will focus on Rho GTPase family.

The Rho family of GTPases are small, approx. 20 kDa, signalling G proteins (Madaule & Axel, 1985). They are highly conserved and universally found in eukaryotes including yeasts and

some plants (Wuichet & Søgaard-Andersen, 2014). There have been 22 members of the Rho family identified with the aid of genome sequencing (Rojas *et al.*, 2012). However, three members, cell division control protein 42 homolog (Cdc42), Ras-related C3 botulinum toxin substrate 1 (Rac1) and Ras homolog gene family, member A (RhoA) are the most widely studied. The latter of which, RhoA, is the focus of this research.

1.4.1 RhoA pathway

RhoA mostly functions in a cytoskeletal contractility capacity (Nobes & Hall, 1995) but acts upon many downstream proteins. RhoA is a highly conserved protein, like the rest of the larger GTPase family, however, it is one of the oldest Rho GTPases with homologues as old as 1.5 billion years (Rojas *et al.*, 2012). The protein sequences between the Rho family are near identical. Its N-terminal contains the majority of the protein coding sequence for GTP binding and hydrolysis whilst the C-terminal is open to modification allowing anchoring into the plasma membrane (Hamel *et al.*, 2011; Schaefer, Reinhard & Hordijk, 2014; Shao *et al.*, 2003; Foster *et al.*, 1996; Lartey & López Bernal, 2009). RhoA can be sequestered from the membrane by inhibitors such as Rho protein GDP dissociation inhibitor (RhoGDI), eliminating downstream interaction (Ohga *et al.*, 1989; Hiraoka *et al.*, 1992). RhoA contains inactive GDP-bound and active GTP-bound conformational states. The presence of both states facilitates the exchange of GDP to GTP to regulate activation. RhoA activity is regulated by guanine nucleotide exchange factors (GEFs) and GTPase activating proteins (GAPs) (Garrett *et al.*, 1989; Hamel *et al.*, 2011; Etienne-Manneville & Hall, 2002) which through phosphorylation of bound GDP function to activate and inactivate RhoA, respectively.

As depicted in Figure 1.10, RhoA can be activated by a wide range of soluble factors including, but not limited to, cytokines, growth factors and hormones (Bhowmick *et al.*, 2001; Kusama *et al.*, 2001; Schwartz, 2004). These extracellular signals bind to membrane bound receptors such as G-protein coupled receptors (GPCRs) and tyrosine kinase receptors (RTKs) (Nobes & Hall, 1995; Keller *et al.*, 1997; Ridley & Hall, 1994) facilitating downstream regulation of RhoA via GEFs and GAPs. RhoA is also activated and regulated by various integrins (extracellular matrix and cell adhesions) and mechanical stresses (tension, compression and shear) (Zhao *et al.*, 2007; Chapados *et al.*, 2006; Wei *et al.*, 2000; Burbelo *et al.*, 1995). Whilst the exact process of mechanosensation is unknown, more

recent research may show a possible interaction with mechano-activated TRPV4 channel (Seminario-Vidal *et al.*, 2011). The Rho family GTPases as a whole regulate a wide array of cellular functions that they cannot be covered in sufficient detail here, however individual GTPases do possess a degree of redundancy between them. RhoA transduces activatory signals downstream to 4 major complexes within the cell, protein kinase N1 (PKN), Citron, mammalian diaphanous protein (mDia) and Rho kinase. PKN is a Rho effector involved in endosomal trafficking to the plasma membrane (Amano *et al.*, 1996b; Flynn *et al.*, 2000). Citron is critical for cytokinesis and regulating the cell cycle (Madaule *et al.*, 1998). mDia regulates microtubule stability and actin polymerisation important for cellular motility (Watanabe *et al.*, 1999). Whilst Rho kinase, also referred to as ROCKI and isoform ROCKII, has several substrates to effectively regulate myosin light chain (MLC) phosphorylation, myosin phosphatase targeting protein (MYPT) phosphorylation, actin polymerisation and membrane linkages, and regulate production of intermediate filament structures (Machesky & Hall, 1997; Chrzanowska-Wodnicka & Burridge, 1996; Kimura *et al.*, 1996; Amano *et al.*, 1996a).

Of interest to us is the effect of Rho kinase on MLC and its phosphorylation, however phosphorylation of MLC can also occur independent of the RhoA pathway, whereby intracellular calcium flux acts as a secondary messenger binding with calmodulin to activate MLC kinase (MLCK) permitting the phosphorylation of MLC (Nairn & Perry, 1979). This process of MLC phosphorylation still results in the contraction of cellular myosin.

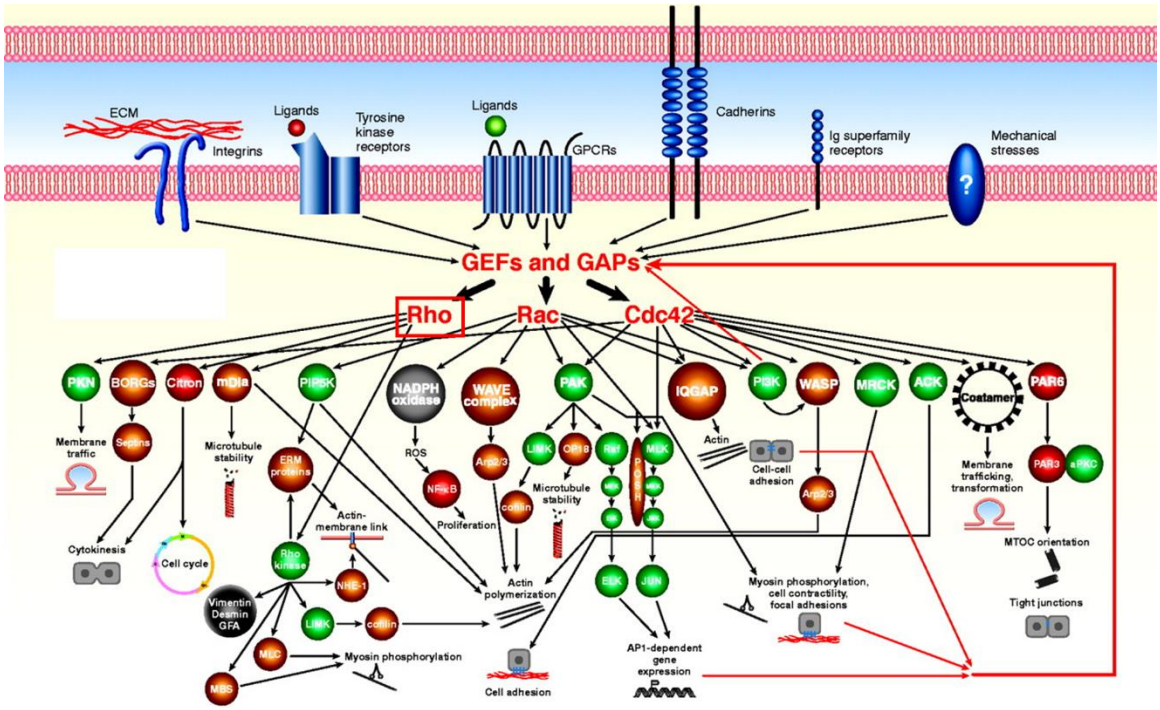

Figure 1.10. ***Simplified overview of small GTPase signalling*** *Rho, Rac and Cdc42 pathways delineated with upstream activatory receptors, integrins, tyrosine kinase receptors, GPCRs, cadherins, immunoglobin superfamily receptors and mechanical stresses. Pathways show significant overlap in downstream targets and resultant end targets. Rho pathway highlighted with red box for significance to discussed literature. [Adapted from* (Schwartz, 2004)*].*

1.4.2 RhoA in the airway and association with TRPV4

Studies have shown an interaction between the RhoA signalling pathway and smooth muscle contractility in airway disease states including asthma and airway hyperresponsiveness (Yoshii *et al.*, 1999; Hunter *et al.*, 2003; Somlyo & Somolyo, 2003; Schaafsma *et al.*, 2006a, 2006b). Airway hyperresponsiveness is a characteristic and common feature to many subtypes of asthma. Briefly, within a healthy airway GEF activation of RhoA facilitates Rho kinase (ROCK) inhibition of MLC phosphatase allowing MLC phosphorylation and causing contraction of actomyosin (Mbikou *et al.*, 2011; Amano *et al.*, 1996a; Van Eyk *et al.*, 1998) (Fig. 1.10). This contraction facilitates cell shape change with concurrent contractility of the airway bronchial smooth muscle but is readily reversed relaxing the airway and bronchi. However, in a disease airway state contractility cannot be readily reversed and can result in hypercontractility of the airway smooth muscle (Roberts *et al.*, 1984). This is thought to occur due to augmented responses of calcium-mediated sensitisation of RhoA and ROCK signalling in smooth muscle (Chiba *et al.*, 2005; Iizuka *et al.*,

1999) in a similar manner to that in the pathogenesis of hypertension (Uehata *et al.*, 1997). Airway contractility was found to be significantly reduced upon the application of ROCK inhibitor Y-27632 (Chiba & Misawa, 2004) demonstrating the role of the RhoA signalling pathway. Furthermore, RhoA protein expression was found to be markedly upregulated in a rodent model of airway hyperresponsiveness (Chiba *et al.*, 1999). Ultimately, increased airway contractility leads to phenotypic changes to the airway smooth muscle as seen in asthmatic airways (Roberts *et al.*, 1984) and demonstrated in animal models (Gavett & Wills-Karp, 1993).

Investigation into the role of TRPV4 in airway remodelling following insult with house dust mite *Dermatophagoides farinae* identified a crucial role of RhoA downstream of TRPV4 activation via cytokine transforming growth factor beta 1 (TGF-β1) (Gombedza *et al.*, 2017). However, this wasn't the first time a link between TRPV4 and RhoA was identified. RhoA also has a defined role in the release of ATP in the airway during hypotonic stimulus (Seminario-Vidal *et al.*, 2011). Through the use of inhibitors and receptor knockdowns, TRPV4 activation was identified to play a pinnacle role in RhoA-mediated signalling and downstream ATP release via pannexin-1 (Seminario-Vidal *et al.*, 2011). Precisely how RhoA and MLC transduce activatory and release signals to pannexin-1 is currently unknown. Figure 1.11 displays a hypothesised pathway where current data suggests potential inhibitory and activatory components leading to ATP release. Physiologically, these data and resultant predicted pathway may provide a mechanism of how under certain conditions, such as altered tonicity including changes in airway mucus, can potentiate a cough through the release of ATP.

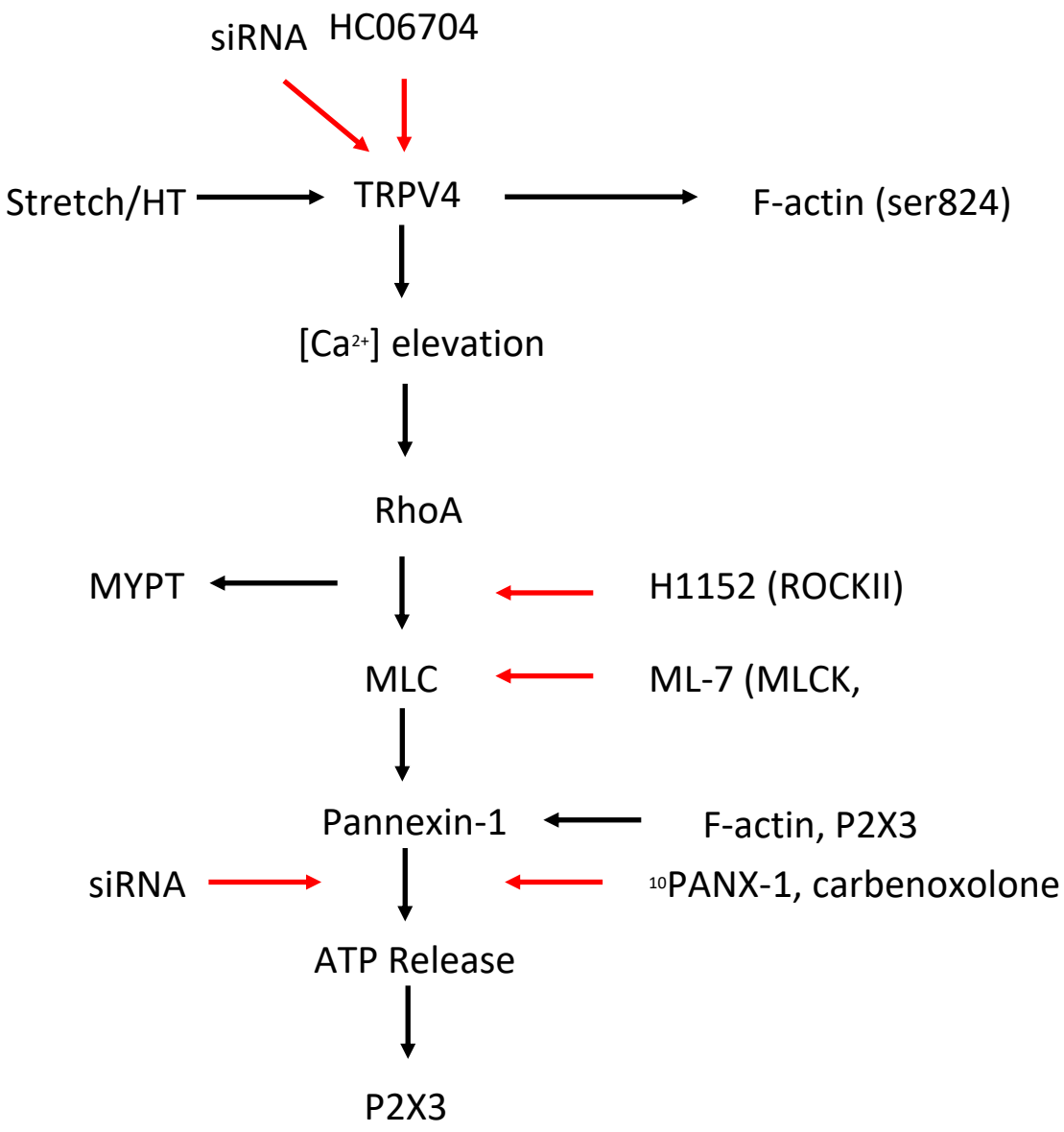

Figure 1.11. ***Diagrammatic representation of the hypothesised 'hypotonic pathway'.*** *Black arrows indicate activatory signal or transduction. Red arrows indicate inhibitory signal or blockade. Pathway developed from data published by* (Seminario-Vidal *et al.*, 2011; Shin *et al.*, 2012; Abdulqawi *et al.*, 2015; Rahman *et al.*, 2018).

1.5 Human Rhinovirus

The most common viral respiratory tract infections (RTI) every year are the common cold, and whilst mostly self-limiting these can occasionally cause severe symptoms and hospitalisation of the chronically ill including asthma and COPD sufferers (Wilkinson *et al.*, 2006; Johnston *et al.*, 1995). Development of a cough in upper respiratory tract infection is a frequent symptom from RV infection and whilst it can be bothersome it is relatively harmless but can occasionally cause distress (Gwaltney *et al.*, 1966; Witek *et al.*, 2015).

Development of a cough in response to viral infection usually resolves within 2-4 weeks (Jones & Stewart, 2002) but can precipitate a post viral cough which lingers up to 8 weeks (Morice *et al.*, 2006). The common cold can be caused by up to 200 different pneumotropic viruses including coronavirus, adenovirus, parainfluenza, respiratory syncytical virus and most commonly, accounting for approximately 80% of cases, rhinovirus (Kainulainen *et al.*, 2010).

1.5.1 Taxonomy and classification

Human rhinovirus (RV) belong to a family of viruses known as *Picornaviridae*, they are positive-sense single stranded RNA (ssRNA) viruses and are among the smallest at only 30 nm in diameter and genome of only 7,200 base pairs (Palmenberg, Rathe & Liggett, 2010). RV are classified based on their phylogenetic sequences as groups designated RV-A, B and C (McIntyre, Knowles & Simmonds, 2013). But the most recent large scale phylogenetic analysis carried out on all currently identified RV serotypes suggests that there may be many more RV-C serotypes undiscovered (Palmenberg *et al.*, 2009) potentially due to the fact that RV-C was not cultured *in vitro* until 2011 (Bochkov *et al.*, 2011). Furthermore, it highlighted the presence of a potentially new clade, RV-D (Palmenberg *et al.*, 2009). Following the discovery of RV-C that was revealed in 2006 (Lamson *et al.*, 2006), it has been possible to finally ascertain why asthma and COPD sufferers experience severe exacerbations when tests would frequently appear negative. Whilst RV has long been known as the causative agent of approximately 60% of asthma exacerbations (Johnston, 2007), the recent discovery of RV-C has allowed its identification as the genotype responsible for the most severe exacerbations, often requiring hospital intervention (Bizzintino *et al.*, 2011) due to the binding mechanism of entry which has been linked to childhood asthma and associated severe exacerbations (Bønnelykke *et al.*, 2014).

RV are extremely diverse with almost 160 serotypes identified and sequenced to date (McIntyre, Knowles & Simmonds, 2013). RV are further classified by their binding mechanism. Major group, which comprises 90% of serotypes, bind to human intercellular adhesion molecular-1 (ICAM-1) (Tomassini *et al.*, 1989) and minor group bind to low density lipoprotein-receptor (LDL-R) (Hofer *et al.*, 1994). RV-C is distinct in that it binds by

a mechanism independent of ICAM-1 and LDL-R and therefore not classified as major or minor group (Bochkov *et al.*, 2011). After several years of failed attempts the binding mechanism of RV-C was finally identified as cadherin-related family member 3 (CDHR3) (Bochkov *et al.*, 2015) a gene linked with childhood asthma and severe exacerbations with no known lung function role (Bønnelykke *et al.*, 2014). Interestingly, some major group serotypes (RV8, 54 and 89) facilitate cell entry by the use of an additional receptor heparin sulphate proteoglycans particularly in studies of knockout ICAM-1 (Khan *et al.*, 2011, 2007).

1.5.2 Structure

RV follow a generic structure shared by all *Picornaviridae*. They are icosahedral (Fig. 1.12) which consist of four viral proteins VP1-4 (Rossmann *et al.*, 1985), with an average diameter of 20-30 nm (McGregor & Mayor, 1971). RV genome is a ssRNA open reading frame of approximately 6,500 base pairs flanked by an untranslated region (UTR) of 650 base pairs, and covalently capped with a viral priming protein (VPg) for replication (Lee *et al.*, 1977). The 5' UTR creates the characteristic cloverleaf structure (Gamarnik & Andino, 1998) which is followed by an internal ribosome entry site (IRES) (Jang *et al.*, 1988; Pelletier & Sonenberg, 1988). These structures play important roles in viral replication and translation, respectively. The 3' flanking polyA tail is suggested to aid the efficiency of viral replication and support stability (Herold & Andino, 2001) and essential for its virulence (Spector & Baltimore, 1974). Schematic representation of the RV viral genome can be seen below (Fig. 1.13).

As seen in Figure. 1.13, RV genome is roughly divided into 3 sections P1, P2 and P3, whereby P1 consists of structural capsid proteins VP1-4, P2 consists of regulatory proteins 2A-C and P3 encodes non-structural proteins required for viral replication and progeny assembly, 3A-D (Callahan, Mizutani & Colonno, 1985; Skern *et al.*, 1985). Crevices formed by flanking regions of VP1, 2 and 3 facilitate the attachment of major group RV to receptor ICAM-1 for host entry (Colonno *et al.*, 1988). Also present within these are hydrophobic binding regions (Smith *et al.*, 1986). Unlike major group RV, minor group RV binds its cognate host entry receptor differently. It binds LDL-R near the tip of the five-fold vertex of the capsid (Hewat *et al.*, 2000).

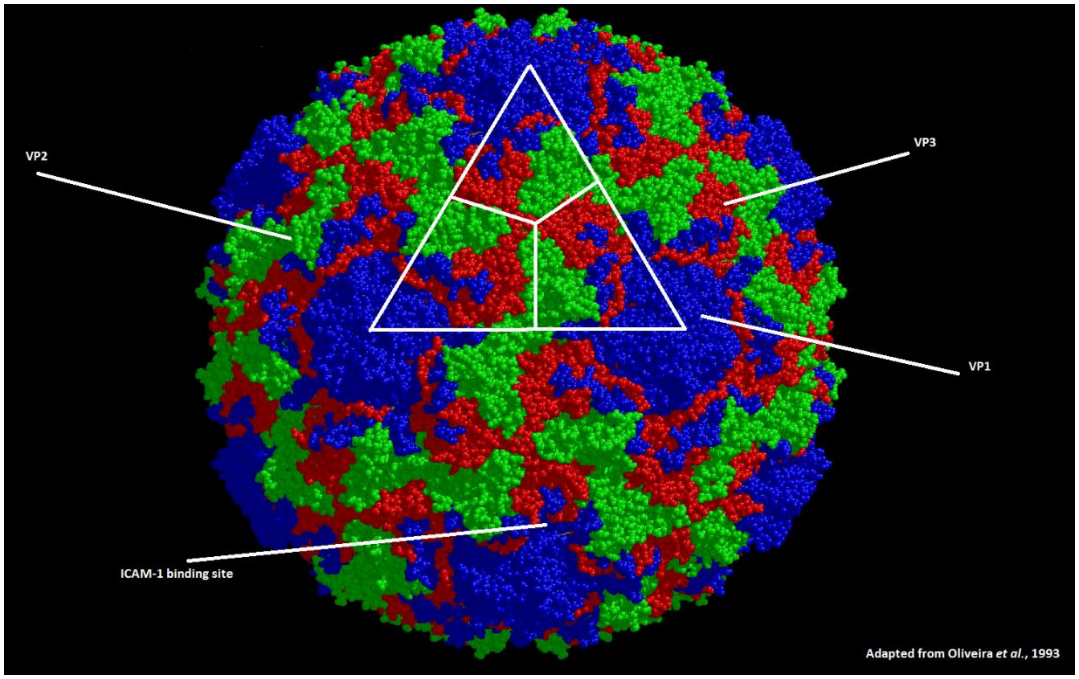

Figure 1.12. ***RV-16 structure.*** *3D modelled structure of human rhinovirus serotype 16 modelled using RASMOL from data obtained from X-ray diffraction. RV-16 is composed of three viral protein components represented by different colours as follows VP1 (blue), VP2 (green) and VP3 (red), with molecular weight of approximately 30,000* (Hadfield *et al.*, 1997)*. The binding site for attachment receptor ICAM-1 is found within VP1, as labelled. The triangle represents a repeating protomer structure containing segments of VP1, VP2, VP3 and ICAM-1 binding region. VP4 cannot be seen on this diagram as it is an internal protein found behind VP1, 2 and 3 protein coat [Adapted from* (Hadfield *et al.*, 1997; Oliveira *et al.*, 1993)*].*

1.5.3 Life cycle

As RV is a positive sense ssRNA virus, it is directly translated by host ribosomes but cannot hijack host machinery for its replication and so encodes a viral replicase, 3D (Palmenberg, Rathe & Liggett, 2010). Polarised epithelial cells of the nasal mucosa are the primary site of RV infection (Bardin *et al.*, 1994). The route of entry is different depending on whether RV is major or minor group (Schober *et al.*, 1998), or RV-C clade which is currently still unknown but independent of that from major and minor. Engagement of major group RV and host receptor triggers endocytosis independent of clathrin and caveolin (Khan *et al.*, 2010) (Fig. 1.14). Upon delivery to early endosomes in a clathrin-dependent pathway (Grunert *et al.*, 1997), the viral capsid begins to undergo a conformational change to hydrophobic subviral A-particles (uncoating) mediated by receptor interaction and low pH conditions which induces virion instability (Hewat & Blaas, 2004; Tsang *et al.*, 2001; Hughes *et al.*, 1973).

Multifactorial evidence has shown that viral ssRNA infiltrates the host cytoplasm through pore formation in the endosome resulting in endosomal rupture (Schober *et al.*, 1998; Kronenberger *et al.*, 1997). This process is facilitated by subunit VP4 (Lee, Monroe & Rueckert, 1993), however its distinct route is currently unknown. In contrast, minor group RV gain entry to host cells through LDL receptor which are scarce at the plasma membrane due to its recycling mechanism. A feature shared between major and minor groups is cellular internalisation in a clathrin dependent pathway (Bayer *et al.*, 2001; Huber *et al.*, 2001). Likewise, minor group capsids also undergo a conformational change but they differ in genome release (Schober *et al.*, 1998). It has been suggested through a compilation of work that VP4 proteins bound to the N-terminal of VP1 proteins insert themselves into the plasma membrane of the encapsulating endosome (Panjwani *et al.*, 2014; Davis *et al.*, 2008) thereby attaching the virus to the endosome. This forms an ion-conducting pore (Brabec *et al.*, 2005) in the membrane altering the membrane potential to create an overall negative charge (Danthi *et al.*, 2003) which drives the release of the viral genome into the cytoplasm. Unfortunately, this is only speculative as real-time visualisation of this has yet to be achieved.

Upon escape from the endosome, the viral VPg cap is cleaved by host enzyme VPg unlinkase (Virgen-Slane *et al.*, 2012; Racaniello, 2001) which exposes the IRES to facilitate its subsequent replication. The IRES initiates translation of the ORF through attachment of 40s ribosome at AUG start codon, but RV differs from other genus of viruses in that it is non-scanning (Belsham & Sonenberg, 2000) and uses the proximity of encoded AUG codons to orient the positioning of the ribosomal subunit to initiate translation (Palmenberg, Rathe & Liggett, 2010). This particular mechanism has not been identified in any other enteroviruses and as such is suggested to aid its survival with minimal energy expenditure. Furthermore, RV encodes a protein (2A) which prevents host protein synthesis through cleavage of eukaryotic initiation factor 4G (eIF-4G) (Barco, Feduchi & Carrasco, 2000; Svitkin *et al.*, 1999), essentially shutting down the host cell in a process so efficient thousands of progeny virions are made within a mere 8 hours post infection (Racaniello, 2001).

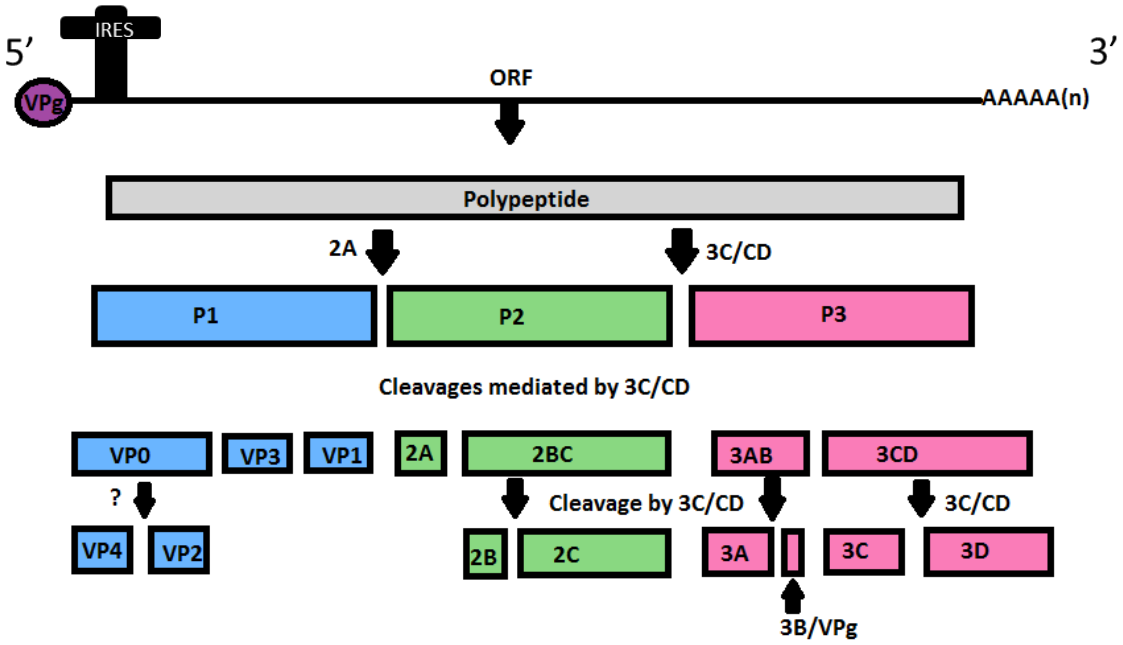

Figure 1.13. ***Human rhinovirus genome.*** *Schematic diagram of translation and post-translational cleavage of human rhinovirus open reading frame genome. Genome consists of 5'- and 3'- UTR as labelled, a poly A-tail and a single open reading frame encoding one protein but post-translationally cleaved into 11 viral structural (P1 blue) and non-structural (P2 green and P3 pink) proteins and are required for viral replication and host interference, respectively. Genome contains an internal ribosome entry site (IRES) essential for ribosome binding and subsequent translation of reading frame. Boxes not to relative genomic size scale.* (Lee *et al.*, 1977; Gamarnik & Andino, 1998; Jang *et al.*, 1988; Pelletier & Sonenberg, 1988; Herold & Andino, 2001; Callahan, Mizutani & Colonno, 1985; Skern *et al.*, 1985).

RV is categorised as a Class IV replicating virus from the Baltimore Classification System (Baltimore, 1971) and therefore has a simple replication cycle. Once ribsomally bound, the ORF is directly translated as a long single polypeptide chain that is autocatalytically and co-translationally cleaved (Palmenberg, Rathe & Liggett, 2010; Blaas & Fuchs, 2016) by encoded viral protease eventually into 11 mature proteins. The single polypeptide chain is initially cleaved by viral proteins 2A and $3C^{pro}$ in to the respective segments P1, P2 and P3 (Racaniello, 2001). Secondary and tertiary cleavages are mediated by viral proteases $3CD^{pro}$ (Racaniello, 2001), except cleavage of VP0 mediated by an as yet unknown protease (Fig. 1.13).

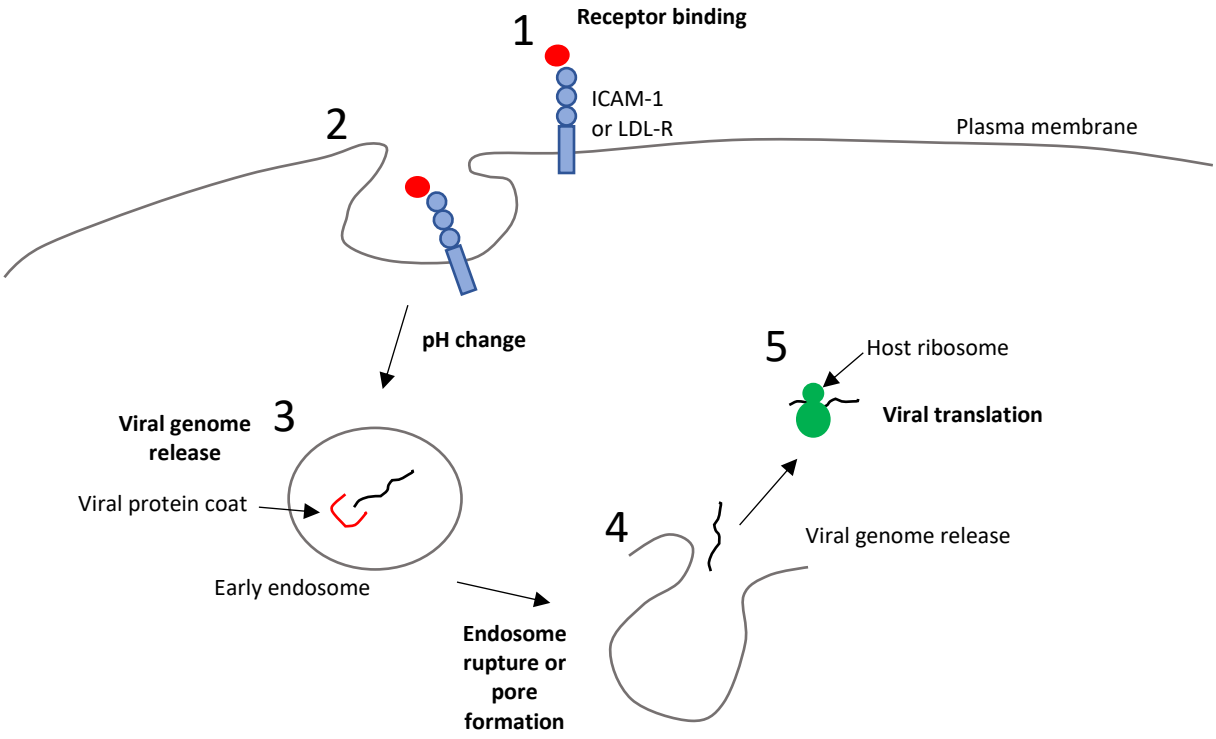

Figure 1.14. ***Lifecycle of human rhinovirus*** *from receptor binding, internalisation and release of viral genome. 1. RV virion binds to cognate receptor (major group – ICAM-1, minor group – LDL). 2. Triggers internalisation of virion and receptor via endocytosis. 3. Endosome encapsulates virion and reduction in pH releases viral genome. 4. Major group rhinovirus – exposed VPg cap facilitates endosome rupture through pore formation in membrane causing release of viral genetic material in the cytoplasm. 4. Minor group rhinovirus – viral VP4 protein inserts into endosome membrane creating a pore allowing conduction pore production to shuttle viral genome out of the endosome without lysis. Host enzymes lead to cleavage of viral cap VPg which exposed IRES and allowed viral genome to bind to host ribosomes for translation (5).*

Once viral protein 3D is translated it initiates replication of the positive stranded viral genome, within membrane vesicles derived from endoplasmic reticulum (ER) (Palmenberg, Rathe & Liggett, 2010), to produce a negative strand which forms a double stranded intermediate (Hewson *et al.*, 2005), an important stimulus to the host innate immune system. Whilst viral 3D functions in a slight regulatory capacity, RV does not encode a dedicated proof-reading mechanism (Palmenberg, Rathe & Liggett, 2010).

A disproportionate percentage of viral RNA copies are positive stranded (Novak & Kirkegaard, 1991), so most of these are packaged and assembled to form progeny. Viral proteins VP1-4 associate to form a pentamer procapsid, and whilst there is no direct evidence to date to suggest how the viral ssRNA is packaged, there are two proposed scenarios that either the genome is inserted into the procapsid or the procapsid forms around the genome, but the general consensus favours the latter (Nugent & Kirkegaard, 1995; Basavappa *et al.*, 1994). The release of RV progeny results in lysis of the host cell (Racaniello, 2001) since they are non-enveloped viruses and therefore do not need to bud from the host cell membrane. Ordinarily, RV are not particularly cytopathic especially in more resilient cells, such as bronchial cells which produce a much lower viral titre than more permissive cells such as HeLa (Winther, Gwaltney & Hendley, 1990).. Cytopathic effects seen from RV infection tend to be limited to, but not exclusively, epithelial barrier disruption at tight junctions leading to leakage (Rezaee *et al.*, 2011; Yeo & Jang, 2010; Sajjan *et al.*, 2008).

1.5.4 Symptoms

In the majority of individuals, the common cold caused by RV is relatively mild, self-limiting and limited to the upper respiratory tract. RV infection is classically characterised by rhinorrhoea and nasal congestion, other symptoms include sore throat, sneezing, headache, muscle aches and cough (Gwaltney *et al.*, 1966; Witek *et al.*, 2015; Arruda *et al.*, 1997; Lessler *et al.*, 2009) (Table 1.1) whilst fever and exhaustion are rarely seen in RV infections. A sore throat is the first symptom frequently reported to appear (Arruda *et al.*, 1997) with median duration of illness lasting 10 days (Witek *et al.*, 2015; Pappas *et al.*, 2008; Gwaltney *et al.*, 1967; Heikkinen & Järvinen, 2003).

RV infection follow a seasonal pattern of infection whereby incidence peaks during autumn months (Winther, Hayden & Hendley, 2006; Arruda *et al.*, 1997) and early spring (Winther, Hayden & Hendley, 2006; Gwaltney *et al.*, 1966), but is a dominant presence, according for approximately 52% of cases, throughout spring, autumn and summer months too (Winther, Hayden & Hendley, 2006).

Incubation is typically 2 days in the majority of cases, but this can vary between 20 hours and 4 days long (Gwaltney, Jr., Hendley & Patrie, 2003; Lessler *et al.*, 2009). The severity of infection is not dependent on the serotype of RV but down to confounding factors of the host such as asthma, age and immunocompetence (Kaiser *et al.*, 2006; Johnston *et al.*, 1995; Louie *et al.*, 2009; Miller *et al.*, 2007).

32-33^{o}C is the optimal temperature for RV replication (Papadopoulos *et al.*, 1999); therefore, RV most frequently infects the upper respiratory tract and nasal passages, however, RV has been found to be capable of infection in the lower respiratory tract (Papadopoulos *et al.*, 2000). RV infection has been identified as a major cause in exacerbation of chronic underlying conditions, particularly asthma and COPD often requiring hospitalisation or intervention (Johnston *et al.*, 1995; Seemungal *et al.*, 2001; Bizzintino *et al.*, 2011). However, a novel method of analysis which measured the presence of pathogens on spirometer filters taken from patients with mechanical ventilation identified that airways harbour a multitude of viruses without causing active infection (Mitchell *et al.*, 2016, 2018). Secondary and co-infection with other viruses or bacteria are detected in as many as 25% of cases of RV infection (Arruda *et al.*, 1997; Louie *et al.*, 2009; Alper *et al.*, 2008; Jartti *et al.*, 2008), this was particularly prevalent in children. The effect of this is cofounding in that RV infection disrupts the epithelial barrier facilitating secondary entry of pathogens and increasing vascular permeability and mucus secretion (Sajjan *et al.*, 2008; Yeo & Jang, 2010; Rezaee *et al.*, 2011; Hewson *et al.*, 2010; Zhu *et al.*, 2009b; Passariello *et al.*, 2006). The significance of this will be discussed in greater detail in the following section 1.6 Rhinoviral Cough.

Table 1.1. ***Symptoms classically associated with human rhinoviral infections and the physiological cause for those symptoms.*** *[*(Gwaltney *et al.*, 1966; Witek *et al.*, 2015; Arruda *et al.*, 1997; Lessler *et al.*, 2009; Eccles, 2005).

Symptom	Cause
Rhinorrhoea	Increased vascular permeability, neutrophilic infiltration; mucus hypersecretion
Nasal congestion	Neutrophilic infiltration, mucus hypersecretion, increased vascular permeability
Sore throat	Lytic response to virus; Irritation from post-nasal drip
Sneezing	Mucus hypersecretion, increased vascular permeability
Headache	Sinus pain from excessive mucus and insufficient drainage
Cough	Largely unknown - Irritation from posterior pharyngeal draining, direct infection of large airways

1.6 Rhinovirus Cough

Cough is a common symptom associated with upper respiratory tract infections (URTI) (Witek *et al.*, 2015; Eccles *et al.*, 2003; Curley *et al.*, 1988; Reid, Williams & Hirch, 1953). In some patients coughing can persist leading to a syndrome known as post-viral or post-infectious cough which is arbitrarily defined as lasting from 3 to 8 weeks, with normal chest radiograph findings (Braman, 2006; Irwin *et al.*, 2006). In some individuals cough persists even longer when it is termed a chronic cough (Morice *et al.*, 2007). Whilst a normal cough is a vital protective reflex preventing aspiration, cough hypersensitivity is the mechanism thought to underlie almost all types of pathological cough (Morice, 2010). This has been demonstrated in URTI (Dicpinigaitis *et al.*, 2014, 2011; O'Connell *et al.*, 1996).

Cough causes a plethora of complications affecting the cardiovascular, gastrointestinal and respiratory systems with far reaching psychological, neurological, and musculoskeletal effects (Morice *et al.*, 2007; Irwin *et al.*, 2006; McGarvey & Morice, 2006). Whilst there are many agents on the market to reduce the frequency of cough and aid in the clearance of mucus, a systematic review of over the counter preparations failed to recommend any available treatment (Schroeder & Fahey, 2002). For example, the use of codeine in respiratory tract infection associated cough was found to be no more effective than its

vehicle (Eccles, Morris & Jawad, 1992), and prescription only medications are often unsuitable for certain groups of individuals (Morice *et al.*, 2006).

There are three metrics which are used to study cough, cough challenge, cough counting and subjective end points such as visual analogue scale (VAS) or quality of life. Cough challenge studies include the use of pro-tussive agents such as capsaicin and citric acid which stimulate transient receptor potential (TRP) ion channels to induce cough (Morice, Kastelik & Thompson, 2001; Laude, Higgins & Morice, 1993; Collier & Fuller, 1984). As previously discussed in section 1.1.1, TRP channels have been popularised as pro-tussive irritant receptors (Benemei *et al.*, 2015; Birrell *et al.*, 2009). However, on account of repeated clinical trial failures using both cough counting and subjective measures TRP antagonists as anti-tussives (Khalid *et al.*, 2014, unpublished RCT of inhaled TRPA1 antagonist GRC 17536 (personal communication AHM, 2015)) have failed to reach the clinic. A recent shift of focus now proposes other channels and receptors, such as P2X receptors, different TRP channels including TRPV4 and TRPM8 (Morice, 2014; Grace *et al.*, 2013; Kamei *et al.*, 2005) may be responsible for the observed hypersensitivity. It seems unlikely that one single channel or receptor is responsible for causing cough hypersensitivity in all subjects in cases of post-viral and chronic cough.

Research into URTI and cough faces many problems. Research which relies on natural infection of human volunteers is open to a range of uncontrollable variability including incubation time and causative agent (virus genus and serotype). There is also a lack of suitable animal models for studying RV due to high host specificity of attachment receptors. For example, ICAM-1 is a human receptor (Tomassini *et al.*, 1989) which is not present in guinea pigs, an animal classically used for studying the cough reflex. However pathogens such as parainfluenza virus, a rarer cause of the common cold, can infect guinea pigs and produce a post-viral cough with a hypersensitive airway response to capsaicin (Ye *et al.*, 2011). As a result, studying the effects of RV infection is often carried out *in vitro* using cell systems. There is a plethora of research into viral induced effects characterised from various respiratory cell lines, leading to a variety of proposed mechanisms for the induction of cough.

1.6.1 Mechanisms

1.6.1.1 Inflammatory mediators

RV infection results in the production a broad profile of inflammatory mediators in the host. The primary inflammatory cytokines reported in RV infection are interferon (IFN), interleukin (IL)-1, IL-6, IL-8, tumour necrosis factor (TNF)-α, granulocyte-macrophage colony-stimulating factor (GM-CSF) and RANTES (Papadopoulos & Johnston, 2000; Stöckl *et al.*, 1999). The infection leads to massive upregulation (Papadopoulos & Johnston, 2000), and consequently it is often described as a 'cytokine disease' (Stöckl *et al.*, 1999). Many symptoms are thought to occur as a result of the effects of inflammatory cytokines releasing of mediators. For example sore throat may occur as a result of the release of bradykinin (Proud *et al.*, 1988). The role of these endogenous mediators is discussed below.

1.6.1.1.1 Bradykinin

The pro-inflammatory mediator bradykinin has been suggested as a potent tussive modulator of TRPA1 and TRPV1 (Bandell *et al.*, 2004; Carr *et al.*, 2003; Fox *et al.*, 1996). It is thought to work through phospholipase C (PLC) causing channel phosphorylation and subsequent sensitisation (Chuang *et al.*, 2001). Elevated levels of bradykinin are found in the BAL fluid of patients with inflammatory airway conditions (Baumgarten *et al.*, 1992). Bradykinin has also been suggested to mediate angiotensin converting enzyme (ACE) inhibitor cough (Fox *et al.*, 1996) which affects 15% of patients (Yeo, Foster & Ramsay, 1991). Bradykinin and PGE2 possess the ability to sensitise the airways to cough stimulus in animal studies which can be effectively abolished upon simultaneous application of antagonists to both TRPV1 and TRPA1 (Grace *et al.*, 2012).

1.6.1.1.2 Tachykinins

Tachykinin peptides, neurokinin A and B, and substance P, are inflammatory neuropeptides which collectively induce airway hyperresponsiveness, bronchial constriction (Joos *et al.*, 1994), and increased vascular permeability (Lundberg *et al.*, 1984). They also generate substantial mucus secretion (Rogers, Aursudkij & Barnes, 1989) and the secretion of inflammatory mediators from immune cells (Holzer, 1998; Numao & Agrawal, 1992; Lotz, Vaughan & Carson, 1988). It has been suggested that inhibition of tachykinin metabolism by ACE inhibitors is an alternate mechanism for ACE inhibitor cough (Morice *et al.*, 1987). In RV infection tachykinins are released from neurons upon TRPV1 activation (Holzer,

1998). Unfortunately, the mechanism underlying this activity is currently unknown and understanding such channel interaction may hold the key to modulating the development of viral and post-viral cough. Reduction of degradation of tachykinins by neutral endopeptidases in respiratory viral infection (Jacoby, 2004) are likely to enhance the noxious effects of tachykinins.

Despite its scarcity, substance P in humans has been found to be upregulated, both in nasal epithelium and plasma in chronic cough sufferers (Bae *et al.*, 2012; Otsuka *et al.*, 2011; Cho *et al.*, 2003). The efficacy of substance P, mediated by tachykinin NK-2 receptors (Moore, Undem & Weinreich, 2000), is greatly enhanced by prior inflammation. Furthermore, in excess it is suggested to lower the threshold of pain perception to noxious stimuli, as demonstrated in several pain associated disease states (Appelgren *et al.*, 1998; Evengard *et al.*, 1998). In guinea pigs, the role of substance P in cough has been extensively investigated. Substance P results in bronchoconstriction but highly variable cough (El-Hashim & Amine, 2005). Likewise, in healthy individuals, inhalation of substance P does not cause cough. However at the same concentration, substance P has the ability to elicit cough in patients with common colds (Katsumata *et al.*, 1989), suggesting a hypersensitive state induced by the virus. Additionally, the microvascular leakage of substance P is thought to activate rapidly adapting receptors (RARs) (Bonham *et al.*, 1996) which may add to the irritant effect in common cold.

1.6.1.1.3 Calcitonin gene related peptide

Evidence for the role of another neuropeptide calcitonin gene related peptide (CGRP) is mixed. TRP channel (TRPV1) activation induces and controls the release (Kichko & Reeh, 2009; Holzer, 1998) from C-fibre terminals (Mak & Barnes, 1988). CGRP has an inhibitory effect in substance P induced bronchoconstriction (Cadieux *et al.*, 1999), and when deficient, causes airway hyperresponsiveness (Dakhama *et al.*, 2002). However, an increase in CGRP has been shown in many pain associated conditions including migraine and various forms of inflammation (Lassen *et al.*, 2002; Hua *et al.*, 1996). Chronic cough sufferers have been shown to have increased neuronal levels of CGRP (Chang *et al.*, 2007; O'Connell *et al.*, 1995) associated with the enhanced sensitivity to capsaicin (O'Connell *et al.*, 1995). These effects appear to be mediated through the cytokines, IL-1β and TNF-α (Hua *et al.*, 1996). In respiratory syncytial virus (RSV) infection, a rarer cause of URTI in the adult, the

development of airway hyperresponsiveness appear to arise through a disruption of CGRP balance (Dakhama *et al.*, 2005, 2002). However, this fails to explain the increased levels found in chronic cough sufferers. Unlike substance P, CGRP does not directly induce mucus secretion (Webber, Lim & Widdicombe, 1991) but may indirectly enhance through vasodilation.

The likelihood that substance P, CGRP or neurokinins have some role in cough hypersensitivity is high. Opiates have been shown to be highly effective in a subgroup of patients with cough (Morice *et al.*, 2006). A possible mode of action is through pre-junctional inhibition of peptide release preventing neurotransmission either centrally, or from afferent nerves adjacent to inflammatory mediator receptors (Holzer, 1998).

1.6.1.1.4 Leukotrienes

Leukotrienes are potent inflammatory mediators of chemotaxis, bronchoconstriction and vascular permeation (Hammarström, 1983), which are predominately produced by leukocytes, but also by other inflammatory immune cells. Data is scarce on the extent leukotrienes play in RV infection. However, Seymour *et al.* (2002) identified a significant increase of precursor enzymes within the airways during RV infection in healthy individuals which can potentially increase the capacity of leukotriene B_4 and C_4 synthesis (Seymour *et al.*, 2002). Muscarinic receptor involvement has been implicated in the production of leukotriene B_4 (Profita *et al.*, 2005). In cough associated eosinophilic inflammation blockade of leukotriene receptors has been shown to be efficacious (Takemura *et al.*, 2012). However in a recent study montelukast, a potent inhibitor of the receptor of leukotriene C_4 and D_4, has no effect on cough in the common cold (Wang *et al.*, 2014).

1.6.1.1.5 Eosinophils

Eosinophils are important mediators of cough in allergic disease but their role in viral infection is less clear. Eosinophils, if activated, during viral infection release a multitude of molecules including leukotrienes, growth factors, cytokines and major basic protein (MBP) (Hogan *et al.*, 2008). MBP both binds to and alters pre-junctional M2 receptor function (Evans *et al.*, 1997; Larsen *et al.*, 1994) and increases tachykinin release (Jacoby, 2004). MBP is cytotoxic (Hisamatsu *et al.*, 1990) and has been implicated in peripheral nerve remodelling (Pégorier *et al.*, 2006). It is found in higher levels in nasal aspirates from children during RV infection (Teran *et al.*, 1999). Not only are eosinophils implicated in

tachykinin modulation but during degranulation they also release a potent peroxidase (EPO) which generates reactive oxygen species (ROS) and reactive nitrogen species (RNS). These harmful oxidants are known potent TRPA1 agonists (Nishio *et al.*, 2013; Andersson *et al.*, 2008) which is a receptor ascribed to cause cough in humans and guinea pigs (Birrell *et al.*, 2009).

1.6.1.1.6 Muscarinic receptors

Muscarinic receptors are highly characterised in airway diseases such as asthma and chronic obstructive pulmonary disease (COPD) with limited evidence of their involvement in respiratory infections. Of the five muscarinic receptors (M1-5) only M1-3 can be found in the respiratory system. M1 is expressed on epithelial cells and submucosal glands of pulmonary veins (Mak & Barnes, 1990). M3 receptors are heavily expressed on smooth muscle, inflammatory and submucosal cells (Gosens *et al.*, 2006) where they mediate bronchoconstriction, mucosal secretion and inflammatory responses (Rogers, 2001). M2 receptors predominately regulate cardiac contraction but can also be localised to respiratory smooth muscle (Mak & Barnes, 1990). However the most important role of M2 receptors in the airway is the pre-junctional inhibition of acetylcholine (ACh) release to limit the degree of bronchoconstriction (Fryer & Maclagan, 1984). Respiratory viral agents parainfluenza and RSV have been shown to cause depletion and dysfunction of M2 receptors (Bowerfind, Fryer & Jacoby, 2002) thereby exaggerating cholinergic activity. This dysfunction of M2 receptors has been further shown in double stranded (ds)-RNA animal models, independent of inflammation (Bowerfind, Fryer & Jacoby, 2002) and mediated by interferon release (Jacoby *et al.*, 1998). Therefore, viral infection induced bronchoconstriction, airway hyperresponsiveness and mucus secretion causing cough may be indirectly mediated through M2 receptors (Jacoby *et al.*, 1998). M2 dysregulation can be reversed with dexamethasone (Jacoby *et al.*, 2001) or pilocarpine (Fryer & Maclagan, 1984). However, Lowry *et al.* (1994) found anticholinergic bronchodilators to be ineffective against cough in natural URTI (Lowry, Wood & Higenbottam, 1994). The potent topical corticosteroid fluticasone was also ineffective in significantly reducing symptoms of viral URTI and indeed significantly increased the bacterial colonisation of the upper airway (Puhakka *et al.*, 1998).

Many of the inflammatory mediators discussed above do not directly evoke cough but work synergistically through other pulmonary fibres where the threshold for cough is lowered to provoke the urge to cough. Thus, this change to sensory nerve functionality secondary to these mediators may potentiate and prolong a cough response during and after respiratory viral infection.

1.6.1.2 Physical damage

In comparison to other respiratory viruses such as influenza, RV is renowned for its minimal cytopathic effects (Winther, Gwaltney & Hendley, 1990). It has been suggested that influenza has a higher incidence of cough than that seen with RV infections (Monto *et al.*, 2000). Thus, physical disruption of airway integrity may be a factor in a heightened cough response. RV, or synthetic ds-RNA stimuli polyinosinic:polycytidylic acid (poly(I:C)), is able to disrupt airway epithelial cells via disruption of tight junction complexes at apicolateral membranes through dissociation of zona occludin(ZO)-1, occludin, claudin-1, E-cadherin and β-catenin. This lead to a significant reduction in transepithelial resistance (Rezaee *et al.*, 2011; Yeo & Jang, 2010; Sajjan *et al.*, 2008) indicating a loss of epithelial integrity (Fig. 1.15A). Transepithelial resistance can also be decreased through respiratory localised TRPV4 activation (Reiter *et al.*, 2006) and causes disruption of tight junction complexes leading to increased permeability. Whether these are related or not is unknown. Whether this viral induced loss of integrity is dependent or independent of an inflammatory response is open to debate.

1.6.1.2.1 Inflammatory independent

Reactive oxygen species (ROS) and other oxidants cause barrier disruption and affect permeability in tissues throughout the body (Yamaya *et al.*, 1995) through cytoskeletal and tight junction interruption. This effect is mirrored in polarised epithelial cells, such as those within the airways (Comstock *et al.*, 2011; Rezaee *et al.*, 2011). During infection, RV causes oxidative stress independent of viral replication or ICAM-1 mediated viral attachment (Kaul *et al.*, 2000). The mechanism is thought to be via NOD-like receptor X-1 (NLRX-1) interaction with ds-RNA causing a translocation of NADPH oxidase-1 (NOX-1) leading to the generation of ROS and oxidants (Unger *et al.*, 2014; Comstock *et al.*, 2011). In contrast, ROS production is necessary for clearance of viral infections but requires stringent regulation. Interaction with ds-RNA receptor NLRX-1 induces mitochondrial ROS generation (Arnoult *et al.*, 2009;

Tattoli *et al.*, 2008). This is likely a result of mitochondrial antiviral signalling protein (MAVS) interaction with ds-RNA (Kawai *et al.*, 2005; Meylan *et al.*, 2005; Seth *et al.*, 2005), an important component of RV lifecycle (Hewson *et al.*, 2005). ROS are also potent agonists of TRPA1 and TRPV1 (Nishio *et al.*, 2013; Andersson *et al.*, 2008) which poses a potential interaction route between RV and TRP channels.

1.6.1.2.2 Inflammatory dependent

Other investigators propose that physical disruption is an inflammatory dependent process caused by TNF-α, IFN-γ, IL-4 and IL-8 which mediate the tight junction dysregulation (Soyka *et al.*, 2012; Bruewer *et al.*, 2003; Biagioli *et al.*, 1999). A cytokine-induced effect may however be secondary to signalling pathways aforementioned and which mechanism predominates may be dependent on specific cell type.

Consequently, varying degrees of barrier disruption and physical damage have the potential to cause a multitude of effects. A loss of integrity to airway barriers enables the transmigration of opportunistic bacteria causing secondary respiratory infection (Sajjan *et al.*, 2008). It can also lead to dysregulation of intracellular signalling facilitating the upregulation of growth factors (Wang, Kwon & Jang, 2009; Leigh *et al.*, 2008; Psarras *et al.*, 2006). Finally, in exposed animals an enhanced activation of sensory nerve fibres leads to airway hyperresponsiveness (Newcomb *et al.*, 2008) and epithelial repair is delayed (Bossios *et al.*, 2005). Thus, there is a cycle of cytokine induced barrier damage (Fig. 1.15B) leading to epithelial shedding. Airway epithelial lining begins to become permeable to larger molecules (Rezaee *et al.*, 2011) leading to a cycle of hypersensitivity and further damage.

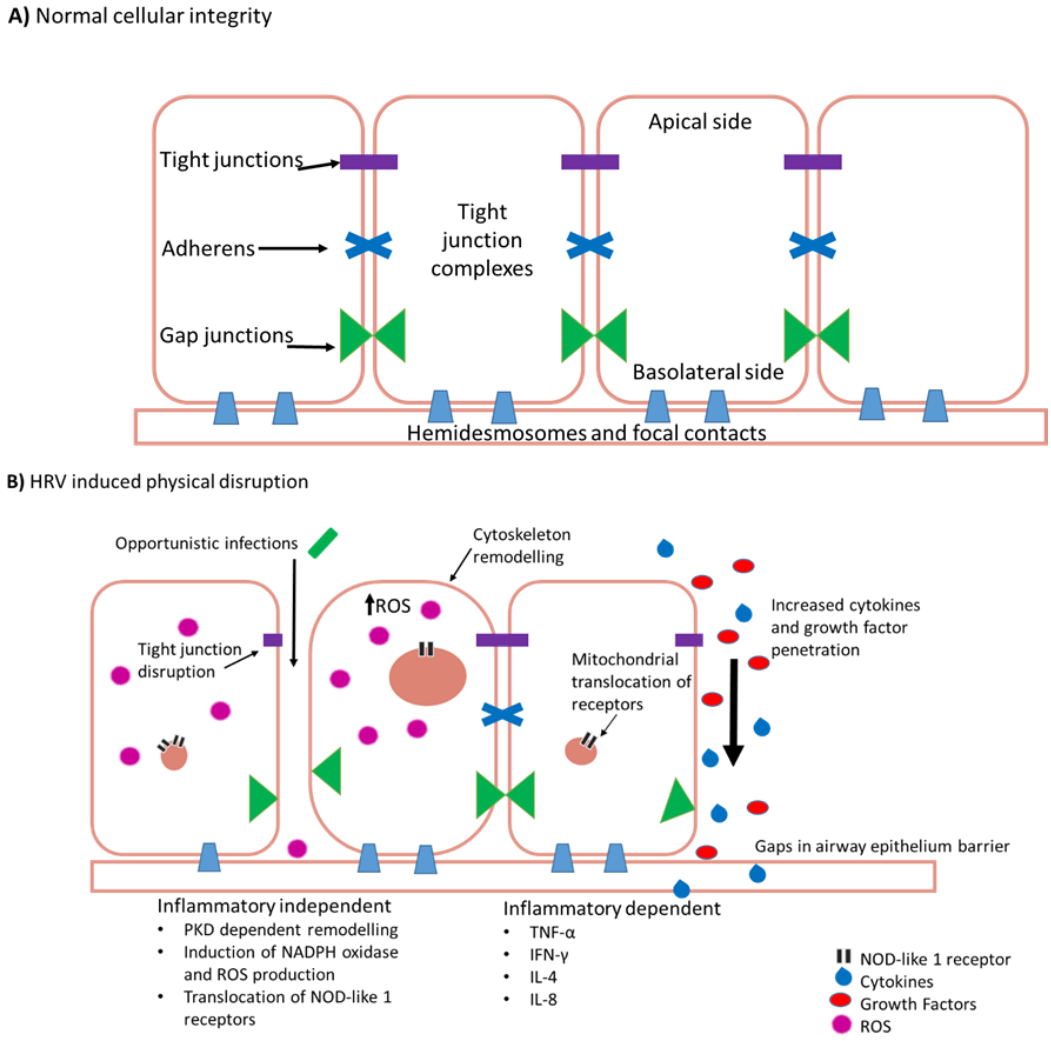

Figure 1.155. ***RV induced physical disruption of airway epithelia. A)*** *Normal healthy airway barrier. In a healthy airway cells are connected together by tight junction complexes including tight junctions, adherens and gap junctions. Cells are attached to basement membranes by hemidesmosomes and focal contacts. Barrier permeability is minimal and tightly regulated to prevent the excessive release of essential molecules, ions and proteins. The barrier is protective against infection.* ***B)*** *Human rhinovirus infection in airway epithelial cells. There are two main ways that RV causes physical disruption of airway barriers, inflammatory dependent and independent. Both replicating and non-replicating virus can interfere with airway membrane integrity by disrupting tight junction complexes. This causes a reduction of transepithelial resistance with the potential consequence of contracting a secondary infection. Cytoskeletal remodelling mediated by protein kinase D (PKD) causes an actin reorganisation within infected cells, altering their structure and integrity further allowing cells to lose their adjoining contacts. Replicating RV produces a dsRNA intermediate structure which can interact and activate NOD-like receptor X-1 ultimately producing reactive oxygen species. These alone are capable of reducing transepithelial resistance and barrier disruption. Loss of gap junctions and cells leaves gaps within epithelial layers. These allow cytokines, growth factors, immune cells and further viral particles to penetrate deeper layers within the airways causing dysregulation of cellular signalling. This dysregulation*

causes further upregulation of various molecules including growth factors which in turn can lead to an increase of receptor expression, such as TRP channels which have a prolific effect to cause cough.

Physical disruption to airways described above is a well-characterised part of the pathophysiology of lung diseases including asthma and cystic fibrosis, but the extent it plays in URTI, such as RV, has only recently begun to become clear, but may be crucially important in patients with pre-existing respiratory disease.

1.6.1.3 Mucus

Excessive mucus production and secretion is common in URTI (Witek *et al.*, 2015; Yuta *et al.*, 1998) initiating symptoms such as a cough and sneezing, and thus facilitating transmission of infection (Phipps & Richardson, 1976; Curley *et al.*, 1988). RV, in particular, upregulates the transcription of various mucin genes including MUC5AC (Hewson *et al.*, 2010; Zhu *et al.*, 2009b; Inoue *et al.*, 2006). This pathway is particularly involved in mucus production and release but this complex process (Fig. 1.16) has yet to be completely characterised. Using NFκB and MAPK inhibitors the pathway induced during RV infection was originally identified. The mechanism is independent of serotype and genotype and is inducible by artificial genomic stimulus using poly(I:C) (Hewson *et al.*, 2010). NFκB is upregulated as part of RV lifecycle (Zhu *et al.*, 1997, 1996) so it is unsurprising that it plays a pivotal role in the production of symptoms during infection and is essential for MUC5AC production. RV is able to induce mucosal cell metaplasia through a novel TLR3-EGFR coupling and the induction of EGFR ligands (Zhu *et al.*, 2009b), including transforming growth factor-α. This results in the production and secretion of mucins via MUC5AC promoter regions (Hewson *et al.*, 2010). The process of mucus secretion and tight junction disruption go hand-in-hand. A loss of epithelial integrity where a dissociation of E-cadherens from adheren tight junction complexes causes the uncoupling of EGFR where it becomes readily activated. However, an excess of EGFR activation promotes goblet metaplasia and thus excessive mucus secretion (Casalino-Matsuda, Monzón & Forteza, 2006). Muscarinic receptors are also involved in mucus secretion, mediated predominately through M3 in cooperation with M1 (Ishihara *et al.*, 1992) and are regulated by M2 (Ramnarine *et al.*, 1996). Since stimulation of muscarinic receptors transactivate EGFR to

stimulate goblet cell mucus secretion (Iwase *et al.*, 2002; Kanno *et al.*, 2002) it is possible that RV possesses the ability to interact with muscarinic receptors to cause this process. The implications of this are far reaching as not only may it begin to explain the aetiology of a viral mucosal cough but also chronic mucus secretion such as occurs in chronic bronchitis.

A counter-regulatory mechanism to RV induced TLR-EGFR coupling is by induction of the transcription factor sterile-alpha-motif (SAM)-pointed domain ETS-factor (SPDEF). SPDEF inhibits TLR signalling and type I IFN release to dampen the pro-inflammatory response induced by RV (Korfhagen *et al.*, 2012). SPDEF is a transcriptional modulator with a wide variety of roles including endocrine and androgen interaction (Park *et al.*, 2007; Oettgen *et al.*, 2000), however recently this transcription modulator was found to regulate goblet cell metaplasia (Chen *et al.*, 2009; Park *et al.*, 2007) and upregulate genes associated with mucus production (Bai *et al.*, 2015), including MUC5AC (Chen *et al.*, 2009). It has been suggested that SPDEF initiates recovery and protects against excessive inflammatory damage during metaplasia. Dysregulation of this pathway may permit the cycle of cough and damage to persist, exposing basal membranes and nerve fibres, allowing RV induced physical damage and mucus overproduction to act synergistically.

Many patients have a dry or non-productive cough and thus whilst an important co-factor mucus production alone is insufficient to explain coughing in URTI. Excessive mucus may exacerbate cough by several mechanisms including a stretch response and altered tonicity. Present within mucus are nucleosides and nucleotides, namely ATP and its breakdown products (Kreda *et al.*, 2010). ATP release occurs through cellular swelling mediated via pannexin-1 (Seminario-Vidal *et al.*, 2011; Ransford *et al.*, 2009) (Bao, Locovei & Dahl, 2004) and subsequent ATP-induced ATP release (Locovei, Wang & Dahl, 2006). Purinergic receptors are increasingly thought to be important mediators of cough hypersensitivity and are discussed previously in section 1.3.2 and further in section 1.6.1.4. In terms of mucus secretion P2Y receptors enhance intracellular calcium concentrations and subsequent ciliary beat frequency (Lieb *et al.*, 2002; Korngreen & Priel, 1996). P2X7 is known to co-localise and interact with Pannexin-1 (Iglesias *et al.*, 2008; Locovei *et al.*, 2007; Pelegrin & Surprenant, 2006). As part of the pore forming complex of P2X7 receptor, pannexin-1 forms a death complex through extended pore dilation and increased permeability (Yan *et al.*, 2010; Locovei *et al.*, 2007; Jiang *et al.*, 2005).

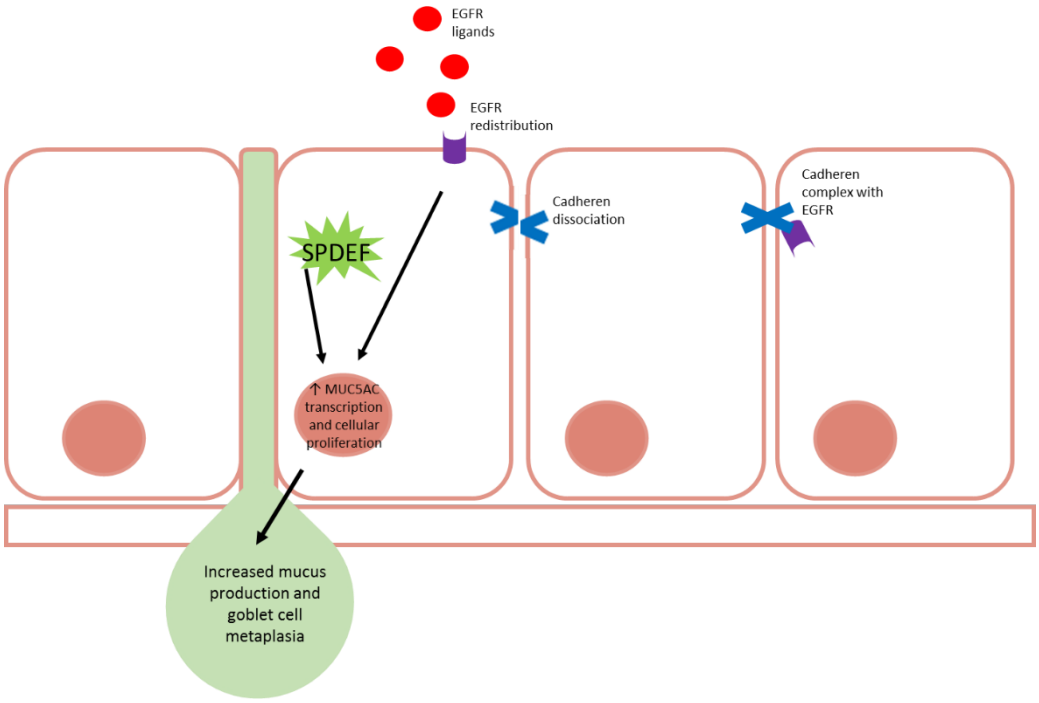

Figure 1.166. ***RV induced mucus production.*** *SPDEF and EGFR regulation of mucus production and goblet cell metaplasia within the airways during URTI. ROS induced uncoupling of epidermal growth factor receptor (EGFR) permits its translocation to the apical membrane of cells which readily allows its activation. Excessive activation of EGFR promotes various cellular processes including goblet cell metaplasia and upregulation of mucus associated genes including MUC5AC. Simultaneously, SPDEF is activated to dampen the inflammatory response mounted against the rhinovirus infection through blockade of TLR signal transduction. SPDEF also functions as a transcription modulator and causes upregulation of MUC5AC. Ultimately, increased MUC5AC and goblet metaplasia results in the hyperproduction of mucus, characteristic of rhinovirus infection.*

As previously discussed in section 1.2.2.2, an increasing number of studies have begun to implicate TRPV4 in mucociliary clearance and airway defence as it is an essential for epithelial barrier function (Reiter *et al.*, 2006) and is highly expressed in ciliated tracheal cells (Alenmyr *et al.*, 2014; Lorenzo *et al.*, 2008; Andrade *et al.*, 2005). As well as arachidonic acid metabolites (Watanabe *et al.*, 2003), TRPV4 can be activated through mechanical and osmotic stimulus (Fernandes *et al.*, 2008), such as viscous and hypotonic mucus, to induce and regulate calcium release (Fernández-Fernández *et al.*, 2008). Not only does this activate the channel but also regulates ciliary beat frequency (Andrade *et al.*, 2005) and mucus secretion, mediated by aquaporin-5 (Liu *et al.*, 2006).

1.6.1.4 Neuronal modulation

Cough is clearly a neuronal reflex so the hypothesis that neuronal modulation underlies the pathogenesis of viral cough is the most convincing. However, at present there is no single comprehensive mechanism that explains the cough induced by RV or indeed any other respiratory pathogen. Theories include a cooperative role of pulmonary oxidative stress in vagal sensory nerves between TRPV1, TRPA1 and P2X receptors (Taylor-Clark & Undem, 2011). It is also thought that direct viral damage to mitochondria leads to ROS production which may modulate or influence cough, previously discussed in 1.6.1.2.

During URTI sensitivity to capsaicin, citric acid and histamine are transiently increased with a reduction in cough threshold (Dicpinigaitis *et al.*, 2011; Grünberg *et al.*, 1997; O'Connell *et al.*, 1996; Empey *et al.*, 1976), without concurrent hyperresponsiveness to methacholine (O'Connell *et al.*, 1996). This suggests RV induced cough is independent of bronchial smooth muscle tone. This was originally proposed to occur through the sensitisation of RARs (Madison & Irwin, 2003) but despite convincing evidence RARs do not express TRPV1 receptors and are insensitive to chemical stimuli (Myers, Kajekar & Undem, 2002). As such they are no longer proposed to be the primary fibre involved in the cough reflex (Grace *et al.*, 2013) but may have a synergistic interaction with C-fibres (Mazzone, Mori & Canning, 2005). As a result of these findings, capsaicin sensitive nerve are not the same nerves known to initiate pathological cough, despite the clear observation that inhaled aerosolised capsaicin produces a cough (Collier & Fuller, 1984). These observed differences may be explained by phenotypic changes to nerve fibres induced during inflammation (Lieu *et al.*, 2012).

Phenotypic changes imply altered gene expression and differentiation. In the guinea pig, low threshold mechanosensitive sensory nerves express TrkA (Lieu *et al.*, 2011) and application of other growth factors induce the functional expression of TRPV1 and TRPA1 *de novo* (Lieu *et al.*, 2012). *In vivo* research in the rat and guinea pig model have found inflammatory states through increased nerve growth factor (NGF) levels causing a phenotypic change of A-delta fibres. They now resemble C-fibres as shown by the co-expression of substance P and NGF (Hunter, Myers & Undem, 2000; Neumann *et al.*, 1996). NGF is transported to sensory neurons via DRG and is able to alter transcription of various proteins and peptides (Woolf, 1996). Further research into the effect of NGF on TRPV1 by

Chuang *et al.* (2001) and Ganju *et al.* (1998) found NGF activates PLC which releases TRPV1 from constitutive inhibition, thus lowering its activation threshold (Chuang *et al.*, 2001; Ganju *et al.*, 1998).

Similarly, RV infection in the human has been shown to cause the upregulation of a number of growth factors (Wang, Kwon & Jang, 2009; Leigh *et al.*, 2008; Psarras *et al.*, 2006). Specifically, RV can induce the upregulation of NGF (Othumpangat, Regier & Piedimonte, 2012) and inhalation of aerosolised NGF can enhance cough in the guinea-pig citric acid induced cough model through TRPV1 and TrkA (nerve growth factor receptor) activation (El-Hashim *et al.*, 2013; El-Hashim & Jaffal, 2009). Despite the differences between human and guinea pig airway innervation, it is these modifications in expression that may lead to a phenotypic change during URTI.

Interest into the role of TRPV4 and P2X receptors in cough have been growing exponentially. Application of TRPV4 agonist GSK1016790A facilitated the subsequent activation of P2X3 receptor through sensitisation of airway sensory nerves (Bonvini *et al.*, 2016). This isn't the first time TRPV4 and P2X3 receptors have been hypothesised to play a cooperative role in pathophysiology (Aizawa *et al.*, 2012). As previously discussed in section 1.2.3 and 1.3.2, it has become apparent that there is significant overlap between TRP channel and purinergic receptor functionality, which have given rise to persuasive theory that TRPV4 and purinergic receptors play a cooperative role in pathological cough. ATP, which has been shown to enhance cough reflex sensitivity (Kamei *et al.*, 2005) in response to citric acid and histamine challenge (Kamei & Takahashi, 2006), potentiates through P2X2/X3 mediated bronchoconstriction (Basoglu *et al.*, 2015, 2005). A successful clinical trial using AF-219, a P2X3 antagonist, reduced the incidence of coughing in patients with chronic cough by 75% (Abdulqawi *et al.*, 2015) provides more convincing evidence that cough sensitivity may be strongly upregulated by the P2X pathway.

Neurogenic inflammation from afferent sensory neurons (Chiu, von Hehn & Woolf, 2012) is mediated mostly but not exclusively by neuropeptides CGRP, neurokinins and substance P. It is thought to be protective reflex, facilitating healing and modulation of local immunity. It is well characterised in numerous diseases, including migraine (Durham, 2006), asthma (Barnes, 2001), and rhinitis the latter of which is common in URTI (Gentile & Skoner, 2001), where it likely amplifies maladaptive responses. Neurogenic inflammation is essential for

sensory neurons to prime and respond to noxious stimuli quickly. Consequently, afferent neurones are abundant in TRP channels, P2X, pathogen-associated molecular pattern (PAMP) and damage-associated molecular pattern (DAMP) receptors. Only a limited set of TLRs, 3, 4, 7 and 9, are present within nociceptive neurons (Diogenes *et al.*, 2011; Qi *et al.*, 2011; Liu *et al.*, 2010), therefore not all pathogens are capable of directly causing neurogenic inflammation, however RV is capable of activating both TLR 3 and 7 within nociceptive neurons (Triantafilou *et al.*, 2011). Stimulation of these TLRs induce an inward depolarisation to elicit neuronal sensitisation to pain stimuli (Diogenes *et al.*, 2011; Qi *et al.*, 2011; Liu *et al.*, 2010). A recent interesting finding identified TLR 7 stimulation leading to an itch specific sensory pathway through intracellular microRNA let-7b (Liu *et al.*, 2010). This in turn induces a rapid inward current in neurons co-expressing TLR7 and TRPA1 to generate pain (Park *et al.*, 2014; Winkler, Taylor & Peterson, 2014). Extracellular ATP is a crucial DAMP ligand that is released during damage and injury. In nociceptive neurons P2X3 receptors are key to ATP recognition and pain production (Souslova *et al.*, 2000). Purinergic receptor P2Y2 is also responsive to ATP and is capable of TRPV1 sensitisation and activation in the absence of TRPV1 stimuli (Lakshmi & Joshi, 2005), a similar sensation previously ascribed to TRPV4 through RV induced mucus overproduction. Cytokines, namely IL-1β and TNF-α, produced as a result of infection cause TRP channel sensitisation and activation through membrane phosphorylation (Binshtok *et al.*, 2008; Nicol, Lopshire & Pafford, 1997). The resultant effect means TRP channels respond to innocuous stimuli as noxious stimuli causing allodynia and perhaps allotussia.

There is a surprising degree of overlap in the physiological location and functionality of thermo-TRP channels and P2X receptors. TRPA1 is reported to possess mechanotransductive properties likely attributable to their distinct characteristic ankyrin repeats (Nagata *et al.*, 2005) in the inner ear to permit hearing (Corey *et al.*, 2004), although this is disputed by other groups (Kwan *et al.*, 2006). However, despite this, an interesting notable finding was the identification of P2X receptors also within the inner ear and that their initial action potential firing is necessary for the maturation of hearing (Tritsch *et al.*, 2007). Like-wise in the bladder, TRPV1, TRPV2, TRPV4, TRPA1 and TRPM8 all have mechanosensory roles (Araki, 2011) to interpret stretch and pain perception (Andersson, Gratzke & Hedlund, 2010), whilst P2X2 and P2X3 play a major role in distension sensation

to excite a micturition reflex (Kaan *et al.*, 2010). Most relevant to cough is their influence on pain. TRPA1 and TRPV1 are well characterised to elicit pain signals in response to noxious stimuli (Laing & Dhaka, 2015; Julius, 2013) P2X2, P2X3, P2X4 and P2X7 having all been identified to play some form of role in various types of pain (Ulmann *et al.*, 2008; Chessell *et al.*, 2005; McGaraughty *et al.*, 2003; Cockayne *et al.*, 2000). Most importantly in neuropathic pain where some pharmacological agents which have shown promising results in clinical trials (Gum, Wakefield & Jarvis, 2012). Relevant to these observations is that P2X2 and P2X3 receptors expressed on afferent neurons are home to classic pain sensation channel TRPV1 (Guo *et al.*, 1999).

The role of TRP channels in RV induced cough has recently been explained in a first of its kind study (Abdullah *et al.*, 2014). In this study, a novel infection site of RV was identified in neuronal cell lines with concomitant upregulation of expressed TRP channels TRPA1, TRPV1 and TRPM8 found on airway sensory nerves. RV infection accounts for up to 50% of exacerbations in asthmatics (Johnston, 2005), and both asthmatic (McGarvey *et al.*, 2014) and chronic cough sufferers (Mitchell *et al.*, 2005; Groneberg *et al.*, 2004) have higher levels of TRP channels expressed in their airways, this finding adds to the mounting evidence that TRP channels play a major role in cough during RV infections but requires further investigation to definitively confirm this.

A post-viral cough is generally unresponsive to conventional pharmacological intervention, but have shown limited responsiveness to anti-cholinergic drug tiotropium (Dicpinigaitis *et al.*, 2008), which leaves a major hole in our therapeutic armamentarium. Currently treatment merely consists of dampening the inflammatory response with the use of anti-inflammatories (such as naproxen) (Pratter, 2006) and cough suppressants (codeine containing products and dextromethorphan) (Morice *et al.*, 2006) in the hope of reducing the frequency, severity and transmission of cough. Opiates although commonly prescribed, are not generally recommended for viral cough due to their poor efficacy and significant adverse effect profile (Morice *et al.*, 2006).

The multiple mechanisms described above provide a confusing and interrelated “soup” of potential therapeutic targets. Dissecting which are the key players involved in this common affliction will be challenging but the rewards for understanding viral induced cough will have enormous impact on human morbidity.

1.7 Working hypothesis

Thermo-TRP channels and ATP may play an important role in the cough response during a respiratory tract infection. Evidence is emerging that blockade of ATP activated P2X3 receptor leads to a life changing reduction in cough but how an airway becomes hypersensitive following a stimulus, such as respiratory tract infection, is largely unknown and subject to speculation. Our overall hypothesis is that common cold causing virus, human rhinovirus-16 (RV-16), causes airway hypersensitivity through an increase in the concentration of ATP found in the airway. This thesis has focused on the expression and function of thermo-TRP channels, TRPA1, TRPV1 and TRPV4 during RV-16 infection, characterisation of the hypotonic pathway and the downstream effect on ATP release, and finally, the role of RV-16 on airway concentration of ATP.

1.8 Aims

1. Determine effect of synthetic viral stimulus polyinosinic:polycytidylic acid (poly(I:C)) on TRPA1, TRPV1, TRPV4 and P2X3 function in A549 airway epithelial and 1321N1 astrocytoma cell lines through measurement of global protein expression and intracellular calcium signalling.
2. Determine effect of RV-16 on TRPA1, TRPV1, TRPV4 and P2X3 function in A549 airway epithelial and 1321N1 astrocytoma cell lines through measurement of global protein expression and intracellular calcium signalling.
3. Pharmacologically characterise hypotonic pathway and determine downstream effect of ATP release and pannexin-1 organisation in A549 cell line.
4. Investigate effect of RV-16 on ATP release on A549 cell line.
5. Determine whether RV-16 affects downstream ATP release following hypotonic stimulation.

Chapter 2

General Methods

2.1 Materials

Cell culture flasks were purchased from Greiner One Bio (Kremsmunster, Austria). Cell culture plates were purchased from Greiner One Bio, Corning (Corning, United States) or Sarstedt (Sarstedt, Nümbrecht, Germany). Foetal bovine serum (FBS) (Gibco, Thermo Fisher Scientific, Loughborough, UK)), penicillin/streptomycin, L-glutamine and Dulbecco's modified Eagles media (DMEM) were all purchased from Lonza (Castleford, UK). RNA extraction kits were purchased from Promega (Wisconsin, United States) and Omega Bio-Tek (Atlanta, United States). RT-PCR primers were ordered from Eurofins (Luxembourg City, Luxembourg). All RT-PCR reagents were purchased from Thermo Fisher Scientific. Poly(I:C) was purchased from Santa Cruz Biotechnology (SCBT) (Texas, United States). All antibodies used for western blotting were purchased from either SCBT or New England Biolabs (Massachusetts, United States). All ELISA reagents, including match ELISA pairs, were purchased from Biolegend (California, United States), except TMB which was purchased from Vectorlabs (California, United States). ATP determination kit, Fluo-AM dyes and DAPI containing Diamond anti-fade mounting media was purchased from Invitrogen (California, United States). Acrylamide and Trans-Blot® Turbo PVDF transfer packs were purchased from Bio-Rad (California, United States), Midori green was purchased from GENEFLOW (Litchfield, UK), sulforhodamine B was purchased from Alfa Aesar, 2-deoxy-D-glucose, H-1152, ML-7, cytochalasin D and phalloidin CruzFluor™ 594 were purchased from SCBT, Seahorse culture plates and sensor cartridges were purchased from Agilent Technologies (California, United States), intracellular ATP measurement kit, HC067047 and RO-31-8220 were purchased from Abcam, *E. coli* cells (XL10-Gold® ultracompetent) were purchased from Stratagene (California, United States), TRPV4 DNA pCMV6-GFP tagged vector was purchased from Origene (Maryland, United States), NucleoSpin® Plasmid DNA purification miniprep kit was purchased from Macherey-Nagel (Düren, Germany), FuGENE® 6 Transfection Reagent was purchased from Promega. Luciferase was purchased from BD Bioscience (New Jersey, United States) All other reagents were purchased from Sigma-Aldrich (Poole, UK) or Fisher Scientific (New Hampshire, United States), except where specified.

2.2 Cell culture and maintenance

Continuous cell lines were thawed from cryopreservation and suspended in cell culture medium. Cells were grown in 75 cm^2 culture flasks at 37^oC with 5% CO_2 and passaged at 70-80% confluence (approximately 3-4 days). A549 cell line was purchased from Public Health England (London, UK). Wild type 1321N1, chimeric P2X2/X3 and hP2X3 transfected 1321N1 cell lines were received from Dr Samuel Fountain, University of East Anglia (Norfolk, UK).

A549 cells were originally derived from immortalised lung cancer cells. A549 cells are type II alveolar cells. The cells are maintained in Dulbecco's modified Eagle medium (DMEM) supplemented with 10% (v/v) heat inactivated FBS, 100 U ml^{-1} penicillin, 100 U ml^{-1} streptomycin and 1% L-glutamine. The cells were passaged every 3-4 days, as appropriate, using HEPES buffered saline-EDTA (HBSE) cell dissociation buffer (10mM HEPES, 1.71mM EDTA and 0.9% (w/v) sodium chloride, pH 7.4).

Transfected A549 cells were transfected in-house using FuGENE® 6 Transfection Reagent as described in section 2.16.5. TRPV4-GFP tagged transfected A549 cells were maintained in the standard supplemented DMEM, as described above, containing additional 0.7mg ml^{-1} G418.

Wild type (WT) 1321N1 cells were used for cell characterisation. WT 1321N1 cells were maintained in DMEM supplemented medium containing 10% (v/v) heat inactivated FBS, 100 U ml^{-1} penicillin and 100 U ml^{-1} streptomycin. The cells were passaged every 3-4 days using HBSE cell dissociation buffer.

Transfected 1321N1 cells were stably transfected with hP2X3 receptor, these cells were a gift from Dr Samuel Fountain, University of East Anglia (Norfolk, UK). The transfected cells were grown in DMEM supplemented with 10% (v/v) heat inactivated FBS, 100 U ml^{-1} penicillin, 100 U ml^{-1} streptomycin, 1% L-glutamine and 0.25µg ml^{-1} puromycin. Cells were passaged every 3-4 days using HBSE cell dissociation buffer.

2.3 Sulforhodamine B assay

Sulforhodamine B (SRB) assay was performed to determine the cellular toxicity of agents added to cell culture during time course experiments. Cells were seeded at 4 x 10^4 density in a 24-well plate and incubated for 16-24 hours at 37°C and 5% CO_2 to adhere. Poly(I:C) or RV was added at increasing concentrations to wells, 10ng ml^{-1}-30µg ml^{-1} or MOI 0.001-1, respectively, of cells over a time course of several days. Assays were stopped by the addition of ice cold 25% trichloroacetic acid (TCA) directly to cells and allowed to fix on ice for 1 hour. Cells were washed 4 times with 1% (v/v) acetic acid and stained with 0.4% (w/v) SRB dissolved in 1% (v/v) acetic acid for 30 minutes and washed 4 times. Cells were dissolved in 10mM unbuffered Tris-base pH 10 and aliquoted into 96-well plate and the absorbance read at 540nm.

2.4 Poly(I:C) stimulus assays

Cells were cultured and seeded at 1 x 10^5 density in 6-well, 96-well plate or 25 cm^2 flasks. Cell were incubated for 16-24 hours at 37°C and 5% CO_2 to adhere. Cells were inoculated with a range of concentrations (30ng-10µg ml^{-1}) of poly(I:C) over various time points to determine the optimal time points and concentration necessary for maximal TRP expression. Supernatants and cells were harvested at 3, 6, 8, 24, 48 and 72-hour time points for downstream analysis including polymerase chain reaction (PCR) (see section 2.6 and 2.7), intracellular calcium signalling (see section 2.8) and western blot analysis (see section 2.9).

2.5 Human rhinovirus-16

Human rhinovirus-16 was a gift Dr Michael Edwards from Imperial College (London, UK). It was initially received as frozen stocks of HeLa Ohio cells infected with RV-16. These stocks had previously been produced by exposing T175 flasks of HeLa Ohio cells to 20ml of high purity RV-16 stocks. Cells were grown in DMEM supplemented media containing 2% (v/v) FBS, 2% 1M HEPES, 1% (7.5% (w/v)) bicarbonate and were incubated for 1 hour at room temperature (RT) with gentle agitation before incubating at 37°C, 5% CO_2 for 16-24 hours until signs of cytopathic effects (CPE) were present. Cells were detached and placed at -

80°C overnight, thawed for 1 hour at RT and re-frozen at -80°C for one hour. Infected HeLa Ohio cells were received at this stage. Cells were thawed at RT and spun at 4000 rpm for 15 minutes to pellet cell debris. Supernatants were filter sterilised through a 0.2 µM filter and stored at -80°C in aliquots.

2.5.1 Determining rhinovirus titre

The titre of RV-16 stocks was determined before use to identify the 50% tissue-culture infective dose end-point (TCID50), the minimum concentration of virus required to induce CPE in 50% of HeLa Ohio cells. HeLa Ohio cells were seeded at 0.5 x 10^5 density in a 96-well plate. An aliquot of RV-16 was thawed and used immediately, and a serial dilution (neat stock to 10^{-5}) was produced from stock in 4% FBS supplemented DMEM media. 50µl was added to each well containing cell suspension. The plate was incubated for up to 4 days at 37°C and 5% CO_2 and checked daily for signs of CPE. Each well including neat virus were read and signs of CPE are recorded. Results were analysed using the Spearman-Kaber equation.

The TCID50 was then used to calculate the multiplicity of infection (MOI) of the virus to be used in infection assays (equation 1).

Equation 2.1. ***Equation used to determine MOI from TCID50ml^{-1} of non-plaque forming viruses****, where N = TCID50, V = volume of virus to be added, X = number of cells seeded, 0.7 = is a non-substitutable standard and m = MOI (unknown to be calculated)*

$$\frac{0.7\ x\ N}{dilution\ factor}\ x\ V = m\ x\ X$$

2.5.2 Production of rhinovirus controls

Virus free filtrates and UV inactivated RV-16 controls were used as a vehicle control. These were used to ensure any effects seen were as a result of the active and infective virus. Both controls do not give a completely negative result but produce a characteristic 'knock down'. UV inactivated controls knock down virally induced cytokines by 50-75% of wild type and filtrates knock down production by 80-90% of wild type (Johnston *et al.*, 1998; personal

communication, Imperial College London). Both controls and wild type virus stocks were titred in HeLa Ohio cells to determine knock down response.

2.5.2.1 UV inactivation

An aliquot of virus stock was thawed into a 35 mm petri dish and UV inactivated at 1200 J/cm^2 for 30 minutes in short wave UV crosslinker at 254 nm, model number CL-1000 (UVP, California, United States).

2.5.2.2 Filtered virus

An aliquot of virus stock was thawed and spun at 12,000 rpm for 5 minutes in 30kDa centrifuge filters (Amicon (Merck Millipore), Massachusetts, United States). The eluted solution was used immediately and the filtrate was kept and stored at -80^{o}C.

2.5.3 RV-16 stimulus assays

Cells were cultured and seeded at 5 x 10^4 – 4.5 x 10^5 density in 6-well plates, 96-well plates or 25 cm^2 flasks. Cell were incubated for 16-24 hours at 37^{o}C and 5% CO_2 to adhere. An aliquot of RV-16 was thawed and used immediately at an MOI of 1 in 4% FCS growth medium. The cells were gently agitated for 30 minutes at room temperature to allow viral attachment. Cells were washed 3 times with 1X PBS, and 10% FCS growth medium was added. Cells were grown and incubated with RV-16 for 3, 6, 8, 24 hours, and at 24-hour increments up to 168 hours with UV inactivated and filtered viral controls. The cells responses to RV-16 were then investigated by PCR (see section 2.6 and 2.7), calcium signalling and calcium imaging (see section 2.8), western blotting (see section 2.9), ATP release (see section 2.11), hypotonic stimulus (see section 2.13), immunofluorescence microscopy (see section 2.14) and Seahorse metabolic analysis (see section 2.16).

2.6 Reverse transcription (RT-PCR)

2.6.1 Primer design

Sequence specific primers were designed for TRPA1, TRPV1, TRPV4, P2X2, P2X3, P2X7 and β-actin (Table 2.1) and purchased through Eurofins. The primers listed in Table 2.1 were designed using National Centre for Biotechnology Information (NCBI) database by analysing sequenced genomes for primers using Primer-BLAST. Briefly, genome accession number

was entered in to Primer-BLAST with specific requirements (melting temperature 50-60^{o}C and GC% <60%). Available primer sequences were then checked against the sequenced genome for areas of overlap, to ensure the primer sequence spanned codons and where the primer binds (C- or N-terminal).

Table 2.1 ***RT-PCR primer sequence with source.***

TRPA1 Forward	5'-CACAGCCATTCATTTTGCTG-3'	Designed 'in house'
TRPA1 Reverse	5'-AAGTGCAGTGTTCCCGTCT-3'	Designed 'in house'
TRPV1 Forward	5'-GACAGCCTGAAGGAGCTTGT-3'	Designed 'in house'
TRPV1 Reverse	5'-CTCCAGCACCGAGTTCTTCT-3'	Designed 'in house'
TRPV4 Forward	5'-CTGAGACCCTCCCTGGACTA-3'	Designed 'in house'
TRPV4 Reverse	5'-GAGAAGACACTGCTTGCTCAGA-3'	Designed 'in house'
P2X2 Forward	5'-GTGATCGTGGTGAGGAACCG-3'	Designed 'in house'
P2X2 Reverse	5'-TTGGAGGGCCCCTGGTAATA-3'	Designed 'in house'
P2X3 Forward	5'-ACCATCGGGATCATCAACCG-3'	Designed 'in house'
P2X3 Reverse	5'-CATGATGGGCGTTTCCACTG-3'	Designed 'in house'
P2X7 Forward	5'-CTGCAACCTAGACCGTTGGT-3'	Designed 'in house'
P2X7 Reverse	5'-CGCAGGTCTTGGGACTTCTT-3'	Designed 'in house'
β-actin Forward	5'-CGTGGGCCGCCCTAGGCACCA-3'	(Ramachandran, Morice & Compton, 2006)
β-actin Reverse	5'-TTGGCCTTAGGGTTCAGGGGG-5'	(Ramachandran, Morice & Compton, 2006)

2.6.2 RNA extraction

RNA was extracted from cells using either E.Z.N.A total HP RNA isolation kit from Omega Bio-Tek or ReliaPrep RNA cell miniprep system from Promega and carried out as per manufacturer instructions. Cells were washed twice in ice cold 1X PBS to remove traces of medium. Briefly, using the E.Z.N.A total HP RNA isolation kit, the cells were lysed in 350µl of cell lysis buffer containing guanidine and sheared by pipetting. An equal volume of 70% ethanol was added and lysates transferred to an elution tube and spun at 10,000 x *g* for 60 seconds. 500µl of RNA wash buffer I was added and spun at 10,000 x *g* for 60 seconds.

500µl of RNA wash buffer II was added and spun at 10,000 x *g* for 60 seconds and carried out twice. The elution tube was spun at maximum speed for 2 minutes to completely dry the membrane before finally, the RNA was eluted from the column in 50µl DEPC-treated water spun at maximum speed for 60 seconds.

Briefly, using the ReliaPrep RNA miniprep system as per manufacturer protocol, cells were lysed in 250µl of cell lysis buffer containing guanidine and sheared by pipetting. 85µl 100% isopropanol was added and cells vortexed briefly. The cell lysate was transferred to an elution tube and spun at 12,000 x *g* for 30 seconds. 500µl of RNA wash solution was added and spun at 12,000 x *g* for 30 seconds. A DNase I incubation mix was prepared with 10% DNase I, 10% 0.09M manganese chloride and 80% yellow core buffer, as supplied by the manufacturer. 30µl of the DNase I mix was incubated with the cell lysate for 15 minutes at room temperature. The lysate was then spun at 12,000 x *g* in column wash and RNA wash for 15 and 30 seconds, respectively. Finally, the lysate was spun at 14,000 x *g* for 2 minutes with RNA wash solution once more, and eluted in 30µl nuclease-free water for 1 minute at 12,000 x *g.*

RNA concentration and quality was quantified with Nanodrop lite spectrophotometer (Thermo Fisher Scientific, Loughborough, UK) using Beer-Lambert Law at absorbance 260 nm. The RNA was stored at -80^{o}C but reverse transcribed to cDNA as soon as possible to prevent degradation of fragile RNA.

2.6.3 Synthesis of cDNA

To convert extracted RNA samples to cDNA for RT-PCR downstream purposes, RevertAid Premium Reverse transcriptase reagents (Thermo Fisher Scientific, Loughborough, UK) were used to convert RNA into cDNA (>2µg). 1µl of random hexamer primers, >14.5µl Nuclease-free water, 1µl 10mM dNTP mix, 4µl 5X buffer, 0.5µl Ribolock and 1µl RevertAid Premium reverse transcriptase was added in specific order to a volume of RNA necessary to transcribe the specified quantity of cDNA (Table 2.2). A duplicate control tube was also made with the omission of RevertAid Premium reverse transcriptase. Table 2.3 details the thermal cycling conditions to produce cDNA.

Table 2.2. ***First strand cDNA synthesis master mix.*** *Reagents required to be added in specific order as listed below. DTT - Dithiothreitol*

Reagent	Volume (µl) or Concentration (µg)
Template RNA	2µg
Random hexamer primers	1µl
Nuclease-free water	>14.5µl
10mM dNTP mix (final concentration)	1µl
5X reaction buffer (250mM Tris-HCl (pH 8.3), 250mM KCl, 20mM $MgCl_2$, 50mM DTT)	4µl
RiboLock RNase inhibitor (20U/µl)	0.5µl
RevertAid reverse transcriptase (200U/µl)	1µl
Total volume	*25µl*

Table 2.3 ***Thermal cycling conditions for RT-PCR used to synthesise cDNA from RNA extraction samples****.*

Process	Temperature (°C)	Time (Minutes)
Activation	-	-
Anneal	50	30
Extension	85	5

2.6.4 RT-PCR

Primers designed in section 2.6.1 were used to amplify the cDNA samples using DreamTaq DNA polymerase reagents (Thermo Scientific). 2.5µl of 10X green DreamTaq buffer, >20.375µl Nuclease-free water, 0.5µl forward and reverse primer, 10mM dNTP mix and 0.125µl (5U μl^{-1}) DreamTaq DNA polymerase was added in specific order to a volume of cDNA (1-2µg) necessary to amplify the required gene sequence (Table 2.4). A duplicate control tube was also made with the omission of DreamTaq DNA polymerase. Table 2.5 details the thermal cycling conditions required to amplify the cDNA samples.

Table 2.4 ***RT-PCR DreamTaq amplification master mix composition.***

Reagent	Volume (µl) or Concentration (µg)
Template cDNA	0.5-20.375µl (1-2µg)
Nuclease-free water	>20.375µl
Forward primer	0.5µl
Reverse primer	0.5µl
10mM dNTP mix (final concentration)	0.5µl
10X DreamTaq green reaction buffer (proprietary formula containing 20mM $MgCl_2$)	2.5µl
DreamTaq DNA polymerase (5U μl^{-1})	0.125µl
Total volume	*25µl*

2.7 Agarose gel electrophoresis

A 1.3% agarose gel was prepared with 1X TAE buffer and stained with Midori Green DNA stain. End product cDNA or other genomic products, including restriction digest products (containing 2.5µl DreamTaq green buffer) and negative controls were loaded into the agarose gel in 1X TAE buffer and electrophoresed with a 1kb DNA ladder for approximately 45 minutes at 100-110 volts. The gel was visualised on molecular imager Bio-Rad Versa Doc at under blue LED light (460-490 nm).

Table 2.5. ***Thermal cycling conditions for RT-PCR used to amplify cDNA using templates of interest.***

Stage	Step	Cycles (number)	Temperature (°C)	Time (seconds)
	Preheat lid		105	
1	Initial denaturation	1	95	180
2	Denaturation	27	95	30
	Annealing		55	30
	Extension		72	60
3	Final extension	1	72	600
	Hold		10	∞

2.8 Intracellular calcium measurements

Cells were assayed to measure intracellular calcium transients in response to TRP and P2X receptor stimuli. As part of protocol optimisation, three techniques were tested and optimised. Firstly, suspension fluorospectrometry, followed by a high throughput plate reader system, Flexstation® (Molecular Devices, California, United States), then using live calcium imaging on Zeiss Axio Observer Z1 fluorescent microscope (Zeiss, Oberkochen, Germany).

Cells were grown to 80-90% confluence in supplemented DMEM and harvested. Cells were washed in 1X PBS and harvested as described in section 2.2 and pelleted by centrifugation for 5 minutes at 300 x *g.* The cell pellet was re-suspended in supplemented DMEM and used as follows according to each subsection technique.

2.8.1 Suspension Fluorospectrometry

Cells were harvested with HBSE and pelleted by centrifugation (300 x *g* for 5 minutes). The pellet was re-suspended in normal growth media and incubated with gentle agitation for 20-30 minutes with 10µg Fluo-3AM from 2.5 µg μl^{-1} stock solution prepared in DMSO. Cells were then washed in 4.5ml 1X PBS and pelleted by centrifugation for 5 minutes at 300 x *g*. Cells were resuspended in 2ml isotonic assay buffer (150mM NaCl, 3mM KCl, 1.5mM $CaCl_2$, 10mM glucose and 20mM HEPES pH 7.4).

A 100µl aliquot of cells was added to cuvettes (Sarstedt) containing 1.9ml isotonic assay buffer and magnetic flea under constant stirring (50 rpm). Transient intracellular calcium responses were measured using PTI fluorospectrometer (Photon Technology International, New Jersey, United States). Cuvettes were individually measured for intensity changes induced by TRP channel or P2X receptor stimuli (e.g. capsaicin or ATP, respectively) at an excitation 506 nm and emission 526 nm wavelengths using Felix GX software (Photon Technology International). Responses were recorded until their plateau or their peak for a minimum of 4 minutes. Responses were analysed as a percentage of control compound 2µM calcium ionophore (A23187) (equation 2), which is assumed to induce a maximum cell response and used to determine the degree of cell decline over the course of an experiment.

Equation 2.2. ***Equation used for calculating calcium signalling responses as a percentage of A23187 control compound.*** *Where x = test agent and RFU = relative fluorescent units.*

$$[Ca_i] = \frac{\Delta\, RFU_x}{\Delta RFU_{A23187}}\, x\, 100$$

Measurements were performed in duplicate on three separate occasions to create a statistical analyses of reproducibility. All repeats were performed on cells between passages 17 to 24.

2.8.2 Flexstation® 3 Multi-mode reader

From the cell suspension, 10µl of cells were used to determine cell concentration using a haemocytometer. The cells were resuspended at 1,000,000 (million) cells ml^{-1} in supplemented DMEM and seeded in an uncoated flat clear bottom 96-well black plate at a density of 5 x 10^4 cells per well. Cells were incubated at 37 ^oC with 5% CO_2 for 16-24 hours. 2X Fluo-4 Direct Assay reagent buffer (Invitrogen) was added directly to cell medium at 1:1 ratio. Cells were incubated for 45 minutes to 1 hour at 37 ^oC, with a total loading time of 1 hour, and plates were immediately read.

Transient intracellular calcium responses were measured using Flexstation (Molecular Devices) and SoftMax Pro 5.2 software (Molecular Devices) at excitation 494 nm and emission 525 nm wavelengths. Baseline measurements were recorded for 30 seconds and responses to TRP channel and P2X receptor stimuli were measured over a period of 300 seconds. Measurements were performed in a minimum duplicate on 3 separate occasions to create a statistical analysis of reproducibility. Responses were calculated as above (Equation 2.) and represented as a percentage of positive control 2µM A23187. All repeats were performed on cells between passages 10-30.

2.8.3 Calcium imaging using Zeiss Microscopy

From the cell suspension, 10µl of cells were used to determine cell concentration using a haemocytometer. The cells were resuspended at 1,000,000 (million) cells ml^{-1} in supplemented DMEM and seeded in a 24 well black Lumox® flat, clear bottom plate (Sarstedt) at a density of 5 x 10^4 cells per well. Cells were incubated at 37 ^oC with 5% CO_2

for 16-24 hours. On the day of the experiment, the cells were washed twice with 1X PBS and overlaid with Hank's buffered saline solution (HBSS) supplemented with 10mM HEPES buffer (HBSS+) containing 2.5 µM Fluo-4 AM from 2 µg μl^{-1} stock solution prepared in DMSO. Cells were incubated for 30 minutes at 37 ^{o}C and a further 30 minutes at room temperature with a total loading time of 1 hour.

Transient intracellular calcium responses were imaged on Zeiss Axio Observer.Z1 inverted microscope (Zeiss) and acquired using Zen Blue Pro software (Zeiss) at excitation 494 nm and emission 525 nm wavelengths. Images were acquired at 2 second intervals for a total time-lapse sequence of 300 seconds. Baseline recordings were taken for the first 20-30 seconds before application of stimulus and calcium flux was measured. Positive response was confirmed with positive control 2µM A23187 at the end of each experimental time course. Recordings were taken in singulate on three separate occasions to create a statistical analysis of reproducibility. All experiments were performed on cells between passage 30-33. All analysis and processing, including playback of image sequences, was carried out using Zen Blue software (Zeiss) and ImageJ with FIJI add-on. Cell responses were calculated using ImageJ with FIJI add on using a standard deviation of Z-stacked movie slices (Rueden *et al.*, 2017; Schindelin *et al.*, 2012). A minimum of 20 independent regions of interest were selected and mean grey value was calculated for each slice and corrected for background fluorescence. Traces were then analysed for area under the curve and statistically analysed using one-way ANOVA followed by Dunnetts analysis.

2.9 Western blot analysis

2.9.1 Sample preparation

The following is applicable to Chapter 3, except section 3.3.4 and Fig. 3.17. Cells were lysed in 6-well plates using 200µl RIPA buffer (G Bioscience, VWR, Pennsylvania, United States) supplemented with Protease Arrest inhibitor cocktail (G Bioscience, VWR) on ice and spun at 10,000 x g for 15 minutes. Lysates were quantified for protein concentration using bicinchoninic acid assay (BCA) (G Bioscience). Briefly, 25µl of lysate sample was added to a clear 96-well flat bottom plate in duplicate with a serial dilution set of standards (bovine serum albumin (BSA) (2mg ml^{-1}-15.625µg ml^{-1})) prepared in cell lysis buffer. Then, 200µl of

working solution was added to each well, prepared with BCA solution and copper solution in a 50:1 ratio. the plate was incubated at 37°C for 30 minutes. The plate was then cooled to room temperature and read at 562nm on Tecan Pro 200 plate reader (Tecan, Männedorf, Switzerland). Following quantification, the lysates were diluted in 2X Laemmli buffer (10% glycerol, 2% sodium dodecyl sulphate (SDS), 50 mM Tris-HCl pH 6.8, 5 mM ethylenediaminotetraactic acid (EDTA), 0.008% bromophenol blue and 5% β-mercaptoethanol) and heated at 80°C for 10 minutes. The samples were spun at 16,000 *x g* for 10 minutes and stored at -80°C or used immediately.

The following is applicable to section 3.3.4 (and Fig. 3.17), Chapter 4 and 5. Cells were lysed in T25 flasks using 500-1000µl 1X cell lysis buffer (New England Biolabs) containing a final concentration of 10mM phenylmethylsulfonyl fluoride (PMSF) (made in isopropanol fresh each time). Cells were lysed on ice for 5 minutes, scraped from the flask and sonicated for 5 cycles. The samples were then spun at 14,000 *x g* for 10 minutes at 4°C and stored at -80°C. Lysates were quantified as above and diluted in 4X Laemmli buffer (40% glycerol, 240mM Tris HCl pH 6.8, 8% SDS, 0.04% bromophenol blue and 5% β-mercaptoethanol) and prepared as described above.

2.9.2 Sodium Dodecyl Sulphate Polyacrylamide Gel Electrophoresis (SDS-PAGE)

Lysates were loaded with sufficient protein (20-50µg, final concentration stated for every experiment in each chapter) into wells and separated using either 10% SDS-polyacrylamide gel Next Gel solution (Next Gel, VWR) throughout Chapter 3 (except 3.3.4 and Fig. 3.17) or in-house prepared 10% SDS polyacrylamide gel throughout from section 3.3.4 (and Fig. 3.17) onwards, using a BioRad electrophoresis system, as shown in Table 2.6. The gel was run in a vertical gel electrophoresis unit in electrode buffer composed of 25mM Tris base, 192 mM glycine and 0.1% SDS. For NextGel solution gels lysates were separated at 200V for approximately 90 minutes. For traditional SDS-PAGE gels, lysates were separated at 120V for 90-120 minutes.

Table 2.6. ***Chemicals used to make SDS polyacrylamide gel****.*

3% Stacking Gel	10% SDS polyacrylamide Gel
3% (30% 37.5:1) acrylamide/bis	10% (30% 37.5:1) acrylamide/bis
Stacking gel buffer, 0.5M tris base pH 6.8	Resolving gel buffer, 1.5M tris base pH 8.8
0.1% SDS	0.1% SDS
0.08% ammonia persulphate	0.05% ammonia persulphate
0.12% TEMED	0.033% TEMED
Deionised water	Deionised water

2.9.3 Transfer

The proteins were then transferred from the SDS-polyacrylamide gel to a polyvinylidene fluoride (PVDF) membrane (Bio-Rad) using Bio-Rad Trans-Blot® Turbo transfer system and midi sandwich membranes at 25V for 10 minutes in a semi-dry system. The PVDF membrane was then incubated in TBS containing 5% non-fat milk solution for at least 1 hour.

2.9.4 Antibody probing and visualisation

The following is applicable to Chapter 3, except section 3.3.4 and Fig. 3.17. The PVDF membrane was washed for 5 minutes three times with 1X PBS-tween 20 (0.1%) before incubation overnight at 4^{o}C with primary antibody in 1X PBS-T (0.1%) containing milk (5%). Primary antibodies were rabbit anti-TRPV1 (1:400), mouse anti-TRPA1 (1:400), rabbit anti-TRPV4 (1:400), rabbit anti-P2X3 (1:400) and mouse anti-α-tubulin, all primary antibodies were purchased from SCBT. Membranes were washed for 5 minutes three times with 1X PBS-T and incubated with corresponding horseradish peroxidase (HRP)-conjugated secondary antibodies (1:7000) at RT for one hour. Membranes were washed a further 3 times with 1X PBS-T and visualised using ECL (Bio-Rad) detection in Bio-Rad Versa Doc under Chemi-ultra sensitive.

From section 3.3.4 (and Fig. 3.17) onwards, PVDF membranes were washed for 5 minutes three times with 1X TBS-T (0.1%) before incubation overnight at 4^{o}C with primary antibody in 1x TBS-T (0.1%) containing BSA (2%). Primary antibodies were rabbit anti-TRPV4 (1:500) (Abcam, Cambridge, UK), rabbit anti-MLC total (1:1000), mouse anti-phospho-MLC (ser19)

(1:1000), mouse anti-pannexin-1 (1:500) and mouse anti-alpha tubulin (1:400). Membranes were washed for 5 minutes three times in 1X TBS-T (0.1%) and incubated with corresponding Licor fluorescent secondary antibodies (1:15000) (Licor, Nebraska, United States) at RT for one hour in the dark. Membranes were washed for 5 minutes three times in 1X TBS-T (0.1%) and visualised on Licor Odyssey CLx (Licor).

2.9.5 Visualisation

For Chapter 3 except section 3.3.4 and Fig. 3.17, membranes were visualised under Chemi ultra-sensitive with flat fielding on the Bio-Rad Versa Doc.

For section 3.3.4 (and Fig. 3.17) onwards, membranes were visualised using Licor Odyssey CLx (Licor) following manufacturer pre-set western auto in channel setting with channels 700 and 800 specific for Licor secondary antibody wavelengths.

2.9.6 Western blot analysis

To quantify western blot data, images were analysed using densitometry of visualised bands using ImageJ software (Rueden *et al.*, 2017). The relative density was calculated as 'percentage of total band area relative to control'. Each individual relative density was adjusted to each corresponding internal loading control α-tubulin. Data was analysed and represented as fold change from control where 1 = baseline. Where applicable, bands were repositioned in order to tally with the order of data on corresponding graphs. All bands come from the same blot. Fold change data was statistically analysed using either two-way ANOVA followed by Tukey analysis or one-way ANOVA followed by either Sidak or Dunnetts analysis, where appropriate.

2.10 Enzyme-linked immunosorbent assay (ELISA)

Levels of IL-8 were measured in supernatants of wild type A549, P2X3 transfected 1321N1 and cells exposed to RV-16. Measurements were made using a commercially available paired antibody kit (Biolegend) and carried out according to manufacturer protocols. The sensitivity of the paired antibodies was 8pg ml^{-1} for IL-8. Plates were read and measured using plate reader at 450 nm.

The day before assay NUNC Maxisorp™ (Thermo Scientific) 96-well plates were coated in 100µl of Capture Antibody diluted 1:200 in 1X Coating Buffer A. The plates were sealed and incubated overnight at 4^{o}C. The antibody was discarded and washed 4 times with 1X PBS-T (0.05%). The plates were blocked with 1X Assay Diluent A for 1 hour at room temperature with 500 rpm agitation. The plates were washed 4 times with 1X PBS-T (0.05%) and 100µl of neat culture sample were added to each well. The plates were sealed and incubated at room temperature for 2 hours with 500 rpm agitation. The plates were washed 4 times with 1X PBS-T (0.05%) and 100µl of Detection Antibody diluted 1:200 in Assay Diluent A was added to each well, the plates were sealed and incubated for 1 hour at room temperature with 500 rpm agitation. The plates were then washed 4 times with 1X PBS-T (0.05%) and 100µl of Avidin-HRP solution diluted 1:1000 in Assay Diluent A was added to each well. The plates were sealed and incubated at room temperature for 30 minutes with 500 rpm agitation. The plates were washed 5 times with 1X PBS-T (0.05%), then, 100µl of Substrate Solution C was added to each well and incubated in the dark for 15 minutes checking for a blue colour change. Finally, the reaction was stopped with the addition of 100µl 2N sulphuric acid (Stop Solution) to each well checking for a positive yellow colour change. The plates were read at 450 nm within 15 minutes of addition.

2.11 ATP determination

2.11.1 Extracellular ATP determination through supernatant sampling

Extracellular ATP levels was measured in two different ways. In the first method, extracellular ATP levels were measured on cell culture supernatants exposed to RV-16 MOI 1 over a period of up to 72 hours using ATP determination kit, as per manufacturer protocol. Briefly, 100µl of 1X reaction buffer (8.9ml dH_2O, 0.5ml 20X Reaction Buffer, 0.1ml 100mM dithiothreitol (DTT), 0.5ml 10mM D-luciferin and 2.5µl 5mg ml^{-1} firefly luciferase) was added to each well of a 96-well plate, the reaction was started upon the addition of standard or sample, making up no more than 10% of the total reaction volume. Samples were assayed in duplicated and luminescence was read 3 times using a Tecan Pro 200 plate reader. Values were standardised to background luminescence and averaged from 3 readings. ATP concentration of each sample was determined using a standard curved constructed at the time of each experiment.

2.11.2 Intracellular ATP determination

Intracellular ATP levels were measured on A549 cells exposed to RV-16 at MOI 1 for up to 168 hours using luminescence ATP detection assay kit (Abcam) as per manufacturer protocol. Briefly, cells were seeded in an uncoated flat clear bottom 96-well white plate at a density of 5 x 10^4 cells per well. Cells were incubated at 37 ^oC, 5% CO_2 for 16-24 hours prior to commencement of RV-16 infections. All work was carried out in subdued lighting or in the dark. At the end of the time course 50µl of Abcam supplied detergent was added to each well and the plate was shaken at 650 rpm on an orbital shaker in the dark for 5 minutes. Then 50µl of substrate solution was added to each well and the plate was shaken for a further 5 minutes at 650 rpm in the dark. The plate was then dark adapted for 10 minutes to ensure minimal background from the plate, and luminescence was measured. Measurements were assayed in duplicate and plates read three times using a Tecan Pro 200 plate reader. Values were standardised to background luminescence and the ATP concentration was quantified in each sample using a standard curved constructed at the time of each experiment.

2.12 pH measurements

Cell culture supernatants harvested from time course experiments of RV-16 MOI 1 were assayed for any change in pH over the duration of the experiment. Briefly, aliquots of supernatants previously obtained, as described in 2.4 and 2.5.3, were thawed from -80^oC and the pH was measured using Hanna HI-2210-02 pH meter (Hanna Instruments, Rhode Island, United States). Measurements were taken at room temperature three times from three independent experiments and averaged.

2.13 Hypotonic stimulus assays

A549 cells (75 cm^2 flask at 70-80% confluence) were lifted with cell dissociation buffer and washed by centrifugation with 1X PBS. The cells were resuspended in 1ml 1X PBS and seeded at a density of 4.5 x 10^5 in 25 cm^2 flasks and incubated for 16-24 hours at 37 ^oC, 5% CO_2 to adhere. Growth media was removed, and cells were washed in 1X PBS before addition of HBSS containing 10mM HEPES (HBSS+) and allowed to equilibrate at 37^oC and

5% CO_2 for 1 hour prior to use. Cells where then incubated with HC067047, H-1152, ML-7, carbenoxolone, vehicle control or no inhibitor in HBSS+ at 37^oC and 5% CO_2 for up to 45 minutes. The cells were then washed with 1X PBS and exposed to 33% hypotonicity or isotonic control for 5 minutes. The cells responses to hypotonic stress were then investigated by calcium signalling and calcium imaging (see section 2.8), western blotting (see section 2.9), ATP release (see section 2.11) and immunofluorescence microscopy (see section 2.14).

2.14 Immunofluorescence microscopy

A549 cells were grown to 70-80% confluence and seeded on to 13 mm (thickness number 1) coverslips, previously cleaned in 70% ethanol and UV sterilised, in a flat bottom 24-well plate at various densities depending on downstream experimentation. Cells were grown in supplemented DMEM growth media for up to 48 hours prior to experimentation at 37^oC with 5% CO_2. The cells were then exposed to RV-16 as described in 2.5.3 or washed twice with 1X PBS then incubated in HBSS+ buffer and allowed to equilibrate for up to 1 hour and exposed to hypotonic stimulus as described in 2.13.

To commence the tri-colour immunofluorescence processing the cells were fixed by incubation with 4% formaldehyde in 1X PBS for 15 minutes at room temperature. The cells were washed three times with 1X PBS and permeabilised with 0.1% Triton X-100 (in 1X PBS) for 10 minutes. The cells were washed three times in 1X PBS again and incubated with 2% BSA in 1X PBS for 1 hour at room temperature to block the coverslip. The cells were washed three times with 1X PBS and incubated with unconjugated primary antibody, monoclonal mouse anti-pannexin-1 (1:200, SCBT) for 1 hour at room temperature or 4^oC overnight. The cells were washed 3 times in 1X PBS again and incubated with fluorescein (FITC) conjugated secondary antibody, mouse IgG kappa chain (1:100, SCBT) for 1 hour at room temperature. The cells were washed 3 times with 1X PBS again and stained with phalloidin CruzFluor™ 594 conjugate stain (1:1000, SCBT) for 1 hour at room temperature. Finally, the cells were washed 3 times with 1X PBS and the coverslips were mounted on to microscope slides using Prolong™ Diamond antifade mounting media containing DAPI for nuclear staining. The coverslips were visualised using Zeiss Axio Observer.Z1 inverted microscope and the images

were captured and processed with Zen Blue pro image acquisition software. Exposure times were determined at the beginning of imaging and remained unchanged through imaging of each experiment to keep conditions consistent.

2.15 Generation of GFP-tagged TRPV4 stably expressing cell line

2.15.1 Bacterial transformation

Competent *E. coli* cells (XL10-Gold® ultracompetent) were thawed on ice before addition of 4µl XL10-Gold® β-mercaptoethanol mix to increase transformation efficiency. Cells were incubated on ice for 10 minutes with gentle agitation every two minutes.

The *E. coli* cells were further incubated on ice for 30 minutes with 100ng μl^{-1} TRPV4 DNA pCMV6-GFP tagged vector. The *E. coli* cell mixture was heat shocked in a 42°C heating block for 30 seconds before a further two minutes on ice. Pre-warmed (500 µl at 42°C) SOB broth was then added to the *E. coli,* the mixture was then incubated for 1 hour at 37°C with agitation (225-250 rpm). The *E. coli* was then plated on LB agar plates containing 100µg ml^{-1} ampicillin and placed upside down in an incubator at 37°C overnight.

2.15.2 Expression of GFP tagged TRPV4 DNA in transformed *E. coli.*

To verify expression of GFP-tagged TRPV4 DNA in transformed *E. coli*, 10 individual colonies were selected from an agar plate grown overnight using a 200µL pipette tip. The colonies were deposited in PCR tubes and the tips were placed in 20ml tubes containing SOB broth and 100µg ml^{-1} ampicillin. The 20ml tubes were then incubated overnight at 37°C in an incubator shaker at 250 rpm to allow for expansion of colonies and to obtain high-copy plasmids. The colonies in PCR tubes, were amplified with DreamTaq PCR master mix by thermal cycling, conditions and reaction mixture as previously described 2.6.4 (Table 2.5 and 2.4, respectively). A positive and negative control (containing plasmid DNA or no colony, respectively) were used. The amplified product was analysed by gel electrophoresis, as described in 2.7.

2.15.3 Plasmid DNA purification and quantification

Plasmid DNA was isolated from *E. coli* grown overnight in SOB broth containing 100µg ml^{-1} ampicillin using NucleoSpin® Plasmid DNA purification miniprep kit according to

manufacturer protocol. Briefly, *E. coli* from saturated SOB broth was pelleted at 11,000 x *g* for 30 seconds. *E. coli* was resuspended in 250µl A1 buffer, followed by a 5 minute incubation at room temperature and lysis in 250µl A2 buffer. Finally, *E. coli* was sheared in 300µl A3 buffer. The lysate was clarified through centrifugation at 11,000 x *g* for 5 minutes. The supernatant was loaded to a hi-bind membrane and spun at 11,000 x *g* for 1 minute. The membrane was washed in 450µl AQ buffer and spun for a further 3 minutes at 11,000 x *g*. The membrane was dried through centrifugation at 11,000 x *g* for 3 minutes. Finally, the dsDNA was eluted in 50µl AE buffer following a 1-minute incubation at room temperature and spun at 11,000 x *g* for 1 further minute. The eluted dsDNA was quantified on the NanoDrop spectrophotometer. Absorbance of samples was measured at 260 nm in triplicate.

2.15.4 Restriction digest of TRPV4 pCMV6-GFP tagged vector

The plasmid dsDNA obtained from the plasmid purification step, as described in 2.15.3, were digested with BamH1 and Xho1 restriction enzymes (New England Bioscience (NEB)) to produce a linear vector and reveal 'sticky end' restriction sites of BamH1 and Xho1 to produce a 2664 and 6536 base pair digests from the plasmid. A double digest was performed as both restriction enzymes required the same incubation temperature and digest buffer. A 20µl reaction mixture containing 5µl plasmid DNA sample, 1mg ml^{-1} BSA, NEB buffer 2, DEPC water and 10U of restriction enzymes BamH1 and Xho1 was incubated for 1 hour at 37^{o}C. A negative control was made for each restriction digest containing all products except restriction enzymes. The restriction digest product was analysed by gel electrophoresis, as described in 2.7.

2.15.5 Generation of stable GFP-tagged TRPV4 A549 cell line

Low passage number A549 cells were grown to 50-80% confluence in a 35 mm petri dish in supplemented DMEM (10% v/v FCS, 1% v/v 100 U ml^{-1} Penicillin- 100 U ml^{-1} Streptomycin, 1% v/v 2mM L-glutamine). On the day of transfection, the culture medium was replaced with 2ml Opti-MEM® (1X) Reduced Serum Medium (Gibco, Life Technologies™). The transfection reagent was prepared in a polystyrene tube containing FuGENE® 6 Transfection Reagent and 157µl Opti-MEM at room temperature and incubated for 5 minutes. At a ratio of 3:1, DNA was added, mixed and incubated for a further 15 minutes at room temperature. The transfection mixture was transferred to the petri-dish containing

cells and incubated at 37°C, 5% CO_2 for 24 hours in a further 2ml Opti-MEM® (1X) Reduced Serum Medium.

The transfection mixture was removed and replaced with complete DMEM and incubated for a further 24 hours at 37°C, 5% CO_2. The media was then replaced once more with fresh complete DMEM containing 0.7mg ml^{-1} G418 (as determined by a kill curve explained in Chapter 5) and incubated for a further 48 hours to allow for G418 selection of A549 transfected cells containing the G418 resistance gene. The culture medium was replaced frequently to remove debris and cellular metabolites and maintain G418 concentration. Once cells became sufficiently confluent they were transferred to at T25 or T75, as appropriate and maintained for 7-14 days in selective G418 DMEM media. The transfected cells were then single cell cloned.

2.15.6 Single cell cloning

The transfected A549 cells were single cell cloned by serial dilution in a flat bottom 96-well plate as per Corning's recommended protocol. Briefly, transfected cells were lifted from culture with HBSE cell dissociation buffer and spun for 5 minutes at 300 *x g*. The cell pellet was resuspended at 1 x 10^5 cells ml^{-1} in supplemented DMEM containing 0.7mg ml^{-1} G418. 100µl of supplemented DMEM containing G418 culture media was added to each well of the 96-well plate and 200µl of cell suspension was added to A1 of the 96-well plate. The cell suspension was diluted 1:2 down the column A1-H1, then using the same pipette tips with a multichannel pipette the cell suspension was further serially diluted 1:2 between each column across the whole plate (Fig. 2.1). 100µl fresh supplemented DMEM containing 0.7mg ml^{-1} G418 was added to each well to make a total volume of 200µl in each well. The plates were set up in duplicate and left for 7-10 days in a 37°C incubator with 5% CO_2.

On day seven, each well was visualised by a light microscopy and wells containing single colonies were marked and allow to expand for a further 3-5 days. After this time the monoclonal cells were transferred in to a T25 cell culture flask containing 0.7mg ml^{-1} DMEM culture media and incubated for a further 7 days at 37°C with 5% CO_2.

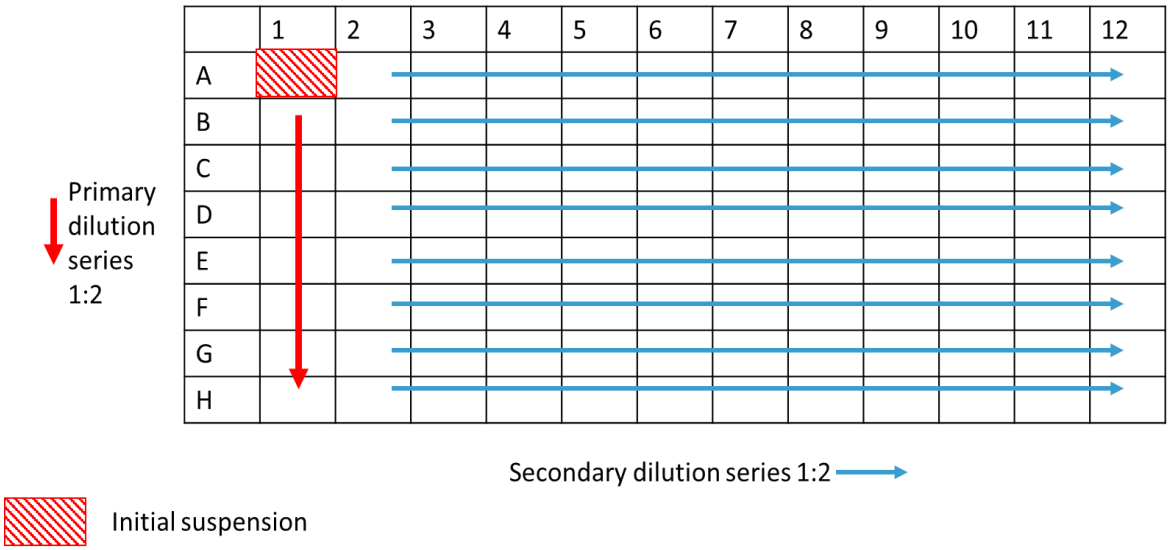

Figure 2.1. ***Diagrammatic representation of single cell cloning serial dilution plate layout.*** *A1 contained initial cell suspension. A1-H1 contained the primary serial dilution of cell suspension. A2-A12 through H2-H12 contained the secondary serial dilution of the initial cell suspension.*

2.15.7 Confirmation of positive TRPV4 transfection with flow cytometry, intracellular calcium signalling and fluorescent microscopy analysis

Once the monoclonal transfected A549 cells had achieved 80-90% confluence they were passaged and initially screened for positive expression of GFP tag to assess global expression of the receptor using flow cytometry. Cells were harvested using HBSE buffer and pelleted by centrifugation for 5 minutes at 300 x *g*. Cell pellets were re-suspended at $1x10^6$ ml^{-1} in 1% BSA in 1X PBS and kept on ice. Cell suspensions were analysed using BD FACSCalibur™ flow cytometer (BD Bioscience, New Jersey, United States) and an argon laser (wavelength 488 nm suitable for excitation of FITC) and captured with BD CellQuest™ Pro Software. Wild type A549 cells were used as control for initially gating for basal auto-fluorescence, size and granularity. Following positive expression of GFP-tag, monoclonal expansions were screened for positive overexpression of TRPV4 using standard potent agonists (GSK1016790A and 4αPDD) by intracellular calcium signalling as described in 2.8.2. Responses were compared to non-transfected A549 cells to determine that TRPV4 was overexpressed in comparison to endogenous expression found in wild type A549 cells. The

transfected cells were also screened for positive expression of GFP protein (bound to transfected TRPV4 protein) using immunofluorescent microscopy as described in 2.14.

2.16 Seahorse analysis of basal and stress cellular metabolism

Cells were seeded in an 8-well Seahorse Bioscience cell culture cartridge at a density required for $4x10^4$ cells per well on the day of experimentation. Cells were treated with RV-16 at MOI 1 as detailed in section 2.5.3. The night before experimentation, an 8-well sensor cartridge was hydrated as per manufacturer protocol ensuring the sensors were fully submerged and incubated at 37°C overnight in a humidified non-CO_2 incubator. One hour prior to running the assay, the sensor cartridge fluid was replaced with 37°C pre-warmed Seahorse calibrant and de-gassed in a 37°C non-CO_2 incubator. One hour prior to running the assay the cell culture plate was washed with 1X PBS and replaced with in-house prepared modified assay media (0.8mM $MgSO_4$, 1.8mM $CaCl_2$, 143mM NaCl, 5.4mM KCl, 0.91mM NaH_2PO_4, 10mM glucose, 1mM pyruvate, 2mM glutamine, pH 7.4) and de-gassed in a 37°C non-CO_2 incubator. Inhibitors were freshly prepared at 10X the required concentration in assay media from stock aliquots dissolved in ethanol. Drug injector ports were loaded with relevant inhibitors (1µM oligomycin, 1µM FCCP, 0.5µM Rotenone/Antimycin and 50mM 2-DG). The sensor cartridge was placed in the Seahorse XFp machine and calibrated for 15-20 minutes prior to loading the cell culture plate and running the assay with a 5-minute initial wait period, followed by 3 cycles of non-mixing, 3-minute wait and measure cycles with 4 injections for approximately 2 hours. Oxygen consumption (OCR) and extracellular acidification rates (ECAR) were measured for the duration of the assay. Data was analysed and displayed using GraphPad Prism.

2.17 Statistical analysis

Unless otherwise stated, data are expressed as the mean of at least three independent experiments $\pm$ S.E.M. Where appropriate data were analysed using two-way analysis of variance (ANOVA) followed by Tukey post hoc test for multiple comparisons of groups. ATP sampling experiments were analysed with one-way ANOVA followed by Dunnett's for multiple comparisons to a control. Western blot data was analysed with either two-way

ANOVA followed by Tukey or one-way ANOVA followed by either Sidak or Dunnetts, where appropriate. Paired and unpaired t-tests were carried out between an individual condition and control in Chapter 5 on some sampling experiments, stated in the text. A *P* value less than 0.05 was used as statistically significant, exact P values are stated where possible.

Chapter 3

TRP Channel and P2XR Expression in Response to Synthetic Stimuli Poly(I:C) and RV-16

The effect of rhinovirus on polymodal nociceptors TRPA1, V1, M8 and V4 has not been fully explored or understood. Presently, the only published data describing the effect of different MOI of RV-16 on thermo-TRP channels has been released by Abdullah *et al.* (2014). Whilst the interest regarding the role of P2XR and cough is rapidly growing, no-one has yet explored the relationship between RV-16 and P2X3. We hope to explore this and also show, for the first time, that RV-16 is able to infect neuronal cell line 1321N1 (transfected with P2X3 receptor). A paper by Qi *et al.* (2011) found TLR ligands, including poly(I:C), has the ability to induce the upregulation of TRPV1 in DRG neurons whilst looking at the effects of neuronal pain. Despite the clear effect URTI has on the tussive response, this finding has not been followed up. We aim to show and confirm this in respiratory A549 and neuronal 1321N1 cell lines.

A549 cells are used extensively in respiratory research including work with RV (Wang, Kim & Jang, 2009; Jang, Kwon & Lee, 2006; Konno *et al.*, 2002; Papi & Johnston, 1999) and studying TRP channels (Büch *et al.*, 2013; Nassini *et al.*, 2012; Mukhopadhyay *et al.*, 2011; Seminario-Vidal *et al.*, 2011; Sidhaye *et al.*, 2006; Reilly *et al.*, 2003). Their extensive history makes them a reliable source to work with, but full cell line characterisation is required to determine endogenous baseline levels of expression and function.

As part of the rhinovirus lifecycle a double stranded RNA (dsRNA) structure is formed, so to study the effects on TRP channels and P2XR from an actively replicating infection a synthetic dsRNA stimulus and TLR3 agonist, poly(I:C) was used. Data using poly(I:C) is useful for determining whether TRP channel and P2XR alteration is due to an actively replicating virus, the sole attachment and entry, or soluble factors from various forms of virus and controls. Each helping to narrow down a potential mechanism starting point.

3.1 Approach and methodology

The purpose of this chapter was study to effect of synthetic viral analogue poly(I:C) and human rhinovirus-16 on thermo-TRP channel and P2X3 receptor expression in airway alveolar epithelial (A549) and neuronal astrocytoma cell lines (P2X3 transfected 1321N1). To carry this out we first characterised our chosen cell lines for endogenous expression of our proteins of interest TRPA1, TRPV1, TRPV4 and P2X3. Then, a series of optimisation

experiments were carried out to determine optimal time points for time courses and to optimise protocols including work to determine that our chosen cell lines were suitable candidates for infection with RV-16.

A549 cells are known to express TRPA1, TRPV1 and TRPV4 (Büch *et al.*, 2013; Nassini *et al.*, 2012; Mukhopadhyay *et al.*, 2011; Seminario-Vidal *et al.*, 2011; Sidhaye *et al.*, 2006; Reilly *et al.*, 2003) and this will be confirmed by us. Both A549 and 1321N1 cell lines are also known to express functional TLR2, 3 and 7 (Sequeira, Senaratne & Riley, 2014; Cherfils-Vicini *et al.*, 2010; Wang, Kim & Jang, 2009; Farina *et al.*, 2005; Olson & Miller, 2004). Here we describe the cellular characterisation undertaken in A549, and wild type and transfected 1321N1 cell lines along with primary infection assays with poly(I:C) and RV-16. All cell lines will undergo several forms of characterisation to ensure the chosen cell lines express the necessary receptors as per published findings. These series of experiments will also provide the baseline measurements for which the stimulated cell line experiments will be compared against. For the characterisation stage, unless where stated otherwise, only wild type 1321N1 cells were used for ease of propagation and determining the presence of P2X7 receptor.

Expression of TRPA1, TRPV1, TRPV4, P2X2 and P2X3 was determined using RT-PCR for mRNA expression, and calcium signalling and western blotting for functional protein expression. The experiments were carried out using materials and procedures as described in detail in Chapter 2. The cell lines were then exposed to varying concentrations of poly(I:C). This was used to determine a suitable concentration with a minimal/acceptable level of cytotoxicity, through the use of the sulforhodamine B (SRB) assay, to ensure sufficient cell density was viable throughout the duration of the time course experiments. Using suitable concentrations as determined from the SRB assay the time points required for maximal retrieval of mRNA for PCR experiments was determined. The cell lines were stimulated with poly(I:C) and results compared for difference in mRNA transcription and protein expression.

3.1.1 Methods: PCR

RNA was isolated separately from unstimulated A549 cells and wild type 1321N1 cells, as described in section 2.6.2, the RNA was reverse transcribed in a thermal cycler to produce

cDNA as described in section 2.6.3. For cell line characterisation, both cell lines underwent end-point RT-PCR to determine endogenous expression of TRPA1, TRPV1, TRPV4, TRPM8, P2X2, P2X3 and P2X7 with endogenous control β-actin using primers designed in-house and conditions described in section 2.6.1 and section 2.6.4, respectively. For time course experiments, each time point sample was subjected to end-point RT-PCR for expression of TRPA1, TRPV1, TRPV4 and P2X3 with endogenous and loading control β-actin under the same conditions used previously.

The reverse transcribed end-product was separated on a 1.3% agarose gel for 45 minutes at 100V and visualised on Bio-Rad Versa Doc, as described in section 2.7.

3.1.2 Methods: Calcium signalling

Intracellular calcium signalling measurements were performed as described in section 2.8. Briefly, cells in suspension (initial cell line characterisation) were loaded with 10μg Fluo-3 AM or cells adhered in microwell plates were loaded with Fluo-4 AM (direct no wash) calcium probes. Intracellular calcium flux was measured using a fluorospectrometer with excitation wavelength 480 nm and emission wavelength 530 nm for Fluo-3 AM or excitation 494 nm and emission 525 nm for Fluo-4. For cell line characterisation, concentration-effect curves were constructed for capsaicin, allyl isothiocyanate, GSK1016790A and ATP by addition of increasing half log concentration increments of agonists to cells. EC_{50} values were calculated for each agonist which displayed a positive response. For time course experiments, the EC_{50} values were used to stimulate intracellular calcium flux. Cell responses were calculated for each cuvette or microwell where baseline (pre-agonist addition) was subtracted from peak fluorescence (post-agonist addition) and overall response expressed as percentage of positive control A23187 as described in section 2.8.1, equation 2.

3.1.3 Methods: Western blot

Western blot analysis carried out in sections 3.2, 3.3.1, 3.3.2 and 3.3.3 (except Fig. 3.17) were undertaken as follows. Cells were seeded at $5x10^5$ into 6 well plates and allowed to adhere overnight prior to commencement of poly(I:C) or RV-16 stimulation time course, as described in section 2.4 and section 2.5.3. Cells were lysed and harvested in 1X RIPA buffer containing anti-proteases and pelleted by centrifugation at 10,000 *x g* for 15 minutes at

4°C. The supernatants were recovered, quantified as described in section 2.9 and diluted to load in 2X Laemmli's buffer and heated at 80°C for 10 minutes. The samples were spun at 16,000 *x g* for 10 minutes and stored at -80°C or used immediately.

The prepared lysates were separated on a 10% SDS-PAGE Next Gel® solution gel and proteins were transferred to PVDF membrane.

The PVDF membranes were blocked in 5% milk solution for 1 hour then incubated overnight at 4°C with primary antibody raised to TRPV1, TRPA1, TRPV4, P2X3 or α-tubulin diluted to 1:400 in 1X PBS-T (0.1%) containing 5% milk. The membranes were then incubated for 1 hour at room temperature with either goat anti-mouse or goat anti-rabbit HRP conjugated secondary antibodies diluted to 1:7000 in 1X PBS-T (0.1%) containing 5% milk before analysis by ECL detection system on Versa Doc followed by densitometry analysis as described in section 2.9.5 and section 2.9.6, respectively. Initial experiments were carried out stripping the membranes with gentle stripping buffer, and re-probing as described. This process eliminated further detectable signals so thereafter all blots were run in duplicate and probed sequentially ensuring there was no overlap in probed molecular weights.

Western blot analysis carried out in section 3.3.4 and Figure 3.17 in section 3.3.3 were undertaken as follows. Cells were seeded at $4.5x10^5$ into T25 flasks and allowed to adhere overnight prior to commencement of RV-16 infections at MOI 1, as described in section 2.5, with hypotonic stimulation assays, as described in section 2.13. Cells were infected for up to 168 hours and either lysed and harvested in 1X cell lysis buffer containing 10mM PMSF and pelleted by centrifugation at 14,000 *x g* for 10 minutes at 4°C, or stimulated with hypotonic stimulus, as described in section 2.13, followed by lysis as described above. The supernatants were recovered, quantified as described in section 2.9.1 and diluted in 4X Laemmli's buffer to 50µg protein and heated at 80°C for 10 minutes. The samples were spun at 16,000 *x g* for 10 minutes and stored at -80°C or used immediately.

The prepared lysates were separated on a 10% SDS-PAGE gel (see section 2.9.2) and proteins were transferred to a PVDF membrane.

The PVDF membranes were blocked in 5% milk solution (1X TBS) for 1 hour then incubated overnight at 4°C with primary antibody raised to TRPV4 (1:500) or α-tubulin (1:500) in 1X TBS-T (0.1%) containing 2% BSA. The proteins were then visualised by incubation for 1 hour

at room temperature with either goat anti-mouse or goat anti-rabbit Licor fluorescent secondary antibodies diluted to 1:15000 in 1X TBS-T (0.1%) containing 2% milk before analysis by Licor fluorescent scanning detection system on Licor Odyssey CLx followed by densitometry analysis as described in section 2.9.5 and section 2.9.6, respectively. Membranes were run in duplicate with sequential probing, to prevent loss of antigen as found during the course of western blotting in section 3.2, 3.3.1, 3.3.2 and 3.3.3.

3.1.4 Methods: ATP measurement

Supernatants from poly(I:C) and RV-16 stimulation experiments were sampled and assayed for extracellular ATP using a commercially available kit as described in section 2.11.1.1. Concentrations of ATP were quantified using a standard curve.

3.1.5 Methods: pH measurement

Supernatants from poly(I:C) and RV-16 stimulation experiments were sampled, and pH measurements were taken as described in section 2.12.

3.1.6 Methods: Enzyme linked immunosorbent assays

Supernatants from RV-16 stimulation experiments were sampled and assayed for TNF-α and IL-8 concentration using a commercially available colorimetric kit as described in section 2.10. Concentrations of cytokines were quantified using a standard curve.

3.2 Optimisation

3.2.1 Calcium signalling

In the first system, PTI spectrofluorometer, none of the cell lines were suitable for long periods of time in suspension. Within a short period of time (<5 minutes) cells had begun to clump and due to the nature of the work to be carried out, calcium chelators to reduce aggregation of cells were unsuitable. With the addition of continual agitation (approximately 50 rpm) cell viability was marginally increased (5-10 minutes). System optimisation was conducted which included the addition of sulphinpyrazone to prevent dye leakage, a shorter incubation time (10-30 minutes) to prevent active efflux of the de-esterified Fluo-3 AM dye, a smaller cell density and shorter assay times reduced from 1 hour to 25 minutes. None of the alterations made a noticeable different. All other options required the addition of calcium chelators, unsuitable for calcium signalling assays. The decision was made to change the detection system to an ABI Flexstation. In this system cells adhered to plate bottoms and pharmacological agents are added to the well from above whilst plates are read from the bottom (Fig. 3.1). Ultimately, future assays were carried out using the ABI Flexstation.

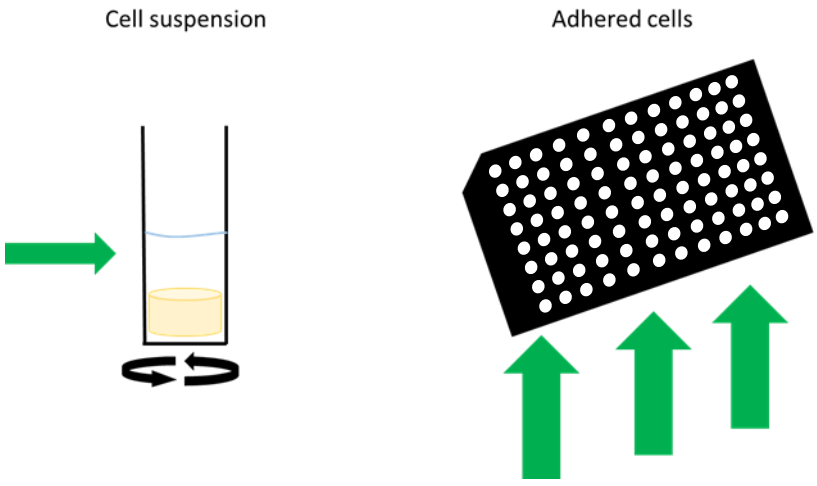

Figure 3.1 ***Comparison between calcium assay read systems****. Suspension systems (PTI spectrofluorometer) read through the cuvette whilst a magnetic flea keeps the cell in suspension. A microplate reader (ABI Flexstation) reads the plates from below, by row with a 1-second delay between wells. The microplate read system had great sensitivity for cells with a tendency to aggregate whist in suspension.*

3.2.2 Polyinosinic:polycytidylic acid

An SRB assay was carried out to assess the degree of cytotoxicity of stimulus poly(I:C) over a course of several days and at a range of concentrations. The recommended working concentration for poly(I:C) is between 10ng ml^{-1}-30µg ml^{-1} with an EC_{50} of 70 ±10ng ml^{-1}. Several papers which have used poly(I:C) and conducted dose responses noted very little change between 30µg ml^{-1} and higher concentrations (Dauletbaev *et al.*, 2015; Shin *et al.*, 2013; Kumar, Zhang & Yu, 2006). Therefore, the decision was made to use 10ng ml^{-1} -10µg ml^{-1} of poly(I:C) in the SRB assay. We carried out a sulforhodamine B (SRB) assay to determine the viability of cell line A549 and WT 1321N1 when stimulated with poly(I:C) at a range of concentrations over a 72-hour period (Fig. 3.2). Cell lines were grown in single culture and treated as they would in experiments, stimulus added and incubated at 37^{o}C, 5% CO_2 for the desired time. When compared to untreated cells, 10µg ml^{-1} maintained cell viability of 95.4% and 110% in A549 and WT 1321N1 cell lines, respectively (Fig. 3.2A and 3.2B, respectively).

To ensure a response could be obtained from this range of concentrations, a time course using only a cell viable concentration was used and carried out over 3 days, as previously used. Using the data obtained from the poly(I:C) SRB assay (Fig. 3.2), 10µg ml^{-1} was chosen to be carried forward in future poly(I:C) stimulation experiments as it displayed minimal cellular toxicity with almost maximal cell viability in comparison to vehicle. Despite almost identical cellular viability of all tested concentrations of poly(I:C), 10µg ml^{-1} is likely to induce maximal change in gene expression whilst maintaining a sufficient cell number. To simultaneously pin point the time of mRNA transcription several time points were included, hourly increments between 1-6 hours then at 8, 24, 48 and 72 hours. RT-PCR was then performed, and the products were electrophoresed on a 1.3% agarose gel and visualised using BioRad Versa Doc imager (Fig. 3.3).

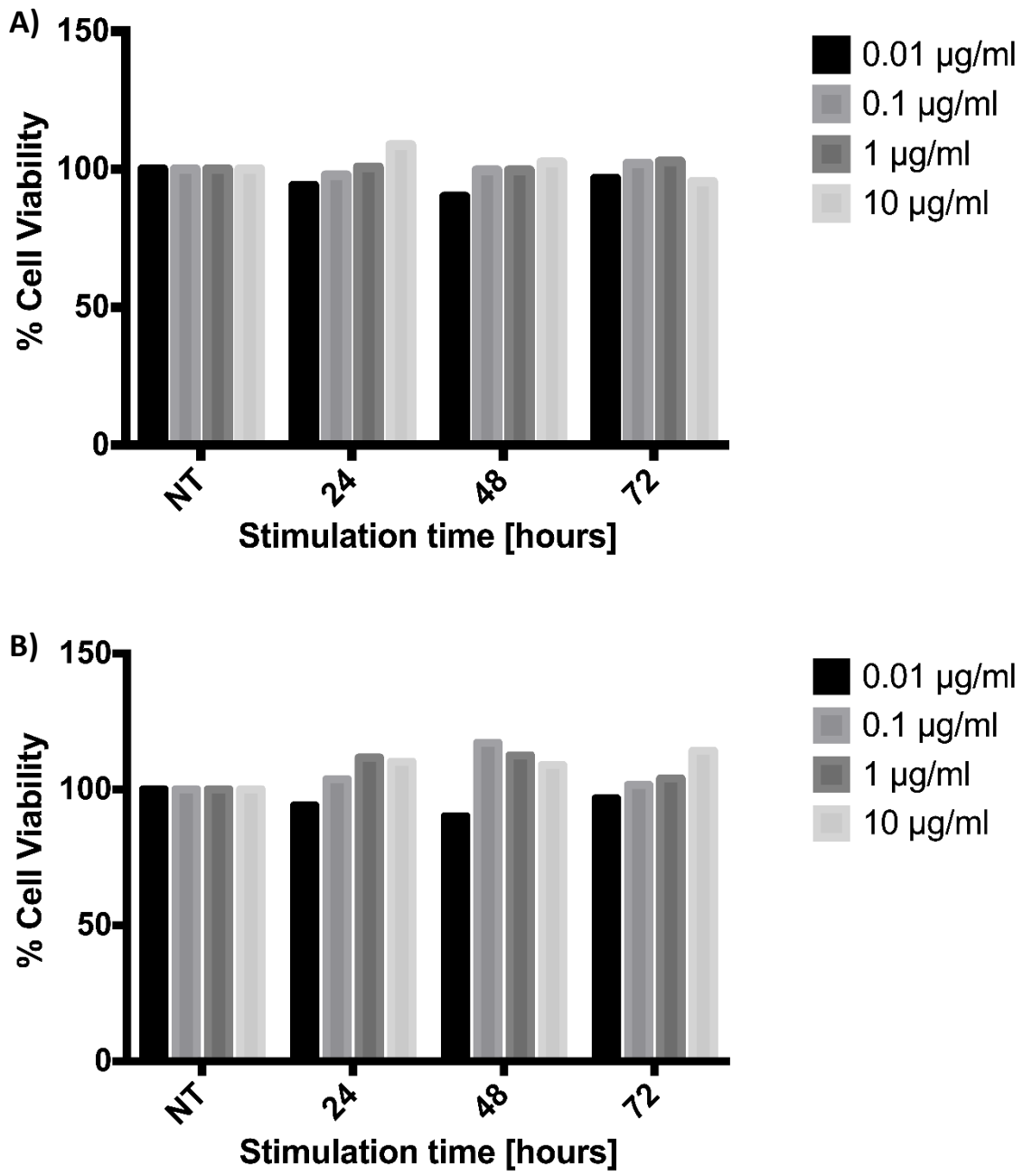

Figure 3.2. ***SRB assay of poly(I:C) on A549 and 1321N1 cell lines****. Percentage of A) A549 cells or B) wild type 1321N1 cells viable after 72-hour time course treated with variable concentrations of poly(I:C) (0.01-10µg ml^{-1}). Each treatment group was carried out in triplicate. Results standardised against 0.9% saline vehicle control (0.1-0.3% total volume of 0.9% (w/v) saline) then represented as percentage of untreated. Data is representative of n=2 therefore no error bars could be applied or statistical analysis carried out.*

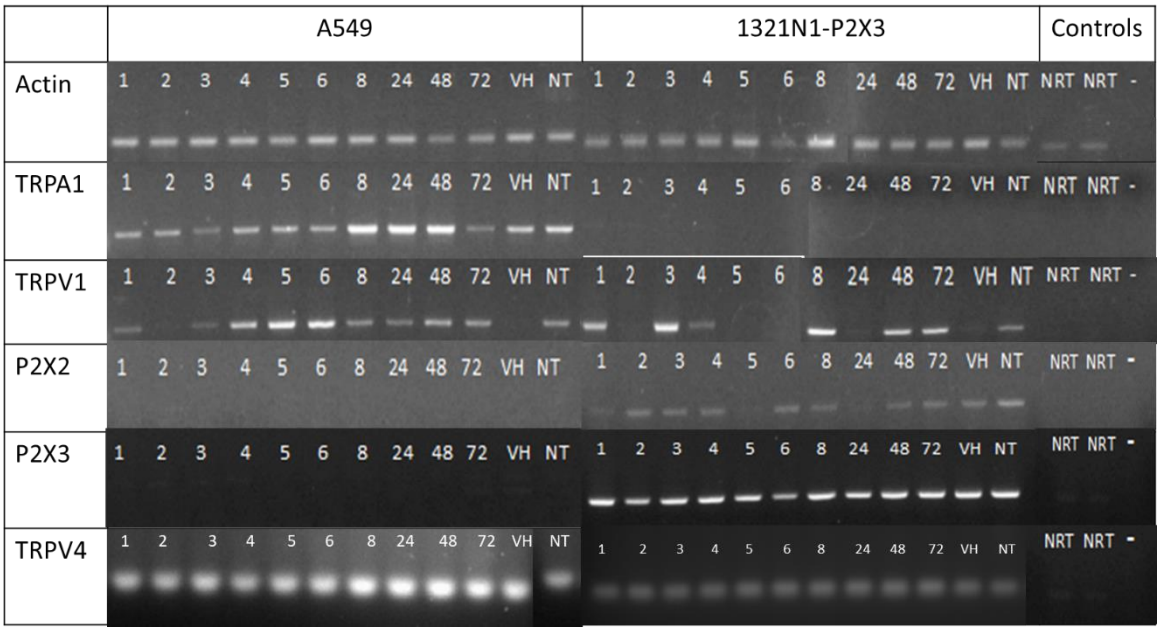

Figure 3.3. ***Representative data gel from poly(I:C) 10ug/mL time course*** *experiment to determine optimal time point for maximal upregulation of mRNA of the target gene. Controls listed were negative (-) control (no cDNA sample), no reverse transcriptase for A549 and 1321N1-P2X3 cell lines, respectively (NRT). Data shown is representative of two independent experiments (N=2).*

Poly(I:C) can be highly variable depending on manufacturer and method of production [unpublished observation, personal communication, 2018]. To account for this variability we carried out all our experiments using poly(I:C) from one manufacturer using the same batch.

3.2.3 Rhinovirus-16

Prior to undertaking optimisation work with RV-16 it was necessary to determine the titre of the viral stocks. This was carried out as per section 2.5.1. Briefly, an endpoint dilution assay was carried out on HeLa Ohio (highly permissible cell line to RV) which were seeded to produce a confluent monolayer in 96 well plates and infected with neat stock virus, or increasing log dilutions (Table 3.1) of neat stock to quantify to volume of virus required to kill 50% of inoculated culture cells over 3 days (Table 3.2), this is known as $TCID_{50}$.

Multiplicity of infection (MOI) is the term used to describe the ratio of virions to cells, whereby MOI 1 refers to 1 virion to 1 cell and MOI 10 means 10 virions to 1 cell. The general consensus for most viral infections, in particular rhinovirus, is to use MOI 1 as the standard

go-to concentration (personal communication, 2015). However, uses of MOI as high as 10 can be used in cases where the virus becomes inactivated over the course of the experiment and used as low as 0.1 where a high titre can be difficult to obtain. Subsequently, we decided to carry out an SRB assay to ascertain the degree of cytotoxicity of RV-16 and ensure sufficient cell survival for downstream applications over a course of several days at a range of MOI. Cell lines were grown and used in single culture. Infections for the SRB assay were carried out as they would in future experiments, where cells were incubated with the virus at room temperature for 1 hour with gentle agitation. The viral supernatant was aspirated, cells washed, and fresh media applied and incubated at 37°C, 5% CO_2 for the desired time. The recommended working MOI for RV-16 is MOI 1, however, data has been published using MOI ranging 0.001-50 (Papi *et al.*, 2013; Abdullah *et al.*, 2014; Schuler *et al.*, 2014; Rajan *et al.*, 2013; Oliver *et al.*, 2008; Chen *et al.*, 2006; Papadopoulos *et al.*, 2000; Johnston *et al.*, 1998; Reza Etemadi *et al.*, 2017). We carried out the SRB assay using only MOI 0.001, 0.01, 0.1 and 1 for up to 3 days. When compared to uninfected cells, MOI 1 was seen to maintain cell viability of 102% and 94% in A549 and WT 1321N1 cell lines, respectively, at 72 hours (Fig. 3.4). This MOI was deemed suitable for further applications.

Table 3.1. ***Endpoint dilution assay ($TCID_{50}$) plate set up****. Rows labelled A-H and columns labelled 1-12 as per standard 96 well plates. Columns 1 and 2 HeLa Ohio cells left uninfected. Columns 3-12 contain serial diluted stock virus inoculating Row A with neat virus stock, row B with a 1:10 dilution of stock, increasing the dilution 1:10 through each row C-H.*

<table>
<tr><th></th><th>1</th><th>2</th><th>3</th><th>4</th><th>5</th><th>6</th><th>7</th><th>8</th><th>9</th><th>10</th><th>11</th><th>12</th></tr>
<tr><td>A</td><td rowspan="8">Control – non-infected HeLa Ohio</td><td colspan="10">NEAT</td></tr>
<tr><td>B</td><td colspan="10">10^{-1}</td></tr>
<tr><td>C</td><td colspan="10">10^{-2}</td></tr>
<tr><td>D</td><td colspan="10">10^{-3}</td></tr>
<tr><td>E</td><td colspan="10">10^{-4}</td></tr>
<tr><td>F</td><td colspan="10">10^{-5}</td></tr>
<tr><td>G</td><td colspan="10">10^{-6}</td></tr>
<tr><td>H</td><td colspan="10">10^{-7}</td></tr>
</table>

Table 3.2. ***Example digitised $TCID_{50}$ sheet of HeLa Ohio cells*** *uninfected, inoculated with RV-16 neat stock or a serial dilution of RV-16 stock. Wells where all cells are dead or show signs of cytopathic effects (CPE) are marked 'X'. Wells where cells are all alive and show no signs of CPE are marked '-'. As Table 1, Columns 1 and 2 were not inoculated with virus and as expected, all cells were alive with no signs of CPE. Row A contained HeLa Ohio cells inoculated with neat stock virus, Row B-H (columns 3-12) contain increasing serial dilution of viral stock. As expected all cells in rows A-D were dead. As expected all cells in rows G and H showed no signs of CPE. The usual working range for RV-16 is $10^{-4} – 10^{-5}$, therefore rows E and F corresponding to those dilutions displayed mixed wells of alive cells and cells with signs of CPE after 3 days, read up to day 5, and used to determine the $TCID_{50}$ of the virus.*

	1	*2*	*3*	*4*	*5*	*6*	*7*	*8*	*9*	*10*	*11*	*12*
A	-	-	X	X	X	X	X	X	X	X	X	X
B	-	-	X	X	X	X	X	X	X	X	X	X
C	-	-	X	X	X	X	X	X	X	X	X	X
D	-	-	X	X	X	X	X	X	X	X	X	X
E	-	-	-	-	X	-	X	-	X	X	X	X
F	-	-	X	-	-	X	-	-	-	-	-	-
G	-	-	-	-	-	-	-	-	-	-	-	-
H	-	-	-	-	-	-	-	-	-	-	-	-

Following the outcome of data acquired in section 3.3.3 we decided to pursue long term infections of RV-16 which required us to carry out a further SRB assay to ascertain the best MOI of RV-16 to use with minimal cell decline over the long period of time. Infections were carried out as previously stated. We carried out the SRB assay using MOI 0.001, 0.01, 0.1 and 1 for up to 216 hours. When compared to non-infected cells (NT control), MOI 1 was seen to maintain cell viability of 100.37% at 216 hours (95% C.I -27.48 to 26.73), 87.16% at 192 hours (95% C.I -14.27-39.94) and 86.82% at 168 hours (95% C.I -13.82 to 40.38) (Fig. 3.5). With no significant change in viability from control at MOI 1 we decided to proceed with long term infections using MOI 1 for 168 hours.

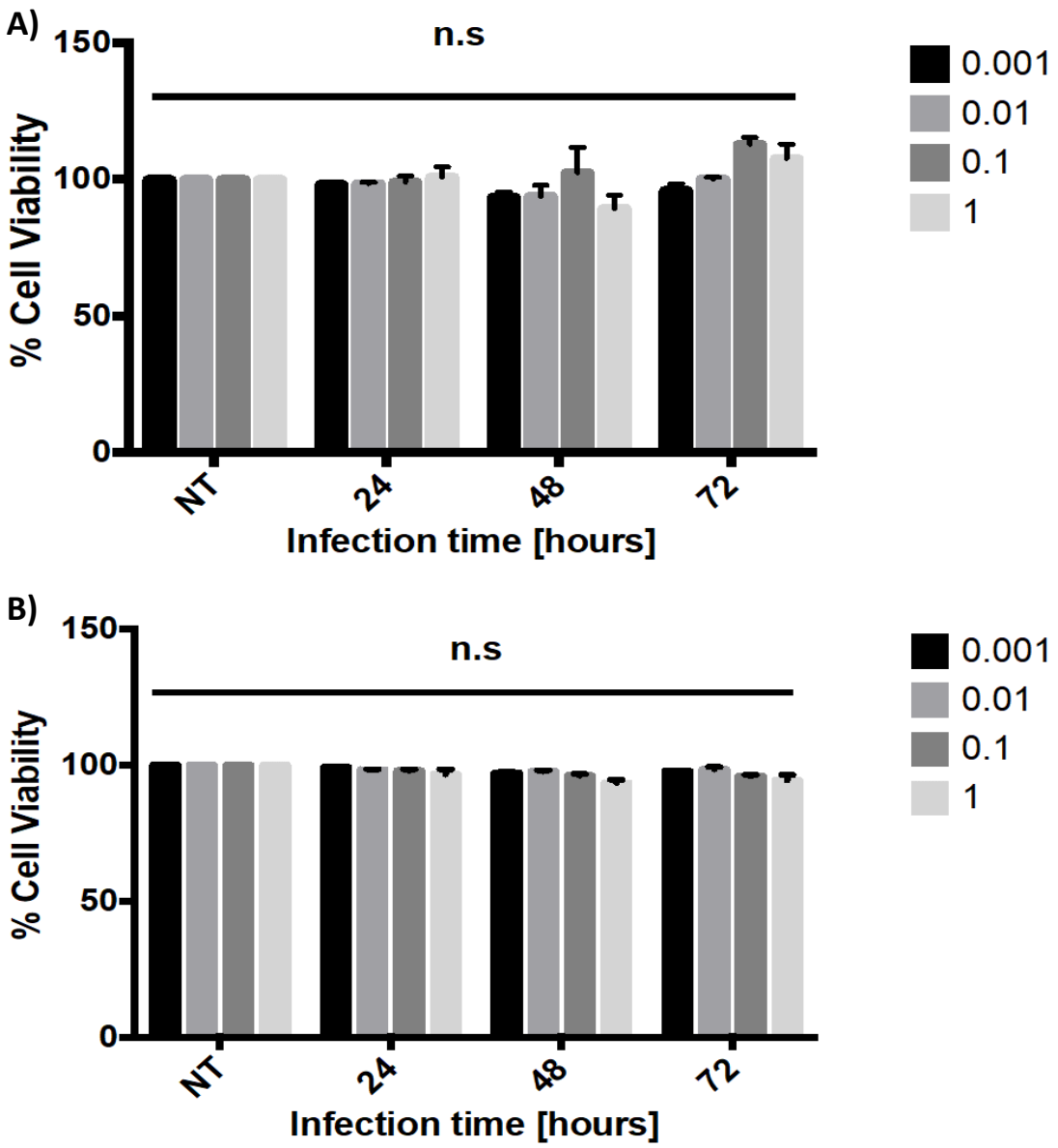

Figure 3.4. ***SRB of RV-16 infected A549 and 1321N1 cell lines****. Percentage of A) A549 cells or B) wild type 1321N1 cells viable after 72-hour time course treated with variable MOI of RV-16 (MOI 0.001-1). Each treatment group was carried out in triplicate. Results standardised against untreated cells grown for the same length of time. Results are displayed as mean ± S.E.M. of three independent experiments (N=3). Statistical analysis was carried out using two-way ANOVA followed by Tukey analysis. P>0.05*

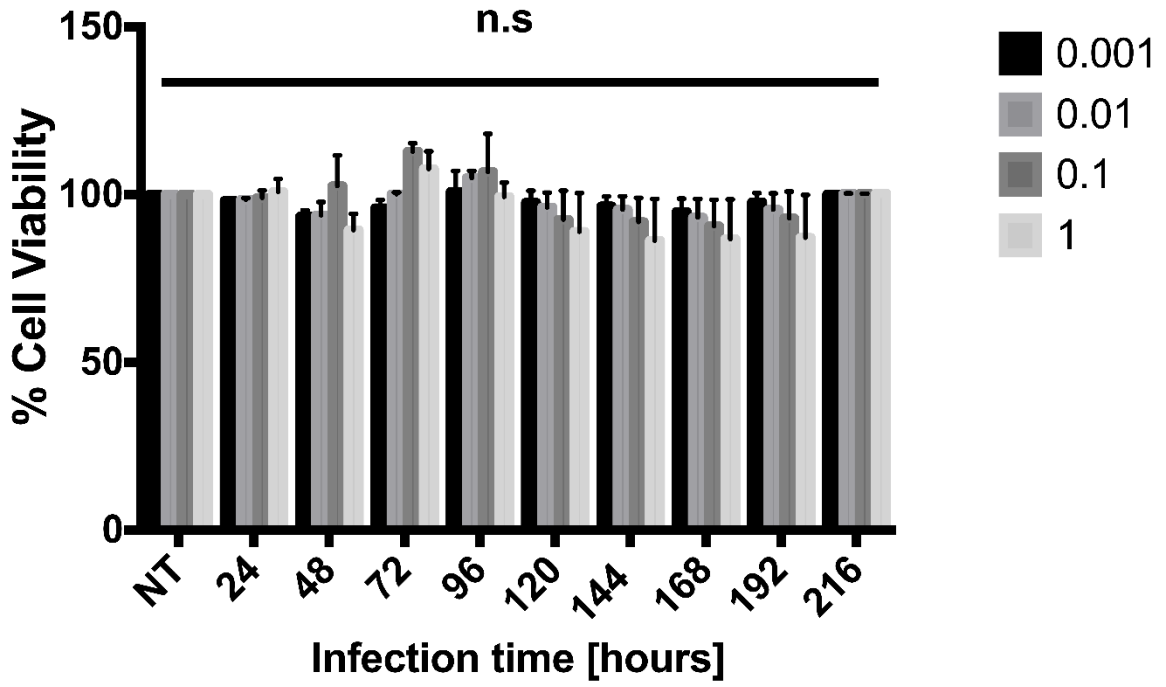

Figure 3.5. ***SRB assay of long-term RV-16 infected A549 cell line****. Percentage of A549 cells viable after 216-hour time course treated with variable MOI of RV-16 (MOI 0.001-1). Each treatment group was carried out in triplicate. Results standardised against untreated cell grown for the same length of time. Results are displayed as mean ± S.E.M. of three independent experiments (n=3). Statistical analysis was carried out using two-way ANOVA followed by Tukey analysis. P>0.05.*

3.2.4 Western blotting

All primary and secondary antibodies purchased from Santa Cruz had not been previously used so required full optimisation. All primary antibody dilutions were titrated using the same transferred membrane and basal protein lysate samples. 20µg P2X2/P2X3 transfected 1321N1 cell lysates were loaded on a 10% SDS gel and run as described section 3.1.3. Membranes were probed with a series of primary antibody dilutions 1:200, 1:400 and 1:700, diagrammatically represented by blue, green and red coloured boxes (Fig. 3.6). All membranes were probed with HRP conjugated antibodies at 1:4000 dilution.

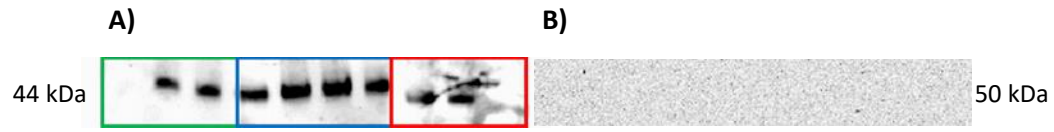

Figure 3.6. ***Western blot of P2X3 and P2X2 from 1321N1 cell line****. Membranes were loaded with 20µg protein from basal P2X2/X3 transfected 1321N1 cell lysate. A) Probed with anti-P2X3 primary antibody at 1:200), 1:400 and 1:700 concentrations (blue, green and red boxes, respectively). B) Probed with anti-P2X2 primary antibody at 1:200, 1:400 and 1:700 concentrations, expected molecular weight 50 kDa. Data representative of N=1.*

Transfected 1321N1 cell lysates were expected to contain overexpressed P2X2 and P2X3 receptors hence the bold and high signal bands for P2X3 (Fig. 3.6A) when only 20µg of protein was loaded. The membrane probed with P2X2 (Fig. 3.6B) displayed no signal for this receptor. The membrane was subject to increasing exposure in an attempt to detect a signal. Further research into this transfected cell line revealed the cell line was not in fact a dual transfected line as originally thought. Instead the cell line was expressing a chimeric P2X2-X3 receptor, possessing only the first 15% of the C-terminus of P2X2 coding and the remaining 85% of the receptor coding region was P2X3 (Gever *et al.*, 2010; Neelands *et al.*, 2003). This explained both the weak signal detected for P2X2 mRNA during RT-PCR (data not shown) and the complete lack of signal during western blotting probing as the antibody was raised against the N-terminus which this transfected cell line lacked. We had initially hoped to use the co-expressing transfected cell line for the stimulus and infection time course experiments to measure any effect poly(I:C) and RV-16 had on both potential tussive receptors P2X2 and P2X3. As a result, we decided to use the P2X3 transfected cell line as we felt this better resembled a physiological model (Bonvini *et al.*, 2016).

3.3 Results

3.3.1 Cell expression of TRP channels and P2XR

A549 cells were purchased to ensure a pure line and no phenotypic changes had occurred as a result of long passages. All characterisation was carried out on passages 3-15. Wild type (WT) 1321N1 cells were obtained at passage 3, and subsequently used for characterisation on passage numbers 6-17.

3.3.1.1 Basal mRNA expression of TRP channels and P2XR using RT-PCR

RNA was isolated from unstimulated A549 cells and WT 1321N1 cells and reverse transcribed in a thermal cycler for end point RT-PCR with primers for TRPA1, TRPV1, TRPM8, P2X2, P2X3 and P2X7, with endogenous control β-actin. The A549 cell line was positive for TRPA1, TRPV1, and P2X7, with low level detection of P2X3 mRNA expression (Fig. 3.7A). WT 1321N1 cell line was positive for TRPV1 and P2X7 mRNA expression (Fig. 3.7B). Results were deemed inconclusive for TRPA1 expression in WT 1321N1 cell line due to the faint positive achieved in two independent experiments of three experiments carried out.

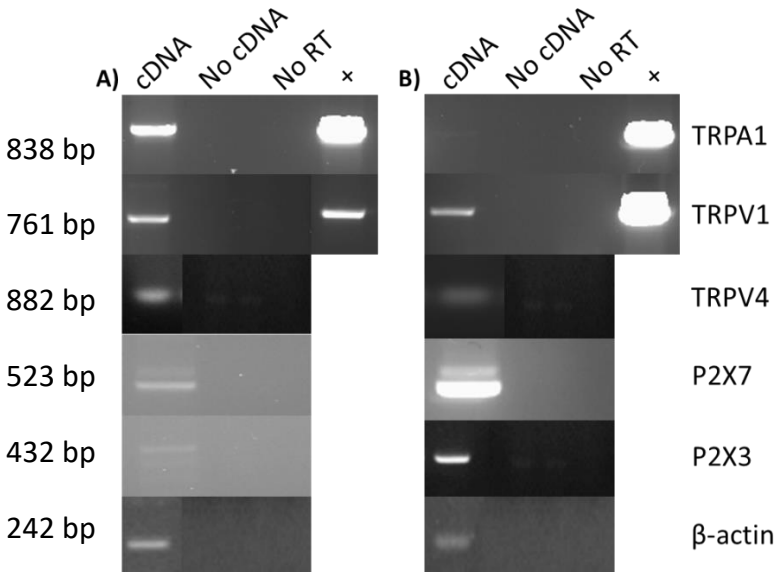

Figure 3.7. ***Endogenous mRNA expression of TRPA1, V1, V4, P2X3, X7 from A549 and 1321N1 cell lines****. End point RT-PCR agarose gel products of A) A549 and B) WT 1321N1 cell lines reverse transcribed for expression of TRPA1, TRPV1, TRPV4, P2X3 and P2X7 with loading control β-actin. Data representative of three independent experiments (N=3). First column – sample cDNA of cell line, second column – no cDNA control (negative control), third column – no reverse transcriptase (RT) added (negative control), fourth column –*

positive (+) control for gene of interest, where available. No positive control was available for TRPV4, P2X3 or P2X7.

3.3.1.2 Cell lines functionally express TRP channels and P2XR

Finally, to definitively confirm that the TRP channels and P2X receptors were responsible for the calcium flux recorded in section 3.3.1, western blotting was carried out on unstimulated cell lysates, as described in section 3.1.3. Following a series of optimisation (see section 3.2.4), A549 cell line was confirmed to be positive for whole cell expression of TRPA1, TRPV1 and TRPV4 (Fig. 3.8A). WT 1321N1 cells were positive for whole cell expression of TRPV1 and TRPV4 (Fig. 3.8B).

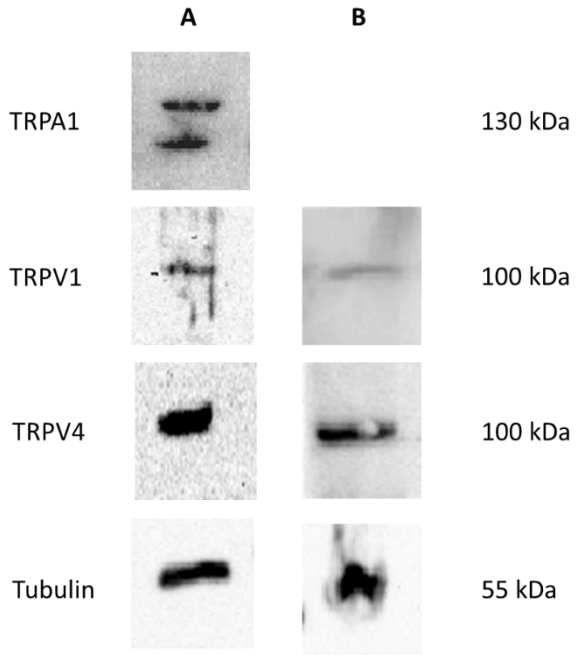

Figure 3.8. ***Endogenous protein expression of TRPA1, V1 and V4 from A549 and 1321N1 cell lines****. SDS-PAGE western blot visualised with HRP conjugated secondary antibody on Bio-Rad VersaDoc. A) A549 whole cell lysate positive signal at approx. 130 kDa when probed with TRPA1, 100 kDa when probed with TRPV1 and TRPV4, and positive signal at 55 kDa when probed with loading control alpha-tubulin primary antibodies. B) WT 1321N1 whole cell lysate positive signal at approx. 100 kDa when probed with TRPV1 and TRPV4 and positive signal at 55 kDa when probed with loading control alpha-tubulin primary antibodies. Cell line characterisation western blots were carried out on 3 different passage numbers. Data representative of N=3.*

3.3.1.3 Cell lines respond to specific channel and receptor agonists

Intracellular calcium signalling assays were used to pharmacologically characterise both cell lines. Corresponding dose response curves were constructed for allyl isothiocyanate (AITC) (TRPA1), capsaicin (TRPV1), WS-5 (TRPM8), GSK1016790A (TRPV4) and ATP (P2X3 and P2X7) using two systems, a PTI spectrofluorometer and ABI Flexstation. Dose response curves were constructed from data from Flexstation system and compared against those obtained from suspension signalling (spectrofluorometer). Cell lines A549 and WT 1321N1 were positive for P2X7 receptor mRNA expression (Fig. 3.7) but functional calcium signalling assays identified the cell lines to be unresponsive to ATP stimulation at any concentration (data not shown). Due to issues with cell clumping during suspension assays (see section 3.2.1), baseline dose response measurements were undertaken in pcDNA3.1 HEK cells (wild type HEK cell line containing empty pcDNA3.1 transfection vector) (Fig. 3.9) to confirm the ATP stock potency and rule out cell related issues. We achieved a positive response to ATP at every concentration used (0.1nM–3µM). We determined that A549 cell line does not express functional P2X7 receptor.

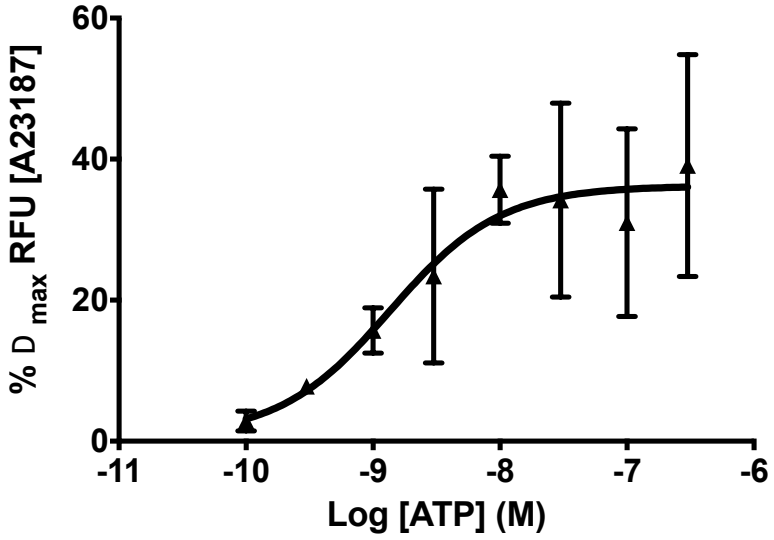

Figure 3.9. ***Dose response curve of ATP carried out in pcDNA3.1 HEK cells*** *using PTI spectrofluorometer system to measure intracellular calcium flux. Results are expressed as mean ± S.E.M. of three independent experiments (N=3).* EC_{50} *= 1.35nM.*

A549 cells were found to be functionally positive for TRPA1, TRPV1 and TRPV4 (Fig. 3.10A, 3.10C and 3.10E). WT 1321N1 cells were positive for TRPV1 and TRPV4 (Fig. 3.10B and

3.10D), whilst confirmation of transfected P2X3 expression in 1321N1-P2X3 was positive using the Flexstation system (Fig. 3.10F).

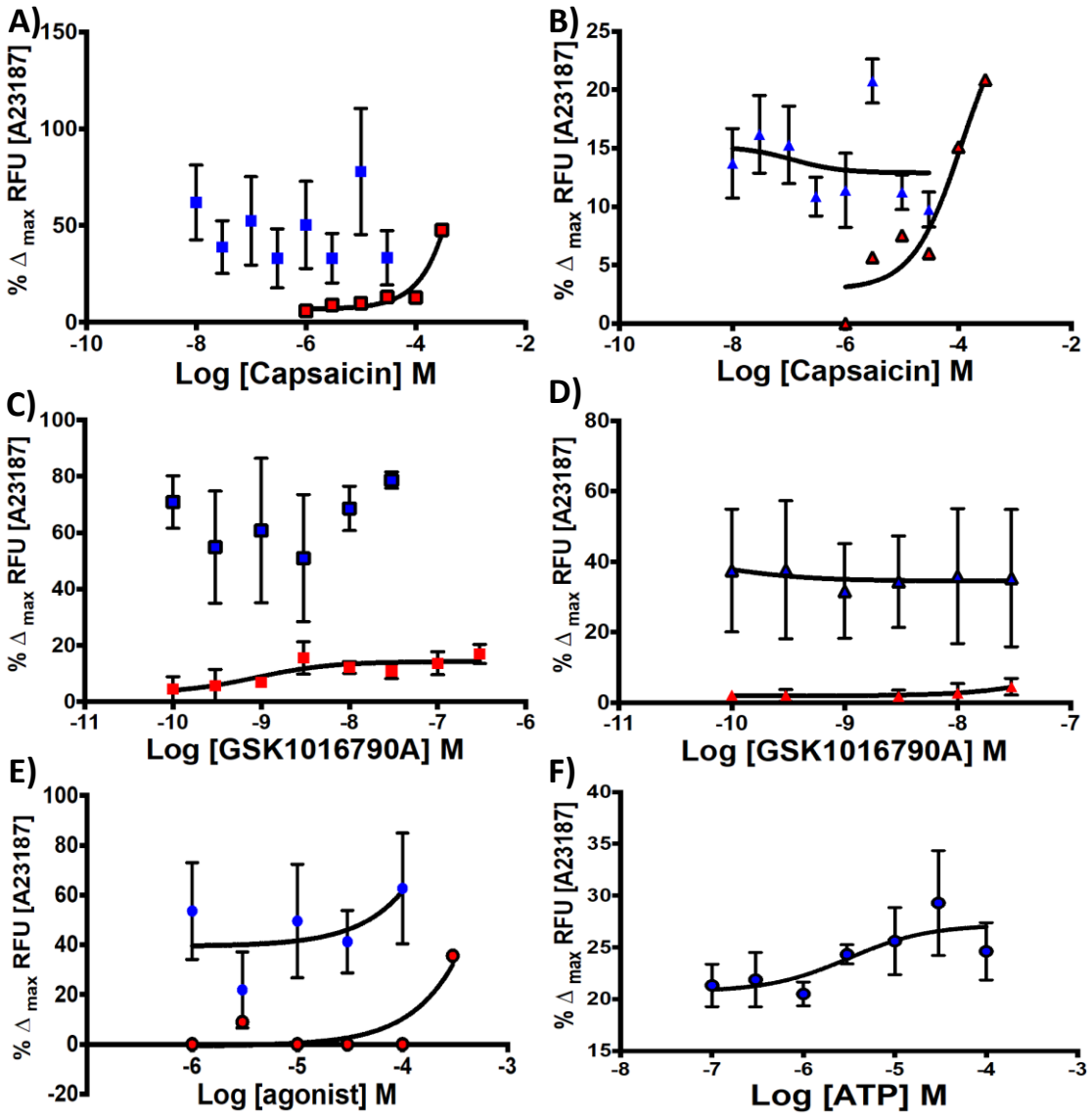

Figure 3.10. ***Log dose response curves comparing intracellular calcium signalling measurement techniques, spectrofluorometer (red) and Flexstation (blue) systems****, unless otherwise stated. A) TRPV1 measurements in A549 cell line using 0.01μM to 30μM capsaicin. B) TRPV1 measurements in WT 1321N1 cell line using 0.01μM to 30μM capsaicin. C) TRPV4 measurements in A549 cell line using 0.1nM to 30nM GSK1016790A. D) TRPV4 measurement in WT 1321N1 cell line using 0.1nM to 30nM GSK1016790A. E) TRPA1 measurements in A549 cell line using 1μM to 300μM cinnamaldehyde (spectrofluorometer system only) or 1μM to 100μM allyl isothiocyanate (Flexstation system only). F) P2X3 measurement in P2X3 transfected 1321N1 cell line using 0.1μM to 100μM ATP. Results for spectrofluorometer measurements were carried out in duplicate and expressed as mean ± S.E.M. of three independent experiments (N=3). Results for Flexstation measurements were carried out in quadruplet and expressed as mean ± S.E.M. of six independent experiments (N=6).*

Both A549 and WT 1321N1 cell lines responded to TRPV1 agonist capsaicin from 10nM to 30µM in both systems (Fig. 3.10A and 3.10B, respectively). No plateau could be achieved with a maximal concentration due to insolubility issues of capsaicin at high concentrations. Therefore, the highest concentration is listed at 30µM. No EC_{50} could be calculated in either system for A549 cell line because the data set was not converged. In the WT 1321N1 cell line an EC_{50} value of $1.153x10^{-7}$ M (115.3nM) was achieved using the Flexstation system, whilst when using the suspension system an EC_{50} value of $1.115x10^{-4}$ M (0.115mM) was achieved. However, given we had made the decision to continue further stimulation experiments using the microplate (flexstation) system, we decided to use a concentration of 1µM for both cell lines, as that concentration elicited a response we hypothesised would be around the EC_{50} range, gave the most consistent response when individual traces were analysed and all concentrations of capsaicin generally resulted in a similar percentage response of A23187.

Both A549 and WT 1321N1 cell lines also responded to TRPV4 agonist GSK1016790A from 100pM to 30nM in both systems (Fig. 3.10C and 3.10D, respectively). In A549 cell line, no EC_{50} could be calculated using the Flexstation system (blue) because the data set was not converged, however, using the suspension system (red) an EC_{50} value was calculated as $8.67x10^{-10}$ M (0.867nM). In the WT 1321N1 cell line an EC_{50} value of $6.357x10^{-11}$ M (63.5pM) was calculated using the Flexstation system whilst using the suspension system an EC_{50} value of $1.427x10^{-3}$ M (1.427mM). However, in both cell lines we chose to carry out further work with 3nM as it gave the most consistent response when individual traces were analysed.

In the Flexstation system (blue), A549 cells responded to TRPA1 agonist AITC from 1µM to 100µM (Fig. 3.10E), the EC_{50} value was calculated as 9.822M. Whilst in the suspension system (red), A549 cells responded to TRPA1 agonist cinnamaldehyde from 1µM to 30 µM, the EC_{50} value was calculated as 1.116M. The results were highly variable for both systems and agonists used. No plateau could be achieved so the EC_{50} values would not have been an accurate representation. Therefore, further experiments carried out used AITC agonist at 30 µM.

Finally, we used the P2X3 transfected 1321N1 cell line (1321N1-P2X3) to confirm their responsiveness to ATP as expected (Fig. 3.10F). Using only the Flexstation, an EC_{50} value of $3.114x10^{-6}$ M (3.114μM) was calculated and used for downstream applications.

3.3.2 Poly(I:C) stimulus causes upregulation of TRP channels and P2XR

It is unknown how RV-16 causes a cough during the common cold but we hypothesise that thermo-TRP channels and P2X3 receptor are part of the causative mechanism of the viral cough response (Atkinson *et al.*, 2016). Previous data have shown an up-regulation of TRPA1 in response to poly(I:C) and RV-16 (Abdullah *et al.*, 2014). The aim of this section was to investigate the effect of poly(I:C) over a 72-hour period on single cell culture A549 and 1321N1-P2X3 cell lines and the effect on TRPA1, TRPV1 and TRPV4 and P2X3 expression.

3.3.2.1 Poly(I:C) causes no effect to TRP channel or P2X3 gene expression

TRPA1, TRPV1, TRPV4 and P2X3 mRNA expression was examined by end point RT-PCR on a thermal cycler, as described in section 3.1.1, using RNA extracted from A549 and 1321N1-P2X3 cell lines following stimulation with 10μg ml^{-1} poly(I:C) over 72 hours, as described in section 2.4. β-actin was used as an endogenous loading control for RT-PCR experiments (Fig 3.11 and Fig. 3.12). In the A549 cell line, poly(I:C) induced upregulation of TRPA1 gene expression by 3-fold from 3 hours post infection (hpi), which reduced to 1-2-fold increase expression from 6 hpi through 72 hpi (Fig. 3.11A, $P>0.05$; n=3), though not significant. TRPV1 gene expression was increased 3-fold from 3 hpi, returning 1-fold from 6 hpi (Fig. 3.11B, $P>0.05$; n=3), though not significant. There was no significant difference in TRPV4 mRNA expression through the time course (Fig. 3.11C, $P>0.05$; n=3). In 1321N1-P2X3 cell line, poly(I:C) induced significant 1.5-fold upregulation of TRPV1 from 3 hpi through 24 hpi (Fig. 3.12A, $P>0.05$; n=3), returning to levels comparable to untreated cells by 48 hpi. There was no significant difference in TRPV4 (Fig. 3.12B) and P2X3 (Fig. 3.12C) mRNA expression from untreated levels throughout the time course ($P>0.05$).

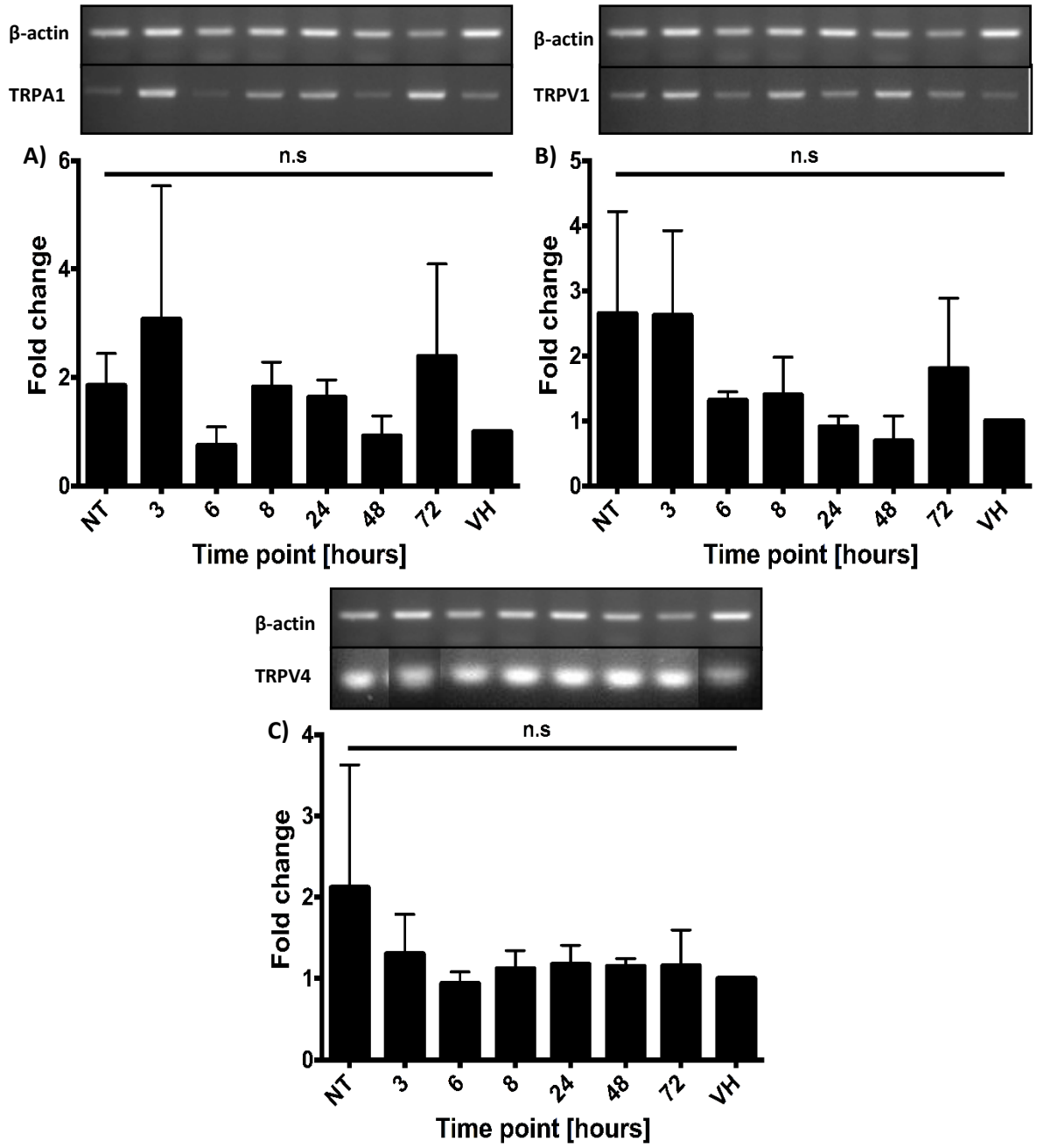

Figure 3.11. ***RT-PCR from Poly(I:C) stimulated A549 cell line time course****. Relative density of RT-PCR of cell line A549 exposed to 10µg ml^{-1} poly(I:C) over a 72-hour time period. A) TRPA1 B) TRPV1 C) TRPV4 gene expression. No treatment – NT, vehicle – VH. Results are calculated from band density and result is standardised against vehicle control, where vehicle=1. Data are normalised to loading control β-actin and displayed as fold change from untreated. Results shown are mean ± S.E.M. of three independent experiments (N=3). Statistical analysis was carried out using two-way ANOVA followed by Tukey analysis. P>0.05.*

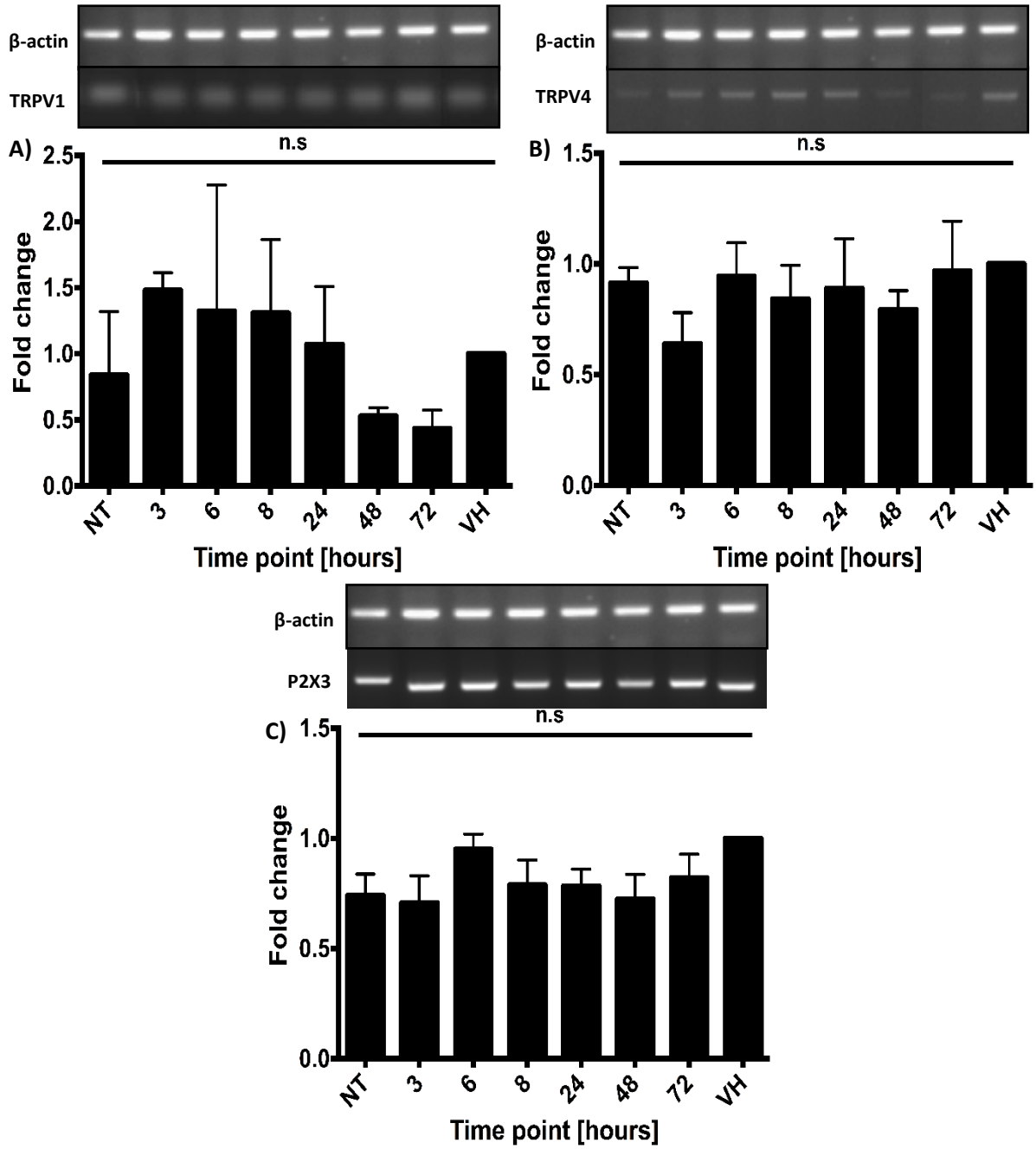

Figure 3.12. ***RT-PCR from Poly(I:C) stimulated 1321N1-P2X3 cell line time course****. Relative density graphs of RT-PCR of transfected cell line 1321N1-P2X3 exposed to 10µg ml^{-1} poly(I:C) over a 72-hour time period. A) TRPV1 gene expression. B) P2X3 gene expression. C) TRPV4 gene expression. No treatment – NT, vehicle – VH. Results are calculated from band density and result is standardised against vehicle control, where vehicle=1. Data are normalised to loading control β-actin and displayed as fold change from untreated. Results are displayed as mean ± S.E.M. of three independent experiments (N=3). Statistical analysis was carried out using two-way ANOVA followed by Tukey analysis. P>0.05*

3.3.2.2 Poly(I:C) causes no effect on thermo-TRP channels and P2X3R protein expression

To further verify the effects of poly(I:C) stimulation, A549 and 1321N1-P2X3 cells were cultured with 10µg ml^{-1} poly(I:C) for up to 72 hours, as described in section 2.4, and lysed. Western blot analysis was carried out as described in section 2.9. Lysates were probed for TRPA1, TRPV1, TRPV4 and P2X3 whole cell protein expression alongside loading control α-tubulin.

In contrast to the mRNA expression results, western blot analysis of TRPA1, TRPV1, TRPV4 and P2X3 expression did not correlate to the previous findings. A549 cell line displayed a 3.5-fold increase in TRPV4 expression at 3 hpi followed by a 2-fold increase of expression at 6-72 hpi (Fig. 3.13). No signal could be obtained for either TRPA1 or TRPV1 despite six independent attempts (data not shown). Under the same conditions, 1321N1-P2X3 cell line displayed 0.5-fold reduction of TRPV4 expression from 3 hpi through 48 hpi, followed by 1.5-fold increase in expression at 72 hpi (Fig. 3.14). In contrast, poly(I:C) stimulation induced a small 2-fold increase of P2X3 expression from 3 hpi through 48 hpi but induced a 15-fold increase at 72 hpi (Fig. 3.15). No statistical analysis could be performed for any protein probed in either cell line as a signal could only be achieved in two independent experiments of six carried out.

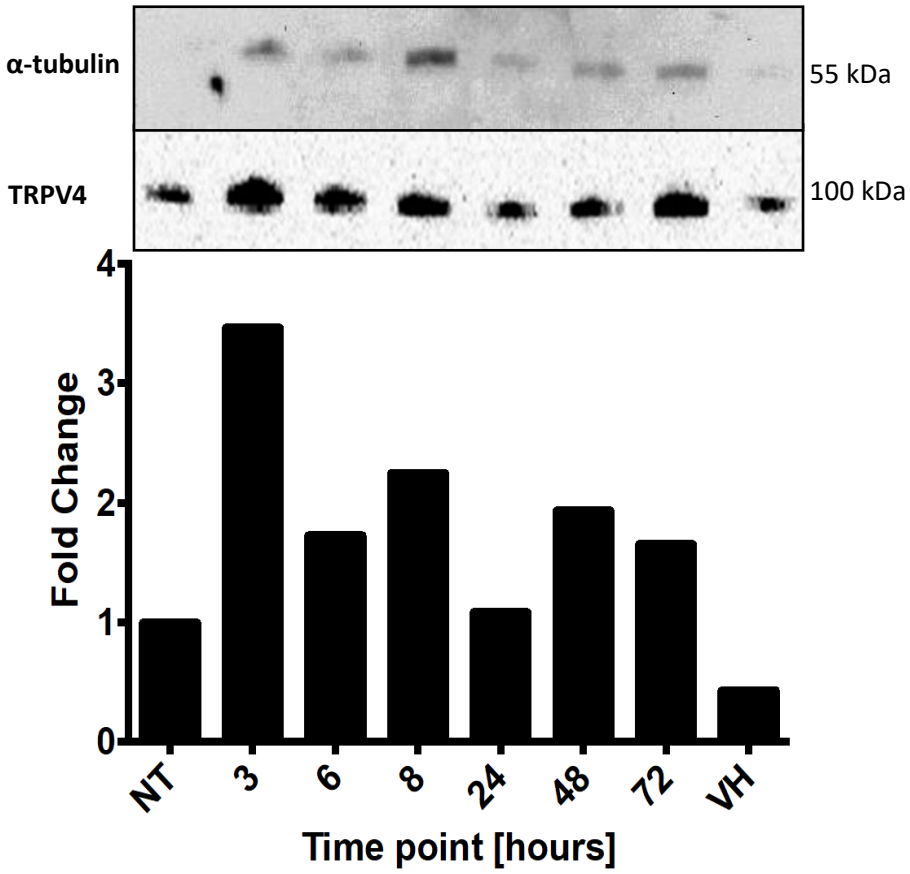

Figure 3.13. ***TRPV4 protein expression in A549 cell line stimulated with poly(I:C).*** *Cell line A549 stimulated with 10µg ml^{-1} poly(I:C) for up to 72 hours, as labelled, treated with vehicle control (VH) 0.9% NaCl solution (final volume 0.1% w/v) or left unstimulated (NT). A549 whole cell lysates (20µg protein) probed for control loading control α-tubulin (55 kDa) and TRPV4 (100 kDa) protein expression, as labelled. Data is representative of n=2 of six independent experiments therefore no error bars could be applied or statistical analysis carried out. Densitometry was carried out and expressed as fold change from basal following normalisation to loading control α-tubulin.*

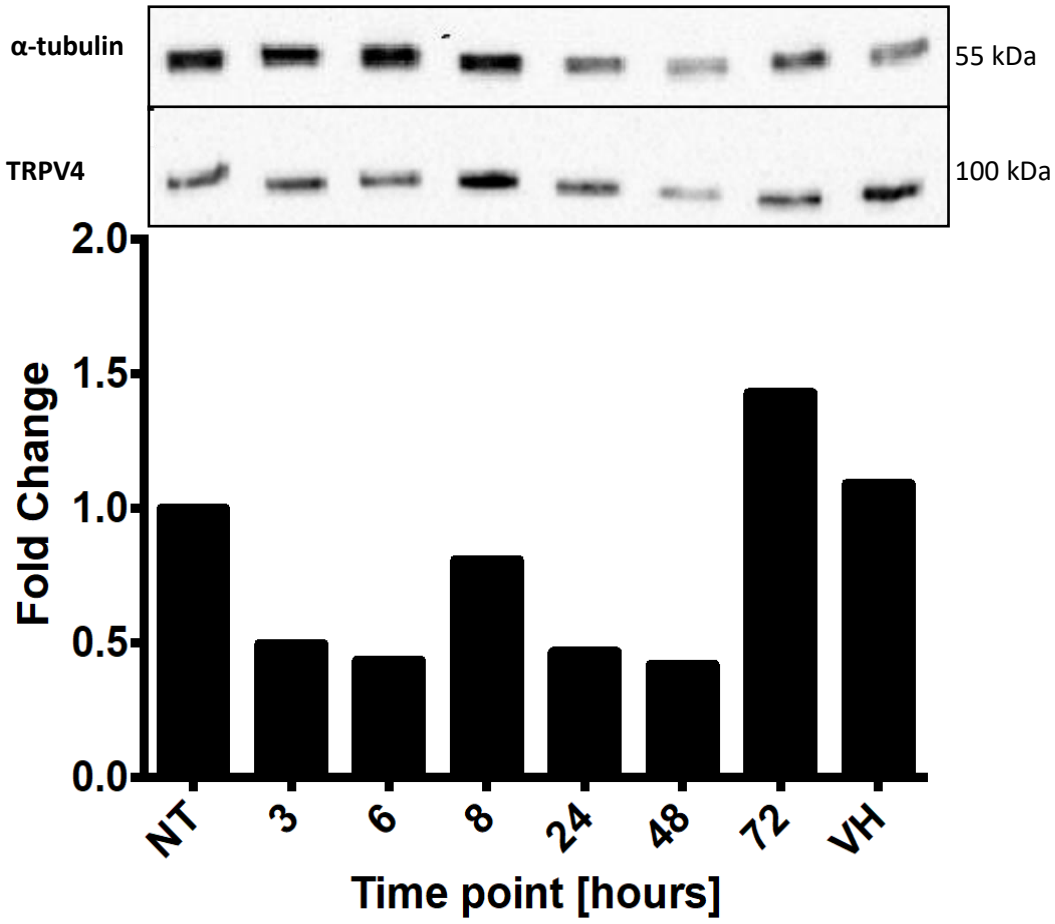

Figure 3.14. ***TRPV4 protein expression in 1321N1-P2X3 cell line stimulated with poly(I:C).*** *Cell line 1321N1-P2X3 stimulated with 10µg ml^{-1} poly(I:C) for up to 72 hours, as labelled, treated with vehicle control (VH) 0.9% NaCl solution (final volume 0.1% w/v) or left unstimulated (NT). 1321N1-P2X3 whole cell lysates (20µg protein) probed for control loading control α-tubulin (55 kDa) and TRPV4 (100 kDa) protein expression, as labelled. Data is representative of n=2 of six independent experiments therefore no error bars could be applied or statistical analysis carried out. Densitometry was carried out and expressed as fold change from basal following normalisation to loading control α-tubulin.*

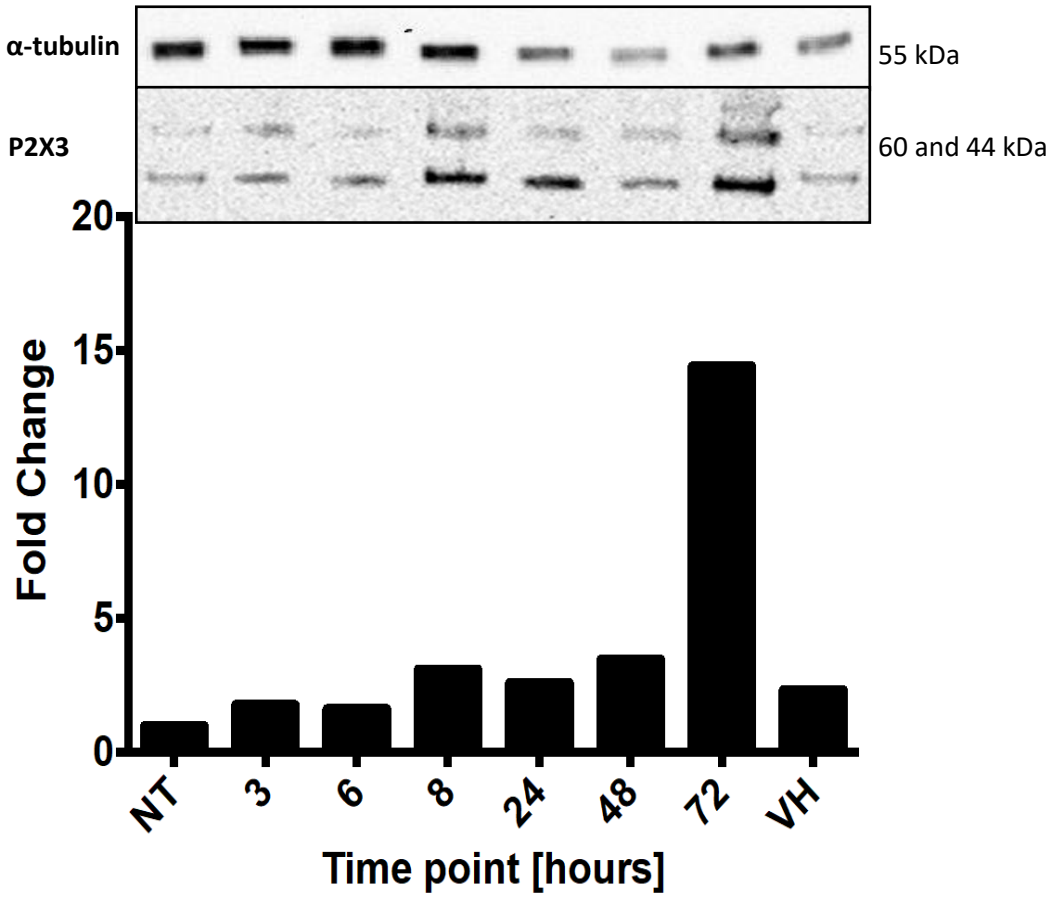

Figure 3.15. ***P2X3 protein expression in 1321N1-P2X3 cell line stimulated with poly(I:C).*** *Cell line 1321N1-P2X3 stimulated with 10µg ml^{-1} poly(I:C) for up to 72 hours, as labelled, treated with vehicle control (VH) 0.9% NaCl solution (final volume 0.1% w/v) or left unstimulated (NT). 1321N1-P2X3 whole cell lysates (20µg protein) probed for control loading control α-tubulin (55 kDa) and P2X3 (66 and 44 kDa) protein expression, as labelled. Data is representative of n=2 of six independent experiments therefore no error bars could be applied or statistical analysis carried out. Densitometry was carried out and expressed as fold change from basal following normalisation to loading control α-tubulin.*

3.3.2.3 Poly(I:C) stimulation causes increased response to TRPV4 agonist GSK1016790A in alveolar and astrocytoma cell lines using intracellular calcium signalling

Finally, to confirm the change in protein expression affects the receptor function in the same manner, calcium signalling responses to receptor specific agonists were measured, using previously determined EC_{50} values, see section 3.3.1.2. Assays were carried out using the same conditions as previously used, see section 3.1.2. Briefly, cells were loaded with Fluo-4 AM direct (no wash) dye and incubated for 30 minutes at 37^{o}C, followed by a further 30 minutes at room temperature for a total loading time of 1 hour. Results are represented as percentage of A23187 (positive control and assumed maximal response) in comparison to unstimulated cells (NT) (Fig. 3.15).

In A549 cell line, stimulation with 10µg ml^{-1} poly(I:C) induced a 50% increase in response from TRPV4 agonist GSK1016790A at 72 hpi (Fig. 3.16A), though not significant (P>0.05). There was no significant change in response to either TRPV1 agonist capsaicin or TRPA1 agonist AITC at any time point in comparison to A23187. In a similar manner, in 1321N1-P2X3 cell line there was a 100% increase in response to TRPV4 agonist GSK1016790A at 8 hpi (Fig. 3.16B), but returned to baseline from 24 hpi, though also not significant (P>0.05). Again, there was no significant change in response to either capsaicin to AITC at any time point in comparison to A23187.

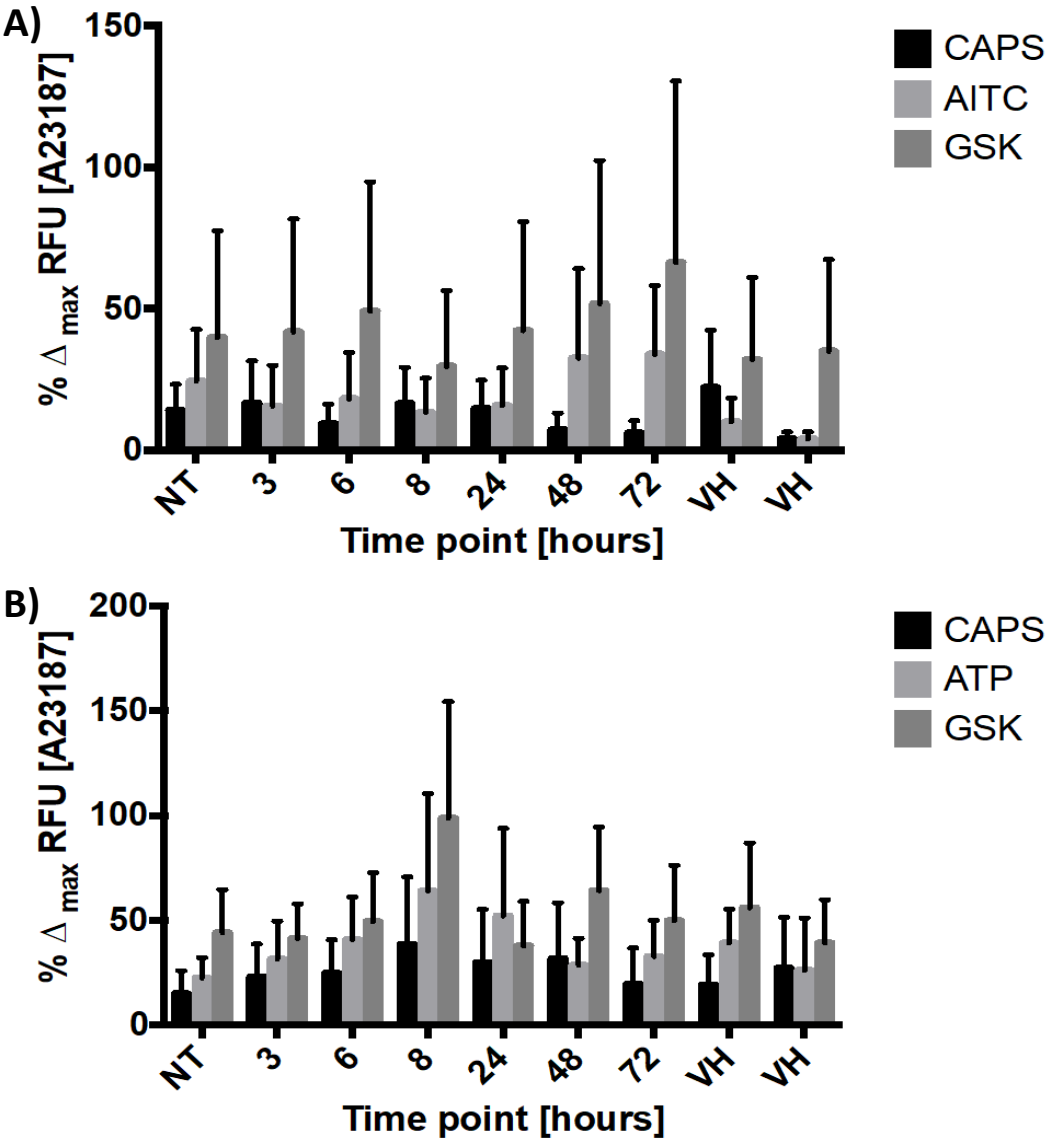

Figure 3.16. ***Calcium signalling responses from A549 and 1321N1-P2X3 cell lines stimulated with poly(I:C).*** *A549 and 1321N1-P2X3 cell lines exposed to poly(I:C) over a 72-hour time course. Cells stimulated with receptor agonist. Responses measured as a percentage of maximal control compound A23187. Results standardised against vehicle control and expressed as a percentage of vehicle response. A) A549 cells stimulated with capsaicin (CAPS), allyl isothiocyanate (AITC) and GSK1016790A (GSK). B) 1321N1-P2X3 cells stimulated with CAPS, ATP and GSK. No treatment – NT, vehicle control 0.9% (w/v) NaCl (final volume 0.01%) – VH. Results are displayed as mean ± S.E.M. of N=3. P>0.05.*

3.3.3 RV-16 stimulus assay causes upregulation of TRP channels and P2XR

This section expands upon the work from section 3.3.2 using a different stimulus. RV-16 is a ssRNA virus whereas poly(I:C) is a synthetic dsRNA stimulus. The effects over 72 hours using two different viral stimuli were compared for any difference in thermo-TRP and P2X3 expression. The purpose of this section was to research the effect RV-16 has over a 72-hour period on single culture A549 and 1321N1-P2X3 cells and the effect of TRPA1, TRPV1 and TRPV4 and P2X3 expression. We also confirmed for the first time that RV-16 can infect and replicate in the astrocytoma 1321N1 cell line.

3.3.3.1 Effect of RV-16 stimulation on protein expression of TRPA1, TRPV1, TRPV4 and P2X3R

To investigate the effect of RV-16 on thermo-TRP and P2X3 receptor expression, A549 and 1321N1-P2X3 cell lines were infected with RV-16 at MOI 1 for 1 hour at room temperature with gentle agitation. The cells were washed and incubated at 37^{o}C for up to 72 hours. We took infected cells, lysed them and carried out western blot analysis, as described in section 2.9. Lysates were probed for TRPA1, TRPV1, TRPV4 and P2X3 whole cell protein expression alongside loading control α-tubulin.

In A549 cell line, infection with RV-16 at MOI 1 caused no significant change in TRPV4 protein expression from baseline (untreated) (Fig. 3.17, $P>0.05$, n=5). No signal could be achieved for either TRPA1 or TRPV1 expression in A549 cell line (data not shown) despite nine independent experiments carried out.

In the 1321N1-P2X3 cell line, RV-16 induced a non-significant upregulation from baseline of TRPV4 whole cell expression by 2-fold from 3-6 hpi (Fig. 3.18), returning to baseline from 8 hpi ($P>0.05$, n=3). However, UV inactivated, and filtered controls stimulated a 2- and 3.5-fold increase in TRPV4 expression, respectively, though not significant ($P>0.05$). We hypothesise this is likely due to imaging problems as can be evidenced by representative blot image for α-tubulin loading control. This problem is discussed further in section 3.4 Conclusion. Infection with RV-16 induced a 30-fold increase from baseline in whole cell expression of TRPV1 at 3 hpi (Fig. 3.19) ($P<0.001$, n=3), dropping to a 4-fold increase at 6 hpi (not significant $P>0.05$) and returning to baseline from 8 hpi. Once again, UV and filtered

control induced an apparent 6-fold increase in TRPV1 expression, though not significant (P>0.05).

Finally, when 1321N1-P2X3 cell line was infected with RV-16 a rapid 15-fold increase in expression of P2X3 from baseline levels was identified at 3 hpi (not significant, P>0.05) (Fig. 3.20), followed by a slow time-dependent decrease in expression to baseline by 48 hpi. Again, UV and filtered controls displayed a 4-fold increase in P2X3 expression, though not significant.

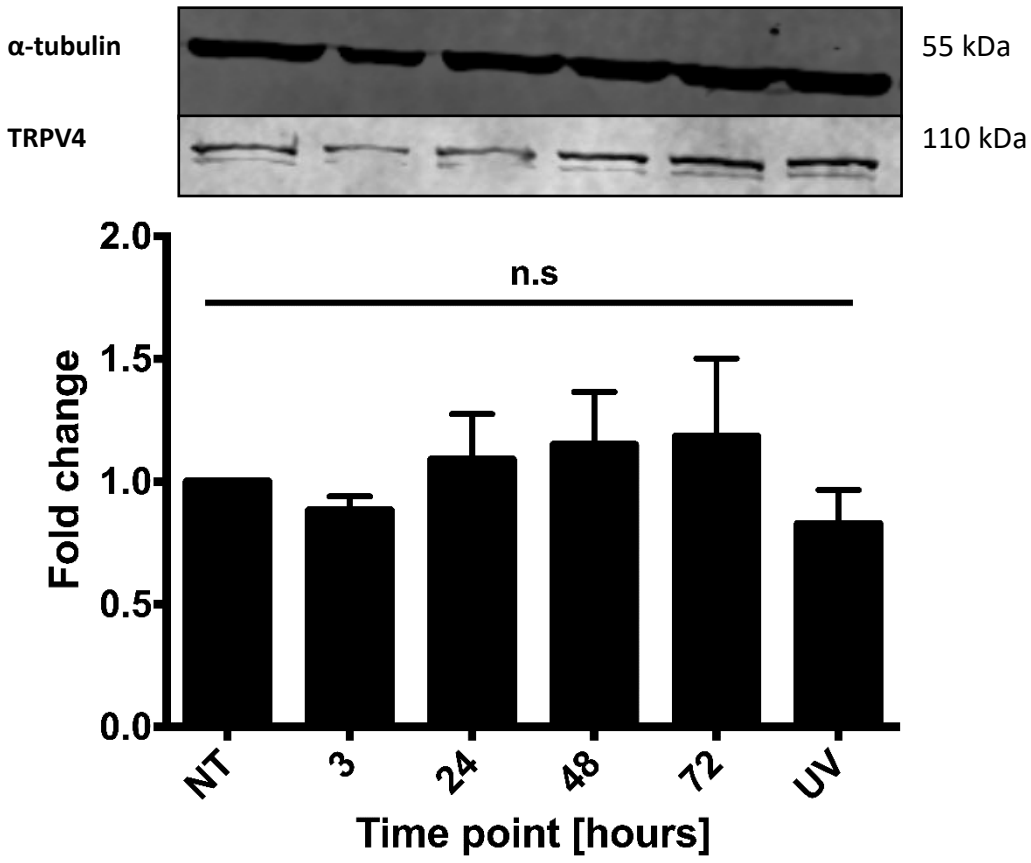

Figure 3.17. ***TRPV4 protein expression in A549 cell line infected with RV-16.*** *A549 cell line stimulated with RV-16 at MOI 1 for up to 72 hours, as labelled, UV-inactivated viral sham control (UV) or left unstimulated (NT). Whole cell lysate (50μg protein) probed for α-tubulin loading control and TRPV4 protein expression, as labelled. Results are displayed as mean ± S.E.M. of five independent experiments (n=5). Statistical analysis was carried out using multiple comparison two-way ANOVA followed by Tukey analysis. Densitometry was carried out and expressed as fold change from basal following normalisation to loading control α-tubulin. P>0.05.*

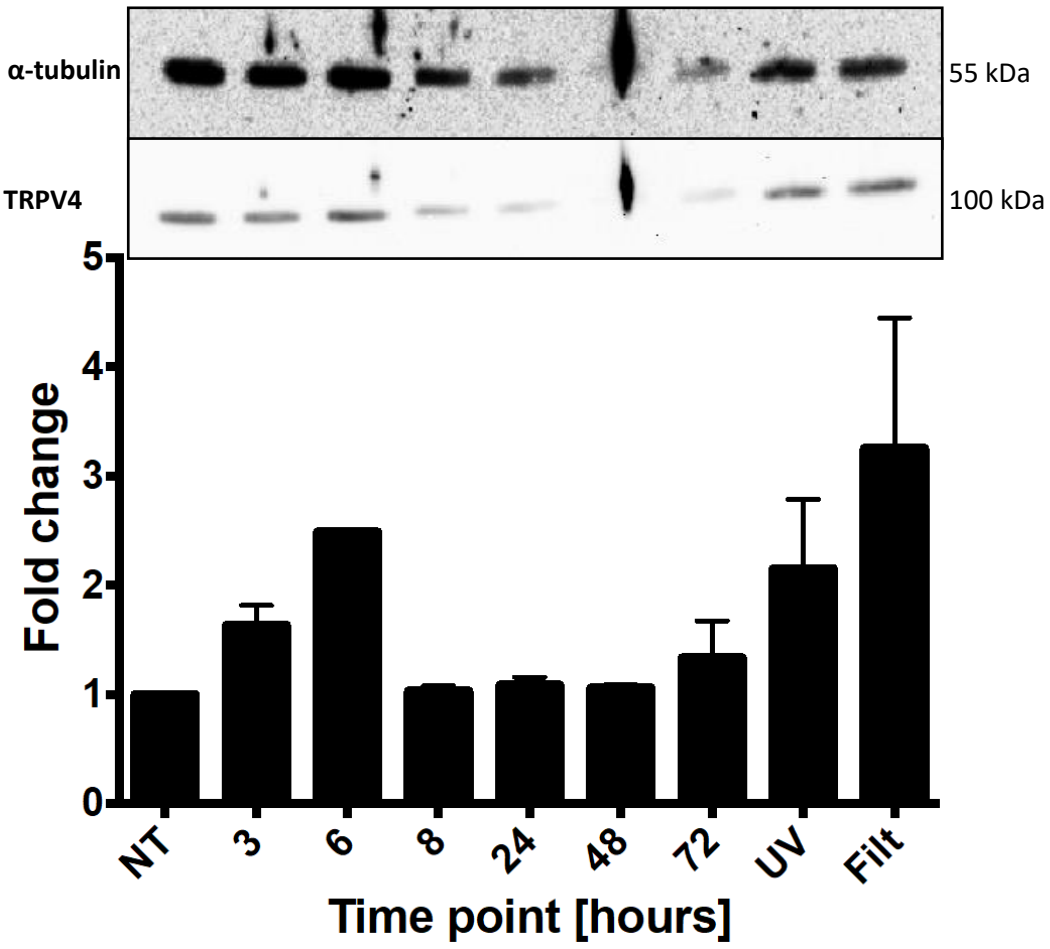

Figure 3.18. ***TRPV4 protein expression in 1321N1-P2X3 cell line infected with RV-16.*** *Cell line 1321N1-P2X3 was stimulated with RV-16 at MOI 1 for up to 72 hours, as labelled, treated with UV inactivated control (UV), filtered viral control (Filt) or left unstimulated (NT). 1321N1-P2X3 whole cell lysate (20µg protein) probed for loading control α-tubulin and TRPV4 protein expression. Data representative of N=3 of nine independent experiments. Densitometry was carried out and expressed as fold change from NT following normalisation to loading control α-tubulin. Statistical analysis was carried out using two-way ANOVA followed by Tukey analysis. P>0.05*

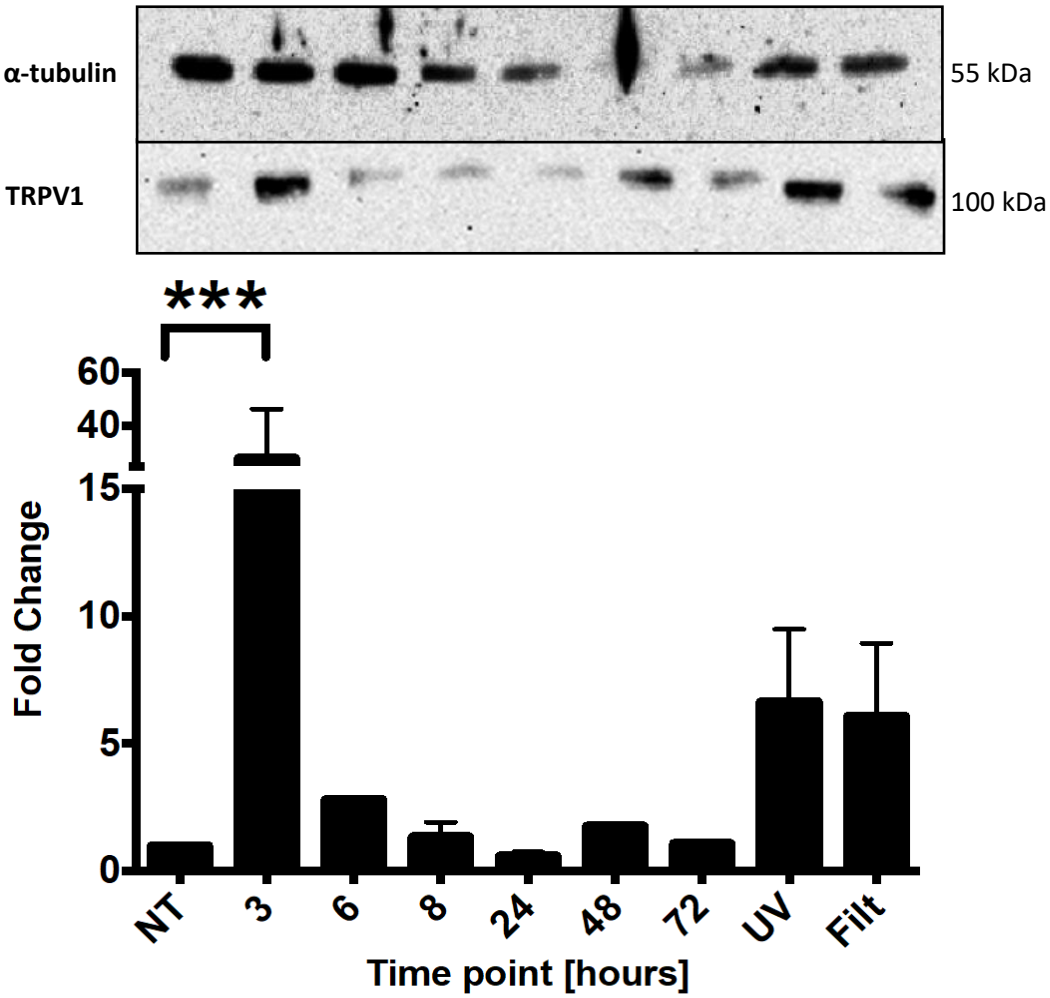

Figure 3.19. ***TRPV1 protein expression in 1321N1-P2X3 cell line infected with RV-16.*** *Cell line 1321N1-P2X3 was stimulated with RV-16 at MOI 1 for up to 72 hours, as labelled, treated with UV inactivated control (UV), filtered viral control (Filt) or left unstimulated (NT). 1321N1-P2X3 whole cell lysate (20µg protein) probed for loading control α-tubulin and TRPV1 protein expression. Data representative of N=3 of nine independent experiments. Densitometry was carried out and expressed as fold change from NT following normalisation to loading control α-tubulin. Statistical analysis was carried out using two-way ANOVA followed by Tukey analysis.***P<0.001.*

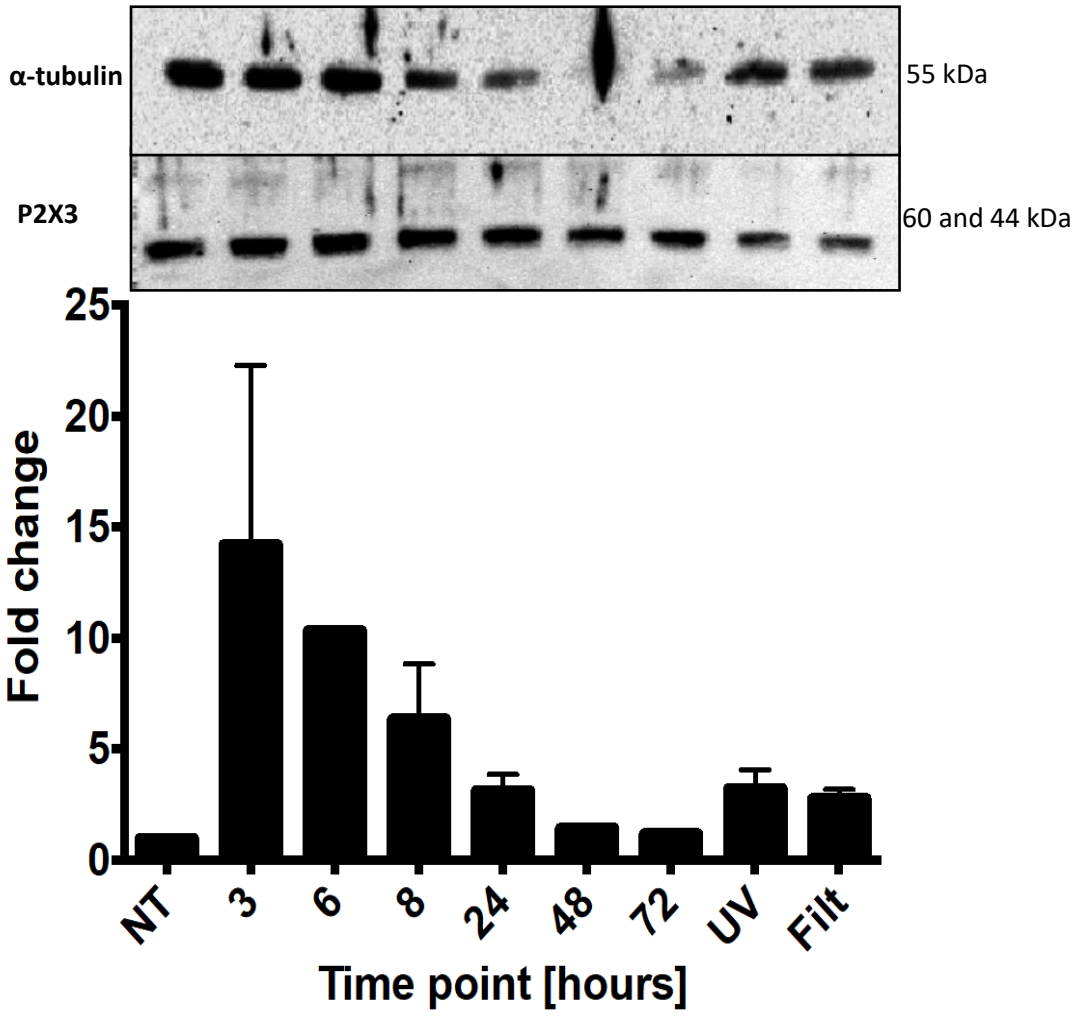

Figure 3.20. ***P2X3 protein expression in 1321N1-P2X3 cell line infected with RV-16.*** *Cell line 1321N1-P2X3 was stimulated with RV-16 at MOI 1 for up to 72 hours, as labelled, treated with UV inactivated control (UV), filtered viral control (Filt) or left unstimulated (NT). 1321N1-P2X3 whole cell lysate (20µg protein) probed for loading control α-tubulin and P2X3 protein expression. Data representative of N=3 of nine independent experiments. Densitometry was carried out and expressed as fold change from NT following normalisation to loading control α-tubulin. Statistical analysis was carried out using two-way ANOVA followed by Tukey analysis. P>0.05*

3.3.3.2 Infection with RV-16 causes early inhibition of TRPA1 function and late inhibition of P2X3

To confirm the change in protein expression also correlates to a shift of receptor function, calcium signalling responses to receptor specific agonists were measured, using previously determined EC_{50} values (See 3.3.1.2) also used in section 3.3.2.3 for poly(I:C) stimulation assays. Assays were carried out using the same conditions as previously used, see section 3.1.2.

In A549 cells exposed to RV-16 at MOI 1 there was no statistical difference of response to either TRPV1 agonist capsaicin or TRPV4 agonist GSK1016790A at any time point (Fig. 3.21A). A549 cells exposed to RV-16 at MOI 1 displayed a significantly diminished response to TRPA1 agonist AITC 3 and 6 hpi, 80% and 90% respectively, when standardised against vehicle control ($P<0.05$, n=3) (Fig. 3.21A and 3.22A). Responses to AITC returned to baseline from 24 hpi. UV control response was reduced to a lesser degree than early time points but was not a significant reduction.

In 1321N1-P2X3 cell line there was a general trend of reduced receptor signalling for all receptors stimulated (Fig. 3.20B). Responses to capsaicin were reduced by on average 50% from 3 hpi to 72 hpi, though not significant ($P>0.05$). Furthermore, responses to GSK1016790A were reduced by 50% at 3 hpi, returning to baseline from 6 hpi, though also not significant ($P>0.05$). However, 1321N1-P2X3 cells showed a reduced response to P2X3 agonist ATP in all time points including UV control with significant reduction, 75% from untreated levels, at 72 hpi ($P<0.05$, n=3) (Fig. 3.21B and 3.22B).

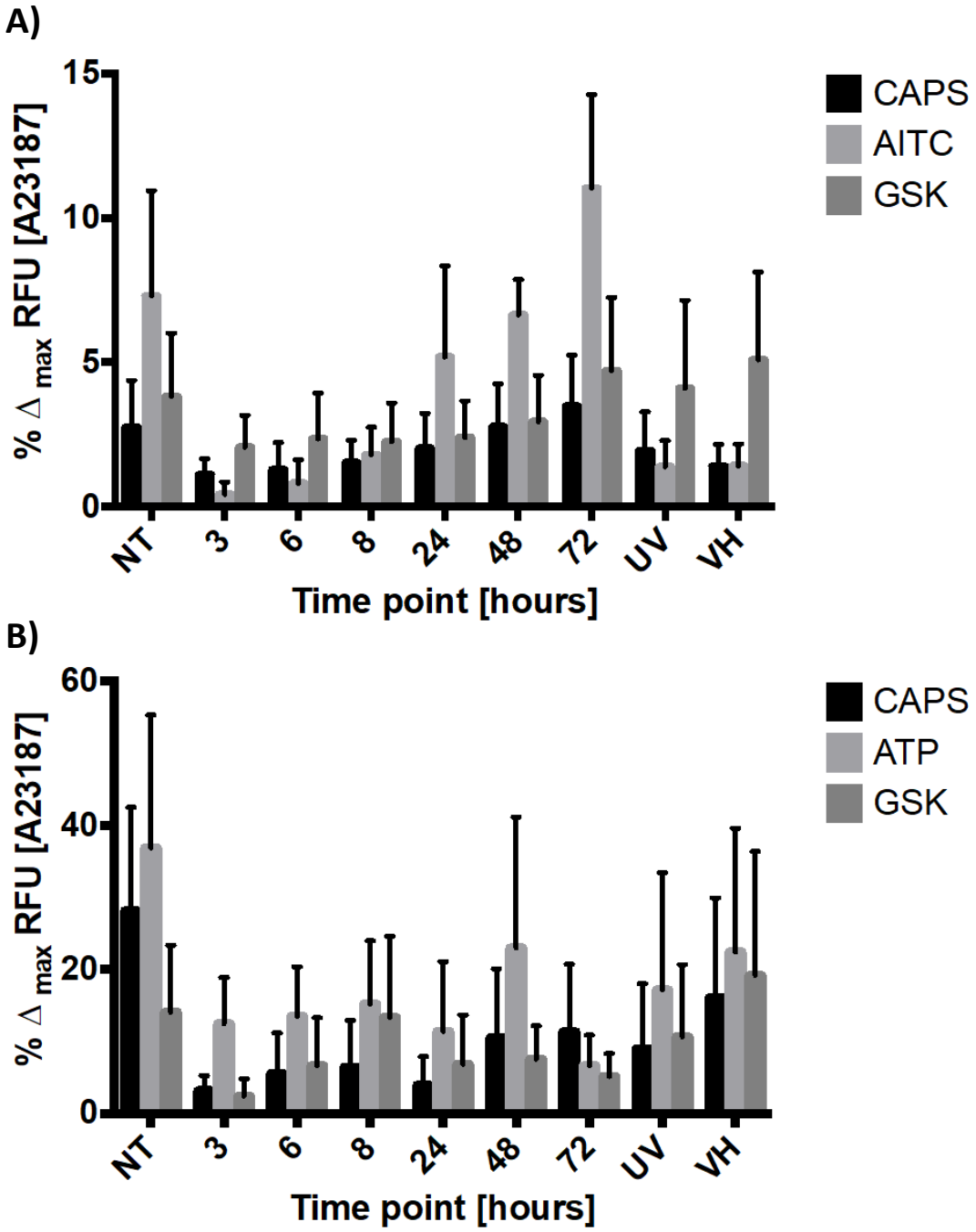

Figure 3.21. ***Calcium signalling responses from A549 and 1321N1-P2X3 cell lines infected with RV-16.*** *A549 and 1321N1-P2X3 cell lines exposed to RV-16 over a 72-hour time course. Cells stimulated with receptor agonist. Responses measured as a percentage of maximal control compound A23187. A) A549 cells stimulated with capsaicin (CAPS), allyl isothiocyanate (AITC) and GSK1016790A (GSK). B) 1321N1-P2X3 cells stimulated with CAPS, ATP and GSK. No treatment – NT. Ultraviolet – UV. Results are displayed as mean ±S.E.M. of three independent experiments (N=3). Statistical analysis was carried out using two-way ANOVA followed by Tukey analysis. P<0.05*

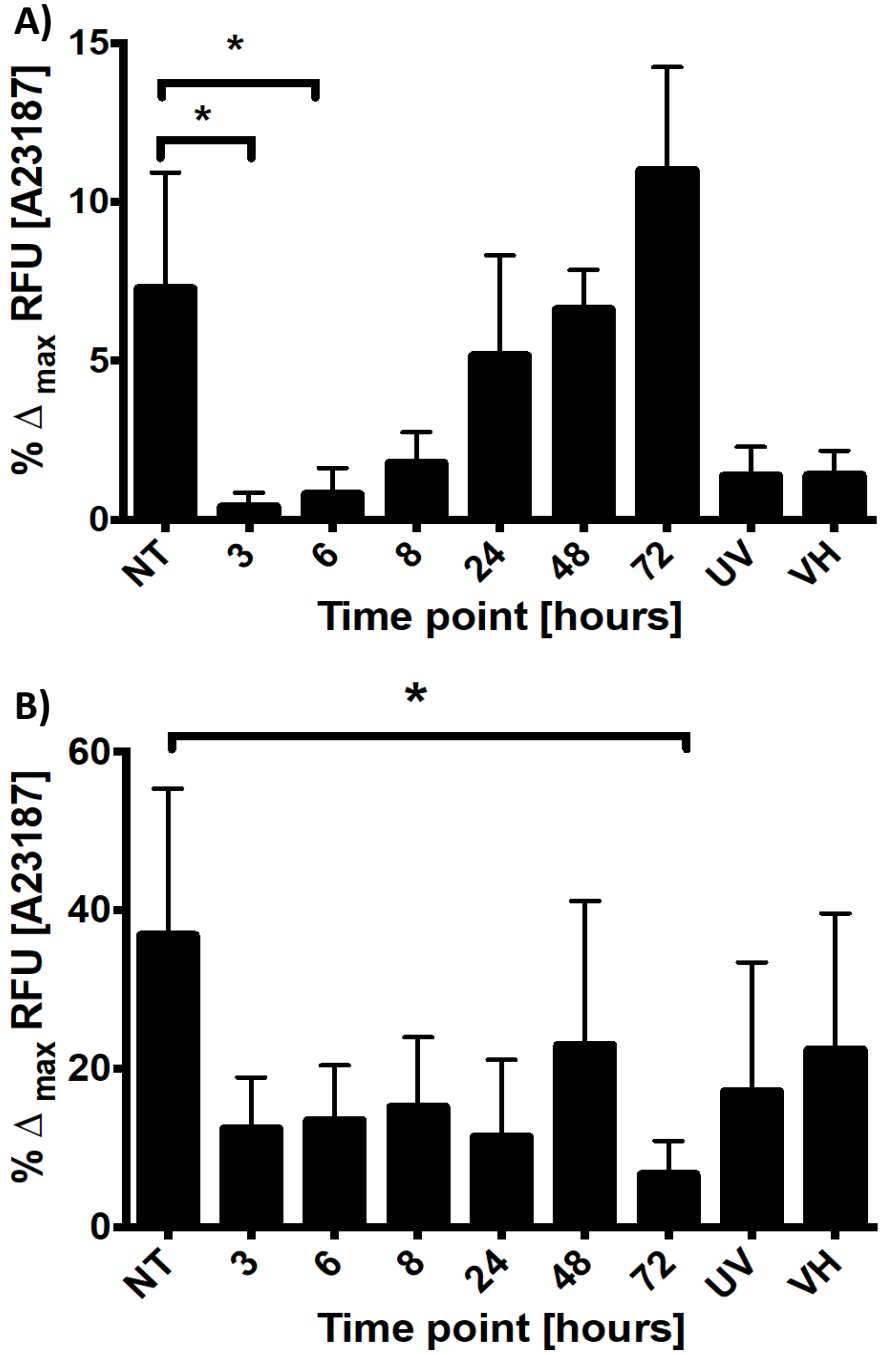

Figure 3.22. ***Calcium signalling response to AITC and ATP from A549 and 1321N1-P2X3 cell lines, respectively, infected with RV-16.*** *RV-16 exposed cell lines over a 72-hour time course. Cells stimulated with receptor specific agonists. Responses measured as a percentage of maximal control compound A23187. Results standardised against vehicle control and expressed as a percentage of vehicle response. A) A549 cells stimulated with allyl isothiocyanate (AITC). B) 1321N1-P2X3 cells stimulated with ATP. No treatment – NT. Ultraviolet – UV. Results are displayed as mean ± S.E.M. of three independent experiments (N=3). Statistical analysis was carried out using two-way ANOVA followed by Tukey analysis. *P<0.05.*

3.3.3.3 RV-16 causes no effect to ATP release or extracellular pH

In addition to monitoring protein expression and functional response of receptors, extracellular ATP levels and pH of culture media was also measured. pH was measured in RV-16 time course media culture samples. No significant change was noted in pH at any time point in either cell line (P>0.05) (Fig. 3.23). Extracellular ATP levels were measured using a luminescence ATP determination kit for offline use, described in section 2.11.1.1. Again, ATP levels were determined in media culture samples of RV-16 time course experiments. No significant change in extracellular ATP levels were noted in either cell line, or time point (P>0.05) (Fig. 3.24). However, we could not rule out the possibility of a viral induced change in expression or activity of ectoATPases present on cell surfaces degrading the released ATP.

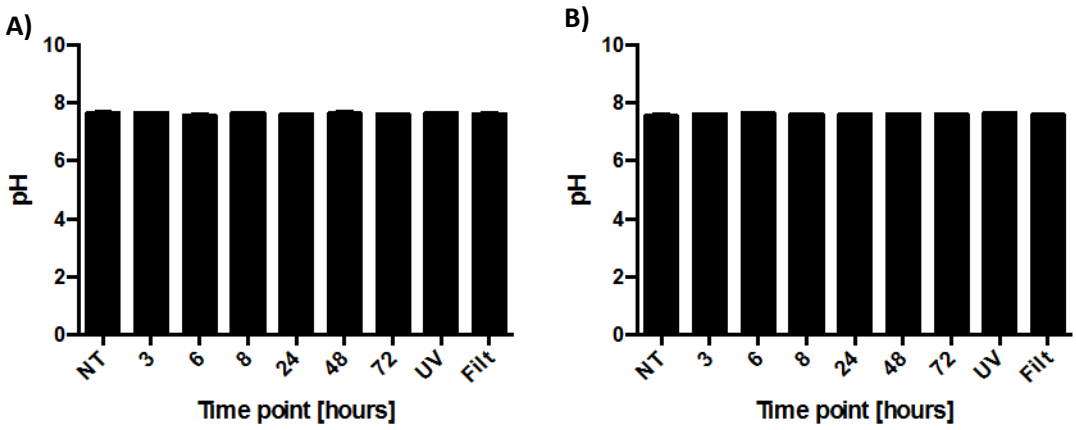

Figure 3.23. ***pH of culture media following stimulation with MOI 1 of RV-16*** *for up to 72 hours, stimulated with UV inactivated viral control (UV), filtered control (filt) or left unstimulated (NT). pH was measured with pre-calibrated pH meter. A) A549 cell line. B) 1321N1-P2X3 cell line. Samples were measured in triplicate and readings averaged. Data shown is mean ± SEM of N=3. Statistical analysis was carried out using two-way ANOVA followed by Tukey analysis. P>0.05*

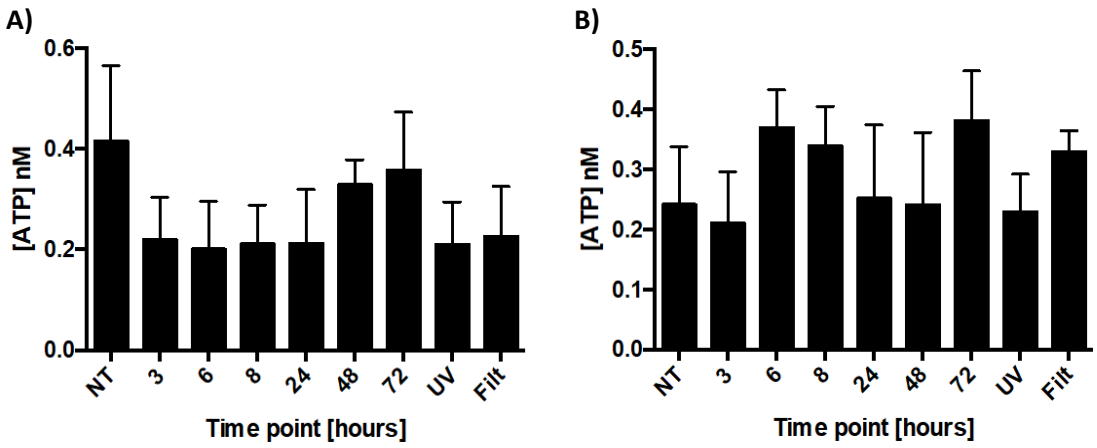

Figure 3.24. ***ATP concentrations in media samples of cells stimulated with RV-16 at MOI 1*** *for up to 72 hours, stimulated with UV inactivated viral control (UV), filtered control (filt) or left unstimulated (NT). Luminescence readings were measured and ATP levels (nM) were quantified using an ATP standard curve. A) A549 cell line. B) 1321N1-P2X3 cell line. Samples were measured in duplicate and each plate was read 3 times and measurements averaged. Data shown is mean ± S.E.M. of three independent experiments (N=3). Statistical analysis was carried out using two-way ANOVA followed by Tukey analysis. P>0.05*

3.3.3.4 RV-16 has no effect on IL-8 cytokine release

ELISA was carried out on cell culture supernatants from both A549 and 1321N1-P2X3 cell lines infected with RV-16 at MOI 1 for presence of inflammatory interleukin IL-8. We found basal uninfected cells displayed higher levels of IL-8 compared to all time points including UV inactivated control in both cell times (data not shown).

3.3.4 Long term RV-16 infection causes no change in TRP channel expression or function in A549 cell line

Following the outcome of the experiments carried out in section 3.3.3 investigating the effect of RV-16 at MOI 1 on TRP channel expression and function to specific receptor agonists on a short-term infection model, we decided to investigate the effect on a long-term infection model. We decided to only investigate this on the A549 airway cell line as we felt there was no significant findings or trends identified when we infected the 1321N1-P2X3 astrocytoma neuronal cell line used throughout the rest of this chapter. All experiments were carried out on similar passage number A549 cells as used in section 3.3.3

to ensure any difference in findings identified were not due to any passage effects or phenotypic drift.

We previously incubated cells with RV-16 for up to 72 hours. However, this length of time would only account for the range of asymptomatic infection known as the incubation phase of infection. We therefore chose to carry out experiments as previously but on cells infected for up to 7 days to begin to delineate the effect of RV-16 *in vitro* during symptomatic infection on TRP channel expression and function. We continued to infect the cells at MOI 1 as used throughout this chapter and in accordance with the SRB assay carried out which determined at MOI 1 there was no significant difference in cellular viability after 216 hours of infection (Fig. 3.5).

Briefly, the cells were infected with RV-16 at MOI 1 and incubated for 1 hour at room temperature with gentle agitation. The cells were washed and incubated at 37^{o}C for up to 168 hours with UV-inactivated sham viral control as used previously. The cells were either lysed and subject to western blot analysis or assayed with calcium fluorescent dye on Flexstation® and using the same concentration of agonists as used in section 3.3.3.

3.3.4.1 Long term infection with RV-16 causes no change in TRPV4 protein expression

We carried out western blot analysis of long-term infection of A549 cells with RV-16 at MOI 1 for up to 168 hours. We investigated the protein expression of TRPA1, TRPV1 and TRPV4 with loading control α-tubulin. We were unable to achieve a signal for either TRPA1 or TRPV1 from any of three independent experiments carried out (data not shown). There was no significant difference in protein expression of TRPV4 (Fig. 3.25) ($P>0.05$, $n=3$).

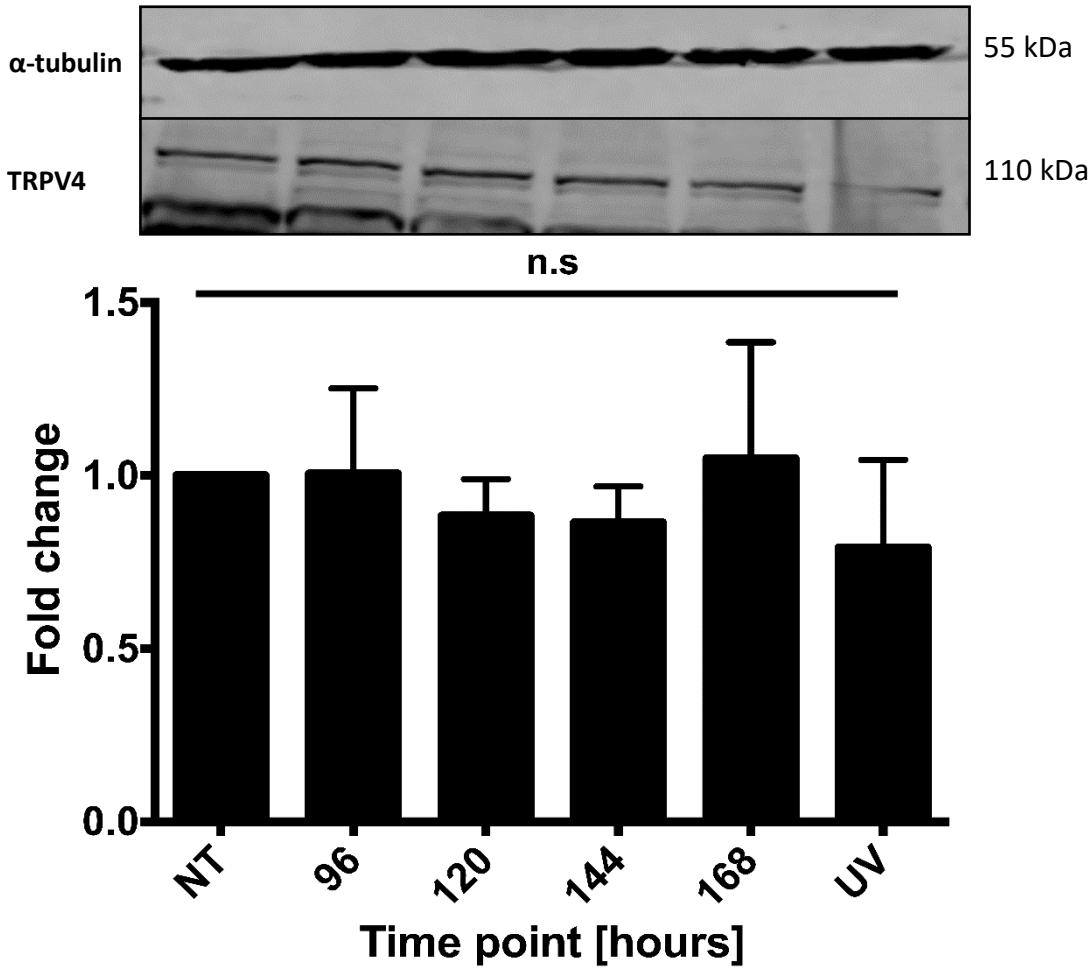

Figure 3.25. ***TRPV4 protein expression in A549 cell line following long term infection of RV-16****. A549 cell line stimulated with RV-16 at MOI 1 for 96 to 168 hours, as labelled, UV-inactivated viral sham control (UV) or left uninfected (NT). Whole cell lysate (50µg protein) probed for α-tubulin loading control and TRPV4 protein expression, as labelled. Results are displayed as mean ± S.E.M. of three independent experiments (n=3). Statistical analysis was carried out using multiple comparison two-way ANOVA followed by Tukey analysis. Densitometry was carried out and expressed as fold change from basal following normalisation to loading control α-tubulin. P>0.05.*

3.3.4.2 Long term infection with RV-16 causes no change in TRP channel function

In A549 cells exposed to RV-16 at MOI 1 there was no significant difference of response to TRPV1 agonist capsaicin, TRPA1 agonist AITC or TRPV4 agonists GSK1106790A or 4αPDD at any time point compared to uninfected control (Fig. 3.26, P>0.05, n=3). Responses remained consistent between all time-points, UV inactivated sham control and uninfected control.

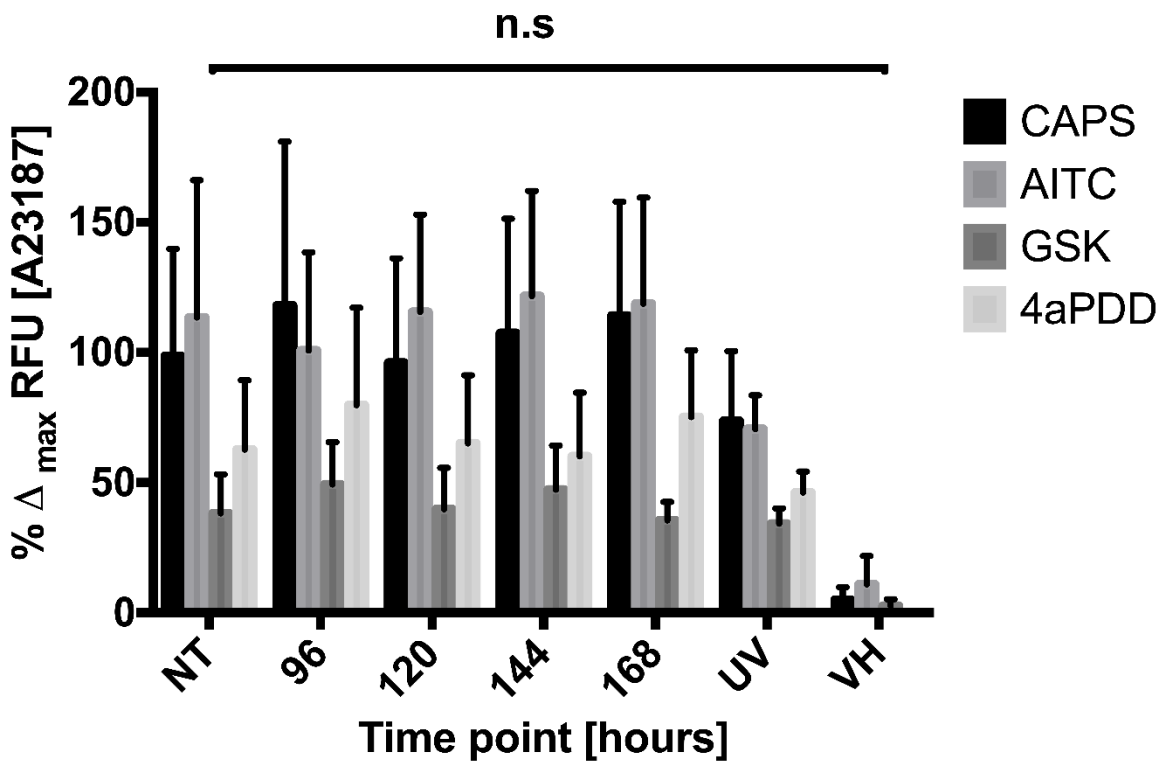

Figure 3.26. ***Calcium signalling responses from A549 cell line following long term infection with RV-16.*** *A549 cell line exposed to RV-16 from 96- to 168-hour long term time course. Cells were stimulated with receptor specific agonists. Responses were measured as a percentage of maximal control compound A23187. A549 cells were stimulated with capsaicin (CAPS), allyl isothiocyanate (AITC), GSK1016790A (GSK) and 4αPDD. NT – uninfected cells, UV – UV inactivated viral sham control, VH – DMSO vehicle control 0.01% v/v. Results are displayed as mean ± S.E.M. of three independent experiments (N=3). Statistical analysis was carried out using two-way ANOVA followed by Tukey analysis. P>0.05.*

3.4 Discussion

In order to gain a better understanding of the molecular mechanism involved in causing a viral cough during the common cold, A549 and 1321N1-P2X3 cell lines were stimulated with synthetic viral analogue poly(I:C) and RV-16 for up to 72 hours. Analysis of gene expression, protein expression and protein function were undertaken to determine if poly(I:C) or RV-16 altered to the expression or function of tussive receptors TRPA1, TRPV1, TRPV4 or P2X3. Through the course of this research we have shown for the first time that astrocytoma cell line 1321N1 can be effectively stimulated with synthetic viral stimulus poly(I:C). We describe that poly(I:C) causes upregulation of TRPV1 transcription, a classical tussive receptor. We observed early upregulation of TRPV1 mRNA from 3 hours post stimulation. We also showed for the first time that astrocytoma cell line 1321N1 can be infected with RV-16. We confirmed this through supernatant sampling during infection time course by infecting RV permissive HeLa Ohio cells in the same manner used for viral titrating, as described in section 2.5.1.

Firstly, we sought to characterise our cell lines, so we carried out a series of experiments to determine basal expression of TRP channels and P2X receptors in A549 and 1321N1 cell lines. RT-PCR data of A549 cell line corresponded with published literature for basal expression clearly expressing TRPA1, TRPV1 and TRPV4 mRNA (Reilly *et al.*, 2003; Mukhopadhyay *et al.*, 2011; Seminario-Vidal *et al.*, 2011). Response to common agonists of TRPA1 (AITC), TRPV1 (capsaicin) and TRPV4 (GSK1016790A) confirmed functional protein expression through the use of intracellular calcium signalling and western blot analysis. Minimal amplification of P2X3 could be found but further analysis with intracellular calcium signalling could not detect protein expression indicating no basal transcribed receptor expression in the cell line. Wild type 1321N1 cell line was used to carry out characterisation due to the ease of propagation over the 1321N1-P2X3 transfected cell line we ultimately used throughout further experimentation. RT-PCR data clearly demonstrated basal mRNA expression of TRPV1 and TRPV4. No mRNA for TRPA1 could be amplified from the cell line. These findings were confirmed with functional intracellular calcium signalling where the cell line responded to capsaicin (TRPV1) and GSK1016790A (TRPV4), at suboptimal concentrations. There was no response to cinnamaldehyde or AITC, two common potent TRPA1 agonists. Inherent problems with agonist GSK1016790A are widely known, but

unfortunately there is only a small pool of available TRPV4 agonists all with poor function or specificity (unpublished observation, personal communication, 2017, 2018) so we have persevered with this choice confirming protein expression with western blot analysis. We confirmed the positive expression of P2X3R in 1321N1-P2X3 transfected cell line with RT-PCR, intracellular calcium signalling and western blot analysis.

Poly(I:C) is a synthetic dsRNA stimulus whereas RV-16 is a ssRNA virus with a dsRNA life cycle stage. One of the controls used in the course of RV-16 infections is UV-inactivated virus which causes the destruction of the viral genome and preventing replication but still capable of binding via ICAM-1 receptor. Therefore, we can determine if any change in mRNA or protein expression, or a change in receptor function is caused by actively replicating virus (poly(I:C)), TLR activation (RV-16) or receptor binding alone (UV-inactivated).

We described that poly(I:C) stimulation induced no significant change in mRNA gene expression or functional response to specific agonists at any point in A549 cell line. Despite this, when we investigated whole cell protein expression, we identified early upregulation of TRPV4 expression and an increased activity to agonist GSK1016790A, albeit at a later time point.

In 1321N1-P2X3 cell line, poly(I:C) did not cause any change in either TRPV4 or P2X3 mRNA expression. However, poly(I:C) did induce a small early upregulation in TRPV1 mRNA, which remained elevated until 48 hpi, where levels returned to baseline. To assess if the increased gene expression translated to increased protein expression, we carried out western blot analysis. Unfortunately, we were unable to achieve a signal for any of the TRPV1 probed membranes so were unable to corroborate this finding. Despite seeing no change in mRNA expression of P2X3 in the 1321N1-P2X3 cell line at any time point and no observable difference in intracellular calcium signalling in response to P2X3 agonist ATP from untreated levels we identified a large increase in protein expression, 2-15 fold increase, throughout the entire time course. Western blot analysis of TRPV4 whole cell protein expression yielded variable results whereby we identified an early decrease (3-48 hpi), followed by a late increase in expression. However, intracellular calcium signalling identified a large increase in activity of TRPV4 in response to GSK1016790A at an early time point when expression was at its lowest point.

Following from the findings of poly(I:C) stimulation we next sought to determine whether a RV-16 produced a similar response over the same period of time. Abdullah *et al.* (2014) is the only published data describing the effect different MOI of RV-16 has on TRP channels resulting in TRP upregulation. As a result of our optimisation, we decided to use MOI of 1 as we felt this better represented a physiological effect whilst ensuring minimal cytotoxicity.

Unlike poly(I:C) stimulation, RV-16 induced significant early inhibition in the A549 cell line when exposed to TRPA1 agonist AITC during intracellular calcium signalling, returning to baseline by 24 hpi. There was no change in signalling responses to capsaicin (TRPV1) and GSK1016790A (TRPV4). However, in the 1321N1-P2X3 cell line, RV-16 induced inhibition of P2X3 signalling in response to ATP at all time points irrespective of exposure to UV inactivated viral control, this was despite a large increase in protein expression from early time points and throughout the time course. Therefore, suggestive that RV-16 infection may inhibit signalling of P2X3 receptor, without the concurrent downregulation of receptor expression. This suggests that this requires not only actively replicating virus but external ICAM-1 receptor binding, due to the fact that poly(I:C) cannot cause this effect alone which would be indicative of an actively replicating viral effect.

We carried out western blot analysis to assess whether the reduction in receptor function corroborated with reduced receptor expression during RV-16 infection. In contrast to intracellular calcium signalling findings, A549 displayed no change in TRPV4 protein expression at any time point. Thereby suggesting RV-16 causes an inhibitory effect to TRPV4 function during early infection without concurrent downregulation of protein expression of the receptor. When exposed to RV-16 the 1321N1-P2X3 cell line also displayed an increased in TRPV4 expression from early infection time point, however, a large increase was also seen in UV and filtered controls. We hypothesise this is likely due to an inherent issue with our western blot analysis system. We have experienced consistent and significant problems with running and visualising western blot membranes. TRP channel antibodies are notoriously unreliable (Fernandes *et al.*, 2013, personal communication, 2016, 2017), as evidenced throughout this chapter whereby we carried out up to nine independent experiments but only achieved a signal on two separate occasions for some targets (TRPV4 and P2X3) or never achieved a signal for other targets

(TRPA1 and TRPV1). Therefore, we are not entirely convinced by our western blot findings for either poly(I:C) or RV-16 experiments. Despite the clear limitations in our western blot system, there is also a possibility that RV-16 may affect our loading control protein α-tubulin (unpublished observation via personal communication, 2018) and because our data are standardised to the loading control, any effect on α-tubulin would massively alter our end densitometry measurement.

We made the decision to measure extracellular ATP levels during the course of the RV-16 time course infections as research is beginning to highlight the important role of ATP in the development of cough (Fowles *et al.*, 2017; Bonvini *et al.*, 2016). However, no observable difference could be noted in ATP release regardless of cell line, treatment or time point up to 72 hours. However, later work has suggested this an ineffective means of accurately measuring ATP levels in culture media and may not be entirely accurate due to the presence of ectoATPases (Seminario-Vidal *et al.*, 2009, 2011; Okada *et al.*, 2006) and the fact we did not use ectoATPase inhibitors to prevent the degradation of ATP in our samples. We stated previously, we could not also rule out the possibility of a virally induced effect on ectoATPase activity on our cell lines.

We carried out ELISA measurements of IL-8 to confirm RV-16 was actively replicating and causing an inflammatory response in our cell lines. Unfortunately, we were unable to confirm this as our ELISA experiments did not work as expected. The literature states there should be an increase in IL-8 release following RV-16 stimulation (Johnston *et al.*, 1998), however, we found lower levels of IL-8 at all time points compared to basal. We would have repeated these experiments to confirm our findings, along with other inflammatory markers such TNF-α and IFN-β.

Finally, following our findings from section 3.3.3, we decided to investigate RV-16 infection long term (96-168 hours). Surprisingly, there was no difference in protein expression of TRPV4 between short- or long-term RV-16 infection as we hypothesised. But most surprisingly was that there was no difference in function of either TRPA1, V1 or V4 during long term infection despite us previously identifying large inhibition of function during short term infection. We hypothesis that this reduction in function seen initially may have been a result of calcium sequestration during early viral infection, possibly a result of TLR and inflammatory pathway activation through RV-16 binding to ICAM-1 receptor and

activation whereby there's a redistribution of calcium stores. However, this hypothesis would require further investigation to confirm.

Two major limitations of this work are that we used A549 alveolar cell line and a transfected cell line. Alveolar cells are not the primary site of infection of RV-16, in fact common cold are generally limited to the upper respiratory tract and only spread to the lower respiratory tract in at risk individuals including those with asthma and COPD. However, we chose to use these cells are they are widely used for RV-16 investigations, are permissible to RV-16 infection (Greiller *et al.*, 2018; Papi *et al.*, 2013; Chun *et al.*, 2013; Wang, Kim & Jang, 2009; Johnston *et al.*, 1998; Papi & Johnston, 1999) and are very easy to propagate. We acknowledge this as a limitation but feel this cell line is still relevant to the unravelling the pathogenesis of the common cold cough. The other major limitation of the work using the transfected 1321N1 cell line is that replication is independent of the nucleus using a promoter within the cell. Therefore, we cannot assume any viral induced changes in expression are due to an effect to the cell and not a result of a viral effect to the promoter expressing the P2X3 gene.

In conclusion, we have shown that A549 and, for the first time, transfected 1321N1-P2X3 cell lines are permissible to poly(I:C) stimulation and infected with RV-16. Collectively our findings suggest RV-16 infection may induce upregulation of cough receptors whilst simultaneously diminishing signalling through the receptor below physiological basal conditions and is an interesting avenue to peruse further.

Table 3.3. ***Comparative table of findings from basal, poly(I:C) and RV-16 experiments****. Data were collated from RT-PCR (PCR), western blot (WB), calcium signalling (CaSig), ATP measurement assays from supernatants (ATP) and pH measurements of supernatants (pH). Basal expression is shown as positive (Y) or negative (N). No change in expression or function from control or baseline during stimulation experiments are shown as NC. Change in expression or function is shown as increase (↑) or decrease (↓) at various time points post-stimulation (hpi) and indicated, were appropriate, with star significance (*P<0.05, ***P<0.001).*

Condition	Technique	A549				1321N1-P2X3			
		TRPA1	TRPV1	TRPV4	P2X3	TRPA1	TRPV1	TRPV4	P2X3
Basal	PCR	Y	Y	Y	N	N	Y	Y	Y
	WB	Y	Y	Y	N	N	Y	Y	Y
	CaSig	Y	Y	Y	N	N	Y	Y	Y
Poly(I:C)	PCR	NC	NC	NC	-	-	NC	NC	NC
	WB	-	-	↑ at 3 and 72 hpi	-	-	-	↓ at 3-48 hpi	↑ at 3-72 hpi
	CaSig	NC	NC	↑ at 72 hpi	-	-	NC	↑ at 8 hpi	NC
RV-16	WB	NC	NC	NC	-	-	***↑ at 3 hpi	↑ at 3 and 6 hpi	↑ at 3-24 hpi
	CaSig	*↓ at 3 and 6 hpi	NC	NC	-	-	↓ at 3-72 hpi	↓ at 3 hpi	*↓ at 72 hpi

Chapter 4

The Effect of Hypotonic TRPV4 Activation on Downstream Signalling and ATP Release

Despite years of research into the common cold cough, the mechanism has yet to be fully elucidated. There is excessive airway mucus production during an URTI which may contribute to hypotonic stimulation of the airway epithelium causing a cough. Data by Seminario-Vidal *et al.*, (2011) showed that hypotonic stimulation of TRPV4 led to ATP release via pannexin-1. ATP is now thought to be a major component in causing cough through stimulation of P2X3 receptor (Fowles *et al.*, 2017; Atkinson *et al.*, 2016; Abdulqawi *et al.*, 2015; Bonvini *et al.*, 2016), which has been shown to be effectively blocked by specific antagonists including MK-7624 (formally AF-219) (Abdulqawi *et al.*, 2015). However, peripheral ATP alone was deemed not to be the primary source of increased coughing (Fowles *et al.*, 2017). With this knowledge, we decided to further investigate ATP release in A549 alveolar cells.

The pathway of hypotonicity induced ATP release was previously partially defined by Seminario-Vidal *et al.*, (2011) using airway derived cells human bronchial, Calu-3 and A549 cells. The pathway identified that hypotonic stimulus caused activation of TRPV4 via a mechanical stretch response. This calcium flux recruited and facilitated the activation of RhoA (Koyama, Oike & Ito, 2001) and subsequent MLC phosphorylation leading to pannexin-1 activation with eventual ATP release through pannexin-1 (Ransford *et al.*, 2009). This was shown through pannexin-1 inhibitor, carbenoxolone, and that inhibition of this channel significantly reduced the extracellular release of ATP by 6-fold. We also know that ATP release via hypotonic stimulation is a calcium dependent mechanism (Boudreault & Grygorczyk, 2004; Tatur *et al.*, 2007; Akopova *et al.*, 2012; Okada *et al.*, 2013).

With limited targeted developments regarding this signalling pathway since the release of the 2011 publication, this leaves a gap in literature to further elucidate the mechanism of ATP release in response to hypotonic stimulation. Through the use of specific inhibitors of TRPV4 (HC067047), RhoA (H1152), MLC (ML-7), pannexin-1 (carbenoxolone), PKC (RO-31-8220), actin cytoskeleton (cytochalasin D) and calcium-calmodulin kinase (KN93) we aim to delineate this pathway further in a hypotonic environment. Further identification of components of this pathway and components which provide an integral role in ATP release may provide a pharmacological target for treatment of cough during respiratory viral infection.

4.1 Approach and methodology

The aim of this chapter was to confirm previously published data and to further our understanding that hypotonic stimulus causes ATP release through pannexin-1 channel (Seminario-Vidal *et al.*, 2011) using soluble luciferase assays, in airway epithelial A549 cells. We decided to employ the use of small molecular weight inhibitors HC067047, H1152, ML-7, carbenoxolone, RO-31-8220, cytochalasin D and KN93 to monitor the change in ATP release during hypotonic stimulus to delineate a full mechanistic pathway.

We aimed to show that hypotonic stimulation leads to ATP release and increased membrane localisation of pannexin-1 through the use of western blotting analysis, whilst visualising cytoskeletal remodelling with and without the presence of inhibitors as TRPV4 and pannexin-1 have both been found to associate and be modulated by actin (Becker, Bereiter-Hahn & Jendrach, 2009; Bao *et al.*, 2012). Literature has previously shown that using a blocking peptide of pannexin-1 only lead to a 50% reduction in ATP release under hypotonic stimulation (Seminario-Vidal *et al.*, 2011), which suggests other components as well as pannexin-1 mediates ATP release.

Throughout Chapter 3 we used A549 airway alveolar and 1321N1-P2X3 astrocytoma neuronal cell lines. However, the focus of this Chapter was to investigate hypotonic stimulation, and physiologically we felt a hypotonic stimulus was unlikely to affect underlying airway nerves. Therefore, we decided to carry out this investigation only on the A549 cell line, as we felt this better represented a physiological effect.

The experiments were carried out using materials and procedures as described in Chapter 2. Briefly, cellular responses to 33% hypotonic stimulus were monitored using western blot analysis to assess changes in global protein expression and activity. Our ultimate end-point measurement was ATP release via pannexin-1 channel.

4.1.1 Methods: Western blot

Cells were seeded at $4.5x10^5$ into T25 flasks and allowed to adhere overnight prior to commencement of hypotonic stimulation assays, as described in section 2.13. Cells were lysed and harvested in 1X cell lysis buffer containing 10mM PMSF and pelleted by centrifugation at 14,000 *x g* for 10 minutes at 4^{o}C. The supernatants were recovered, quantified as described in section 2.9.1 and diluted in 4X Laemmli's buffer to 50µg protein

and heated at 80°C for 10 minutes. The samples were spun at 16,000 *x g* for 10 minutes and stored at -80°C or used immediately.

The prepared lysates were separated on a 10% SDS-PAGE gel (see section 2.9.2) and resolved for 90-120 minutes at 120V. Proteins were transferred to PVDF membrane using Bio-Rad PVDF transfer packs on Tran-Blot Turbo transfer system for 10 minutes at 25V in a semi-dry system.

The PVDF membranes were blocked in 5% milk solution (1X TBS) for 1 hour then incubated overnight at 4°C with primary antibody raised to TRPV4 (1:500), pannexin-1 (1:500), total-MLC (1:1000), phosphor-MLC (ser19) (1:1000) or α-tubulin (1:500) in 1X TBS-T (0.1%) containing 2% BSA. The membranes were then washed and incubated for 1 hour at room temperature with either goat anti-mouse or goat anti-rabbit Licor fluorescent secondary antibodies diluted to 1:15000 in 1X TBS-T (0.1%) containing 2% milk before analysis by Licor fluorescent scanning detection system on Licor Odyssey CLx followed by densitometry analysis as described in section 2.9.5 and section 2.9.6, respectively. Membranes were run in duplicate with sequential probing, so no stripping was carried out. Eliminating any potential problems with loss of antigen as found during the course of western blotting in Chapter 3. Through the use of fluorescent antibodies, we were able to remove the signal by unselecting either 700 or 800 channel for accurate measurement of band density without compromising initial detection.

4.1.2 Methods: ATP measurement

Supernatants from hypotonic stimulation assays were sampled at 15 second intervals for 5 minutes and assayed for extracellular ATP as described in section 2.11.1.1. Concentrations of ATP were quantified using a standard curve.

4.1.3 Methods: Immunofluorescence

Immunofluorescent microscopy was carried out to determine the cellular distribution of pannexin-1, and in relation to the actin cytoskeleton, prior to, during and 5 minutes post hypotonic exposure. Cells were seeded at $4x10^4$ on to 13mm coverslips, previously prepared as described in section 2.14, and allowed to adhere for 48 hours prior to commencement of hypotonic stimulation, as described in section 2.13.

Following a 5-minute exposure to 209mOsm hypotonic buffer or control, the cells were fixed in formaldehyde (4% in PBS) for 15 minutes, followed by permeabilization in triton X-100 (0.1% in PBS) for 10 minutes. The coverslips were then blocked in BSA (2% in PBS) for 1 hour. All washes were carried out with chilled PBS. The cells were then incubated for 1 hour with mouse monoclonal primary antibody raised to pannexin-1 (1:200), followed by incubation with mouse monoclonal anti-mouse IgGκ FITC-conjugated secondary (1:100) for 1 hour. Finally, the cells were stained with phalloidin CruzFluor™ 594 conjugate (1:1000) for 1 hour and mounted on the glass slides with DAPI containing Prolong™ Diamond antifade mounting media.

Fluorescent microscopy analysis was performed as described in section 2.14.

4.1.4 Methods: Calcium Imaging

Calcium imaging measurements were performed as described in section 2.8.3. Briefly, cells were seeded in 12 well Lumox® black clear bottom plates and loaded with 2.5 µg Fluo-4 AM calcium probes. Intracellular calcium flux was imaged and measured using Zeiss axio observer Z1 microscope at excitation wavelength 485 nm and emission 525 nm. Cellular calcium flux was imaged in response to hypotonic stimulus or isotonic control. Positive response was confirmed with positive control A23187 at the end of each experimental time course. Cell responses were calculated using ImageJ with FIJI add on using a standard deviation of Z-stacked movie slices. A minimum of 20 independent regions of interest were selected and mean grey value was calculated for each slice and corrected for background fluorescence. Traces were then analysed for area under the curve and statistically analysed using one-way ANOVA followed by Dunnetts analysis, as described in section 2.8.3.

4.2 Optimisation

4.2.1 Development of hypotonic buffer and ATP measurement assay

We had previously decided to use a pre-determined 200mOsm osmolality for hypotonic assays as this value has been previously used in the literature (Seminario-Vidal *et al.*, 2011; Okada *et al.*, 2013) and we aimed to replicate some of the previous findings of Seminario-Vidal *et al.*, (2011). We managed to achieve a 209mOsm osmolality for the hypotonic assay buffer using a 33% hypotonic solution (Table 4.1)

We decided to continue using a commercially available ATP measurement kit (Thermo) for end-point ATP measurements, as previously used in Chapter 3. We conducted a series of osmolality measurements of the ATP measurement working solution to ensure a hypotonic buffer could be used concurrently with the kit. The measurement kit was made up according to the manufacturer protocol and modified in various ways (as detailed in Table 4.1), osmolarity measurements were made for each working solution (Table 4.1).

To make the kit as per the manufacturer's protocol, the working solution was measured as 52 mOsm and deemed to be too hypotonic for use on live cells with on-line ATP readings. Therefore, the next step was to carry out basic ATP standard curves using the modified isotonic working solutions, as seen in Table 4.1, to ensure the extra solute volume would not cause assay interference or reduced sensitivity as previously found with the modified D-luciferin working solution. ATP standards were prepared ranging from 1nM to 1µM and the luminescence measured using top read luminescence settings on Flexstation® (Molecular Devices). Measurements were taken in duplicate and each standard read twice with standard high sensitivity PMT settings. No signal could be obtained either consistently or at all (data not shown). As a result, these modified working solutions were not suitable for ATP measurements.

We then decided to optimise a protocol for measuring ATP using the individual reagents rather than utilising a pre-made kit. As previously described by Seminario-Vidal, Lazarowski & Okada (2009), luciferase (Sigma) was used at 0.8µg cm^{-2} of culture surface and D-luciferin (BD Bioscience) at 150µM independent of supernatant volume.

Table 4.1. ***Osmolality measurements of ATP working solutions and hypotonic assay buffers****. Dulbecco's modified Eagles media – DMEM; phosphate buffered saline – PBS; Hank's balanced saline solution – HBSS;*

Major constituent	Measurement (osmol kg^{-1})	mOsm L^{-1}
Deionised water – manufacturer standard set up	0.052	52
DMEM – phenol red free	0.331	331
PBS	0.325	325
Deionised water with D-luciferin reconstituted in HBSS	0.076	76
Deionised water and PBS (1:1)	0.193	193
Deionised water and DMEM – phenol red free (1:1)	0.192	192
HBSS – with HEPES (HBSS+)	0.318	318
Hypotonic buffer	0.099	99
Isotonic buffer	0.359	359
HBSS+ and hypotonic buffer (33%) (1:1)	0.209	209
Calcium assay buffer (CAB)	0.324	324
Calcium assay buffer and hypotonic buffer (1:1)	0.209	209

To test the new method, ATP standard curves were read in duplicate using the standard formula (HBSS modified with 10mM HEPES – HBSS+) (318 mOsm) and in a 33% hypotonic solution (209 mOsm) to ensure a signal could be obtained despite the osmolality change and to confirm no interference from solutes. ATP standards were initially read using Flexstation® kinetic top read and read for a duration of 5 minutes. Unfortunately, this setting was insufficient for reading each ATP containing well with a small enough interval (data not shown). Next, we tried using black, clear bottom plates, despite the likelihood of a quenched signal, and running the assay for 5 minutes using Flexstation® bottom read flex mode with 2 second interval. An intermittent signal was achieved but it was significantly damped (data not shown). We decided to use white, clear bottom plates with bottom read setting using 1000ms integration and 2 second interval. Using this method, we successfully obtained a strong, stable signal lasting the full 5-minute measurement time (Fig. 4.1).

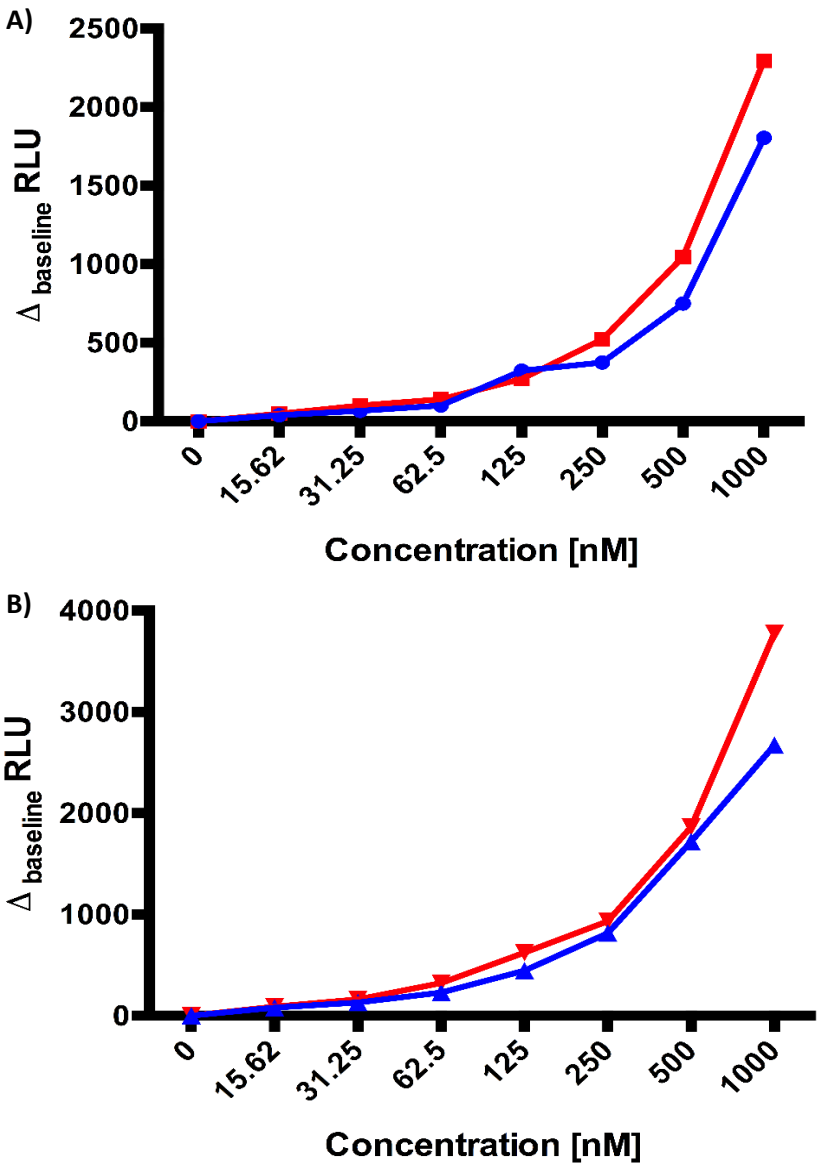

Figure 4.1. ***Test traces of online ATP measurement using in-house prepared luciferin-luciferase mixture*** *made in A) HBSS+ or B) 33% hypotonic buffer read for 30 seconds to measure baseline followed by addition of ATP to mixture. Data displayed are change in relative luminescence (RLU) from baseline following addition of ATP either 60 second (blue) or 300 seconds (red) post addition. Dose response curves using standard curve ATP 1µM to 15nM. Signal obtained at all concentrations for full 300 second duration.*

Finally, to confirm this new method would be suitable to use on live cells we carried out a series of on-line tests to assess extracellular ATP release. Cells were washed 3 times with PBS then equilibrated in HBSS+ for 1 hour at 37°C and 5% CO_2. The cells were allowed to equilibrate and achieve plateau following the addition of luciferase-luciferin to account for shear stress ATP release. A 33% hypotonicity solution was applied to the cells and

luminescence measured for 5 minutes at 1000ms interval. Experiments were run with ATP standards independent of hypotonic stimulus to create a standard curve so luminal ATP concentrations could be quantified. Unfortunately, despite modifications to integration time, method of injection, duration of equilibration and concentration of soluble luciferin-luciferase mixture we were unable to achieve a signal representative of real time flux measurement. Due to the nature of A549 cells and their mechanosensitive properties (Boudreault & Grygorczyk, 2004; Ramsingh *et al.*, 2011; Grygorczyk, Furuya & Sokabe, 2013) we determined this poor luminescent signal was due to saturation of luciferin either from the equilibration period or during the beginning of the hypotonic experiments due to mechanical activation of the cells.

Ultimately due to time constraints, we chose to carry out off-line sampling to measure ATP release in response to hypotonic stimulus using a commercially available kit, used in Chapter 3 and described in section 2.11.1, and quantified the ATP concentration using a standard curve.

4.2.2 Optimisation of fluorescent microscopy imaging using Zeiss axio observer Z1

For the purpose of immunofluorescent analysis used in section 4.3.2 we decided to carry out time point optimisation to determine the optimal duration of hypotonic stimulation. We chose to fix and stain cells at 1-, 3- and 5-minutes post hypotonic exposure and 3- and 5-minutes post isotonic exposure (Fig. 4.2). We identified that there was no visual difference in cellular distribution of pannexin-1 following isotonic exposure at either 3 or 5 minutes. However, following hypotonic exposure we identified that pannexin-1 distribution became less dispersed and more compartmentalised possessing a 'honeycombed' appearance as exposure duration increased (as noted by white arrows in Fig. 4.2). Optimisation was carried out using inhibitors at 3 and 5 minutes of hypotonic exposure but we found negligible difference between images taken (data not shown). Therefore, we chose to continue using the 5-minute hypotonic exposure as stimulus as used throughout section 4.3.

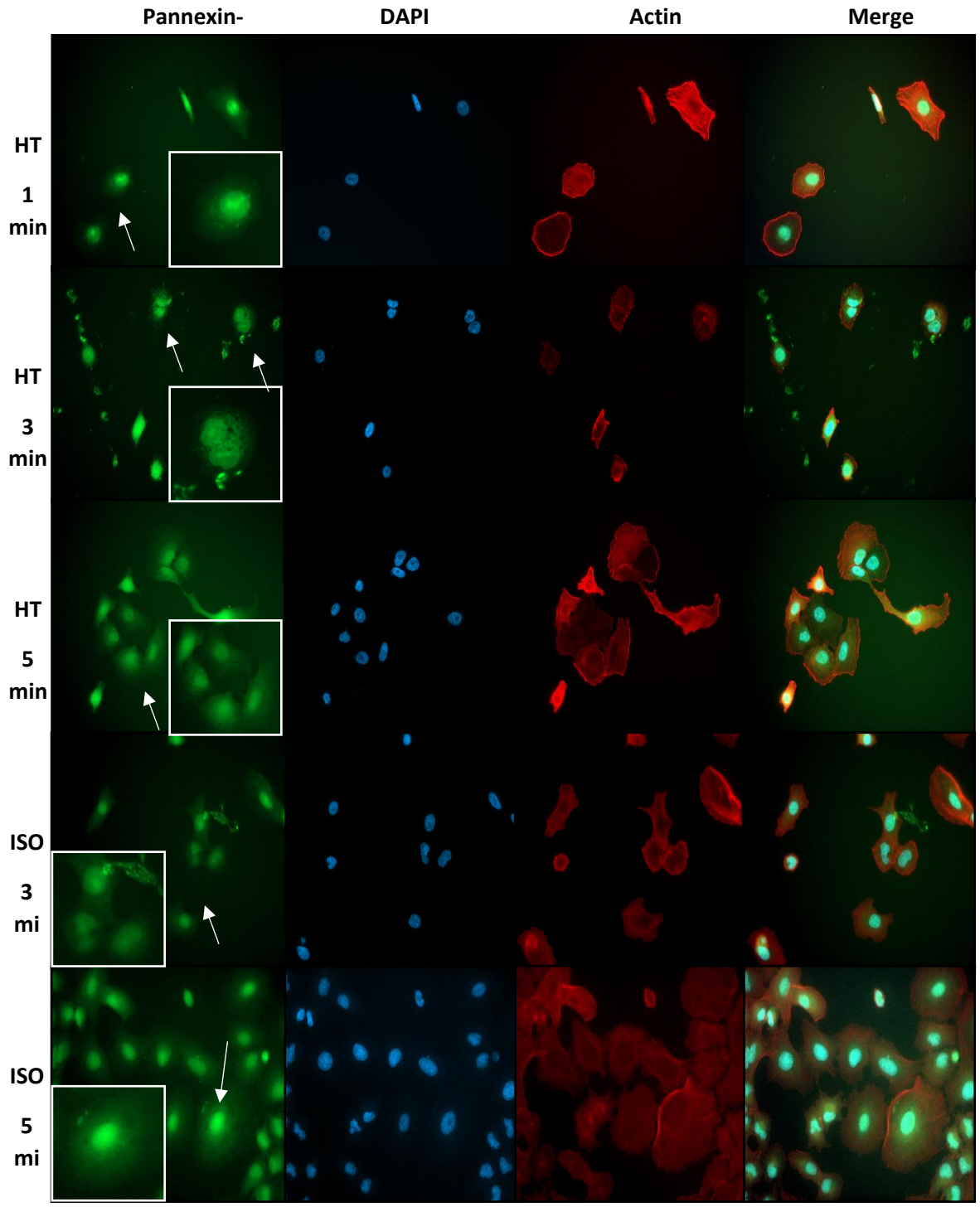

Figure 4.2. ***Immunofluorescent microscopy representative images of A549 cells stimulated with hypotonic (HT) buffer or isotonic (ISO) control buffer for increasing durations of time****. Cells stained for pannexin-1 with FITC (green), nuclei with DAPI (blue) and actin cytoskeleton with phalloidin conjugate 594 (red). Three targets overlaid and merged (merge). Images representative from minimum of 5 images taken from n=1. White arrows indicate areas of interest and are represented with magnified inset boxes.*

4.3 Results

4.3.1 TRPV4 activation through hypotonic shock causes pannexin-1 mediated ATP release via RhoA signalling

The role of TRPV4 activation in the hypotonic stress pathway has been previously characterised in A549 cells (Seminario-Vidal *et al.*, 2011). We aimed to replicate those findings to show the role of RhoA (Seminario-Vidal *et al.*, 2011; Koyama, Oike & Ito, 2001) and MLC downstream of TRPV4 activation and upstream of pannexin-1 channel activation (Seminario-Vidal *et al.*, 2011; Ransford *et al.*, 2009). We then aimed to add to these current findings to further delineate the mechanism of the hypotonic stress pathway.

We have previously confirmed the expression of TRPV4 endogenously in A549 cell line (section 3.3.1) and the A549 cell line has been used in literature characterising pannexin-1 channel (Seminario-Vidal *et al.*, 2011; Ransford *et al.*, 2009; Seminario-Vidal *et al.*, 2009). Therefore, we chose not to carry out any further optimisation of the A549 cell line. Throughout our experiments using inhibitors we decided to use concentrations and durations of incubation others have used previously defined in the literature (Seminario-Vidal *et al.*, 2011; Okada *et al.*, 2013).

Briefly, A549 cells were exposed to inhibitors of known and hypothesised components of the hypotonic stress pathway. Cells were then exposed to hypotonic stimuli of 209 mOsm (33% hypotonicity) or control isotonic 359 mOsm, for a period of 5 minutes. Whole cell lysates were produced and subject to western blot analysis for TRPV4, pannexin-1, total MLC, phospho-MLC (ser19) and α-tubulin, or cell supernatants were sampled in real time and processed post-exposure to quantify the concentration of released ATP. All experiments were carried out on A549 cells from known origin (Public Health England) with passage numbers 15-35.

4.3.1.1 Hypotonic stimulation causes no change to global protein expression of pannexin-1 or TRPV4

Whole cell lysates were isolated from A549 cells incubated with various inhibitors to the hypothesised 'hypotonic pathway'. Lysates were subject to western blot analysis and probed for global protein expression of pannexin-1, TRPV4, total-MLC, phospho-MLC (ser19) and loading control α-tubulin (Fig. 4.3 and 4.4).

As expected, western blots of hypotonic time course experiments yielded no significant change in protein expression over the short incubation and time course. We hoped to monitor MLC phosphorylation of ser19 during the hypotonic incubation and monitor the effect of various inhibitors to the hypotonic stress pathway on MLC phosphorylation using western blotting. However, we only managed to achieve a positive signal for both total-MLC and phospho-MLC (ser19) on one occasion (data not shown). We were therefore unable to carry out any analysis using this data. As a result, we cannot draw any conclusions of the effect of hypotonic stimulation on MLC phosphorylation at ser19. Inhibition of TRPV4, RhoA (via ROCK), MLC (via MLCK) and pannexin-1 followed by hypotonic stimulation caused no significant change in global expression of pannexin-1 from basal (Fig. 4.3, $P>0.05$; $n=3$). Furthermore, no significant change was found in global expression of TRPV4 in comparison to basal, following inhibition of TRPV4, RhoA (via ROCK), MLC (via MLCK) and pannexin-1 followed by hypotonic stimulation (Fig. 4.4, $P>0.05$; $n=3$).

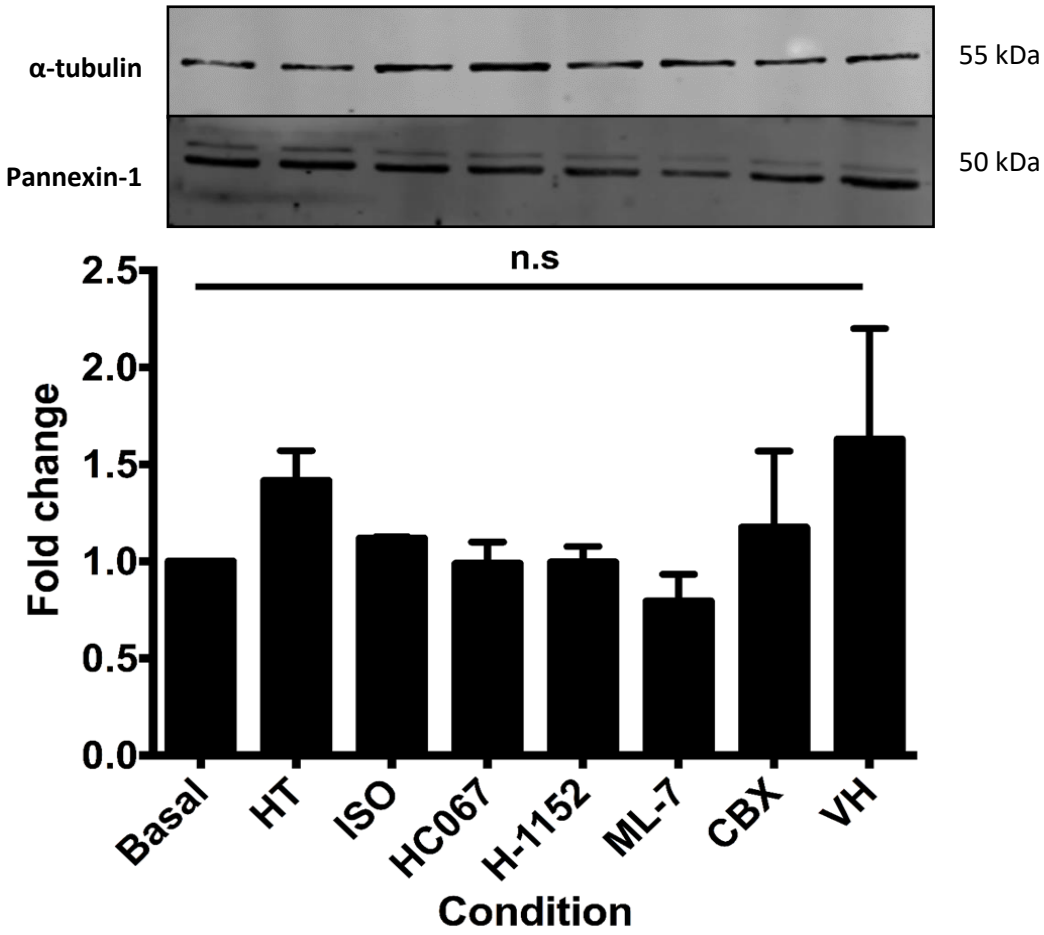

Figure 4.3. ***Pannexin-1 protein expression in A549 following hypotonic stimulation.*** *A549 cell line incubated with inhibitors HC067047 (HC06), H-1152, ML-7, carbenoxolone (CBX) or 0.01% v/v DMSO (VH) then post-treated with 33% hypotonicity (HT) or isotonic control (ISO). Whole cell lysate (50µg protein) probed for α-tubulin (55kDa) loading control and pannexin-1 (50kDa) global expression, as labelled. Densitometry carried out and expressed as fold change from basal following normalisation to loading control α-tubulin and as mean ± S.E.M. Representative blot image of three independent experiments (n=3). Statistical analysis was carried out using multiple comparison two-way ANOVA followed by Tukey analysis. P>0.05.*

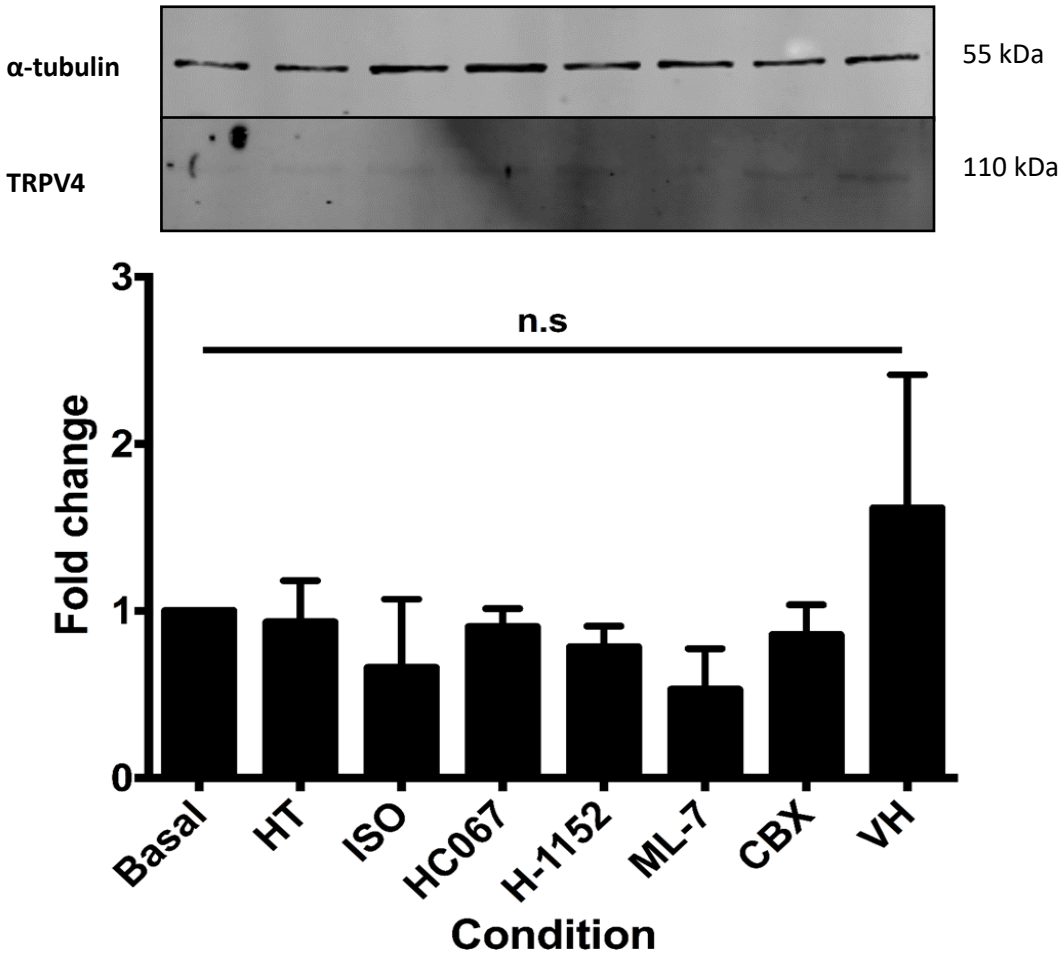

Figure 4.4. ***TRPV4 protein expression in A549 following hypotonic stimulation.*** *A549 cell line incubated with inhibitors HC067047 (HC06), H-1152, ML-7, carbenoxolone (CBX) or 0.01% v/v DMSO (VH) then post-treated with 33% hypotonicity (HT) or isotonic control (ISO). Whole cell lysate (50µg protein) probed for α-tubulin (55kDa) loading control and TRPV4 (110kDa) global expression, as labelled. Densitometry carried out and expressed as fold change from basal following normalisation to loading control α-tubulin and as mean ± S.E.M. Representative blot image of three independent experiments (n=3). Statistical analysis was carried out using multiple comparison two-way ANOVA followed by Tukey analysis. P>0.05.*

4.3.1.2 Hypotonically stimulated ATP release is significantly reduced following inhibition of MLCK and pannexin-1

Hypotonic exposure and mechanical stimulation in A549 cells cause ATP release (Seminario-Vidal *et al.*, 2011; Grygorczyk, Furuya & Sokabe, 2013). We intended to investigate and further delineate the mechanism of hypotonic induced ATP release. Firstly, we aimed to reproduce findings from Seminario-Vidal *et al.* (2011) to ensure hypotonic stimulation lead to ATP release in A549 cells. We endeavoured to optimise an in-house ATP

assay not commercially available as a kit to measure ATP release in real-time on live cells. However due to issues with optimisation (see section 4.2.1), we used a commercially available, ATP determination kit, to assess the release of extracellular ATP on cells stimulated with hypotonic buffer over a 5-minute duration. Briefly, the cells were incubated with inhibitors to TRPV4 (10µM HC067047 – 30 minutes), RhoA (via ROCK) (1 µM H1152 – 45 minutes), MLC (via MLCK) (1 µM ML-7 – 45 minutes), pannexin-1 (10 µM carbenoxolone – 15 minutes) or vehicle control (0.01% v/v DMSO – 45 minutes). The cells were then either sampled undisturbed for basal ATP release or exposed to 209mOsm hypotonic stimulation or isotonic control buffer. Samples were taken every 15 seconds for 5 minutes. The results were displayed as fold change from hypotonic positive control and area under the curve (AUC) analysis was also carried out.

When peak ATP release was determined and analysed, as expected, there was a significant 0.961-fold change reduction in ATP release when A549 cells were exposed to isotonic control buffer (Fig. 4.5, P=0.0031; n=3) to account for mechanosensitive properties of A549 cells in comparison to hypotonic stimulation. Inhibition of MLC via MLCK and pannexin-1 resulted in a significant 0.7821- and 0.7018-fold change reduction in ATP release, respectively, upon hypotonic stimulation in comparison to hypotonic stimulation alone (Fig. 4.5, P=0.0131 and P=0.0276, respectively; n=3). However, there was no significant difference in ATP release when TRPV4 and RhoA were inhibited (P>0.05; n=3).

When each sample trace was subject to AUC analysis there was no significant difference in any condition in comparison to hypotonic stimulation (Fig. 4.6, ISO P=0.1403, H1152 P=0.3172, ML7 P=0.2508, CBX P=0.1669; n=3). However, when the curves of ATP release from cells inhibited with HC067047 (TRPV4 inhibitor) (Fig. 4.7A) were analysed, it was identified that whilst peak ATP release (Fig. 4.5) and overall ATP release (Fig. 4.6) were no different from hypotonic control, ATP release from the cells was much later than the initial stimulus (HT peak at 45 seconds vs HC06 peak at 180 seconds). This trend was consistent through three independent experiments and not seen from any other inhibitor. Finally, in cells incubated with H1152 (RhoA inhibitor), despite there being no significant difference in either peak (Fig. 4.5) or overall (Fig. 4.6) ATP release from hypotonic control, there was a large difference between analyses. This could be explained by interrogation of ATP curves (Fig. 4.7B) where those H1152 treated cells responded with large, brief ATP releases in

comparison to hypotonic stimulation alone which displayed a similar peak ATP release concentration but for a more sustained length of time (Fig. 4.7B).

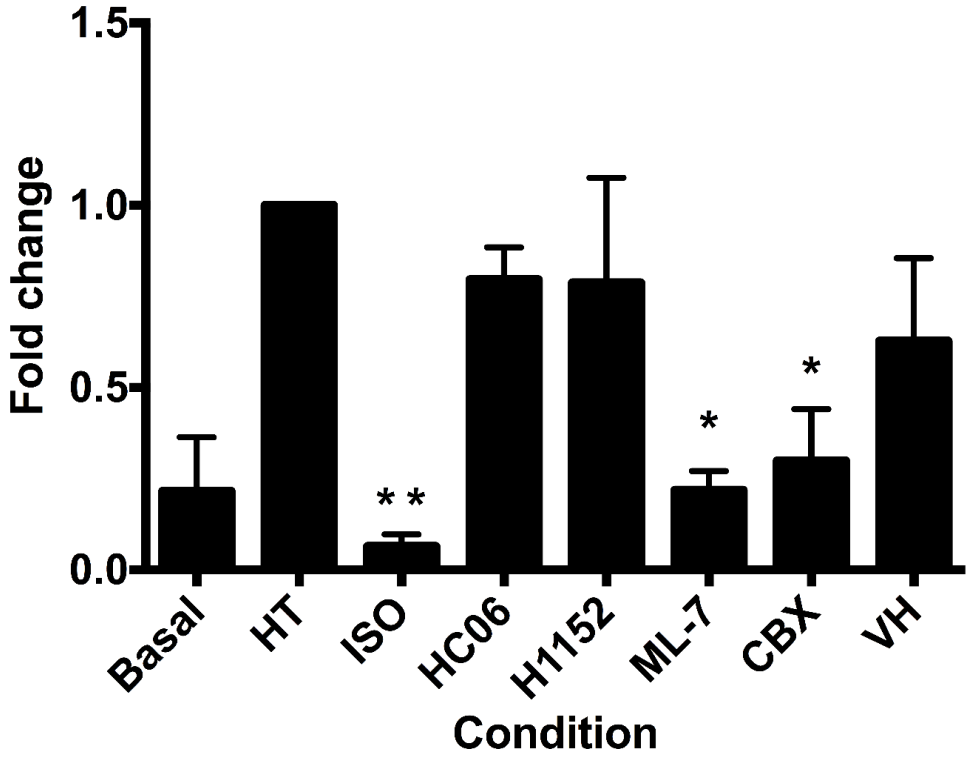

Figure 4.5. ***Extracellular peak ATP release following hypotonic stimulation.*** *A549 cell line incubated with inhibitors HC067047 (HC06), H1152, ML-7, carbenoxolone (CBX) or 0.01% v/v DMSO (VH) then post treated with 33% hypotonicity (HT) or isotonic control (ISO). Supernatants sampled at 15 second intervals for 5 minutes. Peak extracellular ATP release data displayed as fold change from positive control HT (209 mOsm) and as mean ± S.E.M. of three independent experiments (n=3). Statistical analysis was carried out using multiple comparison one-way ANOVA followed by Dunnetts test compared against HT. *P<0.02, **P=0.0031.*

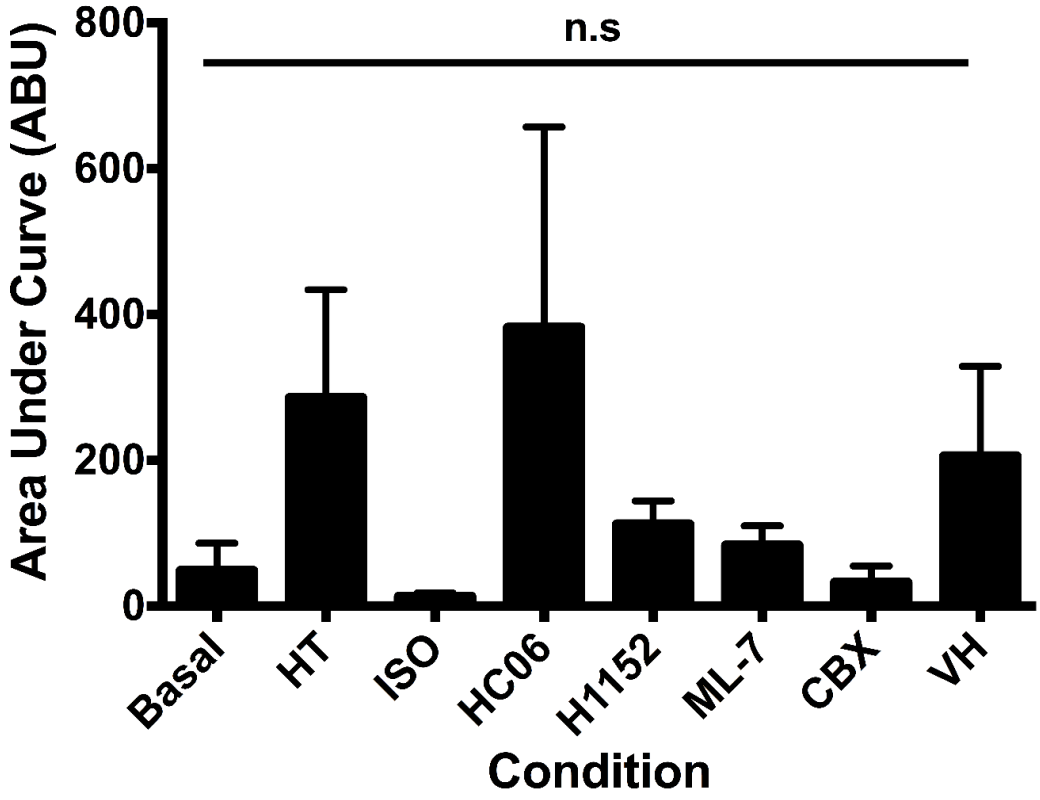

Figure 4.6 ***Area under curve analysis of total extracellular ATP release following hypotonic stimulation.*** *A549 cell line incubated with inhibitors HC067047 (HC06), H1152, ML-7, carbenoxolone (CBX) or 0.01% v/v DMSO (VH) then post treated with 33% hypotonicity (HT) or isotonic control (ISO). Supernatants sampled at 15 second intervals for 5 minutes. Extracellular ATP release data analysed for area under curve for full 5-minute time course from each condition. Data displayed as mean ± S.E.M. of three independent experiments (n=3). Statistical analysis was carried out using multiple comparison one-way ANOVA followed by Dunnetts test compared against HT. P>0.05.*

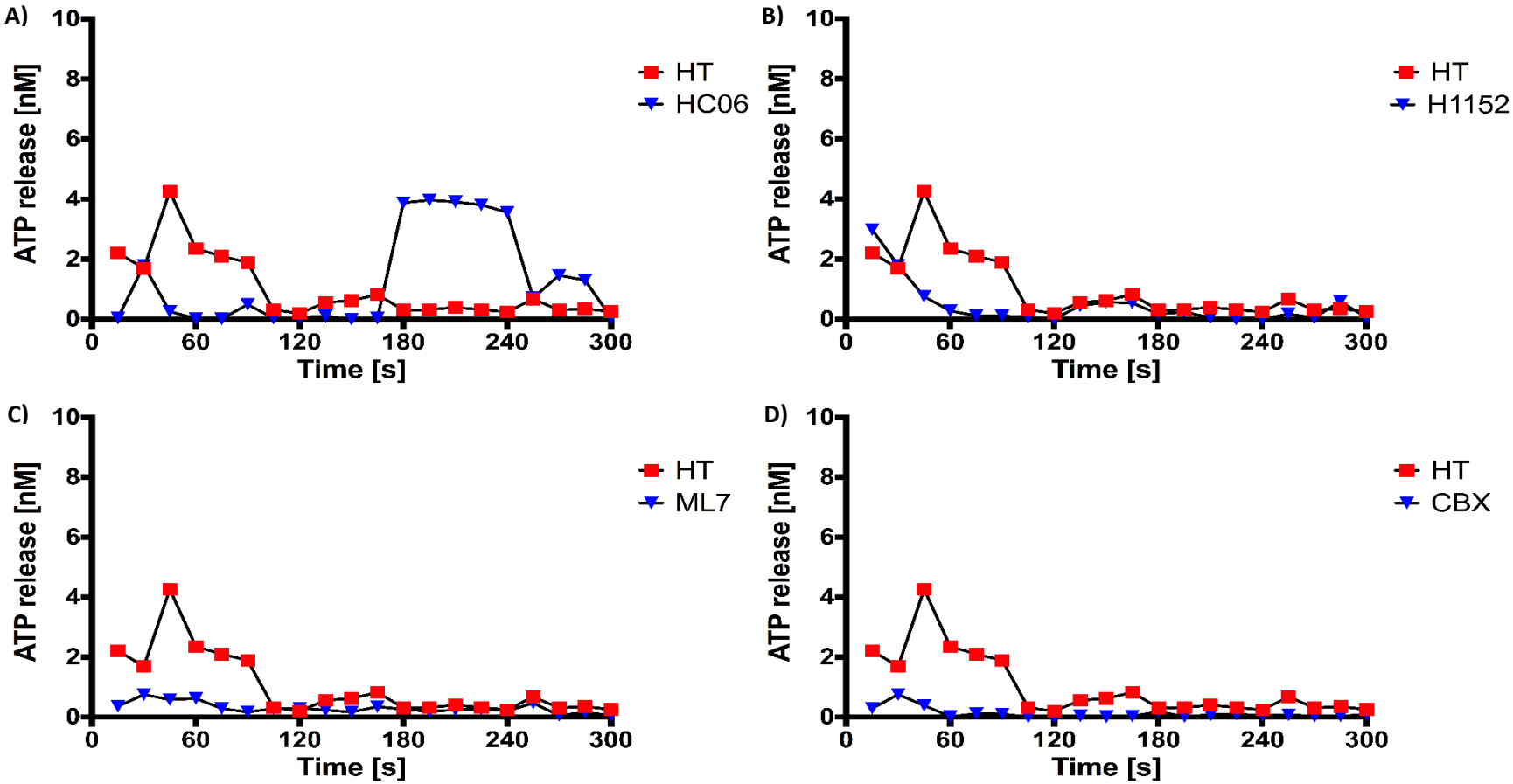

Figure 4.7. ***Quantified ATP sampling traces*** *of A) HC067047 (HC06), B) H1152, C) ML7 and D) carbenoxolone (CBX) compared graphically against hypotonic stimulus (HT). Graphically displayed as mean data points of three independent experiments (n=3) without error bars for visibility. Data processed and statistically analysed as seen in figure 4.6.*

4.3.1.3 Hypotonically stimulated ATP release is significantly reduced following inhibition of PKC, calcium-calmodulin kinase and actin cytoskeleton

We decided to further characterise the mechanism of hypotonic induced ATP release using more inhibitors and sampled cell supernatants once again. We sought to determine if hypotonically stimulated ATP release was facilitated via PKC activation, mediated by calcium-calmodulin kinase or as a result of/or aided by cytoskeletal reorganisation. We did this under the same conditions used in 4.3.1.2 instead incubating A549 cells with 10µM cytochalasin D (actin cytoskeleton), 10µM KN93 (calcium-calmodulin kinase) or 10µM RO-31-8220 (PKC) for 30 minutes, the cells were then exposed to 33% hypotonic stimulus or isotonic control (Fig. 4.8).

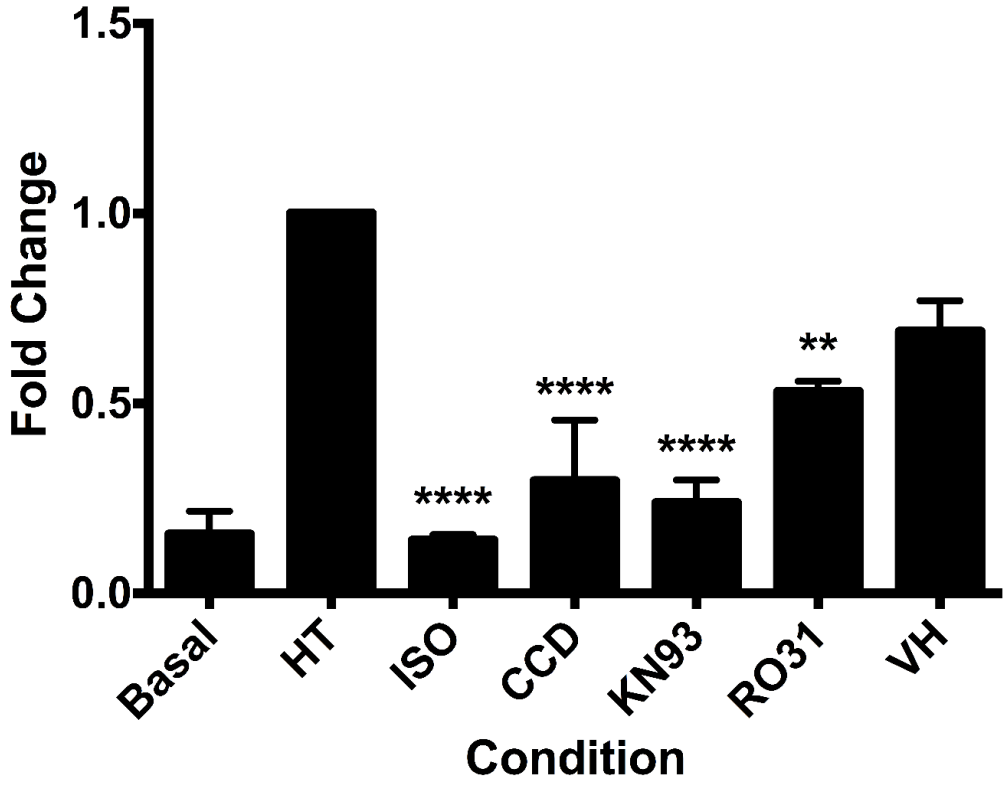

Figure 4.8. ***Extracellular peak ATP release following hypotonic stimulation.*** *A549 cell line incubated with inhibitors cytochalasin D (CCD), KN93, RO-31-8220 (RO31) or 0.01% v/v DMSO (VH) then post treated with 33% hypotonicity (HT) or isotonic control (ISO). Supernatants sampled at 15 second intervals for 5 minutes. Peak extracellular ATP release data displayed as fold change from positive control HT (209 mOsm) and as mean ± S.E.M. of three independent experiments (n=3). Statistical analysis was carried out using multiple comparison one-way ANOVA followed by Dunnetts test compared against HT. **P=0.0033, ****P<0.0001.*

Peak ATP was measured, analysed and displayed as fold change from hypotonic stimulus. Once again, as expected, there was a significant 0.8607-fold change reduction in ATP release when A549 cells were exposed to isotonic control buffer (Fig. 4.8, $P<0.0001$; n=3) in comparison to hypotonic stimulation. Inhibition of the PKC using RO-31-8220 caused a significant 0.469-fold change reduction in peak ATP release in comparison to hypotonic control ($P=0.0033$; n=3). Furthermore, inhibition of actin cytoskeleton using cytochalasin D and calcium-calmodulin kinase using KN93 also caused a significant 0.7046- and 0.7625-fold change reduction in peak ATP release, respectively ($P<0.0001$; n=3).

When each sample trace was subject to AUC analysis there was no significant difference in any condition in comparison to hypotonic stimulation (Fig. 4.9, ISO $P=0.18$, CCD $P=0.0966$, KN93 $P=0.1629$, RO31 $P=0.5104$; n=3). However, curves of ATP release from cells inhibited with RO-31-8220 (PKC inhibitor) (Fig. 4.10B) remained consistently marginally raised for the final 2 minutes of the time course, whereas, in all other conditions ATP release was brief. This trend was consistent throughout three independent experiments and not seen from any other inhibitor used.

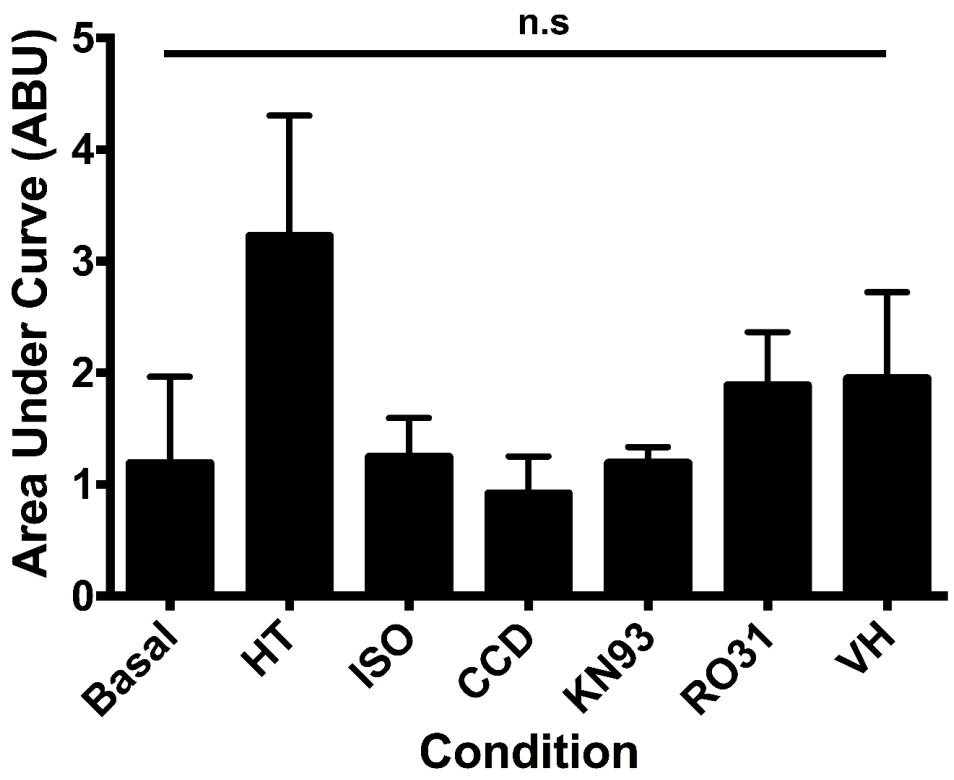

Figure 4.9. ***Area under curve analysis of total extracellular ATP release following hypotonic stimulation.*** *A549 cell line incubated with inhibitors cytochalasin D (CCD), KN93, RO-31-8220 (RO31) or 0.01% v/v DMSO (VH) then post treated with 33% hypotonicity (HT) or isotonic control (ISO). Supernatants sampled at 15 second intervals for 5 minutes. Extracellular ATP release data analysed for area under curve for full 5-minute time course from each condition. Data displayed as mean ± S.E.M. of three independent experiments (n=3). Statistical analysis was carried out using multiple comparison one-way ANOVA followed by Dunnetts test compared against HT. P>0.05.*

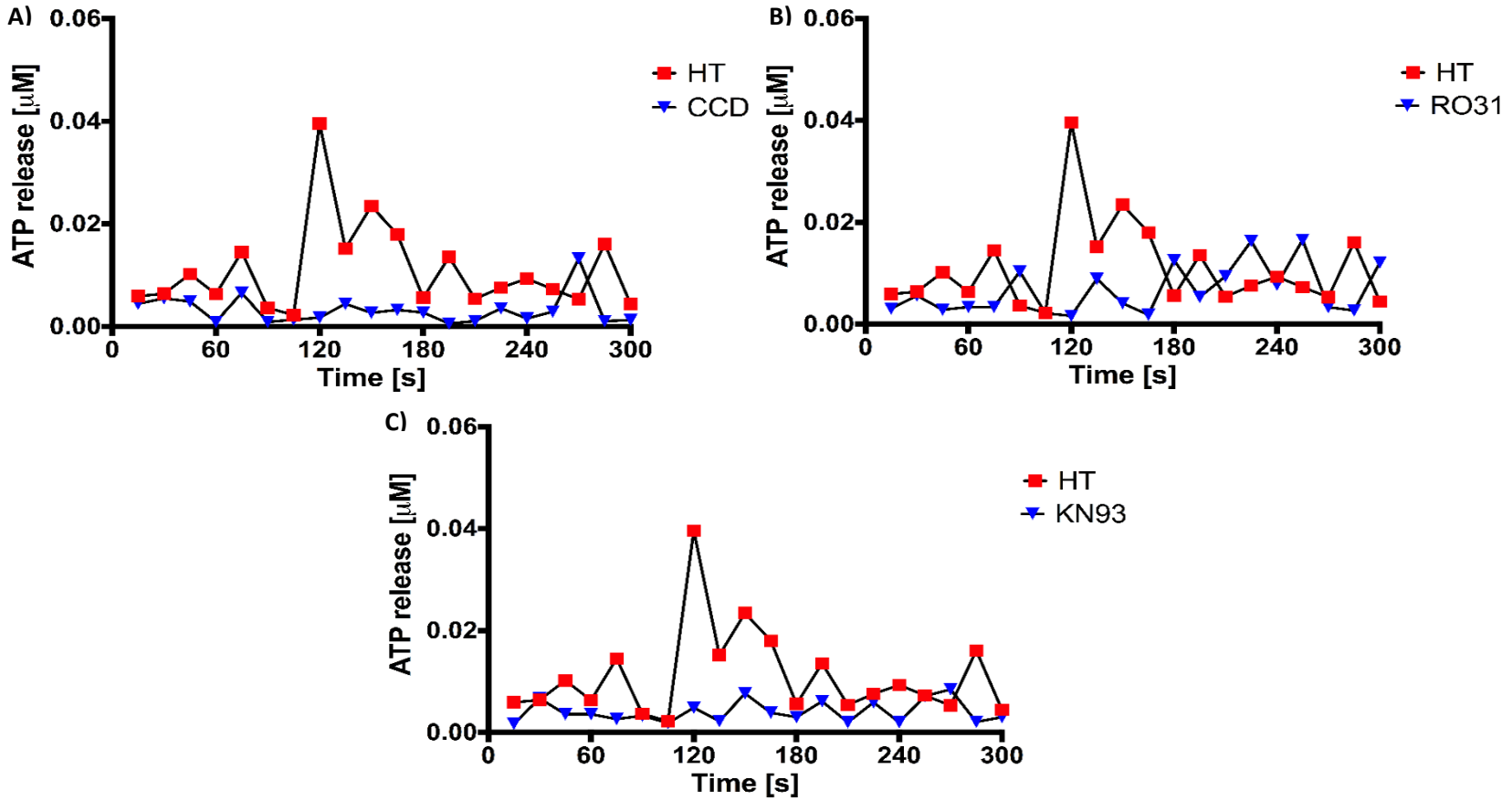

Figure 4.10. ***Quantified ATP sampling traces*** *of A) cytochalasin D (CCD), B) RO-31-8220 (RO31) and C) KN93 compared graphically against hypotonic stimulus (HT). Graphically displayed as mean data points of three independent experiments (n=3) without error bars for visibility. Data processed and statistically analysed as seen in figure 4.9.*

4.3.1.4 Hypotonically stimulated ATP release is dependent on calcium-calmodulin kinase function

Next, we decided to investigate to see if we could knock out the ATP release mechanism following hypotonic stimulation using a combination of inhibitors used previously which displayed the largest inhibition. We used cytochalasin D, carbenoxolone and KN93 in combination, as labelled in Figure 4.11. Peak ATP release was determined and displayed as fold change from hypotonic stimulation. Isotonic control displayed a significant 0.7922-fold change reduction in ATP release (Fig. 4.11, $P<0.0001$; n=3) ensuring the cell responses were not due to mechanical stimulation. A549 cells incubated with a combination of cytochalasin D and carbenoxolone, cytochalasin D and KN93, and carbenoxolone and KN93 displayed a significant 0.7084-, 0.7597-, and 0.7711-fold change reduction in peak ATP release, respectively ($P=0.0004$, $P=0.0002$ and $P=0.0002$, respectively; n=3). However, when A549 cells were incubated with a combination of cytochalasin D, carbenoxolone and KN93, there was still a significant 0.636-fold change reduction in peak ATP release ($P=0.0013$; n=3), but to a lesser extent than any of the inhibitors used in dual combination.

AUC analysis of the quantified ATP curves (Fig. 4.12) from each combination of inhibitors showed that there was a significant reduction in total ATP release following hypotonic stimulation in all combination conditions when compared to hypotonic control (Fig. 4.13). Combination of cytochalasin D and carbenoxolone resulted in a significant reduction in AUC ($P=0.0065$; n=3). However, in any combination where KN93 was used, there was a larger reduction in AUC compared to hypotonic stimulation alone (Fig. 4.13, CCD+KN93 $P=0.0001$, CBX+KN93 $P=0.0001$, CCD+CBX+KN93 $P=0.0003$; n=3). These data suggest inhibition of calcium-calmodulin kinase with KN93 causes the greatest effect to hypotonic induced ATP release, therefore, hypotonic induced ATP release may be dependent on calcium-calmodulin kinase.

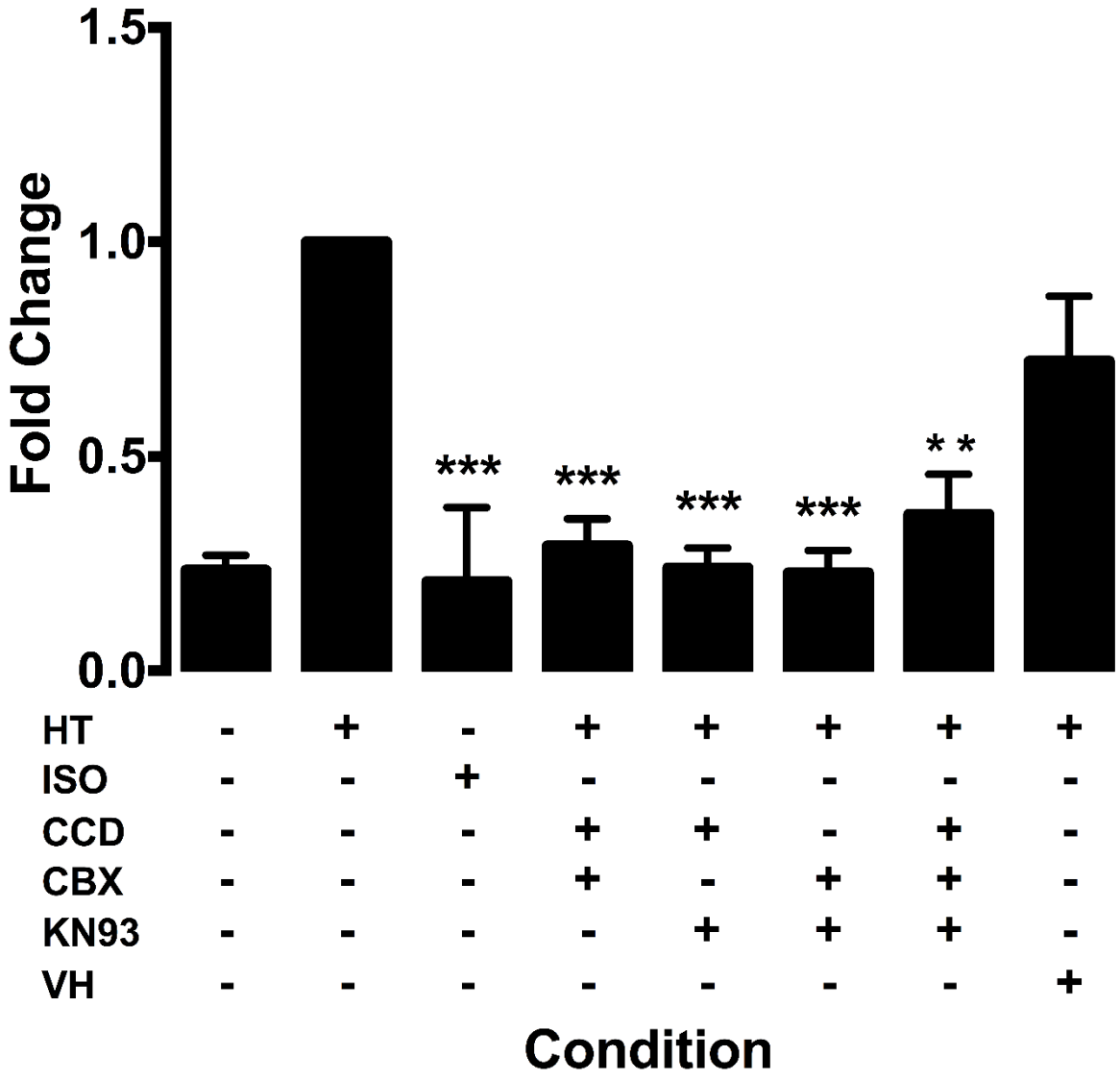

Figure 4.11. ***Extracellular peak ATP release following hypotonic stimulation.*** *A549 cell line incubated with inhibitors cytochalasin D (CCD), carbenoxolone (CBX), KN93 in combination, as labelled, or 0.01% v/v DMSO (VH) then post treated with 33% hypotonicity (HT) or isotonic control (ISO). Supernatants sampled at 15 second intervals for 5 minutes. Peak extracellular ATP release data displayed as fold change from positive control HT (209 mOsm) and as mean ± S.E.M. of three independent experiments (n=3). Statistical analysis was carried out using multiple comparison one-way ANOVA followed by Dunnetts test compared against HT. **P=0.0013, ***P<0.0004.*

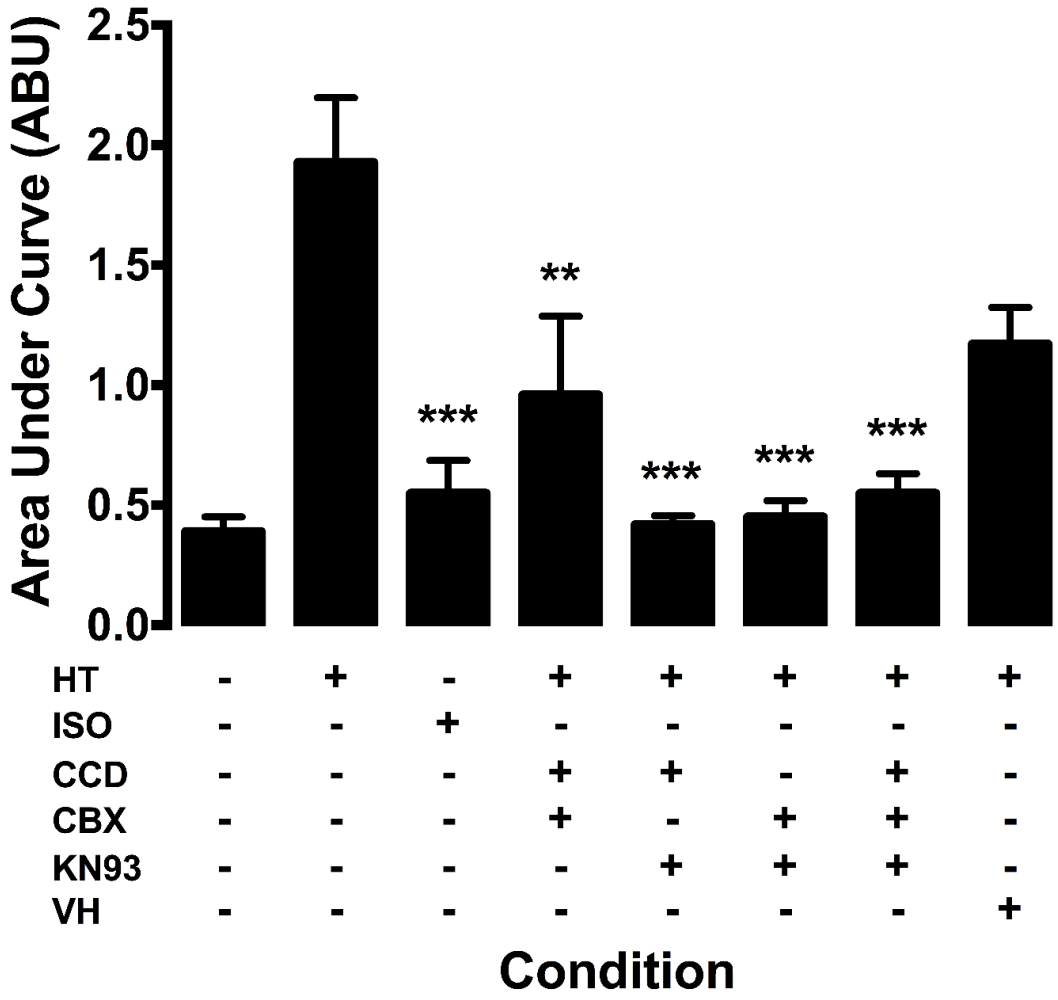

Figure 4.12. ***Area under curve analysis of total extracellular ATP release following hypotonic stimulation.*** *A549 cell line incubated with inhibitors cytochalasin D (CCD), carbenoxolone (CBX), KN93 in combination, as labelled, or 0.01% v/v DMSO (VH) then post treated with 33% hypotonicity (HT) or isotonic control (ISO). Supernatants sampled at 15 second intervals for 5 minutes. Extracellular ATP release data analysed for area under curve for full 5-minute time course from each condition. Data displayed as mean ± S.E.M. of three independent experiments (n=3). Statistical analysis was carried out using multiple comparison one-way ANOVA followed by Dunnetts test compared against HT. **P=0.0065, ***P<0.0003.*

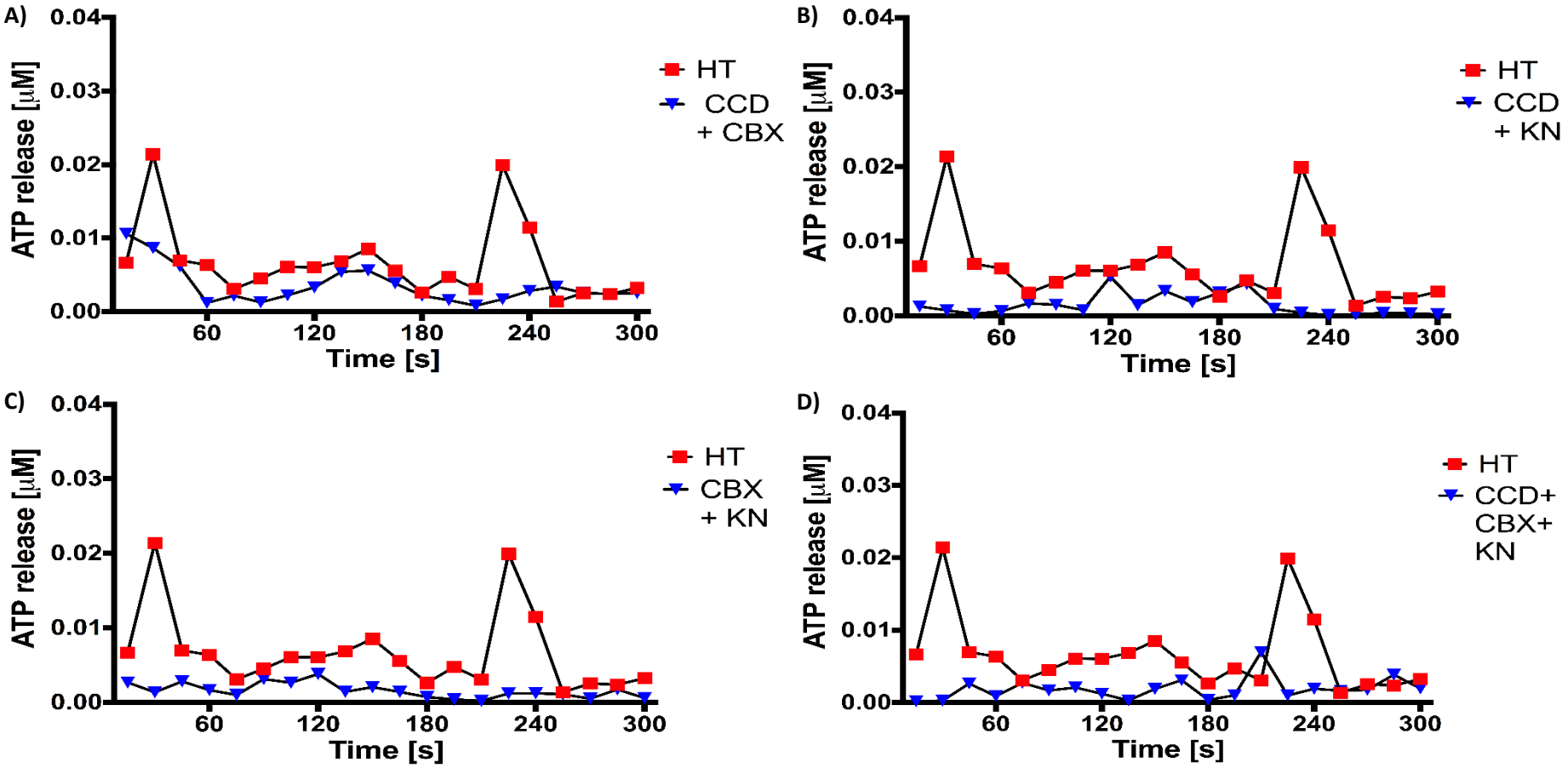

Figure 4.13. ***Quantified ATP sampling traces of various inhibitors used in combination*** *A) cytochalasin D (CCD) and carbenoxolone (CBX), B) CCD and KN93 (KN), C) CBX and KN93 and D) CCD, CBX and KN93 compared graphically against hypotonic stimulus (HT). Graphically displayed as mean data points of three independent experiments (n=3) without error bars for visibility. Data processed and statistically analysed as seen in figure 4.12.*

4.3.2 Hypotonic stimulation alters the cellular distribution of pannexin-1 in A549 cell line

With the knowledge that pannexin-1 plays an integral role in the mechanism of ATP release during hypotonic stimulation, we decided to utilise immunofluorescent microscopy to investigate the cellular distribution of pannexin-1. We hypothesise that hypotonic stimulation causes pannexin-1 release from endosomal compartments and becomes inserted into the cellular plasma membrane to facilitate ATP release.

Briefly, A549 cells were incubated with inhibitors used previously in section 4.3.1, HC067047 (TRPV4), H1152 (RhoA via ROCK), ML-7 (MLC via MLCK), carbenoxolone (pannexin-1), cytochalasin D (actin cytoskeleton), KN93 (calcium-calmodulin kinase) and RO-31-8220 (PKC). The cells were fixed, permeabilised, and stained with FITC conjugated secondary antibody (raised to anti-pannexin-1 primary antibody) and a phalloidin conjugate 594. The stained cells were then mounted with DAPI integrated mounting media. The fixed cells were imaged on Zeiss Axio observer Z1 fluorescent microscope. All experiments were carried out on A549 cells from known origin (Public Health England) with passage numbers 25-30.

Figures 4.14, 4.15 and 4.16 display representative immunofluorescent images for each condition and control stained for pannexin-1 expression with FITC (green), displayed separately, and merged with nuclei stained with DAPI (blue) and actin stained with phalloidin 594 (red). Data was interrogated by carrying out analysis from at least 10 images per condition with regions of interest selected from at least 10 cells per field of view from three independent experiments (n=3) and displayed as corrected (for background) total cell fluorescence (CTCF) (Fig. 4.17).

In comparison to basal unstimulated cells, hypotonic stimulated cells displayed a compartmentalised distribution of pannexin-1 staining producing a ‘honeycombed’ appearance (Fig. 4.14). When cells were pre-incubated with DMSO vehicle control then subject to hypotonic stimulation, pannexin-1 staining resembled that of hypotonic stimulation alone (Fig 4.14), suggestive that DMSO alone causes no effect on pannexin-1 distribution. This ‘honeycombed’ distribution pattern was not seen when cells were incubated with isotonic control buffer. However, the isotonic control caused the cells

distribution of pannexin-1 to become more granular in appearance with a greater degree of overlap with the actin cytoskeleton. Pre-incubation with HC067047, H1152 and ML-7 reduced the hypotonic induced distribution pattern of pannexin-1 compartmentalisation (Fig. 4.15). However, pre-incubation with carbenoxolone reduced the 'honeycombed' appearance of pannexin-1 staining almost entirely, returning the distribution pattern to that resembling basal, this was also seen when cells were pre-incubated with KN93 (Fig. 4.16).

When the A549 cells were pre-incubated with cytochalasin D, cells appeared much smaller in size (Fig. 4.16), as expected, inhibition of the cytoskeleton rendered the cells unable to swell under hypotonic conditions. The pannexin-1 distribution pattern resembled that of other inhibitors HC067047, H1152 and ML-7, with a less compartmentalised appearance of pannexin-1 staining. Finally, when cells were pre-incubated with RO-31-8220 the distribution pattern of pannexin-1 resembled that identified when cells were incubated with isotonic control buffer, however, with less overlap with the actin cytoskeleton likely due to the inhibition of PKC mediated cytoskeleton re-organisation required during hypotonic swelling.

As we would expect due to the nature of the inhibitors, pre-incubation with ML-7, cytochalasin D and RO-31-8220 reduced the formation of stress fibres in cells stimulation with hypotonic buffer. H1152 also reduced the formation of stress fibres but to a lesser extent, as seen with actin staining (shown in red).

Despite the clear and obvious differences in cellular shape and distribution of pannexin-1 caused by hypotonic stimulation and when pre-incubated with different inhibitors, CTCF identified no significant difference in any condition except HC067047 compared to hypotonic stimulation (Fig. 4.17, $P=0.0077$; $n=3$) where CTCF returned to that of basal levels. However, the CTCF of isotonic treated cells was in line of that from basal unstimulated cells despite the clear difference in pannexin-1 distribution. Furthermore, pre-incubation with H1152, KN93 and RO-31-8220 caused CTCF to return to that similar to basal levels. Finally, in cells pre-incubated with ML-7, carbenoxolone and cytochalasin D CTCF resembled that of cells treated with isotonic control, where CTCF was larger than hypotonic but smaller than basal unstimulated cells.

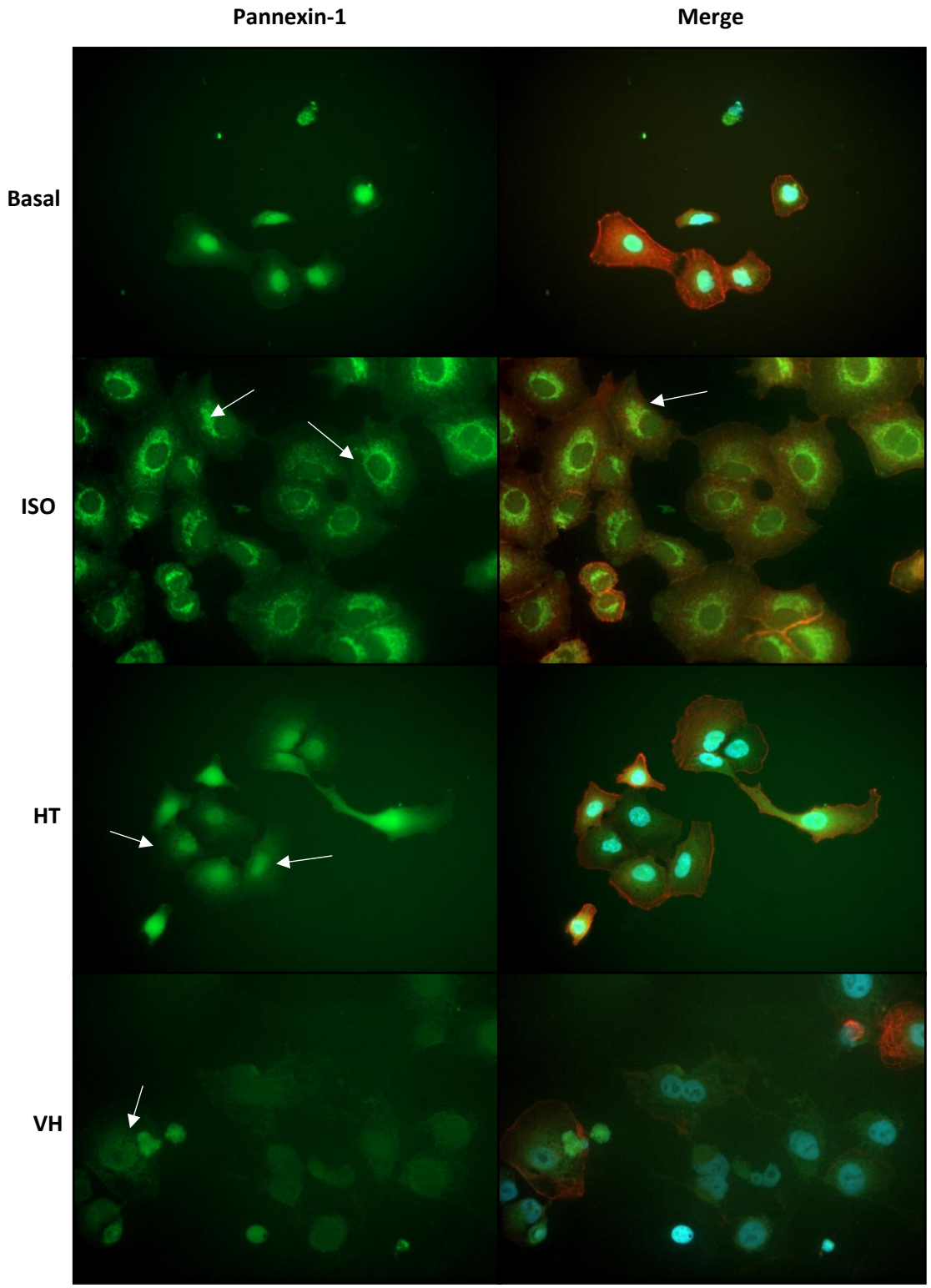

Figure 4.14. ***Immunofluorescent microscopy analysis of A549 cell line stimulated with 33% hypotonicity (HT), isotonic control (ISO), 0.01% v/v DMSO (VH) or basal****. Cells stained for nuclei with DAPI (blue), pannexin-1 with FITC (green) and actin cytoskeleton with phalloidin conjugate 594 (red). Three targets overlaid and merged (merge). Images representative from minimum of 10 images taken from n=3. White arrows indicate areas of interest.*

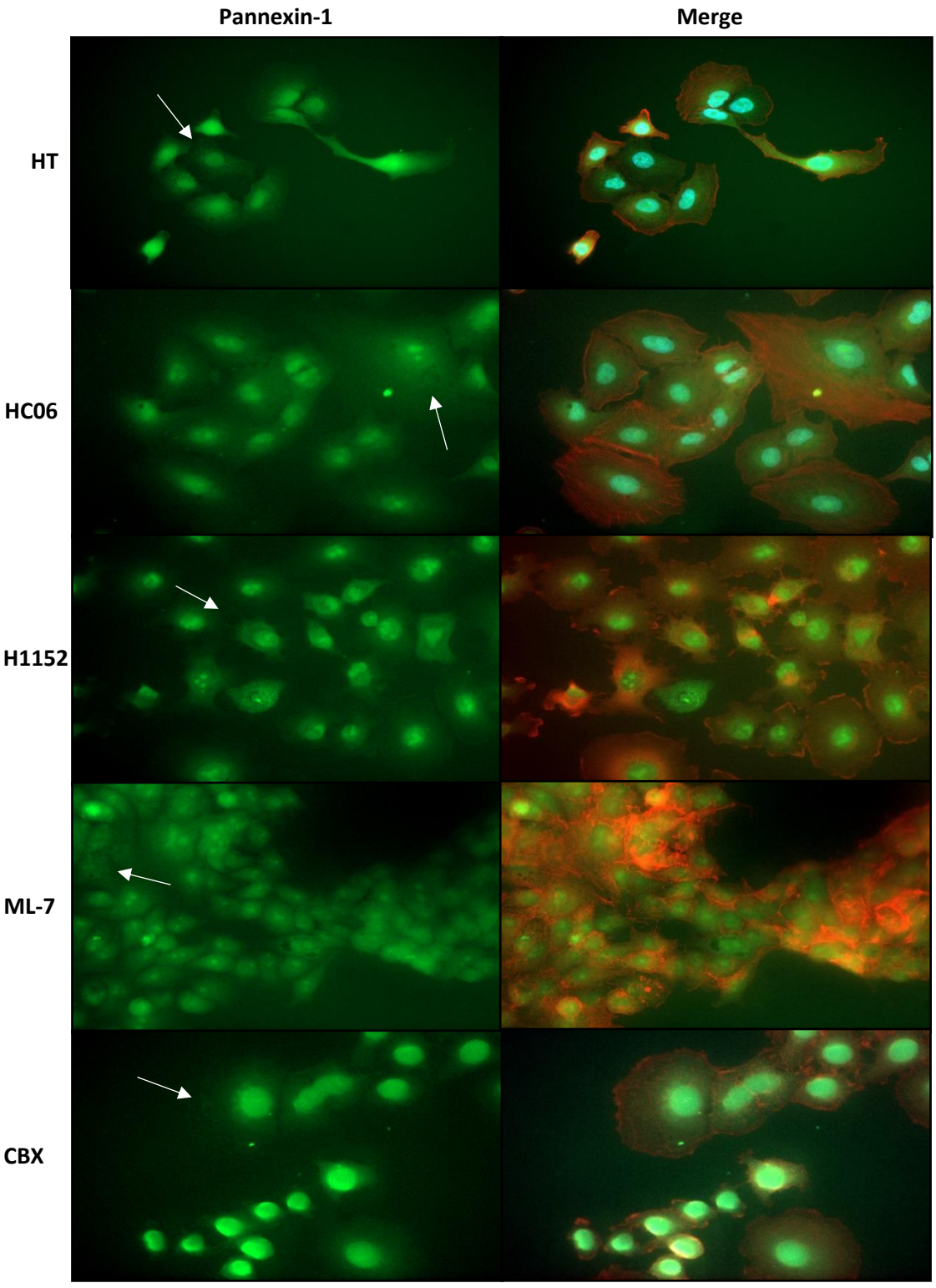

Figure 4.15. ***Immunofluorescent microscopy analysis of A549 cell line incubated with inhibitors, as labelled, and stimulated with 33% hypotonicity (HT).*** *Cells stained for nuclei with DAPI (blue), pannexin-1 with FITC (green) and actin cytoskeleton with phalloidin conjugate 594 (red). Three targets overlaid and merged (merge). Images representative from minimum of 10 images taken from n=3. White arrows indicate areas of interest.*

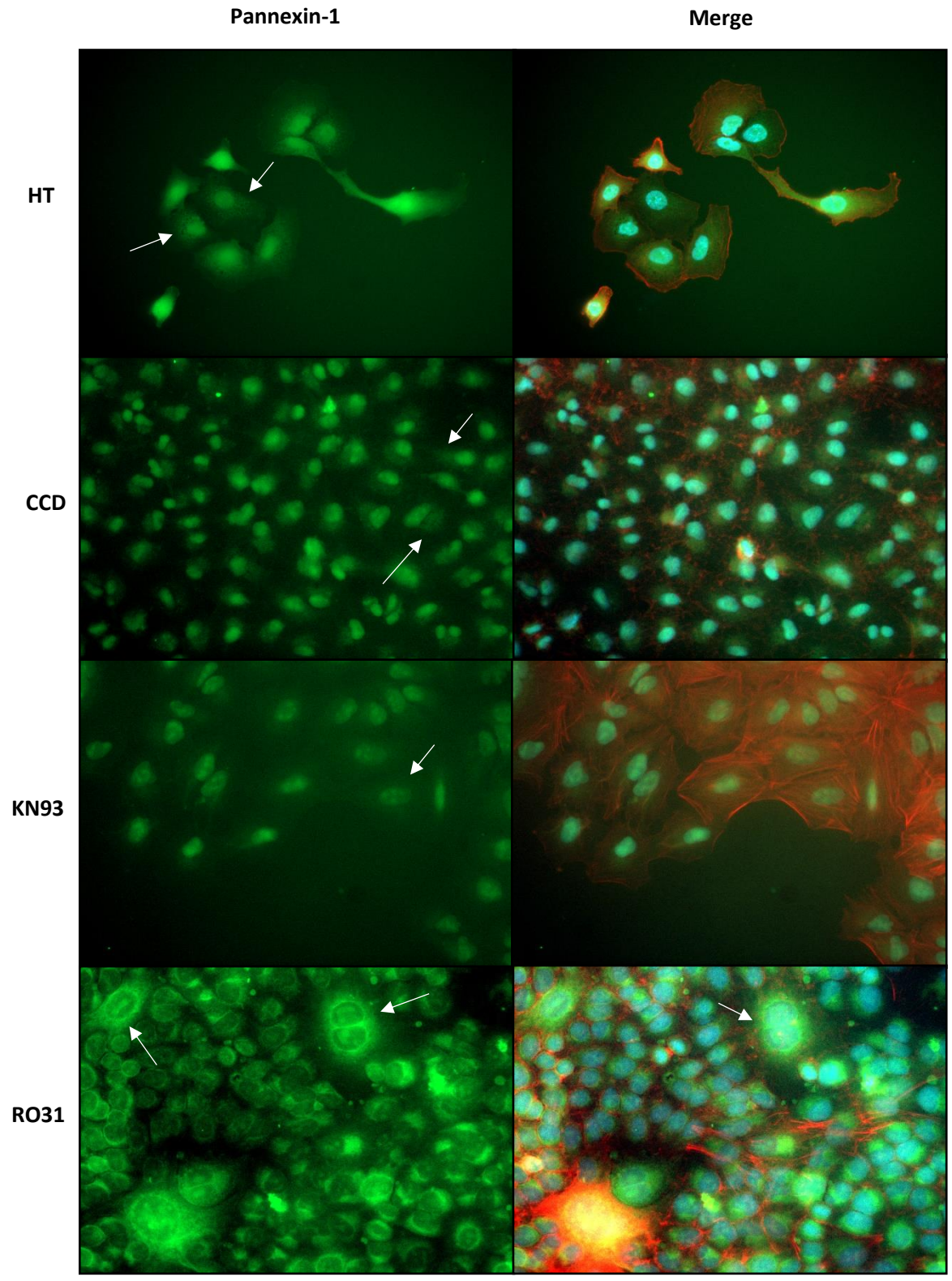

Figure 4.16. ***Immunofluorescent microscopy analysis of A549 cell line incubated with inhibitors, as labelled, and stimulated with 33% hypotonicity (HT).*** *Cells stained for nuclei with DAPI (blue), pannexin-1 with FITC (green) and actin cytoskeleton with phalloidin conjugate 594 (red). Three targets overlaid and merged (merge). Images representative from minimum of 10 images taken from n=3. White arrows indicate areas of interest.*

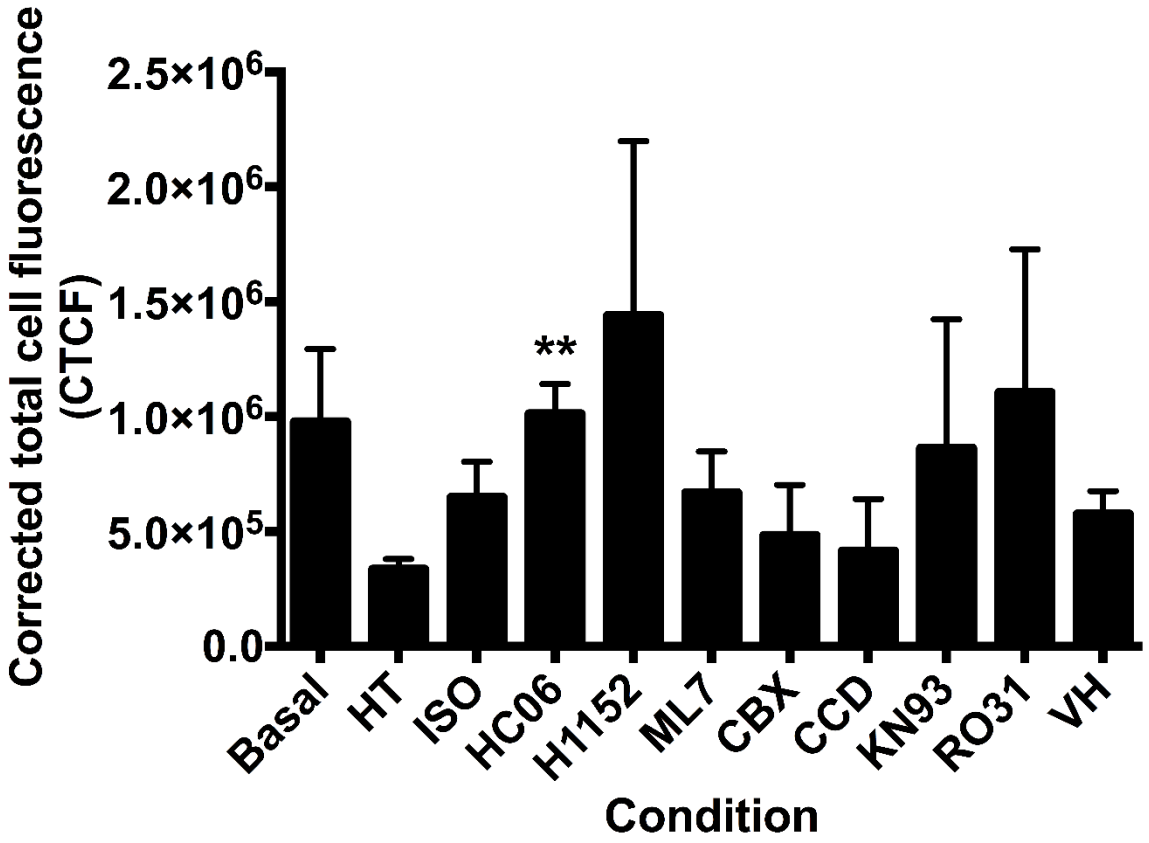

Figure 4.17. ***CTCF of pannexin-1 following hypotonic stimulation.*** *Corrected total cell fluorescence (CTCF) measurements of pannexin-1 probed with FITC conjugated secondary antibody in A549 cell line incubated with inhibitors, HC067047 (HC06), H1152, ML7, carbenoxolone (CBX), cytochalasin D (CCD), KN93, RO-31-8220 (RO31) or 0.01% v/v DMSO (VH) then post-treated with 33% hypotonicity (HT), or isotonic control (ISO). Measurements accompany fluorescent images Fig. 4. 13-15. CTCF calculated from integrated density correct for background fluorescence from a minimum of 10 independent images containing at least 10 cells per field of view from three independent experiments. Data displayed as mean ± S.E.M. of three independent experiments (n=3). Statistical analysis was carried out using multiple comparison one-way ANOVA followed by Dunnetts test compared against HT. **P=0.0077.*

4.3.3 Calcium imaging of A549 cell line exposed to hypotonic stimuli

Finally, we investigated the role of calcium and the intracellular flux during hypotonic stimulation and the role of inhibitors previously used. It has been previously shown that hypotonic stimulation and its subsequent swelling causes intracellular calcium elevations (Tatur *et al.*, 2007), furthermore, that intracellular calcium regulates exocytosis of ATP during hypotonic stimulation (Boudreault & Grygorczyk, 2004; Tatur *et al.*, 2008). We hypothesised that hypotonic stimulation causes elevations in intracellular calcium which can be reduced or inhibited with inhibitors to components of the 'hypotonic pathway', used previously.

Briefly, A549 cells were incubated with inhibitors used previously in section 4.3.1, HC067047 (TRPV4), H1152 (RhoA via ROCK), ML-7 (MLC via MLCK), carbenoxolone (pannexin-1), cytochalasin D (actin cytoskeleton), KN93 (calcium-calmodulin kinase) and RO-31-8220 (PKC). The cells were loaded with fluo-4 AM fluorescence dye and imaged live on Zeiss Axio observer Z1 fluorescent microscope at wavelength excitation 480 nm and emission 525 nm at 3 second intervals prior to and following hypotonic stimulation, isotonic control or positive maximal flux stimulant A23187.

Figures 4.18, 4.19 and 4.20 display representative calcium flux snapshots pre and post hypotonic stimulation and standard deviation images of Z-stacked slices of the time course for each condition and control. Data was interrogated by carrying out analysis from at least 20 regions of interest per condition from three independent experiments (n=3) and displayed as mean grey value. Traces were then subject to AUC analysis and statistical analysis carried out (Fig. 4.21).

Despite published literature stating that hypotonic stimulation results in intracellular calcium elevation (Tatur *et al.*, 2007; Boudreault & Grygorczyk, 2004), we were unable to replicate those findings. Our positive control calcium ionophore A23187 stimulated a strong and rapid intracellular calcium flux, so we were sure that our assay and dye was working as it should have and the cells were still alive. However, we did identify that pre-incubation with ML-7 significantly increased mean calcium fluorescence from hypotonic control following hypotonic stimulation (Fig. 4.21, P=0.0407; n=3). Furthermore, pre-incubation with RO-31-8220 also significantly increased mean calcium fluorescence

following hypotonic stimulation (P<0.0001; n=3). Basal fluorescence was massively increased in cells pre-incubated with RO-31-8220 (Fig. 4.20) likely due to the more generalised inhibitory effect on the cell causing endosomal compartmentalisation of intracellular calcium stores, partially accounting for this increase in mean calcium fluorescence.

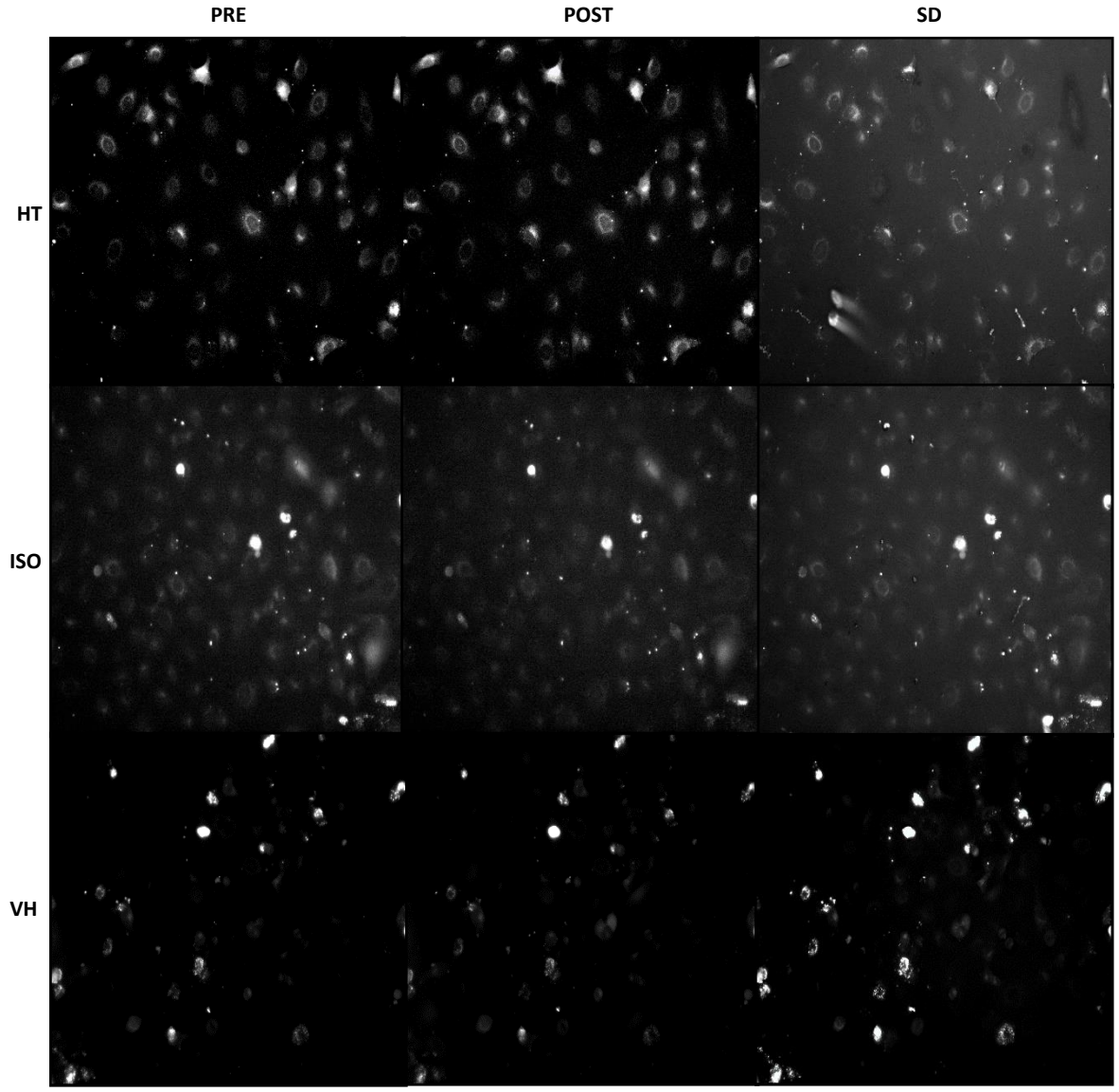

Figure 4.18. ***Calcium imaging snapshots prior (PRE) to hypotonic (HT) stimulation, peak response following HT stimulation (POST) and standard deviation (SD) of Z-stacked slices of the time course.*** *Experiments carried out on A549 cells, loaded with fluo-4, stimulated with 33% hypotonicity (HT), isotonic control (ISO) or 0.01% v/v DMSO vehicle control (VH). Images representative from three independent experiments (n=3). Representative images accompany analysed data in Fig. 4.21.*

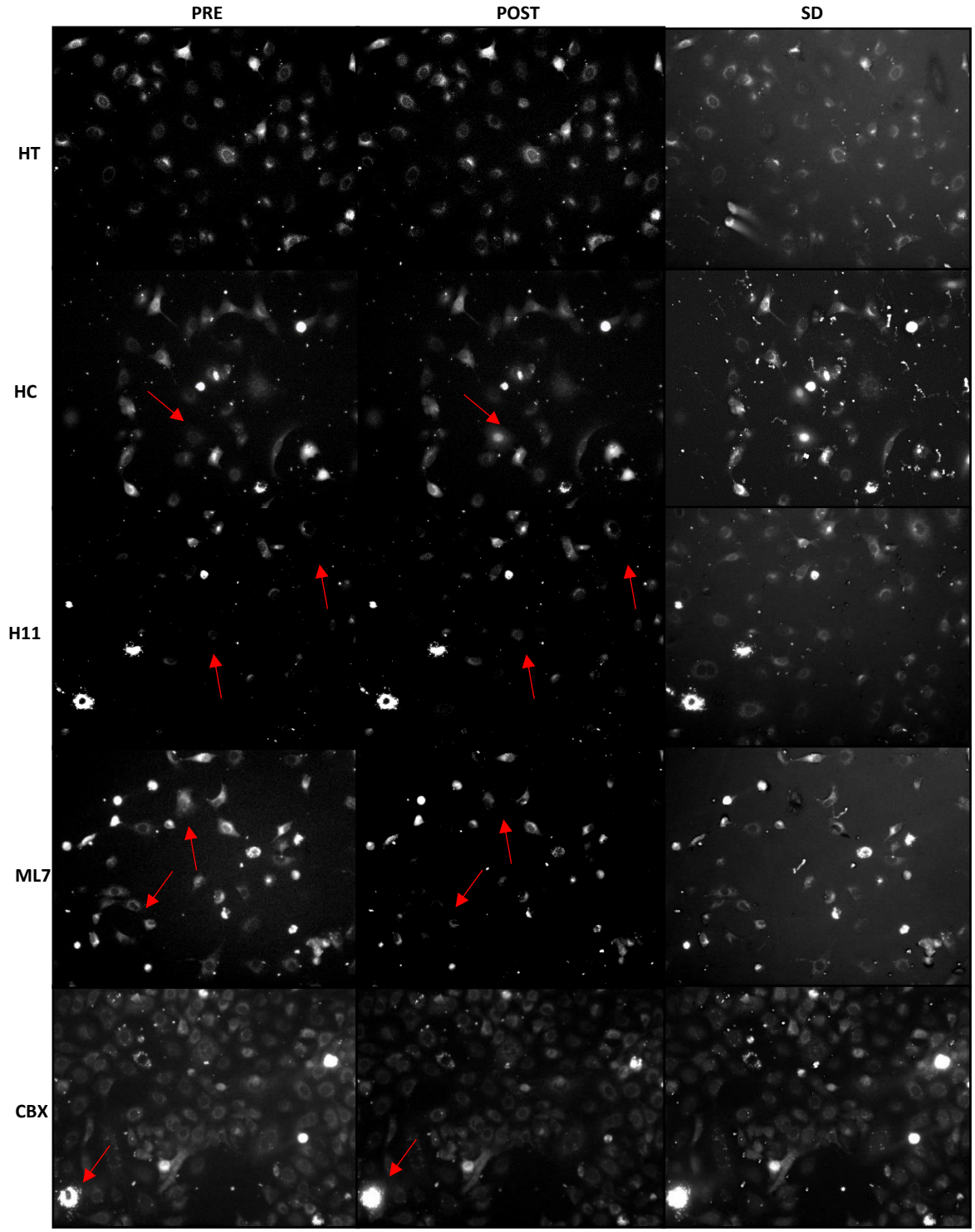

Figure 4.19. ***Calcium imaging snapshots prior (PRE) to hypotonic (HT) stimulation, peak response following HT stimulation (POST) and standard deviation (SD) of Z-stacked slices of the time course of A549 cell incubated with inhibitors****. Experiments carried out on A549 cells, loaded with fluo-4, incubated with inhibitors HC067047 (HC), H1152 (H11), ML7 and carbenoxolone (CBX) then post-treated with 33% hypotonicity (HT). Images representative from three independent experiments (n=3). Representative images accompany analysed data in Fig. 4.21. Red arrows indicate areas of interest.*

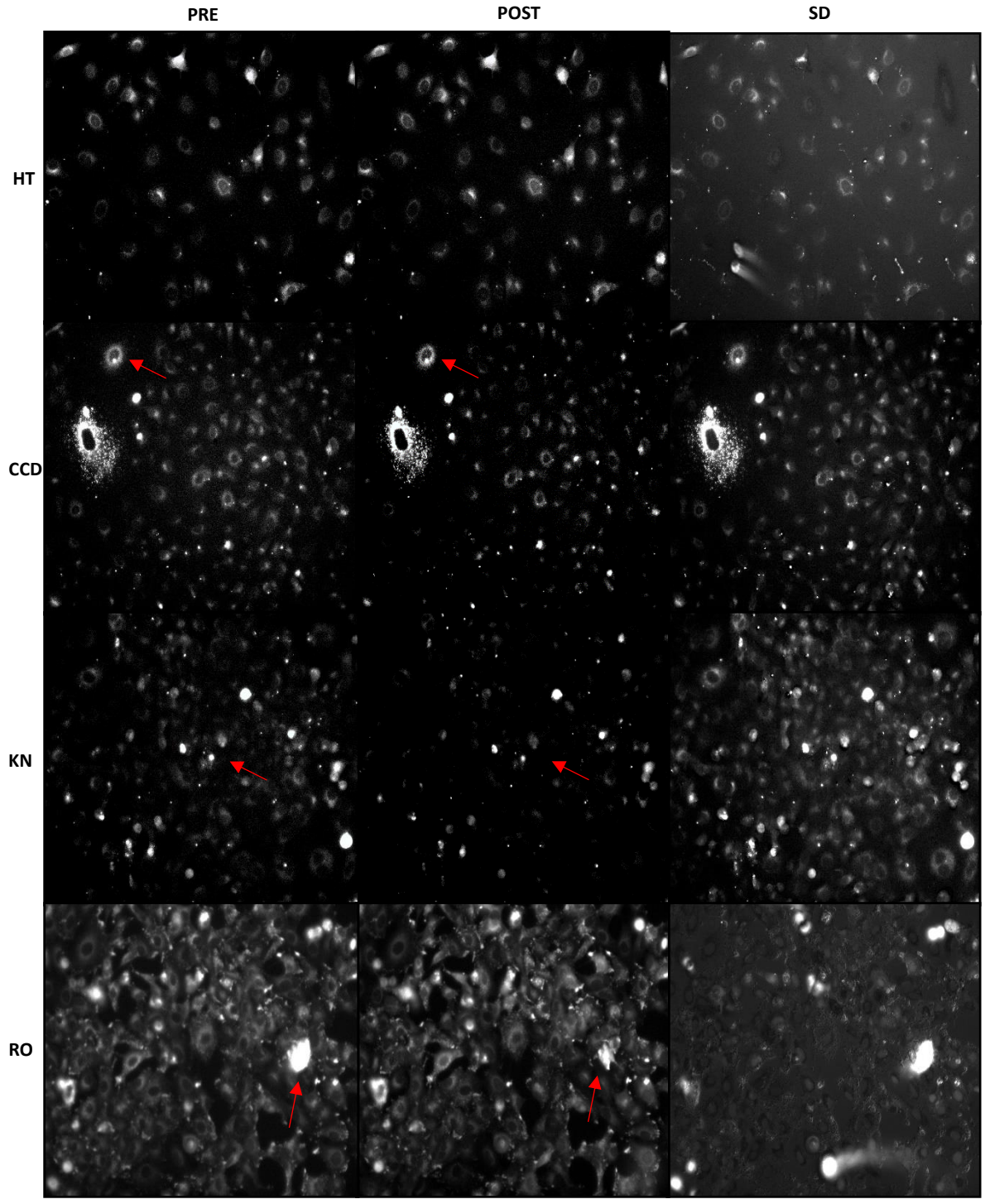

Figure 4.20. ***Calcium imaging snapshots prior (PRE) to hypotonic (HT) stimulation, peak response following HT stimulation (POST) and standard deviation (SD) of Z-stacked slices of the time course of A549 cell incubated with inhibitors.*** *Experiments carried out on A549 cells, loaded with fluo-4, incubated with inhibitors cytochalasin D (CCD), KN93 (KN) and RO-31-8220 (RO) then post-treated with 33% hypotonicity (HT). Images representative from three independent experiments (n=3). Representative images accompany analysed data in Fig. 4.21. Red arrows indicate areas of interest.*

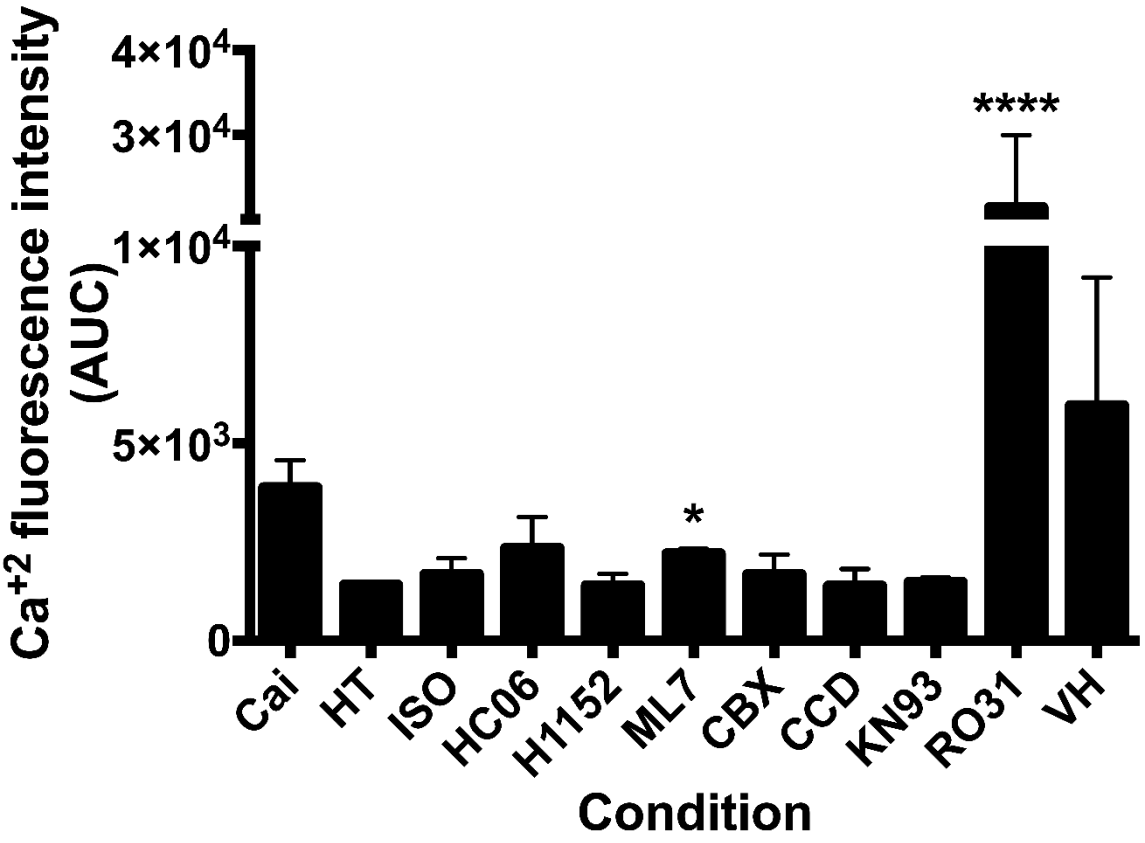

Figure 4.21. ***Area under curve analysis of calcium imaging traces*** *calculated from mean grey value corrected for background from a minimum of 20 independent regions of interest from three independent experiments (n=3). Experiments carried out on A549 cells, loaded with fluo-4, incubated with inhibitors, HC067047 (HC06), H1152, ML7, carbenoxolone (CBX), cytochalasin D (CCD), KN93, RO-31-8220 (RO31) and 0.01% v/v DMSO (VH) then post-treated with 33% hypotonicity (HT) or isotonic control (ISO). Measurements accompany representative field of view fluorescent images Fig. 4. 18-20. Data displayed as mean ± S.E.M. of three independent experiments (n=3). Statistical analysis was carried out using multiple comparison one-way ANOVA followed by Dunnetts test compared against HT. *P=0.0407, ****P<0.0001.*

Overall, when analysing snapshot images of cells incubated with HC067047 (Fig. 4.19), ML-7 (Fig. 4.19) and KN93 (Fig. 4.20), following hypotonic stimulation there was a reduction in fluorescence intensity of intracellular calcium. This trend was not seen in any other condition or when treated with any other inhibitor (Fig. 4.18, 4.19 and 4.20).

4.4 Discussion

Through the work investigated here, we have further delineated the mechanism of the hypotonic pathway through the use of inhibitors to TRPV4, RhoA (via ROCK), MLC (via MLCK), pannexin-1, actin cytoskeleton, calcium-calmodulin kinase and PKC. Here we show that calcium-calmodulin kinase plays a crucial role in hypotonic induced ATP release, and for the first time show that through blockade of this with KN93 we were able to almost knock out hypotonically stimulated ATP release in combination with either pannexin-1 or actin cytoskeleton inhibition. Our data also strongly suggests, that hypotonic stimulation may lead to compartmentalisation of pannexin-1 within cells facilitating the ATP release. This compartmentalisation could be inhibited through blockade of calcium-calmodulin kinase and pannexin-1. Here we also show for the first time that incubation with isotonic buffer changes the cellular distribution of pannexin-1 without concurrent release of ATP. We hypothesise this could be a shear stress response to mechanical stimulation, but insufficient to cause ATP release.

We initially sought to replicate previous findings that hypotonic stimulation leads to MLC phosphorylation at ser19 (Seminario-Vidal *et al.*, 2011). Unfortunately, we were not able to consistently achieve a signal for either total-MLC or phospho-MLC (ser19) using western blot analysis to definitively confirm the role of hypotonic stimulation on MLC phosphorylation status. Furthermore, given more time we would have planned to carry out RhoA pull down assays to ascertain if RhoA was activated upon hypotonic stimulation, as previously identified (Seminario-Vidal *et al.*, 2011), and if this could be manipulated through our inhibitors used.

We then carried out extracellular ATP release analysis using sampled supernatants pre-incubated with inhibitors and exposed to hypotonic stimulation or isotonic control. We identified that inhibition of MLC (via MLCK) and pannexin-1 significantly reduced the peak ATP response compared to hypotonic stimulus alone. When we interrogated the quantified traces of ATP release following hypotonic stimulus, we found HC067047 (TRPV4 inhibitor) did not affect the peak ATP release but caused delayed response. We suggest this is a result of a redundancy system that must be by-passed when TRPV4 is inhibited. Therefore, because the stimulus cannot transduce down the primary route the end product of ATP release is delayed as the system is not as efficient. Findings from immunofluorescent

analysis support the fact that the cells were still able to undergo cellular swelling as a result of the hypotonic stimulus despite the inhibition of TRPV4. This may explain the redundancy mechanism we hypothesised as TRPV4 has been identified to play an important role in the regulation of cell volume during hypotonic stimulation (Becker *et al.*, 2005; Liu *et al.*, 2006). Furthermore, that knockout of TRPV4 impaired the regulatory volume decrease mechanism following hypotonic stimulation (Jo *et al.*, 2015). Another point to consider is that TRPV4 inhibitor HC067047 just functions poorly as an inhibitor and works more like a competitive antagonist, whereby the initial stimulus (hypotonicity) competes and overcomes the inhibition of TRPV4. Ideally, we would have carried out ATP sampling of HC067047 in combination with other inhibitors to confirm its role as a partial inhibitor or determine if TRPV4 plays an integral role in hypotonically induced ATP release, or if its function is solely tied to the pathway, therefore, knocking out TRPV4 does not affect ATP release (personal communication, 2018).

Previously published literature has found that inhibition of pannexin-1 activation with KN93 prevented ATP release but couldn't identify a mechanism in human pulmonary fibroblasts (Rahman *et al.*, 2018). They hypothesised it was likely a result of either calcium-calmodulin kinase II activity, directly mediated by calcium flux, or a calcium mediated secondary effector such as Src family kinase phosphorylation of pannexin-1 (Rahman *et al.*, 2018; Weilinger, Tang & Thompson, 2012). We also found that inhibition of calcium-calmodulin kinase alone resulted in the largest inhibition of ATP release following hypotonic stimulation in airway epithelial A549 cell line. Furthermore, in line with other published work which identified coupling of TRPV4 and pannexin-1 (Rahman *et al.*, 2018; Seminario-Vidal *et al.*, 2011), we found inhibition of TRPV4 led to less ATP release following hypotonic stimulation (direct TRPV4 activation).

We showed that collective inhibition of calcium-calmodulin kinase and either pannexin-1 or actin cytoskeleton resulted in the largest reduction in peak ATP release and overall total ATP release in comparison to hypotonic stimulus alone. We therefore propose that hypotonically induced ATP release is largely mediated by calcium-calmodulin kinase activity and therefore, intracellular calcium. However, we cannot rule out that when A549 cells are incubated in a combination of cytochalasin D, KN93 and RO-31-8220, any ATP release we see is a result of hypotonic stimulation or as a result of a delirious effect of toxic inhibitors

on the cells activating an apoptotic pathway leading to ATP release from alternative pathways. We would ideally have carried out a propidium iodide uptake assay to confirm if an apoptotic pathway becomes activated.

Next, we made the decision to carry out immunofluorescent analysis to investigate the expression and distribution of pannexin-1 during hypotonic stimulation. Whilst we were unable to accurately quantify the changes we saw, there were stark differences between conditions. Most abundantly clear was the effect hypotonic stimulation has on the physical appearance of A549 cells. Pannexin-1 staining became highly characteristic whereby staining became compartmentalised with areas of complete lack of staining leaving 'gaps' within the cell. This phenotype could be effectively abolished when pre-incubated with pannexin-1 inhibitor, and could be significantly diminished with TRPV4, MLC, RhoA and calcium-calmodulin kinase inhibition. However, the most interesting finding from these experiments were the outcome of incubating cells in isotonic buffer where pannexin-1 staining became highly granular. This suggests that whilst the stimulation was insufficient to cause ATP release, the mechanosensitive A549 cells were stimulated enough through shear stress to cause movement of pannexin-1 through the cell. A similar pattern of distribution was also seen in mechanically stimulated astrocytes and primary airway epithelial cultures (Ransford *et al.*, 2009; Albalawi *et al.*, 2017). A clear limitation with the total cellular fluorescent analysis carried out on these cells is that whilst overall fluorescence isn't changed, the physical appearance is and the distribution of pannexin-1 was changed. This data is in line with western blot analysis where global protein expression was unchanged. Collectively, these data suggest that there is movement of endosomal compartments through the cell to transport pannexin-1 protein to the plasma membrane for insertion. To date, there is no published data exploring the effect of endosomal trafficking on pannexin-1 distribution during hypotonic stimulation. This would be an avenue we would like to pursue further given more time. During the process of optimisation to choose a duration of hypotonic stimulation we identified that the 'honeycombed' appearance we saw increased as duration of hypotonic stimulation increased. A possible explanation for this 'honeycombing' appearance seen in cells is that pannexin-1 may undergo the formation of homohexamers in readiness for membrane

insertion and is stored within endosomal compartments in cells as monomers. Currently there is no data to support this hypothesis.

Finally, the calcium imaging we carried out failed to replicate previous published findings, so we were unable to add any new findings using this method to investigate the hypotonic mechanism of ATP release. However, we did identify the reduction in cellular fluorescence following hypotonic stimulation. It is possible this reduction in fluorescence intensity seen was as a result of unbound calcium. A better alternative to counter this problem would have been to use fura-2 calcium dye. We initially attempted to use this, but our microscope lacked the 340 nm laser required for exciting the dye capable of measuring bound calcium.

ATP sampling and measurement was carried out off-line using a commercially available kit as our efforts to develop and optimise an on-line ATP measurement assay proved unsuccessful despite months of development. We are aware our method of assaying ATP was not ideal, however, this method has been used and published previously (Seminario-Vidal, Lazarowski & Okada, 2009). Our method proved less sensitive than others used, with a shorter overall response time and duration of peak ATP release. We had initially planned to use ectoATPase inhibitors to inhibit the degradation of ATP at the extracellular cell surface however we repeatedly found inconsistent and unreliable results and ultimately decided not to use them.

Moving on from this we hope to determine if common cold virus, rhinovirus-16, causes any effect to ATP release basally and during hypotonic stimulation. In conclusion, we identified that calcium-calmodulin kinase was an integral component of ATP release during hypotonic stimulation and that cells stimulated with hypotonic buffer underwent major physical changes in their pannexin-1 distribution.

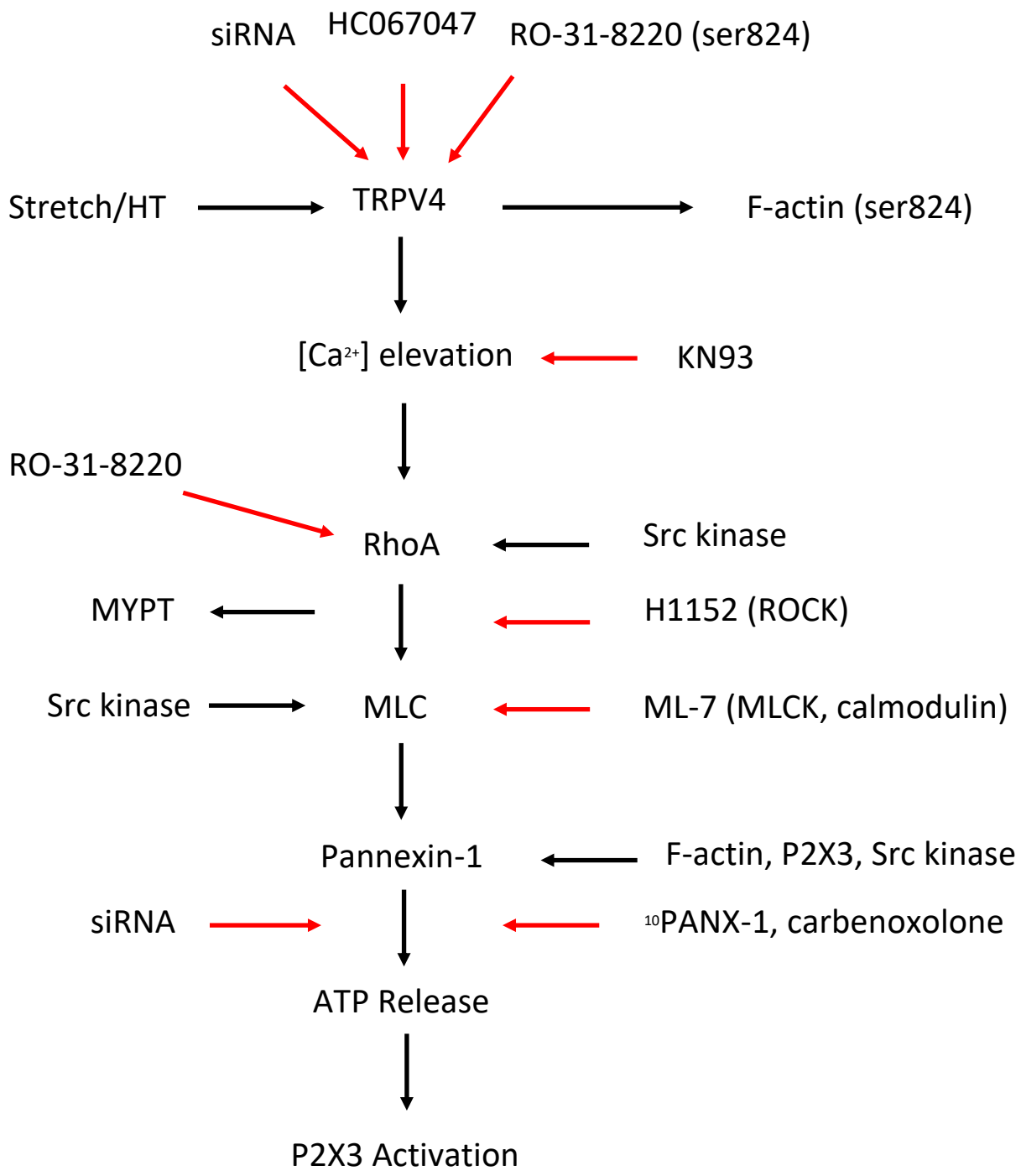

Figure 4.22. ***Hypotonic pathway diagram detailing hypothesised pathway components****, where individual components interact and where inhibited of components lead to reduced ATP release following hypotonic stimulation. Black lines indicate interaction, red lines indicate inhibition. Pathway developed from data published by* (Seminario-Vidal *et al.*, 2011; Shin *et al.*, 2012; Abdulqawi *et al.*, 2015; Rahman *et al.*, 2018; Weilinger, Tang & Thompson, 2012; Garcia *et al.*, 1999).

Chapter 5

Exploring the Effect of Human Rhinovirus-16 on the Hypotonic Pathway, ATP Release and TRPV4 Expression

Rhinoviral infections are a major causative agent of URTI and are associated with acute exacerbation of asthma and COPD. During URTI, airways become hypersensitive to various stimuli including the tussive chemical, capsaicin (Dicpinigaitis *et al.*, 2014; O'Connell *et al.*, 1996) and innocuous stimuli (saline control) (Dicpinigaitis *et al.*, 2011). Airway hypersensitivity in URTI has yet to be fully characterised. Airway hypersensitivity is hypothesised to contribute to the cause of cough in URTI (O'Connell *et al.*, 1996; Dicpinigaitis *et al.*, 2011; Atkinson *et al*., 2016; Jacoby, 2004; Eccles & Lee, 2004) but the mechanisms surrounding its function is unknown. URTI is also associated with excessive production of mucus within the airway, particularly in sufferers of chronic respiratory conditions. This mucus may lead to altered osmolarity within the airway and contribute to hypotonic stimulus of the airway epithelium and airway hypersensitivity leading to cough. We know that pannexin-1 is present within the airway and that its stimulation via hypotonic exposure, which has previously been shown to activate TRPV4, ultimately leads to ATP release via pannexin-1 (Seminario-Vidal *et al.*, 2011; Ransford *et al.*, 2009; Seminario-Vidal *et al.*, 2009). With a recent shift in focus to ATP as a major component in causing cough (Fowles *et al.*, 2017; Atkinson *et al.*, 2016; Abdulqawi *et al.*, 2015; Bonvini *et al.*, 2016) we decided to further investigate ATP release in A549 alveolar cells during RV-16 infection to determine if the common cold increased the concentration of ATP in the airways.

Modern advancements in technologies to accurately and simply measure metabolic profiles has led to an increase in interest on the impact viral infection has on host cell metabolism. In particular, rhinovirus (major group RV-B14) was found to induce an anabolic reprogramming of host metabolism and it's replication was identified as dependent on host glycolysis (Gualdoni *et al.*, 2018). However, this was determined in Hela and fibroblast cells using a non-physiological MOI (3.5-5), therefore, we cannot assume RV induces the same reprogramming response in airway cells during an URTI. We decided to investigate this further using A549 alveolar cells and utilising Seahorse metabolic analyser to measure oxygen consumption and by extension ATP production.

Through our work carried out in Chapter 4 characterising the hypotonic pathway, we decided to investigate the effect of RV-16 on extracellular ATP release during infection and following further stimulation to determine if TRPV4 plays a crucial role in this response and if RV-16 alters the function and expression of pannexin-1 within the airway.

Presently, there is no published literature regarding the effect of hypotonic stimulation during RV-16 infection in the airway and no published literature investigating the effect of RV-16 on intracellular ATP levels and extracellular ATP release. We aim to fill these gaps in our knowledge with this work.

5.1 Approach and methodology

In a similar fashion to section 3.3.4 and Chapter 4, we chose to peruse this line of investigation using only A549 epithelial alveolar cells instead of the previously characterised 1321N1-P2X3 transfected astrocytoma neuronal cells as used throughout the majority of Chapter 3. Following our decision to only investigate the effect of hypotonic stimulation on A549 cell line in Chapter 4 we carried this on here. Once again, we felt a hypotonic stimulus was unlikely to affect underlying airway nerves and we found no significant findings from our RV-16 infection model of the 1321N1 astrocytoma cell line. Furthermore, the A549 cell line has previously been characterised through our own findings (Chapter 3) and published literature (Zhu *et al.*, 1997; Papi & Johnston, 1999), to be permissible to RV-16 infection. We felt this gave a better representation of the viral infection on the airway *in vivo* than we could have hoped to achieve with an astrocytoma neuronal cell line. Therefore, we felt the A549 cell line better represented a physiological effect.

The work carried out in Chapter 4 allowed us to further characterise the hypo-osmotically induced ATP release in A549 cells. We chose to apply that knowledge here and determine if infection with RV-16 altered that response and if it had any effect on ATP release. We utilised similar techniques used previously through Chapter 3 and Chapter 4 to measure ATP release. We also utilised a new technique to measure metabolic function and cell line profile during RV-16 infection. Finally, we generated and characterised a transfected A549 cell line with exogenous TRPV4 expression and sought to measure the effect of RV-16 on TRPV4 expression.

The experiments were carried out using materials and procedures as described in Chapter 2. Briefly, cellular responses to hypotonic stimuli and RV-16 infection were monitored using western blot analysis to assess changes in protein expression and activity. Our ultimate

end-point measurement was ATP release via pannexin-1 channel. Extracellular ATP release was compared against total cellular concentration to determine if stimulation caused an overall increased output, these are both measured using commercially available kits as described in section 2.11. UV inactivated viral control (destroyed genetic material but with an intact protein coat) was used alongside infection experiments to determine if any response or change seen in the airway epithelial cells were a result of actively replicating virus (RV-16) or from ICAM-1 receptor binding alone (UV inactivated).

An obvious limitation of measuring intracellular ATP levels of cell culture is that it only provides a current snapshot of the cells stores. Therefore, we decided to measure the cellular metabolism of RV-16 infected cells using Seahorse analysis and determine if RV-16 infection alters the metabolic profile of A549 cells and their ATP production rates by measuring their mitochondrial function.

All experiments were carried out on A549 cells from known origin (Public Health England) with passage number 3-10 for sections 5.3.3, 5.3.4 and for generating the G418 kill curve, whilst passage number 13-50 was used through section 5.2 to section 5.3.2.

5.1.1 Methods: Western blot

Cells were seeded at $4.5x10^5$ into T25 flasks and allowed to adhere overnight prior to commencement of RV-16 infections at MOI 1, as described in section 2.5, with hypotonic stimulation assays, as described in section 2.13. Cells were infected for up to 168 hours and either lysed and harvested in 1X cell lysis buffer containing 10mM PMSF and pelleted by centrifugation at 14, 000 *x g* for 10 minutes at 4^{o}C, or stimulated with hypotonic stimulus, as described in section 2.13, followed by lysis as described above. The supernatants were recovered, quantified as described in section 2.9.1 and diluted in 4X Laemmli's buffer to 50µg protein and heated at 80^{o}C for 10 minutes. The samples were spun at 16,000 *x g* for 10 minutes and stored at -80^{o}C or used immediately.

The prepared lysates were separated on a 10% SDS-PAGE gel (see section 2.9.2) and proteins were transferred to a PVDF membrane.

The PVDF membranes were blocked in 5% milk solution (1X TBS) for 1 hour then incubated overnight at 4^{o}C with primary antibody raised to TRPV4 (1:500), pannexin-1 (1:500), total-MLC (1:1000), phospho-MLC (ser19) (1:1000) or α-tubulin (1:500) in 1X TBS-T (0.1%)

containing 2% BSA. The membranes were then incubated for 1 hour at room temperature with either goat anti-mouse or goat anti-rabbit Licor fluorescent secondary antibodies diluted to 1:15000 in 1X TBS-T (0.1%) containing 2% milk before analysis by Licor fluorescent scanning detection system on Licor Odyssey CLx followed by densitometry analysis as described in section 2.9.5 and section 2.9.6, respectively. Membranes were run in duplicate with sequential probing, to prevent loss of antigen as found during the course of western blotting in Chapter 3.

5.1.2 Methods: ATP measurement

Supernatants from hypotonic stimulation assays were sampled at 15 second intervals for 5 minutes and assayed for extracellular ATP as described in section 2.11.1.1. ATP concentrations were quantified using a standard curve.

Intracellular ATP levels were quantified using a commercially available kit as described in section 2.11.2. Briefly, A549 cells were seeded in a 96-well plate at $5x10^4$ and infected with RV-16 at MOI 1 for up to 168 hours, as described in section 2.5.3. Cells were lysed in detergent, stabilised with a substrate and luminescence was measured. ATP concentrations were quantified using a standard curve.

5.1.3 Methods: OCR and ECAR measurement

Oxygen Consumption (OCR) and extracellular acidification (ECAR) rate measurements were performed as described in section 2.16. Briefly, cells were infected with RV-16 at MOI 1 for up to 168 hours, as described in section 2.5.3. One hour prior to beginning the measurements the cell plate and drug cartridge were de-gassed in a 37^{o}C non-CO_2 incubator incubated with in-house prepared assay media (as described in section 2.16) supplemented with 10mM glucose, 1mM L-glutamine and 2mM pyruvate or calibrant, respectively. The assay to measure OCR and ECAR was run to 2 hours with non-mix protocol with initial 5-minute wait period. Following measurements, the cells were lysed in 20 µl of 1X lysis buffer and quantified for protein concentration. Results were normalised to µg of protein.

5.1.4 Methods: Generation of GFP-tagged TRPV4 expressing cell line

A549 cells were transfected with GFP-tagged TRPV4 in pCMV6 vector, as described in section 2.15, and cultured as described in section 2.2. Single cell cloning was carried out as

described in section 2.15.6 for selection of monoclonal expansions of the transfected cells. The monoclonal expansions were initially screened for positive expression of the GFP-tagged vector by flow cytometry, as described in section 2.15.7 and further selected for by degree of responsiveness to TRPV4 agonists GSK1016790A (30 and 3nM) and 4αPDD (2µM) using intracellular calcium signalling assays as described in section 2.8.2.

5.1.5 Methods: Immunofluorescent microscopy

Immunofluorescent microscopy was carried out on the GFP tagged-TRPV4 transfected A549 cells (A549-TRPV4-GFP) as part of the characterisation process confirming GFP-tagged TRPV4 expression. Cells from each monoclonal expansion were seeded at $2x10^4$ on coverslips and allowed to adhere for 48 hours. The cells were then fixed, permeabilised and blocked as described in section 2.14. The cells were mounted on glass slides with DAPI containing Prolong™ Diamond antifade mounting media with wild type A549 for non GFP tag control. Fluorescent microscopy analysis was performed as described in section 2.14.

Immunofluorescent microscopy was also carried out on RV-16 infected A549-TRPV4-GFP cells to determine the effect of RV-16 infection on TRPV4 expression and distribution over a 168-hour time course. Cells were seeded at $5x10^3$ on coverslips and infected with RV-16 at MOI 1 for up to 168 hours, as described in section 2.5.3. The cells were than fixed, permeabilised and blocked as described in section 2.15. Finally, the cells were stained with phalloidin conjugated CruzFluor™ 594 conjugate (1:1000) for 1 hour and mounted on the glass slides with DAPI containing Prolong™ Diamond antifade mounting media. Fluorescent microscopy analysis was performed as described in section 2.15.

5.1.6 Methods: Flow cytometry

FACS analysis was used for the initial screening of A549 cells. The GFP tag fused to the receptor was used to assess global expression of the receptor. Ten thousand cells were analysed by FACS using the argon laser (wavelength 488 nm), as described in section 2.15.7.

5.2 Optimisation

5.2.1 Geneticin kill curve in A549 cell for transfection

Prior to beginning transfection of the A549 cell line with GFP-tagged TRPV4 construct, a G418 kill curve was performed to determine the lowest suitable concentration of G418 antibiotic to give a high degree of cell death within 3 days and complete death by 2 weeks. Briefly, we seeded A549 cells at passage 35 at $1.5x10^5$ in 24 well plate. Cells were allowed 16 hours to adhere prior to commencement of treatment. Cells were then treated in duplicate with increasing concentrations of G418, 50µg ml^{-1} – 1mg ml^{-1}. Cells were kept in culture for 14 days and complete growth media containing G418 was replaced every 2 days. Cells were visually assessed daily for signs of toxicity (Fig. 5.2) and results recorded.

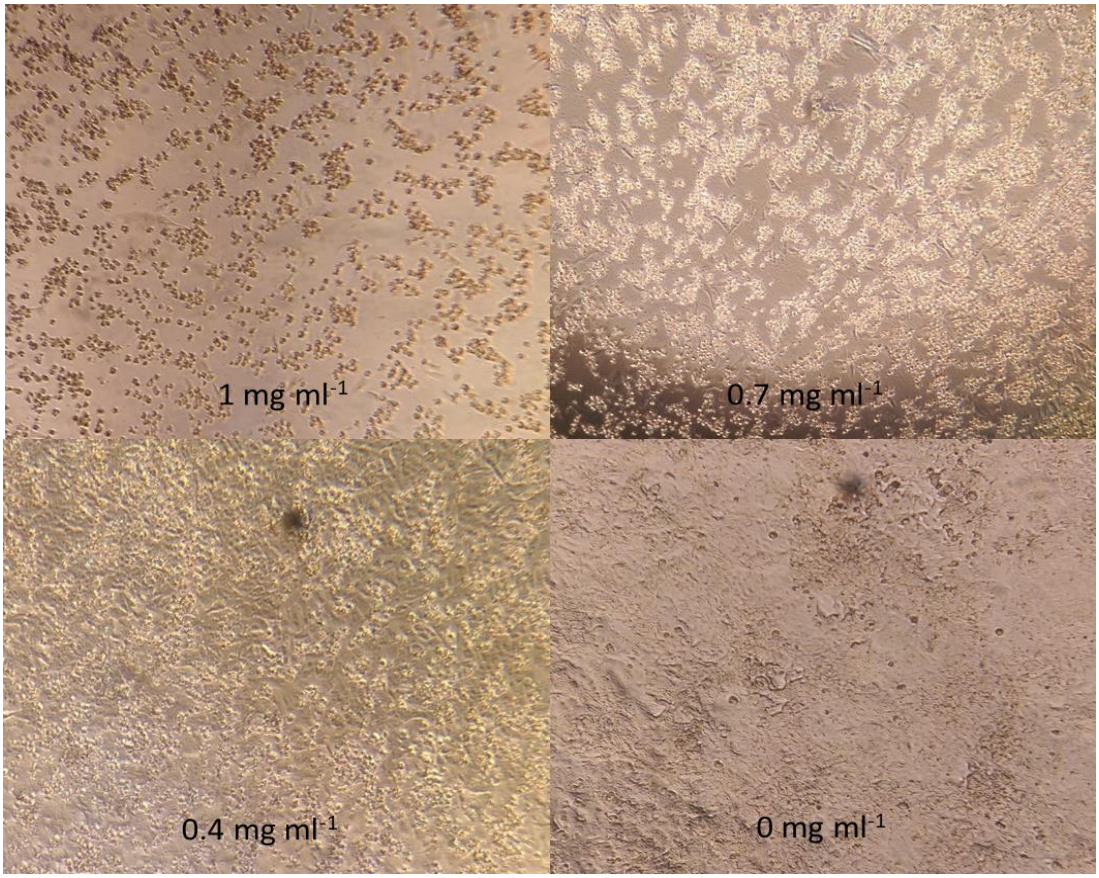

Figure 5.1. ***Kill curve of G418 in A549 cell line*** *passage 39. Images representative of kill curve 1mg ml^{-1} – 0.05mg ml^{-1}*

We determined that the optimal concentration of G418 to use for transfection of A549 cells was 0.7mg ml^{-1}. This concentration is in line with published literature (Oh *et al.*, 2006).

5.3 Results

5.3.1 RV-16 infection induces increased ATP release

Following our characterisation of the hypotonic pathway in Chapter 4 we decided to investigate the effect of RV-16 on this pathway to see if the viral infection caused any alteration to the cellular response. We employed the same techniques as previously used in section 4.3.1 including western blot analysis using whole cell lysates to study global protein expression of hypotonic pathway targets and MLC phosphorylation during RV-16 infection. We further utilised our capabilities to measure both extra- and intracellular ATP levels during hypotonic exposure and basally during RV-16 infection. Building on our previous work with RV-16 from Chapter 3, we carried out infections for longer durations up to and including 7 days (168 hours). We felt this was more accurate representation of the common cold infection instead of purely the incubation period (ranges 1-4 days).

5.3.1.1 RV-16 causes no effect on global pannexin-1 protein expression

Whole cell lysates were isolated from A549 cells infected with RV-16 at MOI 1. Lysates were subject to western blot analysis, as described in section 2.9, and probed for global expression of pannexin-1, total-MLC, phospho-MLC (ser19) and loading control α-tubulin (Fig. 5.2, 5.3, 5.4 and 5.5).

We were able to conclude that infection with RV-16 at MOI 1 caused no significant change in pannexin-1 global protein expression at any time point over a 168-hour infection time course (Fig. 5.2, $P>0.05$; n=5 and Fig. 5.3, $P>0.05$; n=3).

We investigated the effect of RV-16 on total-MLC expression and MLC phosphorylation at serine19. Unfortunately, we were not able to detect any positive signal from total-MLC or phospho-MLC (ser19) including on our positive control for any of the short-term infection (>72 hours) time courses carried out (data not shown). We were therefore unable to determine if RV-16 infection caused any change of MLC whole cell protein expression over a 72-hour period, nor if RV-16 caused any change in MLC phosphorylation status at serine19. When investigated over a longer infection time course 96-168 hours we found no significant different in either total-MLC or phospho-MLC (ser19) expression compared to basal at any time point (Fig. 5.4, $P>0.05$; n=3). Although not significant, there was a

difference between total-MLC and phospho-MLC expression at 168 hours (P=0.0915; n=3). When phospho-MLC was expressed as a percentage of total-MLC (Fig. 5.5) and compared to basal there was a significant reduction in MLC phosphorylation at ser19 at 168 hours (P=0.0245; n=3). Although not significant, there was a general trend in reduction of MLC phosphorylation at ser19 in all time points including UV control compared to basal (96 hours P=0.0711, 120 hours P=0.053, 144 hours P=0.1889, UV P=0.071; n=3).

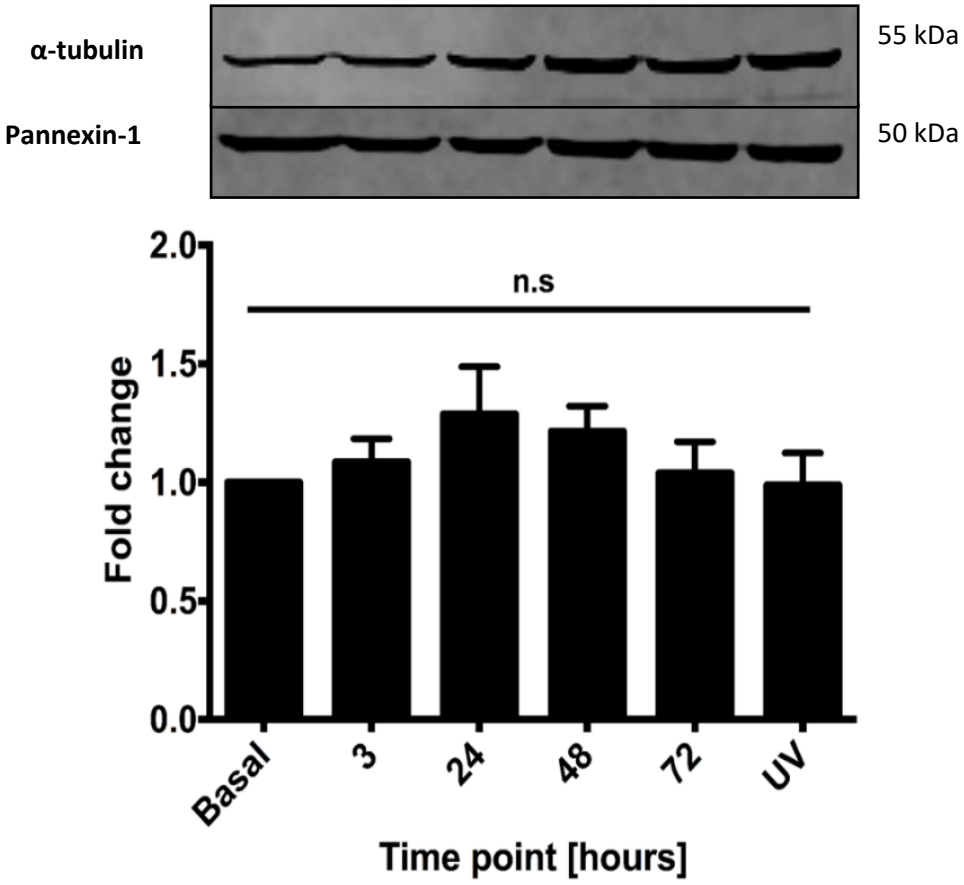

Figure 5.2. ***Pannexin-1 protein expression in A549 cell line infected with RV-16.*** *A549 cell line stimulated with RV-16 at MOI 1 for up to 72 hours, as labelled, UV-inactivated viral sham control (UV) or left unstimulated (basal). Whole cell lysate (50µg protein) probed for α-tubulin loading control and pannexin-1 protein expression, as labelled. Results are displayed as mean ± S.E.M. of five independent experiments (n=5). Statistical analysis was carried out using multiple comparison two-way ANOVA followed by Sidak analysis. Densitometry was carried out and expressed as fold change from basal following normalisation to loading control α-tubulin. P>0.05.*

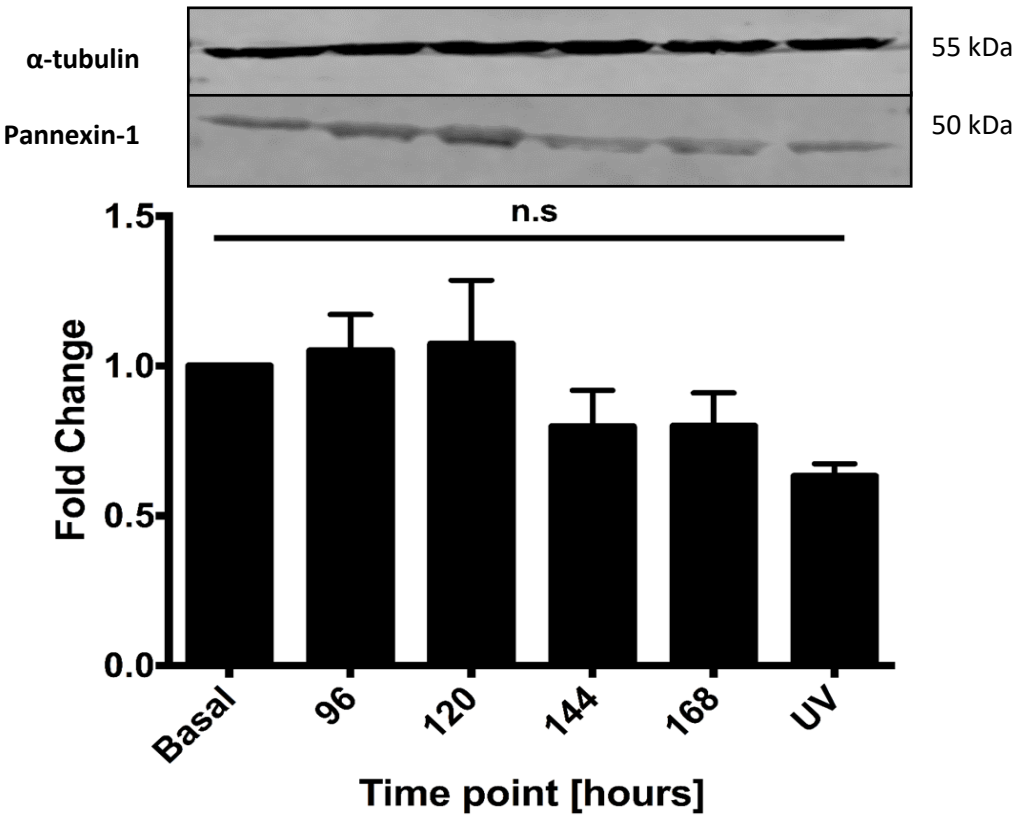

Figure 5.3. ***Pannexin-1 protein expression in A549 cell line infected long-term with RV-16.*** *A549 cell line stimulated with RV-16 at MOI 1 for 96 to 168 hours, as labelled, UV-inactivated viral sham control (UV) or left unstimulated (basal). Whole cell lysate (50µg protein) probed for α-tubulin loading control and pannexin-1 protein expression, as labelled. Results are displayed as mean ± S.E.M. of three independent experiments (n=3). Statistical analysis was carried out using multiple comparison two-way ANOVA followed by Sidak analysis. Densitometry was carried out and expressed as fold change from basal following normalisation to loading control α-tubulin. P>0.05.*

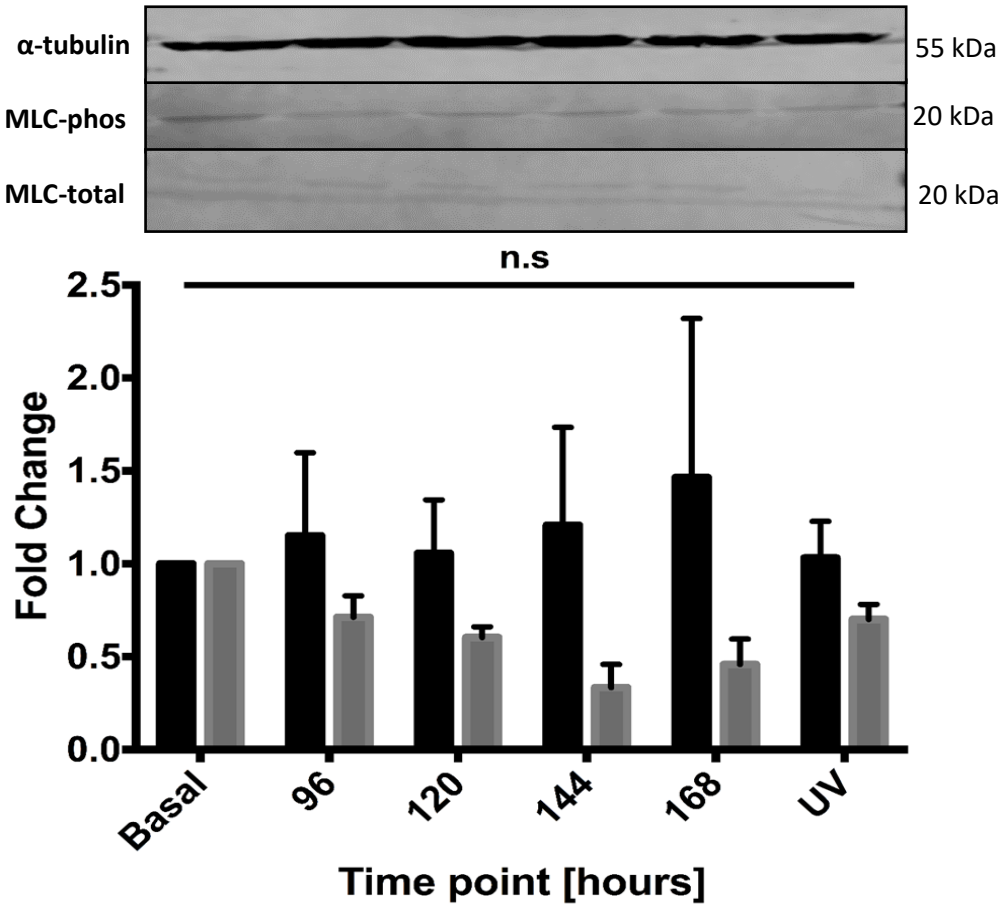

Figure 5.4. ***Total- and phospho-MLC protein expression in A549 cell line infected long-term with RV-16.*** *A549 cell line stimulated with RV-16 at MOI 1 for 96 to 168 hours, as labelled, UV-inactivated viral sham control (UV) or left unstimulated (basal). Whole cell lysate (50µg protein) probed for α-tubulin loading control, ser19 phospho-MLC (grey) and total-MLC (black), as labelled. Results are displayed as mean ± S.E.M. of three independent experiments (n=3). Statistical analysis was carried out using multiple comparison two-way ANOVA followed by Sidak analysis. Densitometry was carried out and expressed as fold change from basal following normalisation to loading control α-tubulin. P>0.05.*

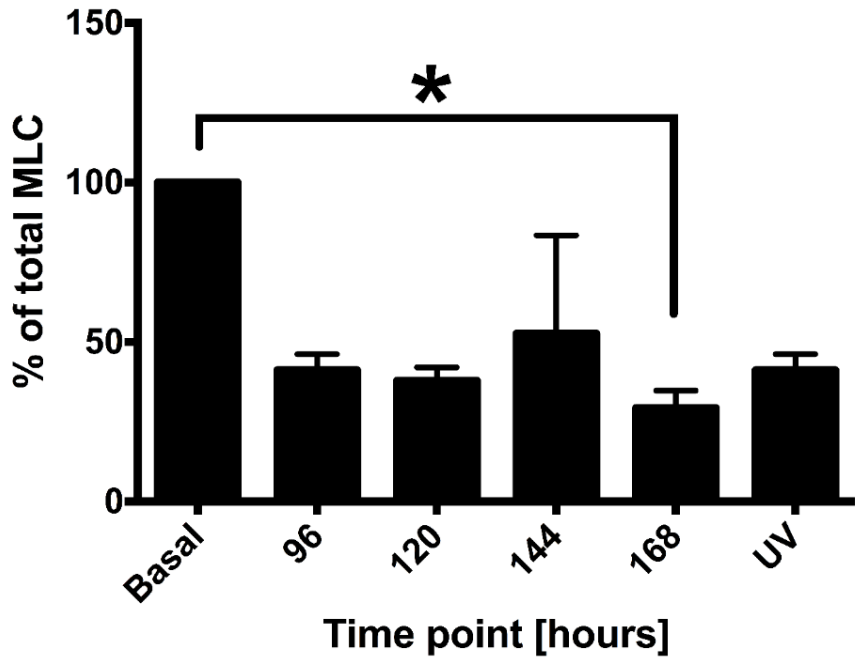

Figure 5.5. ***Phospho-MLC protein expression as a percentage of total-MLC in A549 cell line infected long-term with RV-16.*** *A549 cell line stimulated with RV-16 at MOI 1 for 96 to 168 hours, as labelled, UV-inactivated viral sham control (UV) or left unstimulated (basal). Data displayed is phospho-MLC standardised as a percentage of total-MLC as a result of densitometry data collected from western blot analysis (see Fig.5.7). Results are displayed as mean ± S.E.M. of three independent experiments (n=3). Statistical analysis was carried out using multiple comparison one-way ANOVA followed by Tukey analysis. *P=0.0245.*

5.3.1.2 RV-16 infection causes increased pannexin-1 and TRPV4 expression following pathway inhibition and hypotonic exposure

A549 cells were infected with RV-16 at MOI 1 or with UV inactivated sham viral control. Infected cells were then incubated with inhibitors to the hypotonic pathway (HC067047 – TRPV4, H1152 – RhoA, ML-7 – MLCK, carbenoxolone – pannexin, vehicle control – 0.01% v/v DMSO) then exposed to either isotonic control or hypotonic stimulation. The cells were lysed, and western blot analysis was carried out, as described in section 2.9. Whole cell lysates were probed for TRPV4, pannexin-1, total-MLC, phospho-MLC (ser19) and loading control α-tubulin (Fig. 5.6 and Fig. 5.7). Membranes were visualised with Licor fluorescent conjugated secondary antibodies on a Licor scanner, as previously described.

Once again, we hoped to monitor MLC phosphorylation of ser19 during the hypotonic stimulation and monitor the effect of various inhibitors to the hypotonic stress pathway on

MLC phosphorylation at ser19 using western blot analysis. However, we only managed to achieve a positive signal for both total-MLC and phospho-MLC (ser19) on two separate occasions. We were therefore unable to carry out any analysis using this data (data not shown).

At 48 hours, RV-16 at MOI 1 caused a significant increase in global expression of pannexin-1 at all conditions compared to their respective uninfected control (Fig. 5.8, HT $P<0.0001$, ISO $P=0.0196$, HC06 $P=0.0001$, H1152 $P=0.0002$, ML-7 $P=0.0033$, CBX $P<0.0001$, VH $P=0.005$; $n=3$). There was no significant difference between any condition (inhibitors or hypotonic stimulation) from basal for any other time point (Fig. 5.6, $P>0.05$; $n=3$).

At 72 hours, RV-16 at MOI 1 caused a significant increase in global expression of TRPV4 when pre-treated with HC067047 ($P=0.0298$; $n=3$), H1152 ($P=0.0274$; $n=3$) and ML-7 ($P=0.0162$; $n=3$) then exposed to hypotonic stimulation when compared to their respective uninfected control condition (Fig. 5.9). Furthermore, UV inactivated sham viral control induced a significant increase in global expression of TRPV4 when pre-treated with HC067047 ($P=0.0005$; $n=3$), H1152 ($P=0.0008$; $n=3$), ML-7 ($P=0.002$) then exposed to hypotonic stimulation when compared to their respective uninfected control condition (Fig. 5.13). There was also a significant increase in global TRPV4 expression when stimulated with hypotonic ($P=0.0068$; $n=3$) or isotonic control ($P=0.0003$; $n=3$) (Fig. 5.10).

Whilst this data doesn't corroborate the findings from section 5.3.1.1 and section 3.33, where no significant change was found in either pannexin-1 or TRPV4 global protein expression during standard time course experiments with RV-16 infected cells, the data here is consistent and highly significant. We can therefore not disregard the changes seen here.

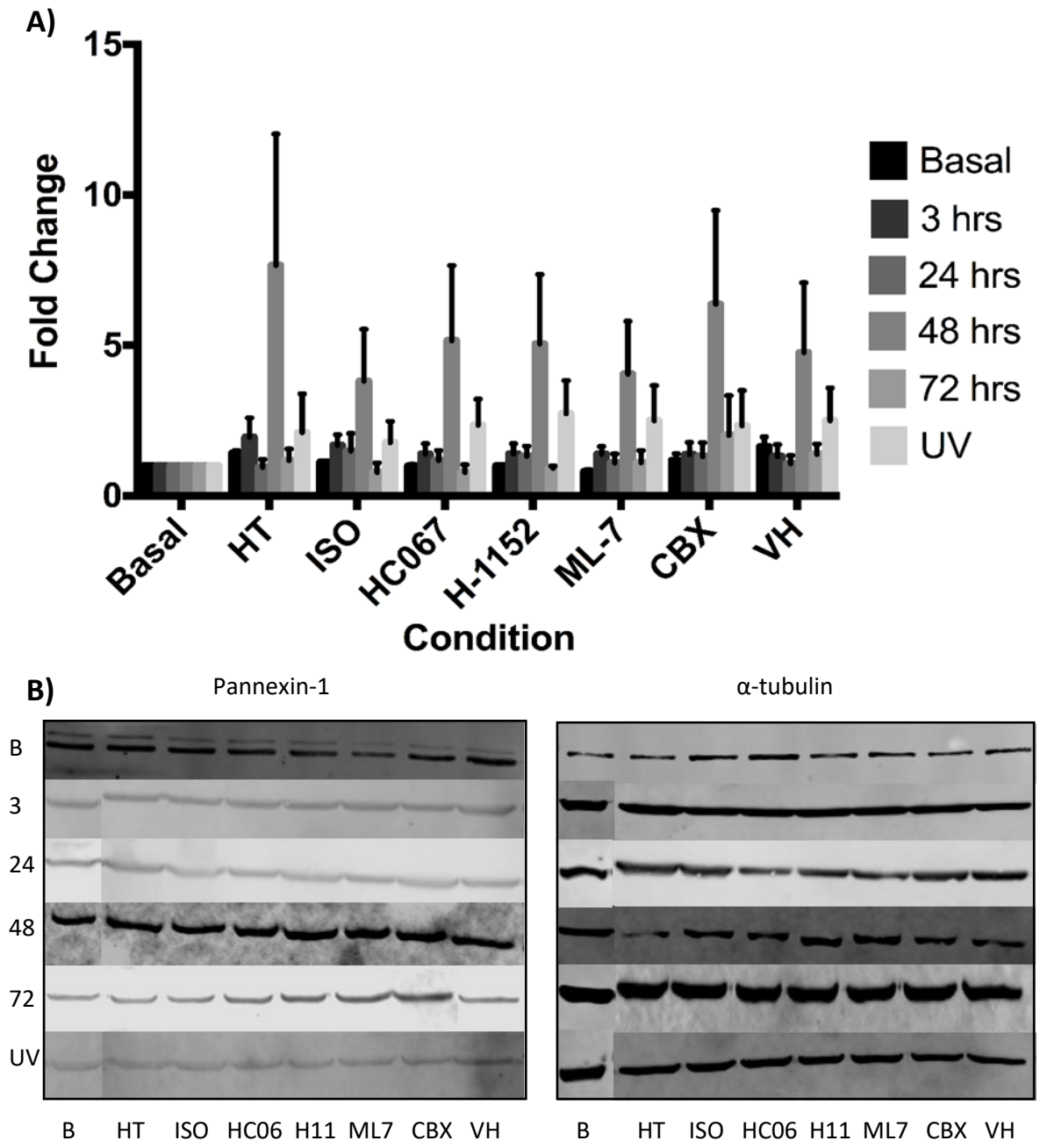

Figure 5.6. ***Pannexin-1 protein expression in RV-16 infected A549 cell line followed by hypotonic stimulation.*** *A549 cell line initially stimulated with RV-16 at MOI 1 for up to 72 hours, as labelled, UV-inactivated viral sham control or left unstimulated (basal), then incubated with inhibitors HC067047 (HC06), H-1152 (H11), ML-7 (ML7), carbenoxolone (CBX), 0.01% v/v DMSO (VH) and post-treated with 33% hypotonic (HT) exposure or isotonic (ISO) control. Whole cell lysate (50µg protein) probed for pannexin-1 and α-tubulin loading control protein expression, as labelled. Densitometry was carried out and expressed as fold change from basal following normalisation to loading control α-tubulin. A) densitometry shown as fold change B) Representative blot images of three independent experiments (N=3) for pannexin-1 (50 kDa) and α-tubulin (55 kDa) loading control expression. Statistical analysis was carried out using multiple comparison two-way ANOVA followed by Dunnetts analysis.*

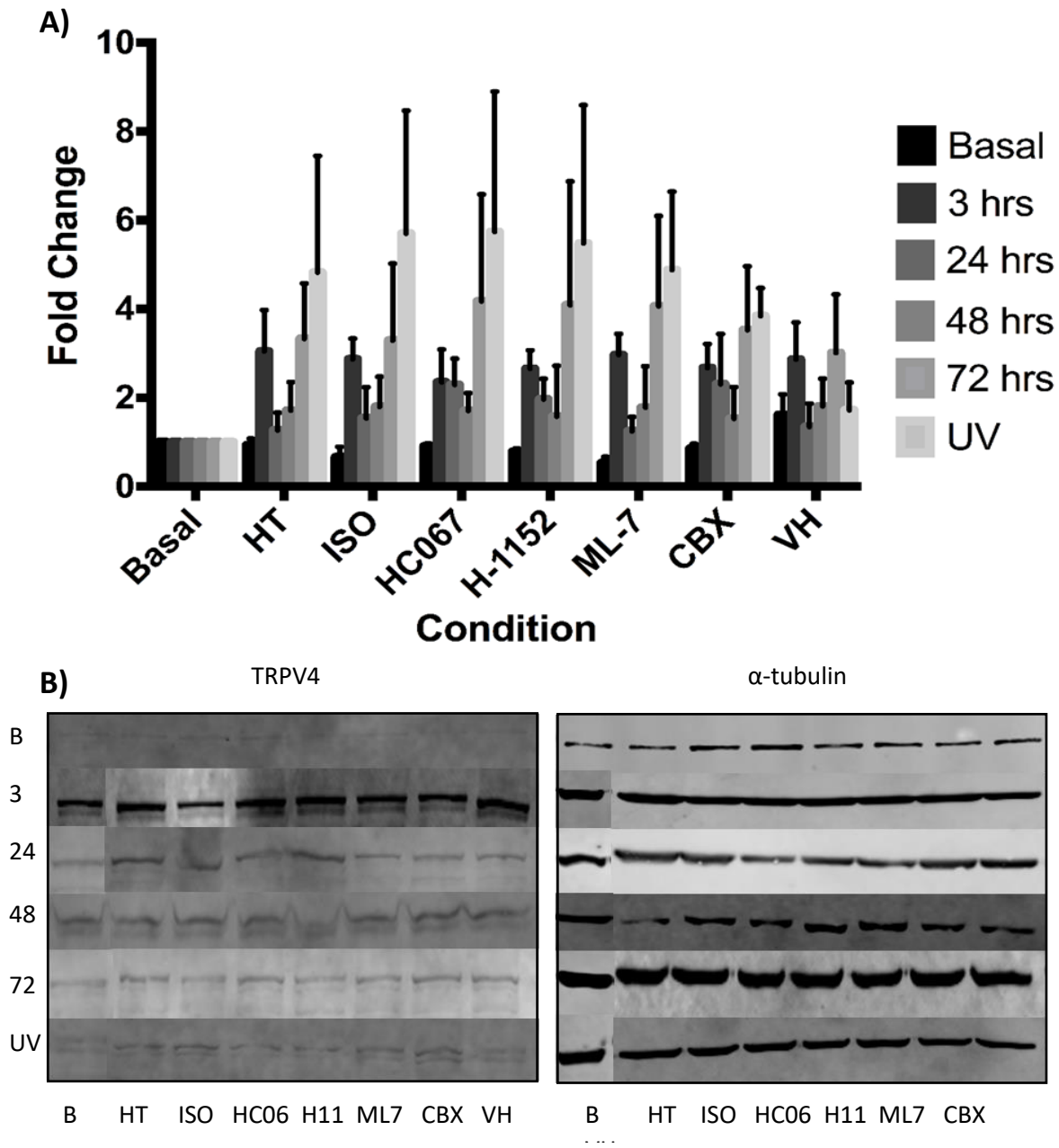

Figure 5.7. ***TRPV4 protein expression in RV-16 infected A549 cell line followed by hypotonic stimulation.*** *A549 cell line initially stimulated with RV-16 at MOI 1 for up to 72 hours, as labelled, UV-inactivated viral sham control or left unstimulated (basal), then incubated with inhibitors HC067047 (HC06), H-1152 (H11), ML-7 (ML7), carbenoxolone (CBX), 0.01% v/v DMSO (VH) and post-treated with 33% hypotonic (HT) exposure or isotonic (ISO) control. Whole cell lysate (50µg protein) probed for TRPV4 and α-tubulin loading control protein expression, as labelled. Densitometry was carried out and expressed as fold change from basal following normalisation to loading control α-tubulin. A) densitometry shown as fold change B) Representative blot images of three independent experiments (N=3) for TRPV4 (110 kDa) and α-tubulin (55 kDa) loading control expression. Statistical analysis was carried out using multiple comparison two-way ANOVA followed by Dunnetts analysis.*

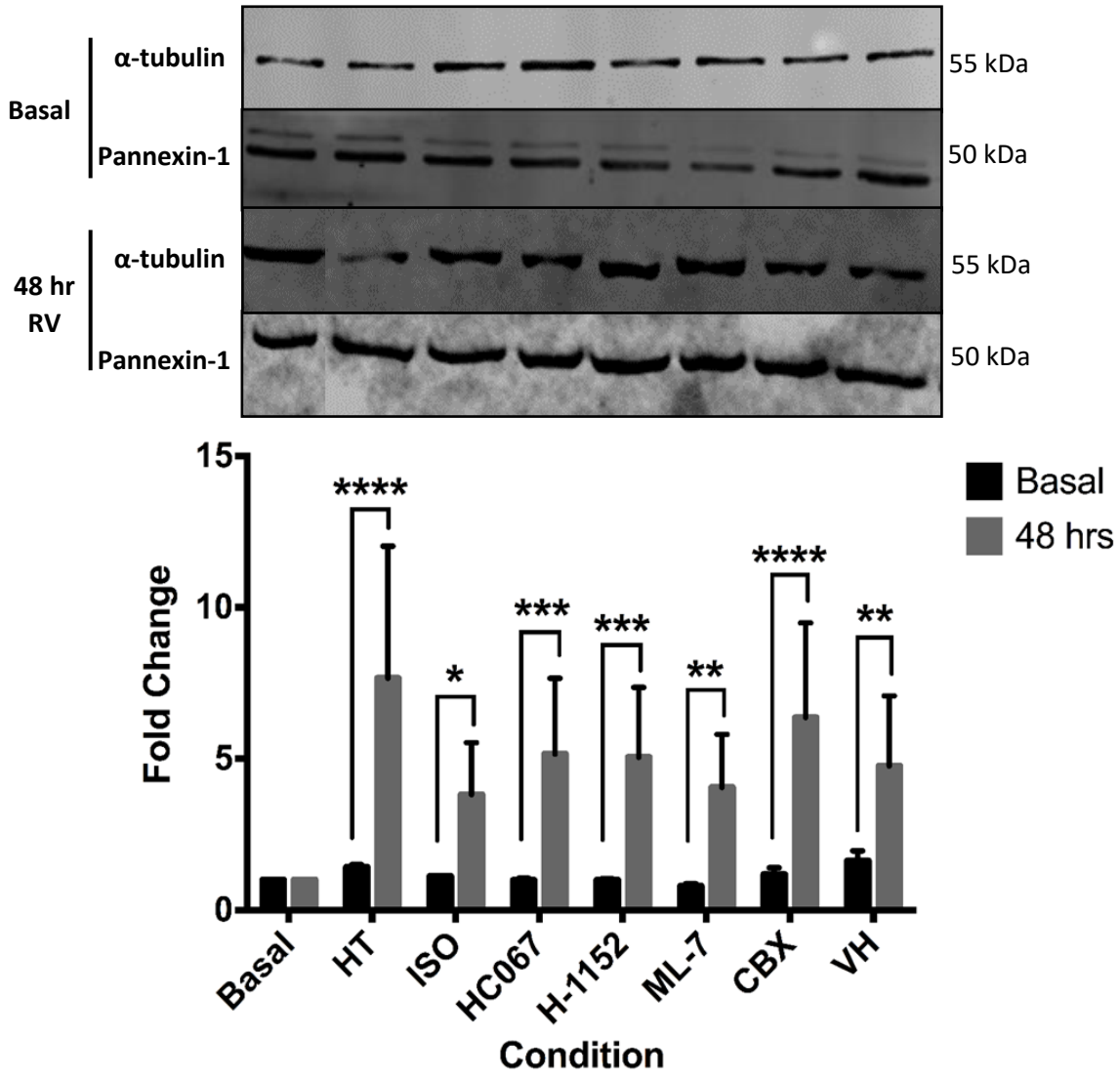

Figure 5.8. ***Pannexin-1 protein expression from A549 cell line after 48 hours RV-16 infection followed by hypotonic stimulation.*** *As detailed from Fig. 5.6, A549 cell line initially stimulated with RV-16 at MOI 1 for 48 hours then incubated with inhibitors HC067047 (HC06), H-1152 (H11), ML-7 (ML7), carbenoxolone (CBX), 0.01% v/v DMSO (VH) and post-treated with 33% hypotonic (HT) exposure or isotonic (ISO) control, as labelled. Whole cell lysate (50µg protein) probed for pannexin-1 and α-tubulin loading control protein expression, as labelled. Densitometry was carried out and expressed as fold change from basal following normalisation to loading control α-tubulin. Densitometry shown as fold change and representative blot images of three independent experiments (N=3) for pannexin-1 (50 kDa) and α-tubulin (55 kDa) loading control expression. Statistical analysis was carried out using multiple comparison two-way ANOVA followed by Dunnetts analysis for change from basal of each condition. *P<0.0196, **P<0. 0.005, ***P< 0.0002, ****P<0.0001*

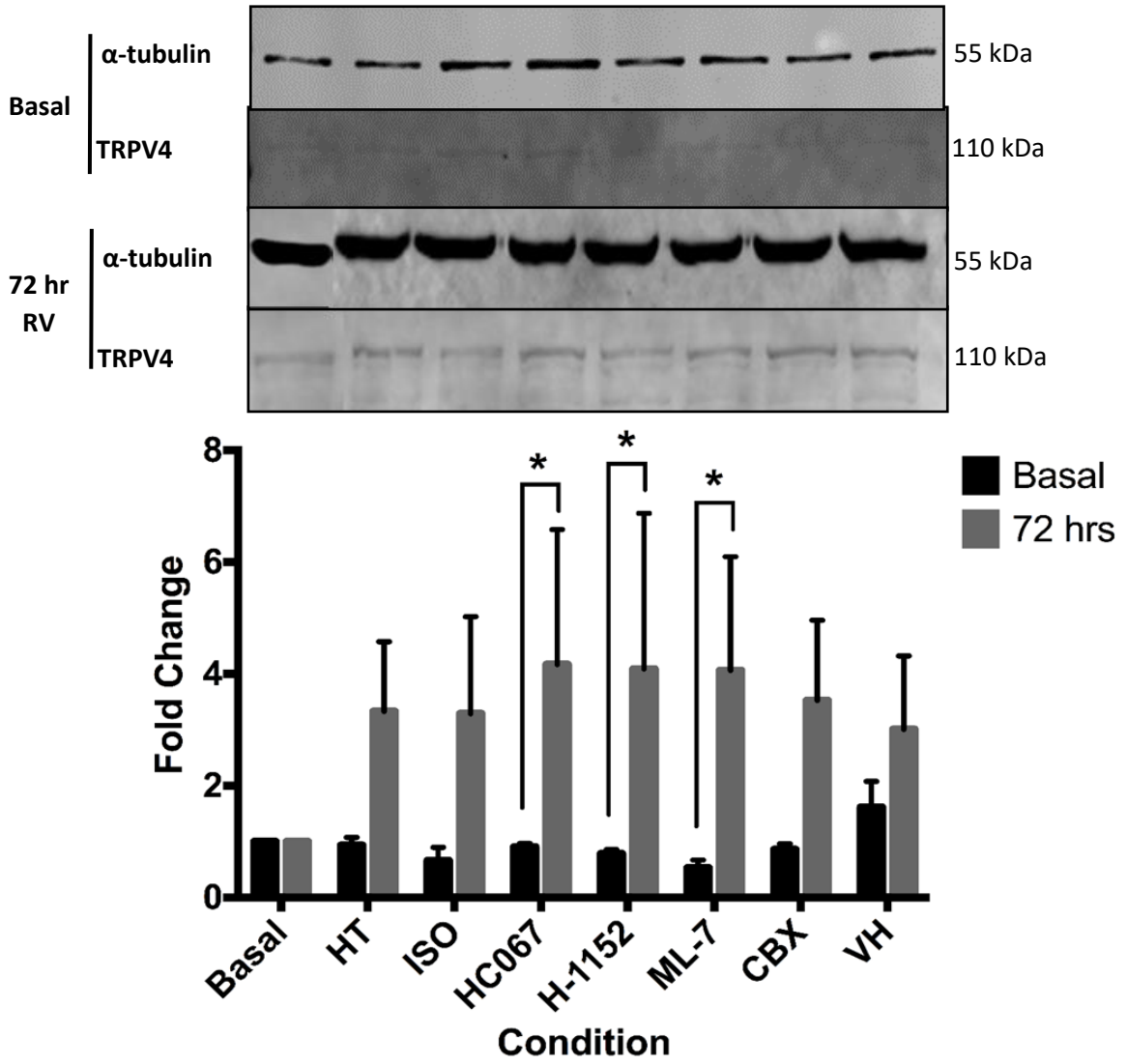

Figure 5.9. ***TRPV4 protein expression from A549 cell line after 72 hours RV-16 infection followed by hypotonic stimulation.*** *As detailed from Fig. 5.7, A549 cell line initially stimulated with RV-16 at MOI 1 for 72 hours then incubated with inhibitors HC067047 (HC06), H-1152 (H11), ML-7 (ML7), carbenoxolone (CBX), 0.01% v/v DMSO (VH) and post-treated with 33% hypotonic (HT) exposure or isotonic (ISO) control, as labelled. Whole cell lysate (50µg protein) probed for TRPV4 and α-tubulin loading control protein expression, as labelled. Densitometry was carried out and expressed as fold change from basal following normalisation to loading control α-tubulin. Densitometry shown as fold change and representative blot images of three independent experiments (N=3) for TRPV4 (110 kDa) and α-tubulin (55 kDa) loading control expression. Statistical analysis was carried out using multiple comparison two-way ANOVA followed by Dunnetts analysis for change from basal of each condition. *P<0.05.*

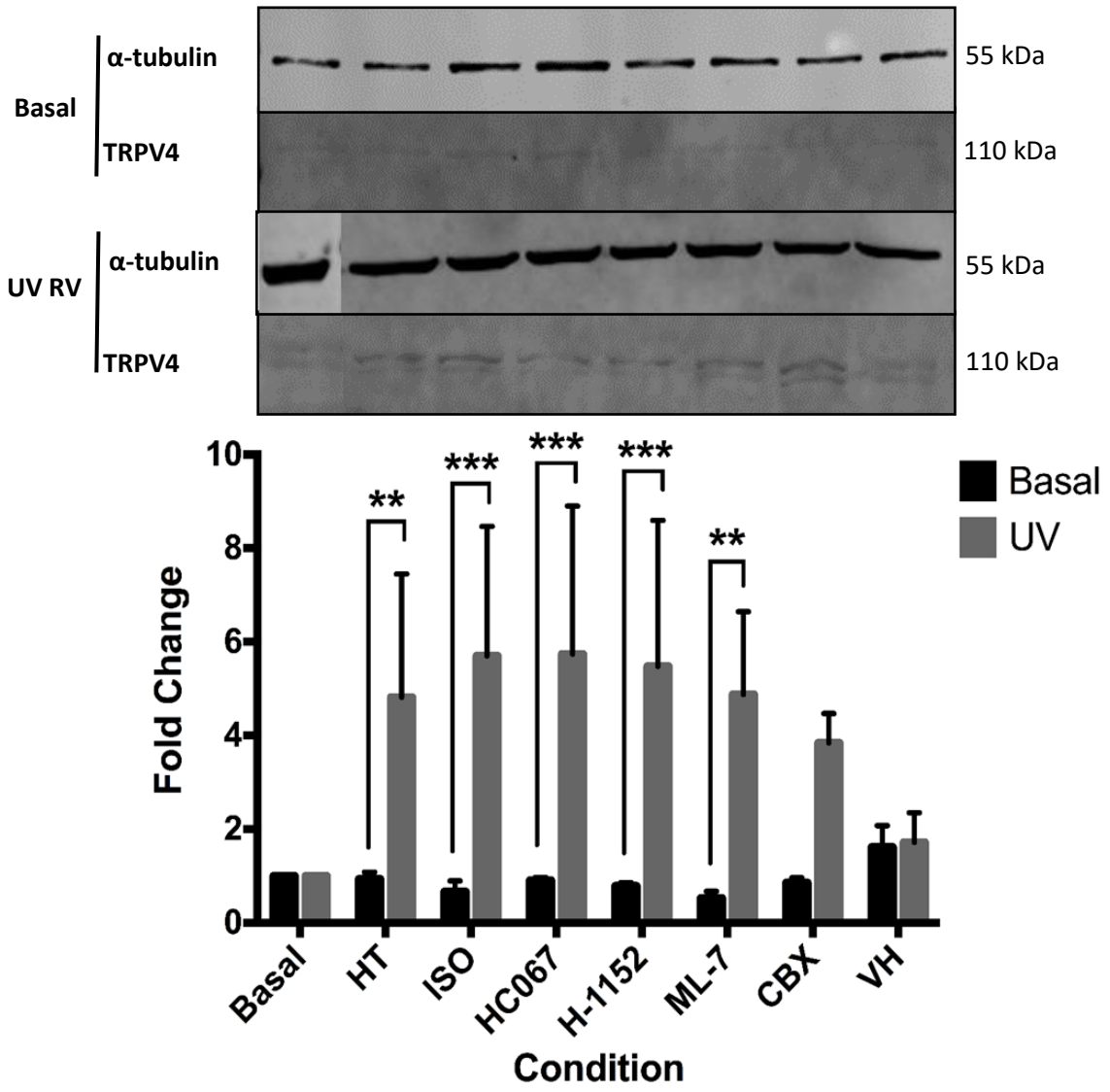

Figure 5.10. ***TRPV4 protein expression from A549 cell line following UV inactivated RV-16 infection followed by hypotonic stimulation.*** *As detailed from Fig. 5.7, A549 cell line initially stimulated with UV-inactivated viral sham control of RV-16 at MOI 1 for 24 hours then incubated with inhibitors HC067047 (HC06), H-1152 (H11), ML-7 (ML7), carbenoxolone (CBX), 0.01% v/v DMSO (VH) and post-treated with 33% hypotonic (HT) exposure or isotonic (ISO) control, as labelled. Whole cell lysate (50µg protein) probed for TRPV4 and α-tubulin loading control protein expression, as labelled. Densitometry was carried out and expressed as fold change from basal following normalisation to loading control α-tubulin. Densitometry shown as fold change and representative blot images of three independent experiments (N=3) for TRPV4 (110 kDa) and α-tubulin (55 kDa) loading control expression. Statistical analysis was carried out using multiple comparison two-way ANOVA followed by Dunnetts analysis for change from basal of each condition. **P<0.002, ***P<0.0005.*

5.3.1.3 RV-16 infection causes increased basal and hypotonic stimulated release of ATP in A549 cell line

Hypotonic exposure and mechanical stimulation in A549 cells cause ATP release (Seminario-Vidal *et al.*, 2011; Grygorczyk, Furuya & Sokabe, 2013). Therefore, we decided to investigate the effect of RV-16 infection on production, storage and release of ATP. We had previously quantified the ATP release in cell culture supernatant at different time points in a one-time sampling and concluded there was no significant change in ATP concentration from basal (see section 3.3.3.3). However, at the time we hadn't considered the impact of ectoATPases so we took a wider approach here. First, we investigated the effect of RV-16 at MOI 1 on total intracellular stores of ATP at both short-term (Fig.5.11A) and long-term infection (5.11B). Between 96-168 hours there was no significant difference in intracellular ATP stores from basal control including UV inactivated sham viral control (Fig. 5.11B, $P>0.05$; n=4). However, there was a 50% increase in intracellular ATP concentration at 24 hours (Fig. 5.11A, $P=0.0034$; n=4) and UV sham control ($P=0.0022$; n=4). Followed by a 50% decrease in intracellular ATP concentration at 48 and 72 hours ($P<0.0001$; n=4) from basal control.

Having previously determined the effect of various inhibitors of the hypotonic pathway on ATP release (see section 4.3.1) we decided to assay extracellular supernatant for ATP concentration on RV-16 infected A549 cells basally (unstimulated), when stimulated with hypotonic stimulus or isotonic control (to account for mechano-activation) over a 5-minute period. Cells were treated in the same way as carried out previously (see section 4.3.1). Briefly, the cells were infected with RV-16 at MOI 1 and incubated for 1 hour at room temperature with gentle agitation. The cells were washed and incubated at 37^{o}C for up to 72 or 168 hours with UV-inactivated sham viral control. The cells were washed and incubated in modified HBSS (HBSS +10mM HEPES) (HBSS+) and allowed to equilibrate for 1 hour prior to commencement of the assay. The cells were then either sampled undisturbed for basal ATP release or exposed to 200mOsm hypotonic buffer or isotonic control buffer. Samples were taken every 15 seconds for 5 minutes. The results were displayed as fold change from uninfected cells and area under the curve (AUC) analysis was also carried out.

Over a 72-hour time course there was no significant change in ATP release basally (unstimulated) (Fig. 5.12A, $P>0.05$; n=3). However, when AUC analysis was carried out

there was a significant increase in ATP release at 72 hours when compared to basal control (Fig. 5.12B, P=0.0185; n=3), all other time points were not significant (P>0.05; n=3).

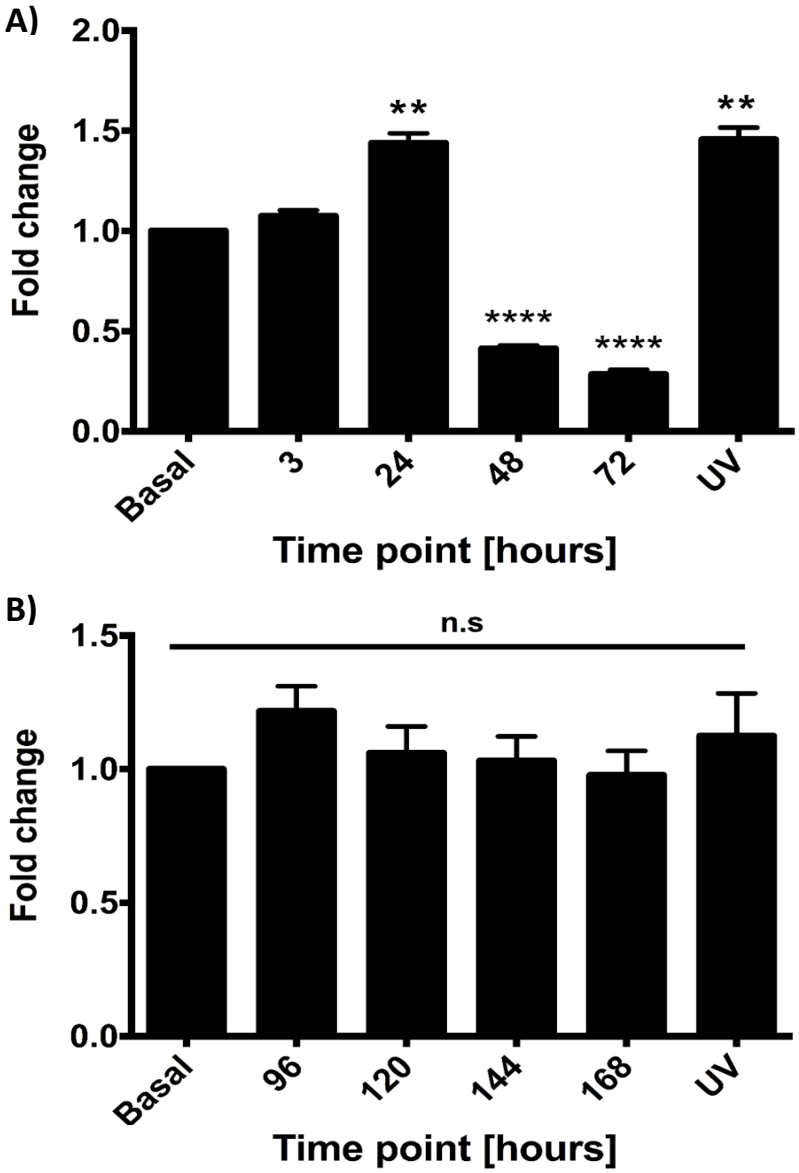

Figure 5.11. ***Total intracellular ATP concentration of RV-16 infected A549 cell line.*** *A549 cells stimulated with RV-16 at MOI 1 for A) 3-72 hours, B) 96-168 hours, UV-inactivated viral sham control or left unstimulated (basal). Intracellular ATP concentration quantified using commercially available kit at each time point. Results are displayed as mean ± S.E.M. of four independent experiments (n=4). Statistical analysis was carried out using multiple comparison one-way ANOVA followed by Dunnetts. **P<0.0034. ****P<0.0001.*

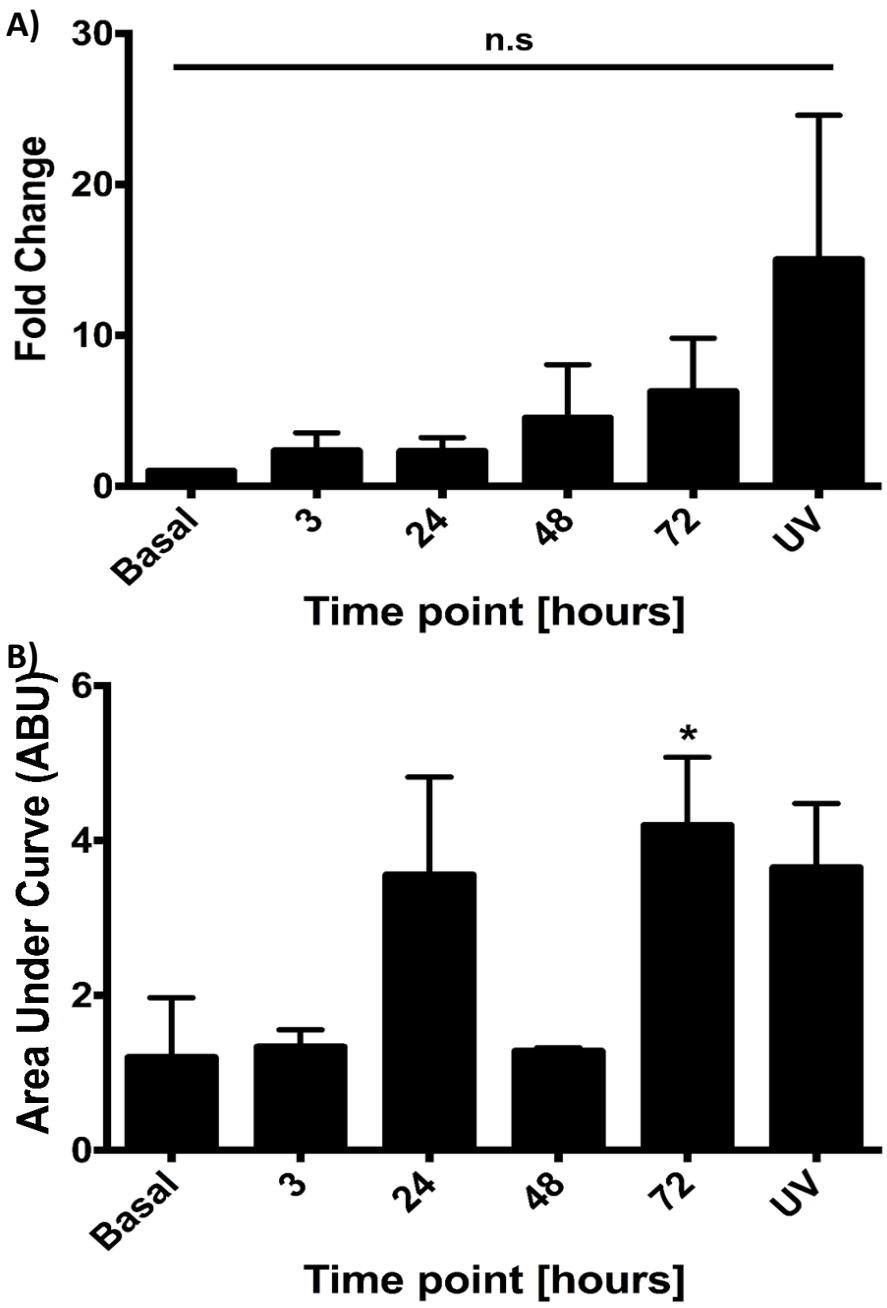

Figure 5.12. ***Peak and total ATP release from A549 cells infected with RV-16.*** *A549 cells stimulated with RV-16 at MOI 1 for up to 72 hours, UV-inactivated viral sham control or left unstimulated. Supernatants sampled at 15 second intervals for 5 minutes. A) Peak ATP release shown as fold change from basal. B) Area under curve analysis of full 5-minute time course. Results are displayed as mean ± S.E.M. of three independent experiments (n=3). Statistical analysis was carried out using multiple comparison one-way ANOVA followed by with Dunnetts. ABU arbitrary units. *P=0.0185.*

When we looked at the effect of RV-16 at MOI 1 over a long-term infection (96-168 hours), there was no significant change in unstimulated ATP release (Fig. 5.13A, P>0.05; n=3), despite a larger fold change increase due to variability in experiments. However, once again when we carried out AUC analysis there was a significant increase in ATP release from 120-168 hours including UV inactivated viral sham control (Fig. 5.13B, 120 hours P=0.03, 144 hours P=0.0012, 168 hours P=0.0028, UV P=0.0006; n=3), 96 hours was not significant (P>0.05; n=3).

We then investigated the effect of isotonic control on ATP release in RV-16 infected A549 cells to determine if the cells become more sensitive to mechanosensation when infected with RV-16. During short term infections with RV-16 there was no significant change in ATP release following isotonic addition at any time point due to variable increases between experiments (Fig. 5.14A, P>0.05; n=3). However, AUC analysis identified significant increases in ATP release at 24 and 72 hours (Fig. 5.14B, P=0.0233 and P=0.0464, respectively; n=3) when compared to uninfected isotonic control. There was no significant difference in ATP release at either 3 hours, 48 hours or UV control (P>0.05; n=3).

Over long-term infection with RV-16, isotonic control induced a general trend of increased ATP increase from 96-168 hours including UV control. Only 168 hours was deemed significant with a 9.5-fold increase in ATP release from basal control (Fig. 5.15A, P=0.0204; n=3). Following AUC analysis, there was no significant change in ATP release at 96 and 168 hours following isotonic control (Fig. 5.15B, P>0.05; n=3). However, there was a significant increase in ATP release at 120 hours, 144 hours and UV control (Fig. 5.15B, P=0.0097, P=0.0005 and P=0.0012, respectively; n=3).

Finally, we looked at the effect of hypotonic stimulation on A549 cells following RV-16 infection. Once again, despite a general trend of increased ATP release over short-term infection when compared to uninfected hypotonic control, only 72 hours was deemed significant with a 7.38-fold increase in ATP release (Fig. 5.16A, P=0.0099; n=3). All other time points were not significant when compared to uninfected hypotonic control (P>0.05; n=3). Following the application of AUC analysis, 72 hours remained significant (Fig. 5.16B, P=0.0127; n=3) whilst all over time points were not significant (P>0.05; n=3).

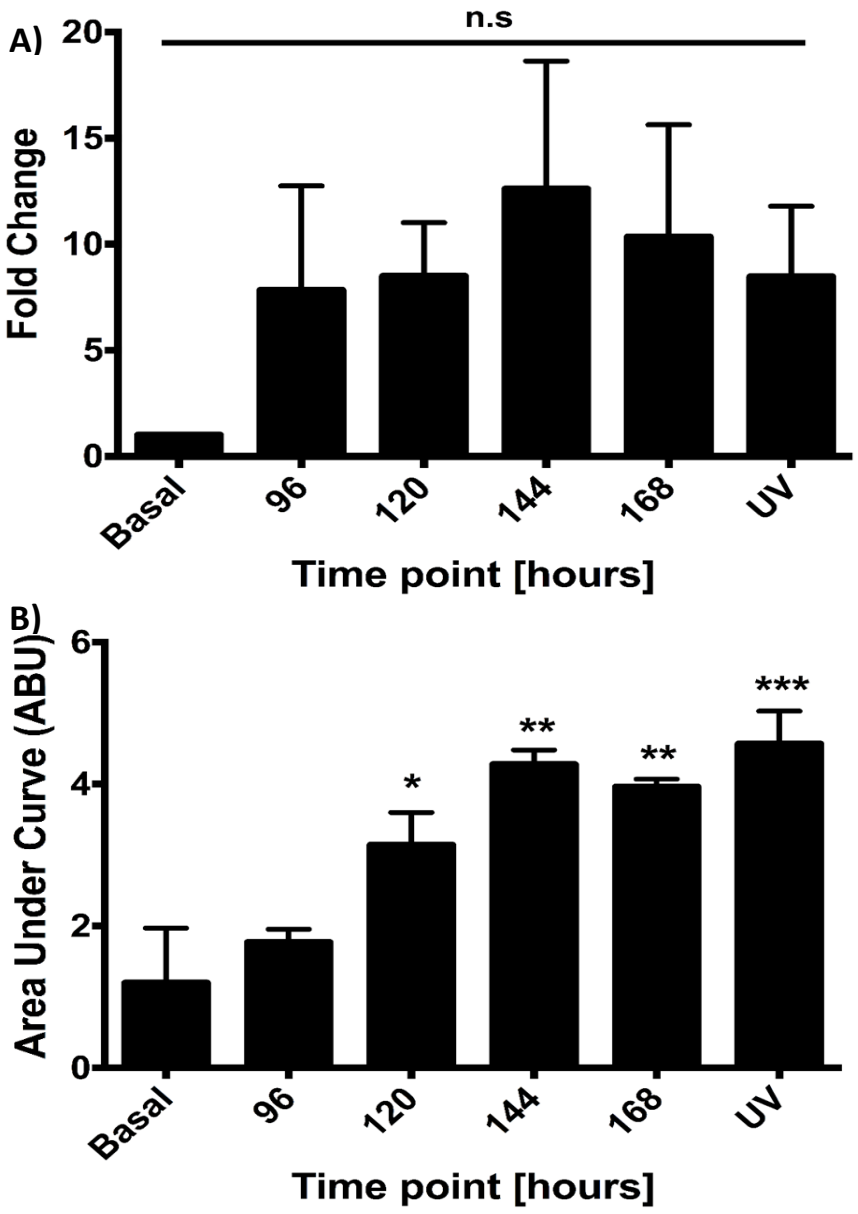

Figure 5.13. ***Peak and total ATP release from A549 cells infected long-term with RV-16.*** *A549 cells stimulated with RV-16 at MOI 1 for 96 to 168 hours, UV-inactivated viral sham control or left unstimulated. Supernatants sampled at 15 second intervals for 5 minutes. A) Peak ATP release shown as fold change from basal. B) Area under curve analysis of full 5-minute time course. Results are displayed as mean ± S.E.M. of three independent experiments (n=3). Statistical analysis was carried out using multiple comparison one-way ANOVA followed by with Dunnetts. ABU arbitrary units. *P=0.0.03, **P<0.0028, ***P=0.0006.*

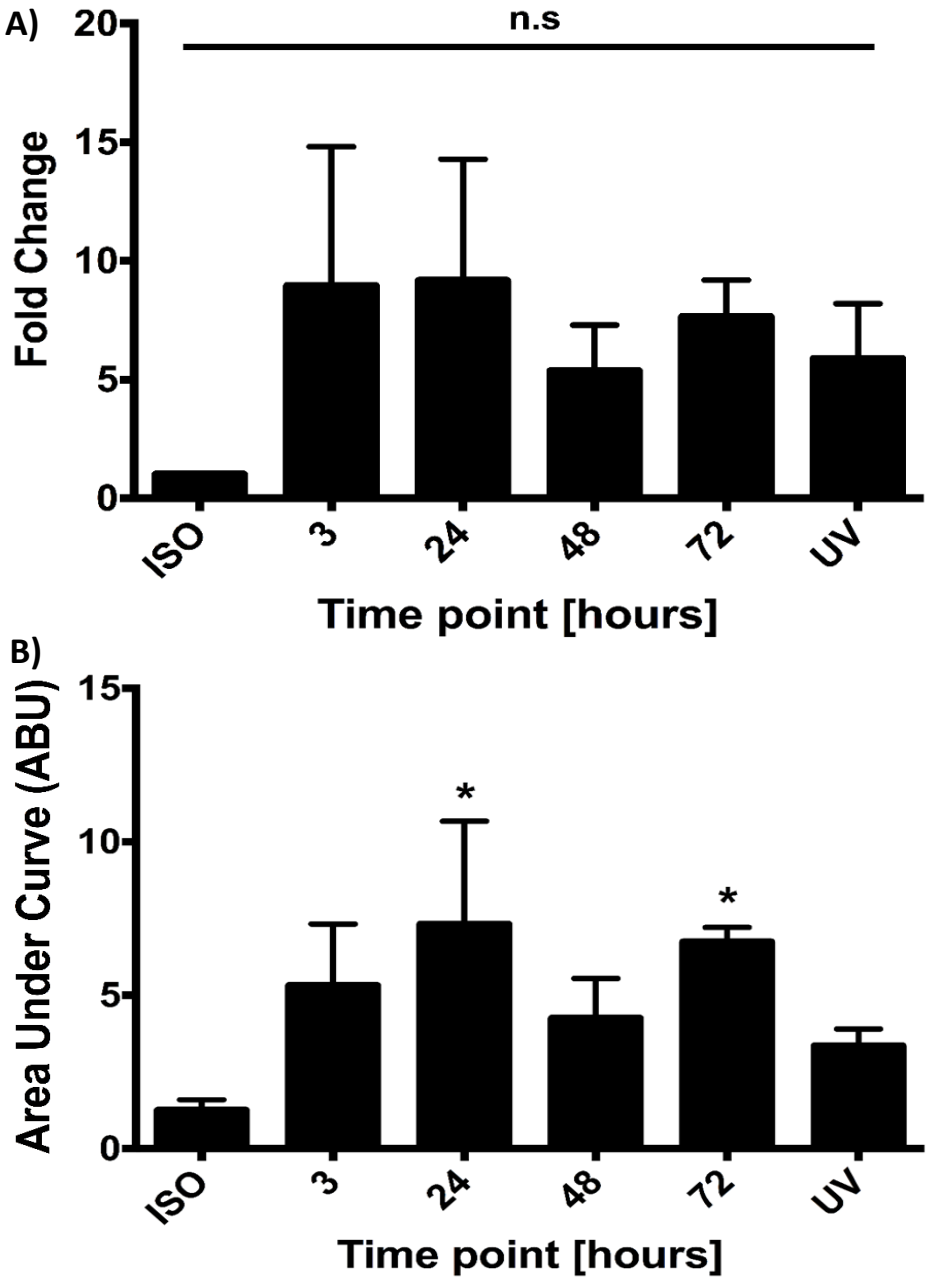

Figure 5.14. ***Peak and total ATP release from A549 cells infected with RV-16 and exposed to isotonic stimulus.*** *A549 cells stimulated with RV-16 at MOI 1 for up to 72 hours, UV-inactivated viral sham control or left unstimulated. Cells exposed to isotonic buffer and supernatants sampled at 15 second intervals for 5 minutes. A) Peak ATP release shown as fold change from basal. B) Area under curve analysis of full 5-minute time course. Results are displayed as mean ± S.E.M. of three independent experiments (n=3). Statistical analysis was carried out using multiple comparison one-way ANOVA followed by with Dunnetts. ABU arbitrary units. *P<0.04.*

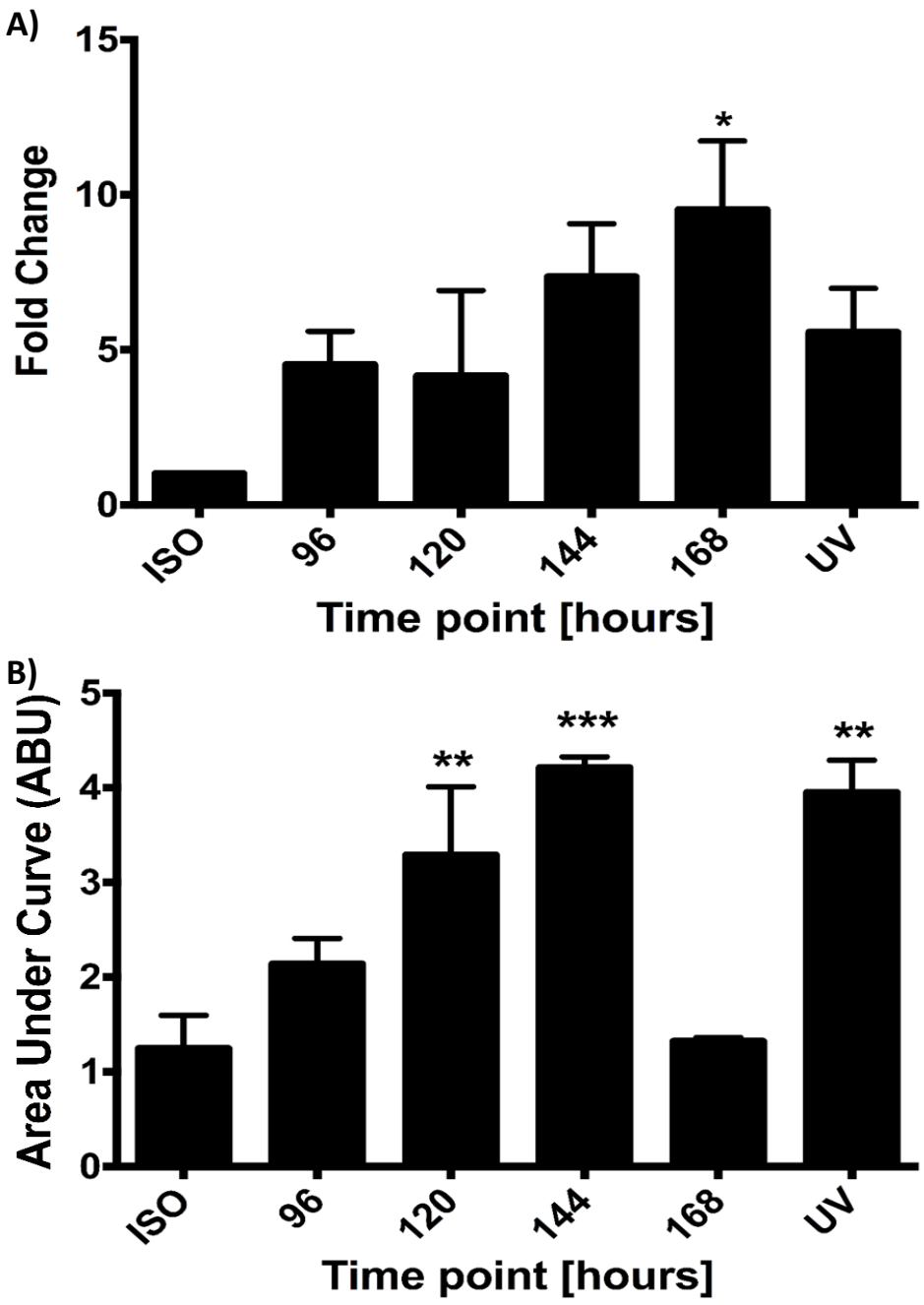

Figure 5.15. ***Peak and total ATP release from A549 cells infected long-term with RV-16 and exposed to isotonic stimulus.*** *A549 cells stimulated with RV-16 at MOI 1 for 96 to 168 hours, UV-inactivated viral sham control or left unstimulated. Cells exposed to isotonic buffer and supernatants sampled at 15 second intervals for 5 minutes. A) Peak ATP release shown as fold change from basal. B) Area under curve analysis of full 5-minute time course. Results are displayed as mean ± S.E.M. of three independent experiments (n=3). Statistical analysis was carried out using multiple comparison one-way ANOVA followed by with Dunnetts. ABU arbitrary units. *P=0.0204, **P<0.0097, ***P=0.0005.*

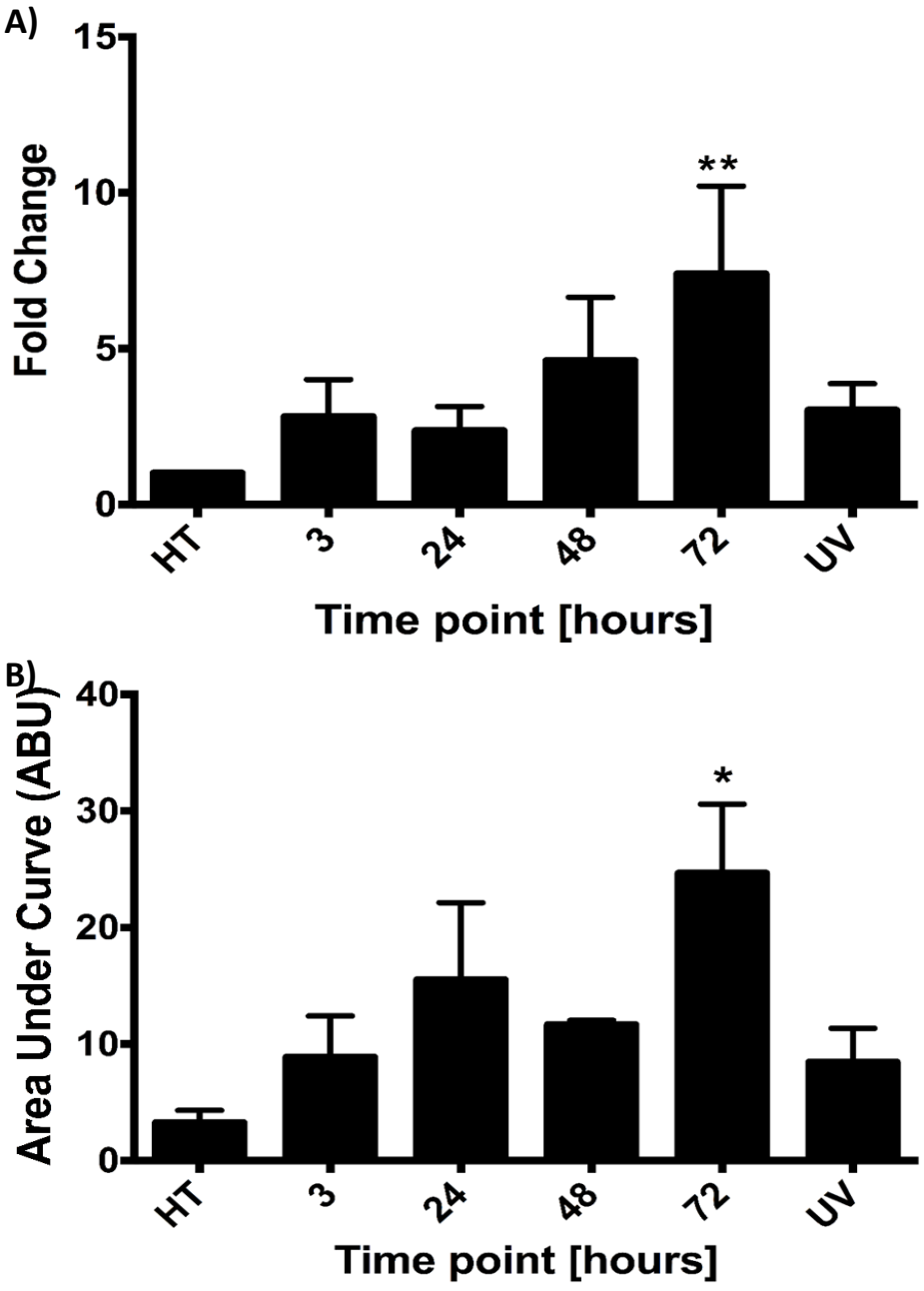

Figure 5.16. ***Peak and total ATP release from A549 cells infected with RV-16 and exposed to hypotonic stimulus.*** *A549 cells stimulated with RV-16 at MOI 1 for up to 72 hours, UV-inactivated viral sham control or left unstimulated. Cells exposed to hypotonic buffer and supernatants sampled at 15 second intervals for 5 minutes. A) Peak ATP release shown as fold change from basal. B) Area under curve analysis of full 5-minute time course. Results are displayed as mean ± S.E.M. of three independent experiments (n=3). Statistical analysis was carried out using multiple comparison one-way ANOVA followed by with Dunnetts. ABU arbitrary units. *P=0.0099, **P=0.0127.*

We found a significant trend of increased ATP release following hypotonic stimulation as time progressed over long-term infection with RV-16 at MOI 1 (Fig. 5.17A). At 96 hours there was a significant 2.7-fold increase in ATP release from uninfected hypotonic control ($P=0.0185$; n=3), at 120 hours there was a significant 4-fold increase ($P=0.0068$; n=3), at 144 hours there was a 4.3-fold increase ($P=0.0028$; n=3), at 168 hours there was a 5-fold increase ($P<0.0001$; n=3), and finally, the UV inactivated viral sham control induced a 2.9-fold increase in ATP release from uninfected hypotonic control ($P=0.0394$; n=3).

Following AUC analysis, there was no significant difference between uninfected hypotonic control and 96 hours (Fig. 5.17B, $P=0.2466$; n=3). All other time points and UV control remained significant (120 hours $P=0.0011$, 144 hours $P=0.0035$, 168 hours $P<0.0001$, UV $P=0.0049$; n=3).

To tie together the quantified intracellular ATP concentration and extracellular release we carried out ratio analysis of short (Fig. 5.18) and long-term infection (Fig. 5.19). A ratio was determined for intracellular concentration to extracellular unstimulated release, intracellular to extracellular isotonic control and intracellular to extracellular hypotonic stimulation for each time point over the 168-hour time course. At 72 hours, there was a significant increase in the ratio of intracellular ATP to unstimulated release when compared to basal (Fig. 5.18, $P=0.0001$; n=3). At 48 and 72 hours, there was a significant increase in the ratio of intracellular ATP to isotonic induced release when compared to basal ($P<0.0001$; n=3). Finally, at 72 hours, there was a significant increase in the ratio of intracellular ATP to hypotonic induced release when compared to basal ($P=0.0041$; n=3). No other time points in any condition had significant change in their ratio of intra:extracellular ATP release ($P>0.05$).

Finally, during long term infection with RV-16 there was a significant increase at 144 and 168 hours in the ratio of intracellular ATP to unstimulated release when compared to basal (Fig. 5.19, $P=0.0003$ and $P=0.016$, respectively; n=3). There was no significant change at any time point in ratio of intracellular to isotonic induced release ($P>0.05$; n=3). Finally, all time points and UV control had significant increases in ratio of intracellular ATP to hypotonic induced release when compared to basal (96 hours $P=0.0125$, 120 hours $P=0.0004$, 144 hours $P=0.0001$, 168 hours $P<0.0001$ and UV $P=0.0313$; n=3).

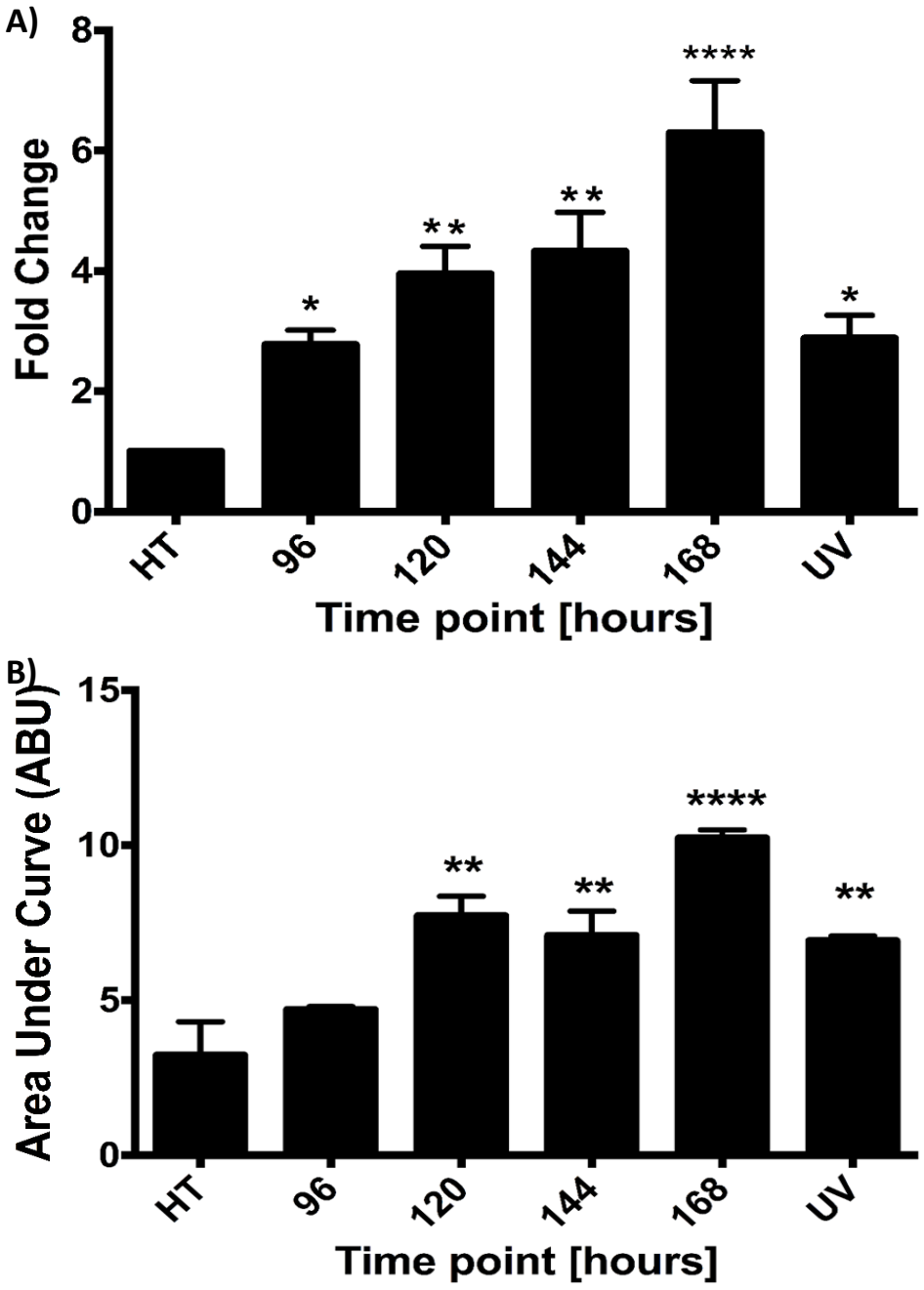

Figure 5.17. ***Peak and total ATP release from A549 cells infected long-term with RV-16 and exposed to isotonic stimulus.*** *A549 cells stimulated with RV-16 at MOI 1 for 96 to 168 hours, UV-inactivated viral sham control or left unstimulated. Cells exposed to hypotonic buffer and supernatants sampled at 15 second intervals for 5 minutes. A) Peak ATP release shown as fold change from basal. B) Area under curve analysis of full 5-minute time course. Results are displayed as mean ± S.E.M. of three independent experiments (n=3). Statistical analysis was carried out using multiple comparison one-way ANOVA followed by with Dunnetts. ABU arbitrary units. *P<0.0394, **P<0.0068, ****P<0.0001.*

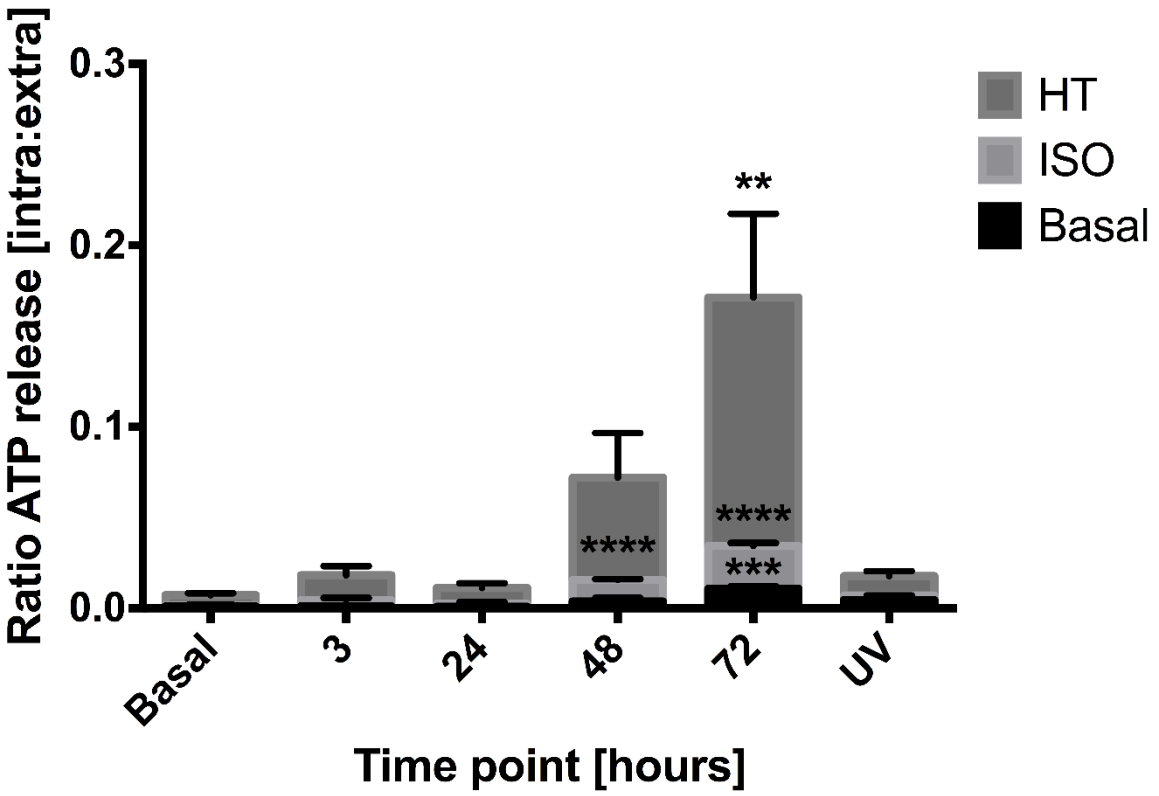

Figure 5.18. ***ATP ratio in RV-16 infected A549 cells.*** *Ratio analysis of sampled supernatant from basal, isotonic and hypotonic sampling experiments against intracellular ATP concentration (see accompanying figures 5.11-5.17 of A549 cells infected with RV-16 at MOI for up to 72 hours, UV-inactivated viral sham control or left unstimulated. Results are displayed as mean ± S.E.M. of three independent experiments (n=3). Statistical analysis was carried out using multiple comparison one-way ANOVA followed by Dunnetts. **P=0.0041, ***P=0.0001, ****P<0.0001.*

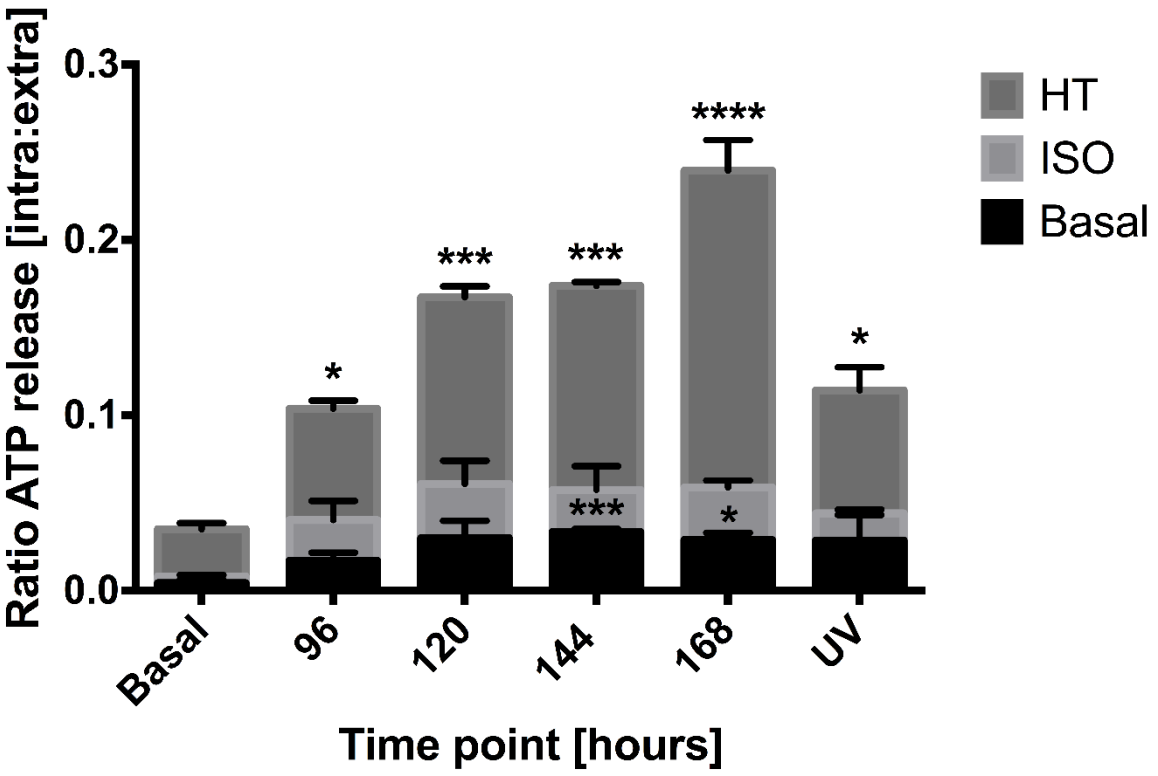

Figure 5.19. ***ATP ratio in long term RV-16 infected A549 cells.*** *Ratio analysis of sampled supernatant from basal, isotonic and hypotonic sampling experiments against intracellular ATP concentration (see accompanying figures 5.11-5.17) of A549 cells infected with RV-16 at MOI for 96 to 168 hours, UV-inactivated viral sham control or left unstimulated. Results are displayed as mean ± S.E.M. of three independent experiments (n=3). Statistical analysis was carried out using multiple comparison one-way ANOVA followed by Dunnetts and paired t-tests (basal vs 144, basal vs 168, HT vs 96). *P<0.03, ***P<0.0004, ****P<0.0001.*

5.3.1.4 RV-16 infection induced a glycolytic metabolic profile shift with no change in overall ATP production rates

To create a complete picture of the effect RV-16 infection plays on airway epithelial A549 cells we carried out seahorse metabolic measurements. This was to determine if there was any change on ATP production, to account for the increases in ATP release we found, any change in mitochondrial respiration and proton leak. We also looked at their metabolic profiles to see if RV-16 causes a switch in cellular metabolism as previously found with another serotype of RV (Gualdoni *et al.*, 2018).

We made the decision to drop the 3-hour time point of RV-16 infection for the purposes of the seahorse measurements as we found no significant change in any ATP measurements

carried out at that time point. The following seahorse metabolic measurements were carried out at 24-72 hours for short term infection and 96-168 hours for long term infection, with respectively UV inactivated viral sham controls.

Metabolism measurements were carried out with the use of drugs to inhibit or uncouple the electron transport chain (ETC). Oligomycin was used to inhibit ATP synthase complex V and determine the cells capability of ATP production, FCCP uncouples the ETC to uncouple oxygen consumption from ATP production to measure maximal respiration capability, and rotenone and antimycin A (Rot/A) inhibits complex I and III of the ETC to completely knock out functionality of the ETC to measure non-mitochondrial respiration. Other parameters can be measured as a result of these drugs. We also utilised 2-DG to inhibit glycolysis and determine the cells glycolytic capacity.

To investigate how mitochondrial respiration was affected during RV-16 infection we measured oxygen consumption rates (OCR) and extracellular acidification rates (ECAR) (Fig. 5.20 and 5.21). The data demonstrate that during short term infection ATP linked and respiration and proton leak was no affected by RV-16 infection (Fig. 5.22, $P>0.05$; n=3). However, non-mitochondrial respiration was significantly increased (35% vs. 69%) when incubated with UV inactivated viral sham control ($P=0.0299$) when compared to basal control. During long-term infection there was no significant change in ATP linked respiration, non-mitochondrial respiration or proton leak at any time point (96-168 hours) or UV control when compared to basal (Fig. 5.23, $P>0.05$; n=3).

RV-16 did not significantly change ATP production rates in either short (Fig. 5.24, $P>0.05$; n=3) or long-term (Fig. 5.25, $P>0.05$; n=3) infection.

Finally, we investigated if RV-16 caused any change in the cellular energy profile (Fig. 5.26). The data suggests infection with RV-16 induces a phenotypic switch at all time points during short- and long-term infection to become more glycolytic at short term (Fig. 5.26A) and more glycolytic and energetic at long-term infection (Fig. 5.26B).

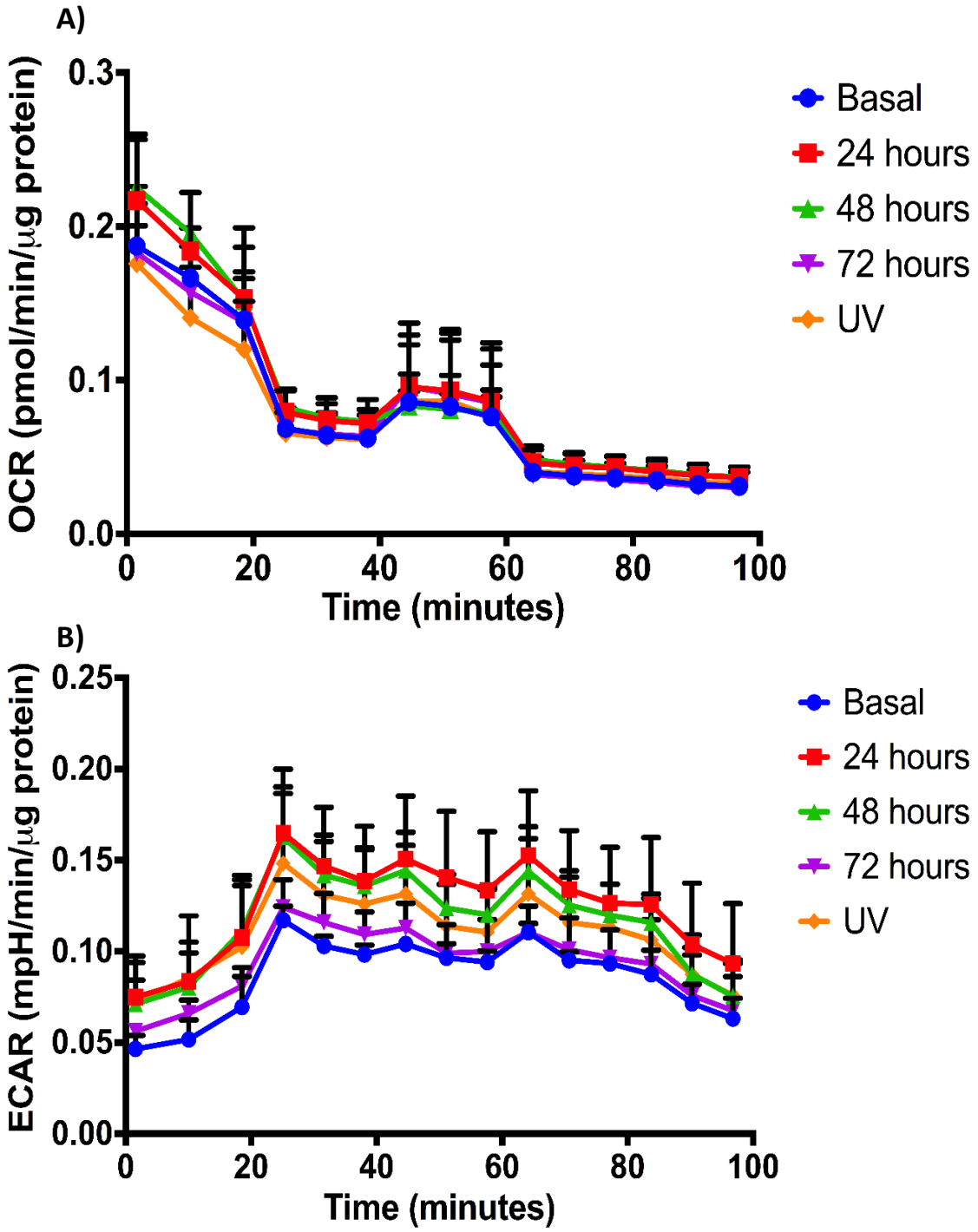

Figure 5.20. ***Mitochondrial stress test traces of RV-16 infected A459 cells.*** *A) OCR and B) ECAR measurements carried out on A549 cells infected with RV-16 at MOI 1 for 24-72 hours during the addition of drugs oligomycin, FCCP, rotenone/antimycin A and 2-DG. Data are standardised to µg protein. Data displayed as mean ± S.E.M. from three independent experiments (n=3) carried out in singulate. P>0.05.*

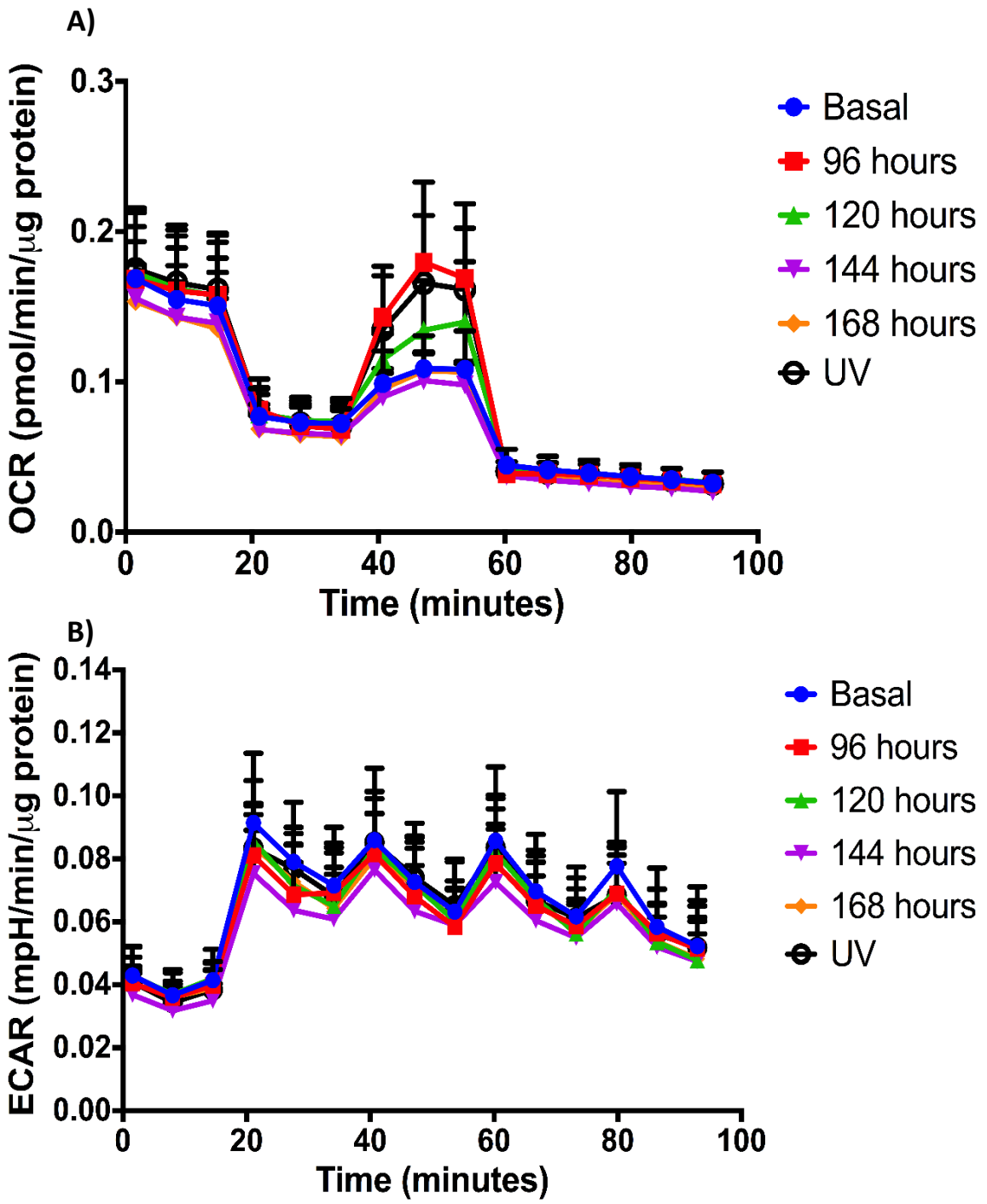

Figure 5.21. ***Mitochondrial stress test traces of long-term RV-16 infected A459 cells.*** *A) OCR and B) ECAR measurements carried out on A549 cells infected with RV-16 at MOI 1 for 96-168 hours during the addition of drugs oligomycin, FCCP, rotenone/antimycin A and 2-DG. Data are standardised to µg protein. Data displayed as mean ± S.E.M. from three independent experiments (n=3) carried out in singulate. P>0.05.*

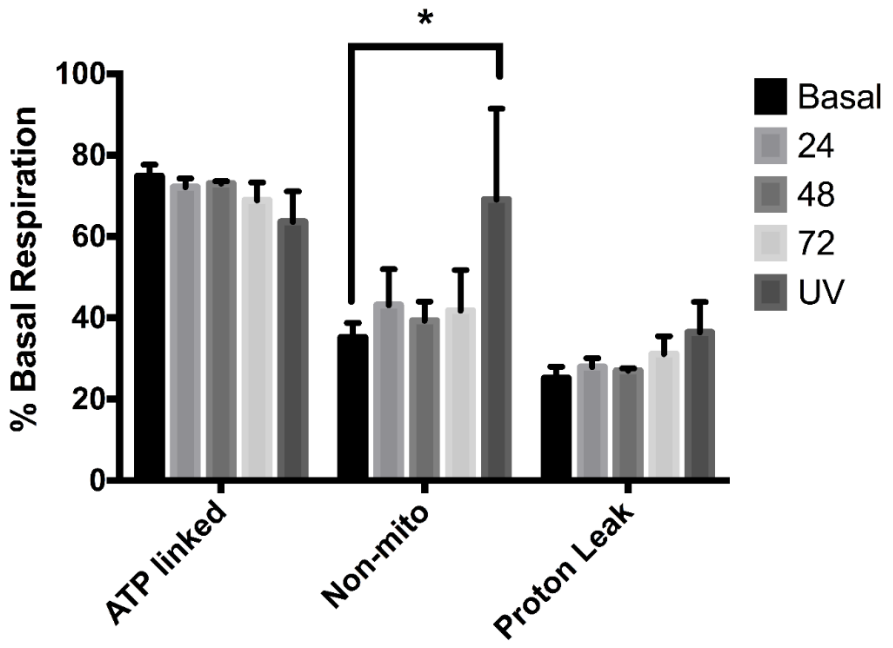

Figure 5.22. ***Short term infection rates of ATP linked respiration, non-mitochondrial respiration and proton leak*** *was quantified by normalisation of OCR from RV-16 infection at MOI 1 (see accompanying figure 5.23) to µg protein and standardised as a percentage of basal respiration. Data displayed as mean ± S.E.M. from three independent experiments (n=3) carried out in singulate. Statistical analysis was carried out using two-way ANOVA followed by Tukey analysis for comparison to basal. *P=0.0299.*

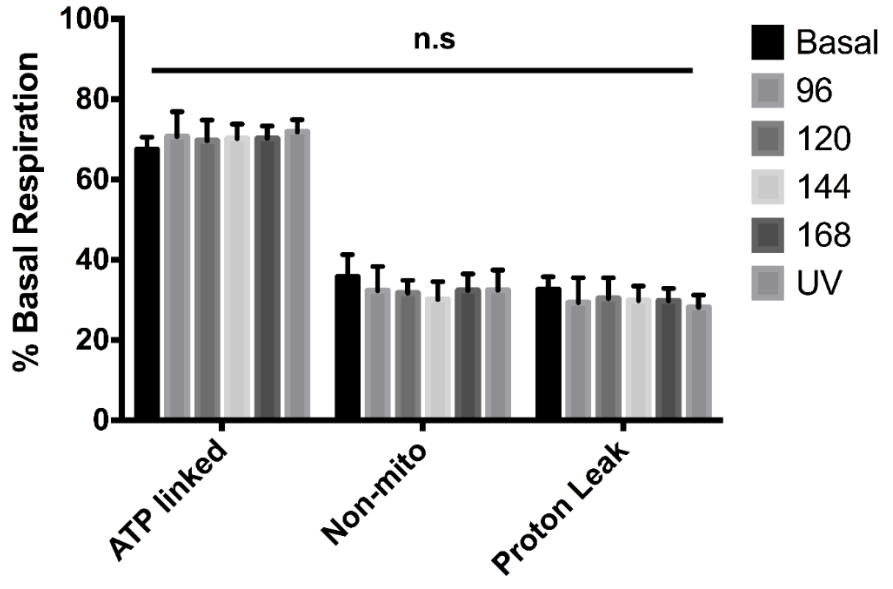

Figure 5.23. ***Long term infection rates of ATP linked respiration, non-mitochondrial respiration and proton leak*** *was quantified by normalisation of OCR from RV-16 infection at MOI 1 (see accompanying figure 5.24) to µg protein and standardised as a percentage of basal respiration. Data displayed as mean ± S.E.M. from three independent experiments (n=3) carried out in singulate. Statistical analysis was carried out using two-way ANOVA followed by Tukey analysis for comparison to basal. P>0.05*

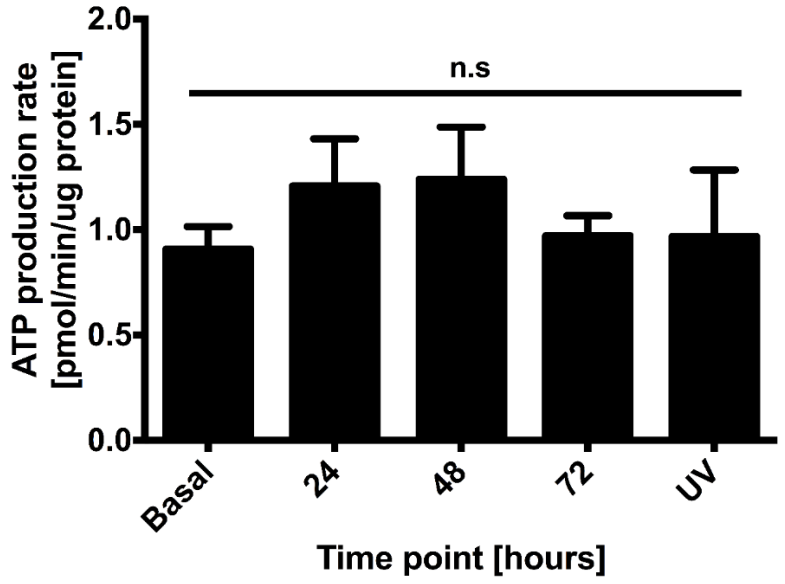

Figure 5.24. ***ATP production rate of A549 cells infected with RV-16 at MOI 1 for up to 72 hours****, UV-inactivated viral sham control or left unstimulated. Data calculated from OCR raw data (accompanying graph figure 5.23) prior to and following the addition of oligomycin. Data displayed are normalised to µg protein and displayed as mean ± S.E.M. from three independent experiments (n=3) carried out in singulate. Statistical analysis was carried out using multiple comparison one-way ANOVA followed by Tukey analysis. P>0.05.*

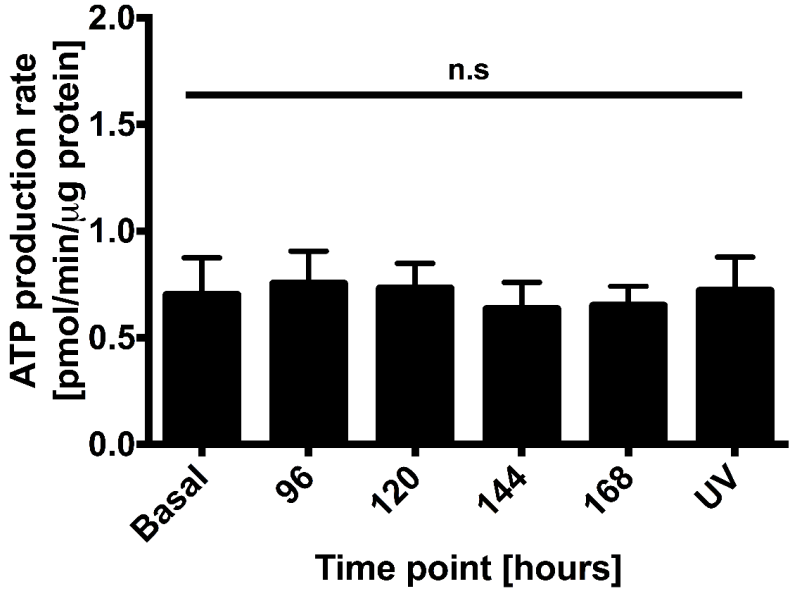

Figure 5.25. ***ATP production rate of A549 cells infected with RV-16 at MOI 1 for 96 to 168 hours****, UV-inactivated viral sham control or left unstimulated. Data calculated from OCR raw data (accompanying graph figure 5.24) prior to and following the addition of oligomycin. Data displayed are normalised to µg protein and displayed as mean ± S.E.M. from three independent experiments (n=3) carried out in singulate. Statistical analysis was carried out using multiple comparison one-way ANOVA followed by Tukey analysis. P>0.05.*

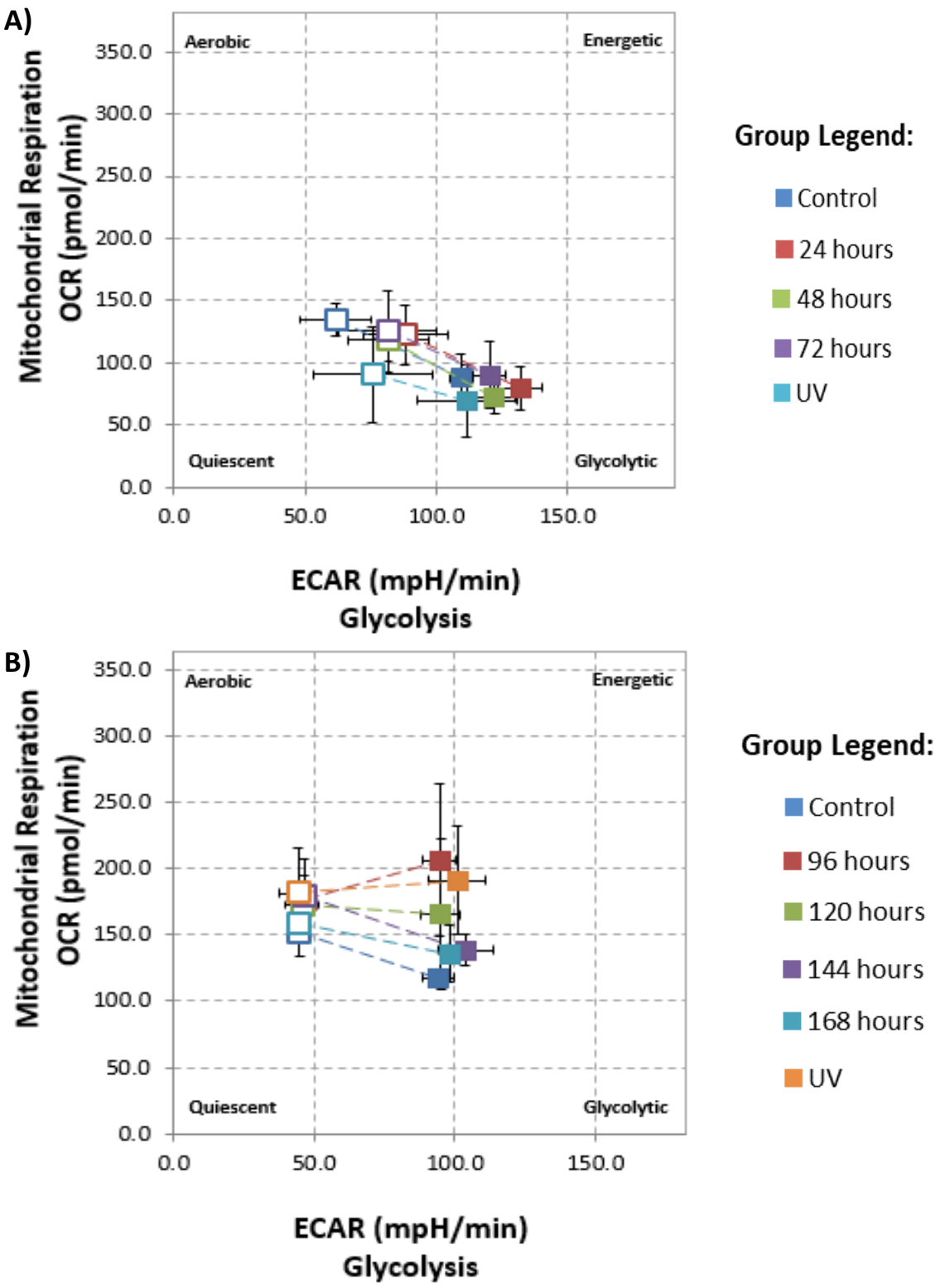

Figure 5.26. ***Metabolic energy profiles developed from A549 cells infected with RV-16*** *at MOI 1 depicted as a phenogram showing a shift in metabolic phenotype during mitochondrial stress. A) Short term (24-72 hours) B) long term (96-168 hours). Data displayed as mean ± S.E.M. from three independent experiments (n=3) carried out in singulate.*

5.3.2 Generation of stably transfected A549 cell line with GFP-tagged TRPV4

Alveolar airway epithelial cell line A549 endogenously expresses TRPV4 as determined by our group (section 3.3.1) and others (Seminario-Vidal *et al.*, 2011; Sidhaye *et al.*, 2006; Seminario-Vidal *et al.*, 2009). We characterised the A549 cell line in Chapter 3 and determined whilst the cell line expressed mRNA and protein of TRPV4, functionally it responded weakly to specific agonist GSK1016790A. This agonist is widely regarded as highly variable in the size of response it elicits (unpublished data, personal communication, 2017, 2018). Therefore, we could not rule out the possibility that agonist GSK1016790A was not able to induce a strong response. So, we decided to generate a stably transfected A549 cell line permanently and overexpressing TRPV4.

5.3.2.1 Transfection of wild type A549 with GFP-tagged TRPV4 pCMV vector

GFP-tagged TRPV4 (in pCMV vector) was successfully amplified from 10 individual transformed *E. coli* colonies (data not shown). Plasmid DNA from two transformed colonies displaying the highest TRPV4 expression was isolated and a double restriction digest was carried out, as detailed in section 2.15.4, to confirm the presence of the TRPV4 pCMV vector (Fig. 5.27). Early passage wild type A549 (passage 3) cells were transfected with the GFP-tagged TRPV4 DNA isolated from the transformed *E. coli* using Fugene® 3 at a ratio 3:1, as described in section 2.15.5. At 48 hours post-transfection, 0.7 mg ml^{-1} G418 was added, concentration determined in section 5.2.1, to select for expression of pCMV vector containing G418 resistance gene. Once the transfected cells became confluent, the cells were transferred to a T25 flask and maintained in culture for 7-14 days.

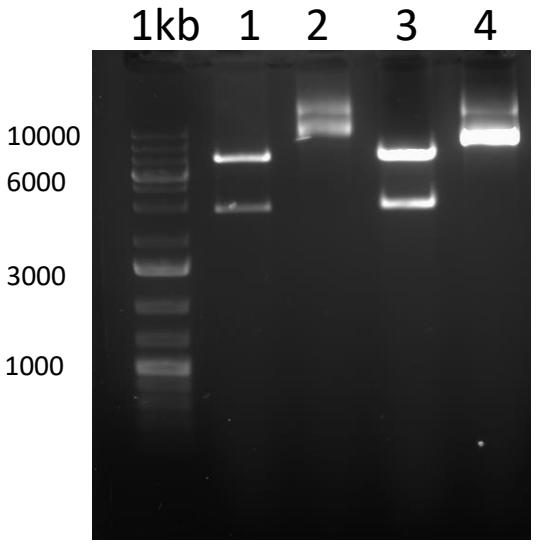

Figure 5.27. ***Enzymatic restriction digest of TRPV4 pCMV vector.*** *1 kb – 1 kb ladder. 1 – colony sample 2 cleaved vector (2664 and 6536 bp digests). 2 – colony sample 2 uncleaved vector (9200 bp vector). 3 – colony sample 5 cleaved vector (2664 and 6536 bp digests). 4 – colony sample 5 uncleaved vector (9200 bp vector). Vectors were purified from positive colonies as determined from initial screening PCR screening and digested with BamH1 and Xho1 to check for the presence of the GFP-tagged TRPV4 containing vectors.*

5.3.2.2 Confirmation of positive expression GFP tagged TRPV4 in transfected A549 cell line

To ensure the transfected cell line originated from a single cell, the G418 resistant cells were taken through a round of single cell cloning, as described in section 2.15.6. Briefly, transfected cells were seeded in serial dilution across a 96 well plate and incubated in G418 containing DMEM for 7 days and assessed for the presence of cell colonies growing from a single colony. Cells were incubated for a further 7 days to allow for expansion. Eight monoclonal cell expansions were assayed for expression of GFP-tagged TRPV4. Firstly, flow cytometry analysis (FACS) was performed using a FACS Calibur as described in section 2.15.7. to determine if the cells globally expressed the GFP tag and therefore possessed the TRPV4 gene. Ten thousand cells were analysed using 488nm Argon laser (suitable for excitation of FITC). Wild type A549 cells were used to gate for basal auto-fluorescence and determine size and granularity. All monoclonal expansions tested displayed a shift in fluorescence intensity when compared against wild type A549 cells (Fig. 5.28), as confirmed by geometric mean analysis (Fig. 5.29).

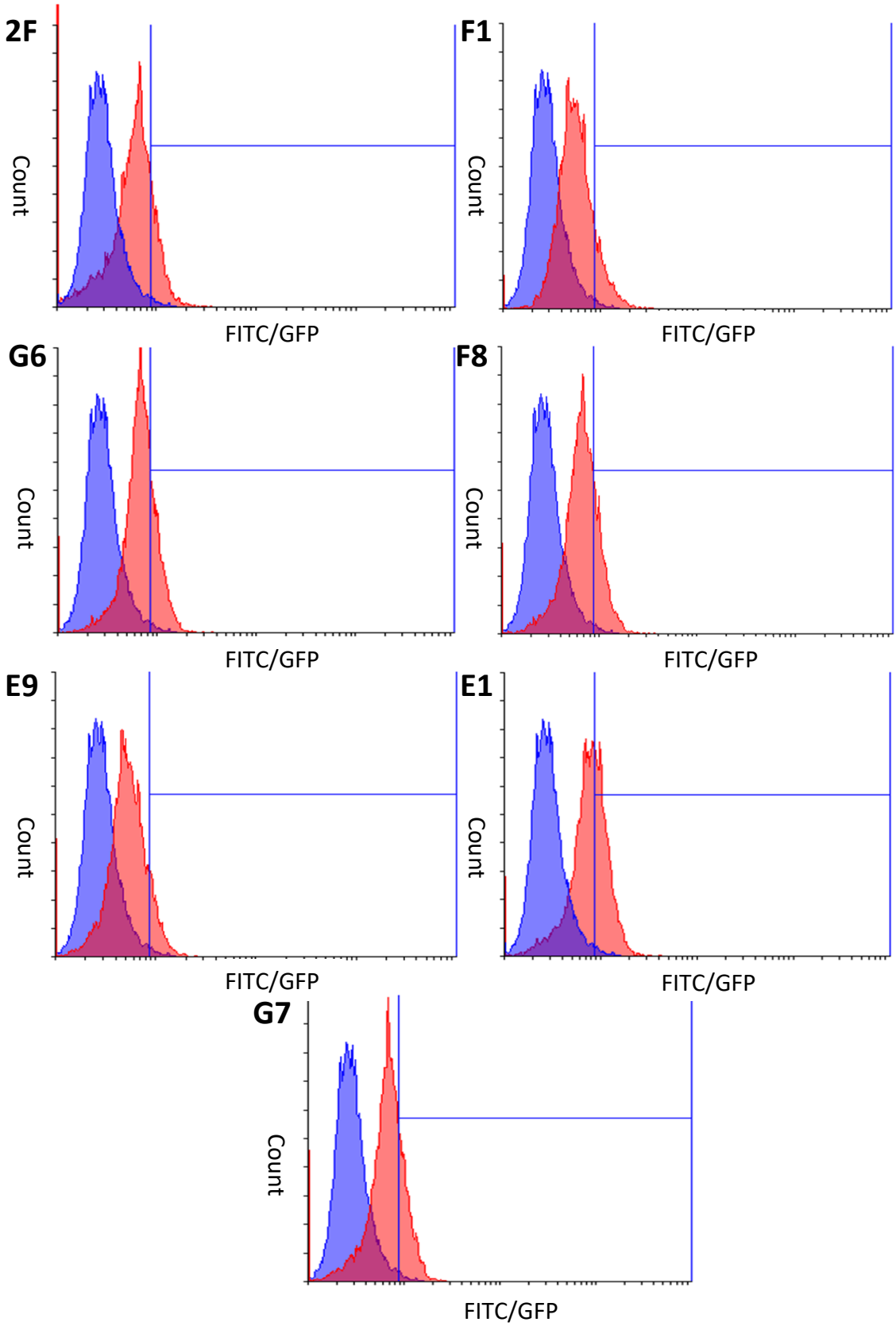

Figure 5.28. ***FACS analysis histograms constructed for each monoclonal expansion*** *(red) produced from single cell cloning of A549 transfection with GFP-tagged TRPV4 pCMV vector. Data initially gated to wild type A549 (blue). Data displayed from one independent experiment (n=1) from ten thousand events counted.*

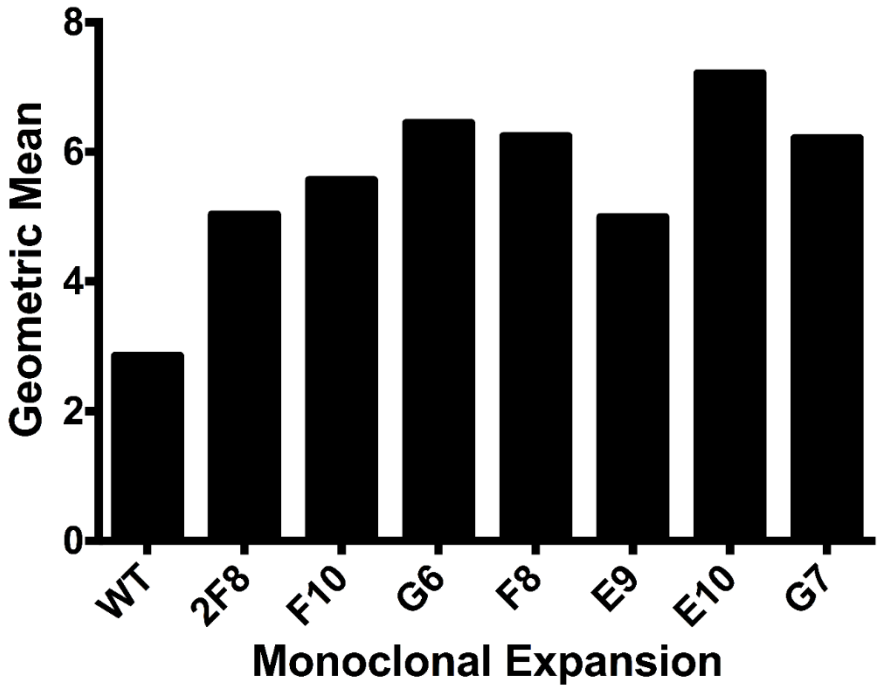

Figure 5.29. ***Geometric mean analysis calculated from FACS histograms*** *obtained following FACS analysis of each monoclonal expansion produced from single cell cloning of A549 transfection with GFP-tagged TRPV4 pCMV vector. Data displayed from one independent experiment (n=1) from ten thousand events counted.*

We noticed an upward shift in side scatter (SSC) in all transfected cells without a concurrent shift in forward scatter (FSC). We determined this was likely due to a change in granularity of the transfected cells. We hypothesised this may be due to an internalisation of the GFP-tagged vector, and therefore the protein may not have been membrane expressed. To determine if this was the case, we carried out immunofluorescence microscopy of all eight monoclonal expansions to clarify if the GFP-tagged TRPV4 receptor was expressed throughout the cell or had been compartmentalised within the cell and not expressing the receptor (Fig. 5.30). Briefly, the cells were fixed, permeabilised and mounted with DAPI integrated mounting media and imaged on Zeiss Axio observer Z1 fluorescent microscope.

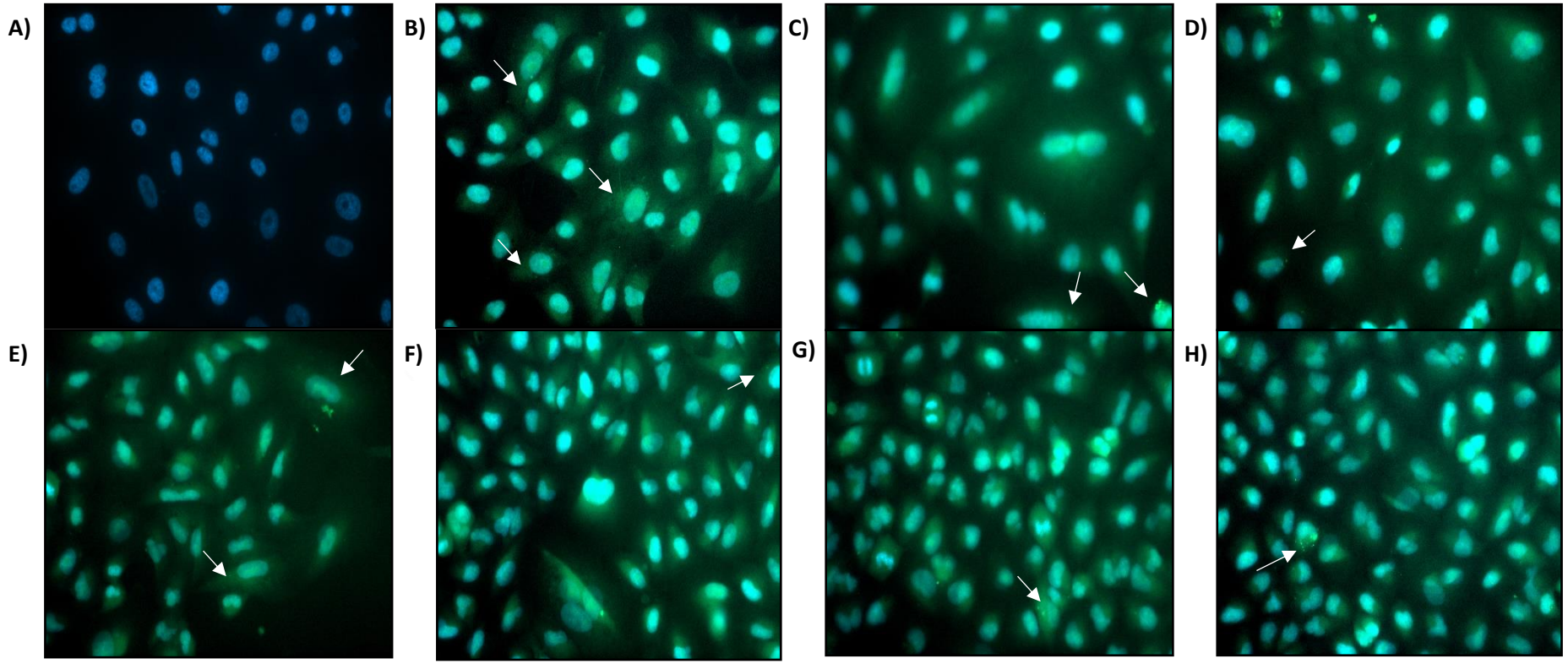

Figure 5.30. ***Immunofluorescent microscopy analysis of monoclonal expansions.*** *Cells stained for nuclei with DAPI (blue) and GFP tagged TRPV4 expression (green). A) wild type DAPI stained. B)-H) monoclonal expansions with GFP tag receptor and DAPI stained. B) – 2F8; C) – F10; D) – G6; E) – F8; F) – E9; - G) – E10; H) – G7. White arrows indicate areas of interest where granularity is dense and highly fluorescent. Images representative from minimum of 10 images taken from each experiment of n=2.*

Finally, all eight monoclonal expansions were tested for responsiveness to specific agonists GSK1016790A and 4αPDD using intracellular calcium signalling, as described in section 2.8.2. Briefly, Fluo-4 AM probe was loaded into cells and increases in intracellular calcium levels were measured at room temperature on a Flexstation® plate reader at excitation 485nm and emission 525nm. For each monoclonal expansion the change in fluorescence in response to a specific agonist was expressed as a percentage of positive control A23187 (Fig. 5.31). When responsiveness to agonist GSK1016709A (30nM) was analysed for significance from wild type, there was a 1631% increase in response from monoclonal expansion 2F8 (Fig. 5.32A, P<0.0001; n=2) and a 366% increase in response from monoclonal expansion E9 (Fig. 5.32B, P=0.0005; n=2).

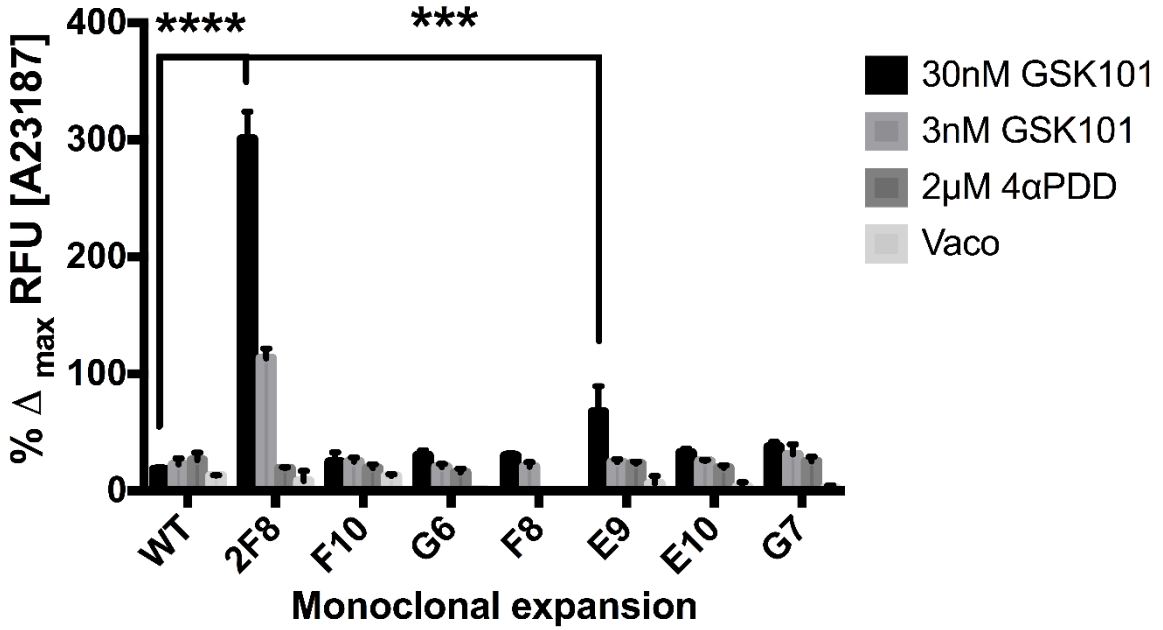

Figure 5.31. ***Intracellular calcium signalling responses from wild type (WT) and eight monoclonal expansions*** *(2F8, F10, G6, F8, E9, E10 and G7). Cells were stimulated with TRPV4 receptor specific agonists GSK1016790A (GSK101) and 4αPDD and vehicle control 0.01% v/v DMSO (Vaco). Responses were measured as a percentage of maximal control compound A23187. Results are displayed as mean ± S.E.M. of two independent experiments (N=2) carried out in duplicate. Statistical analysis was carried out using two-way ANOVA followed by Tukey analysis compared to wild type responses. ***P=0.0005, ****P<0.0001.*

Due to the large shift in fluorescence from FACS analysis, the clearer and more define images from immunofluorescence and the highly significant responses to specific agonist GSK1016790A, we decided to pursue further work using monoclonal expansion 2F8.

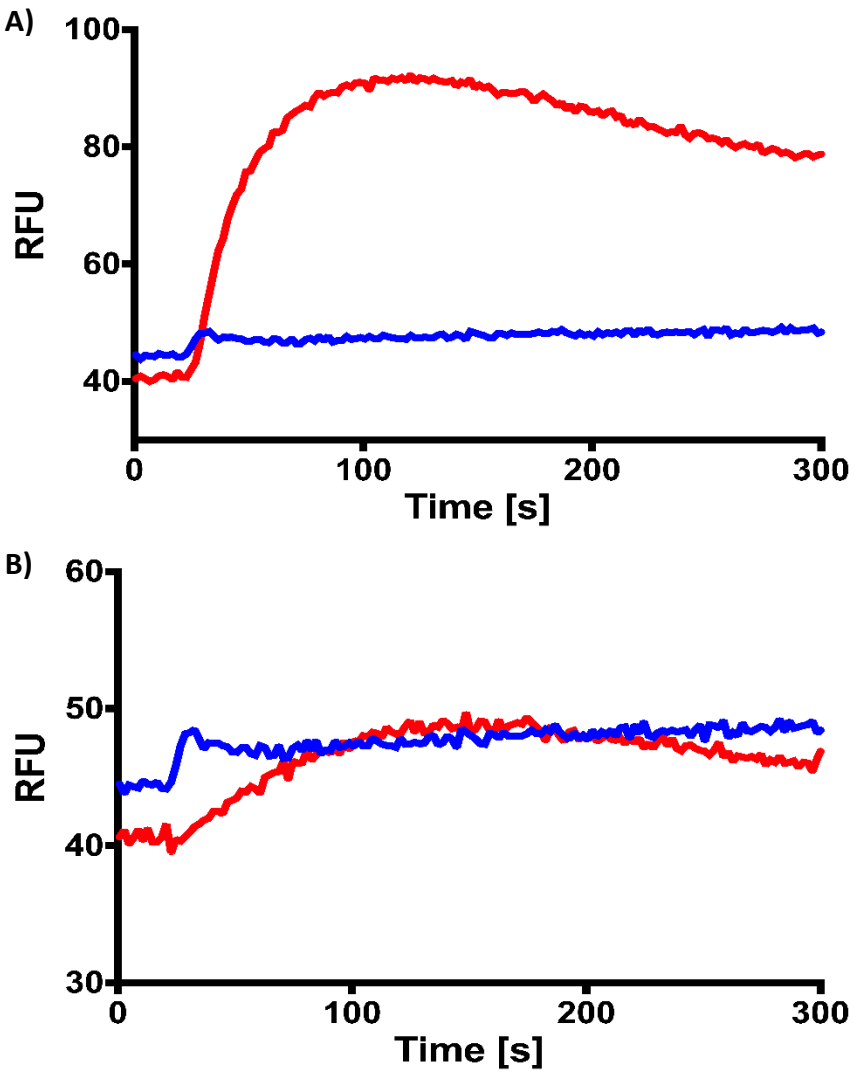

Figure 5.32. ***Representative intracellular calcium signalling traces of monoclonal expansions*** *(red) A) 2F8 and B) E9 intracellular calcium signalling response to TRPV4 agonists GSK1016790A against wild type A549 response (blue). Traces accompany Figure 5.31.*

5.3.3 Rhinovirus infection of A549-GFP-TRPV4 transfected cell line causes a reduction in total cellular fluorescence from 48 hours

With the knowledge that TRPV4 plays an integral role in the mechanism of ATP release during stimulation and that RV-16 increases the amount of ATP airway epithelial cells secrete, we decided to utilise the TRPV4 overexpressing cell line we generated to investigate the role of RV-16 on TRPV4 expression and distribution. Through the process of transfection of the A549 cell line we discovered extensive cellular granulation (see section 5.3.2) which meant using immunofluorescence as an end point read out was not a viable

option as we initially planned to do. However, we decided to try a single time of RV-16 infected transfected A549-GFP-TRPV4 cell line using strategically picked time points.

Briefly, the GFP-tagged TRPV4 transfected cells (monoclonal expansion 2F8) were infected with RV-16 at MOI 1 and incubated for 1 hour at room temperature with gentle agitation. The cells were washed and incubated at 37^{o}C for up to 168 hours with UV-inactivated sham viral control as used previously. The cells were fixed and permeabilised, stained with phalloidin conjugate 594 for 1 hour at room temperature and mounted with DAPI integrated mounting media then imaged on Zeiss Axio observer Z1 fluorescent microscope.

Figure 5.33 displays images of A549-GFP-TRPV4 cells uninfected (basal), at 48-, 96- and 168-hours including UV control for nuclei (DAPI), TRPV4 (GFP tag) and the actin cytoskeleton (phalloidin), these images are displayed separately and merged. No statistical analysis could be undertaken as only a single replicate of the experiment was carried out.

Measurements of each time point were taken using ImageJ with FIJI add-on to measure total cellular fluorescence of GFP corrected for background fluorescence (CTCF) from a minimum of 5 independent images containing at least 10 cells. At 48 hours, there was a 71% drop in CTCF from basal (Fig. 5.34), followed by a 45% drop in CTCF from basal at 96 hours. CTCF returned to basal levels at 168 hours. UV-inactivated sham viral control caused a 47% reduction in CTCF from basal. Limited conclusions must be drawn from this as the data is only n=1.

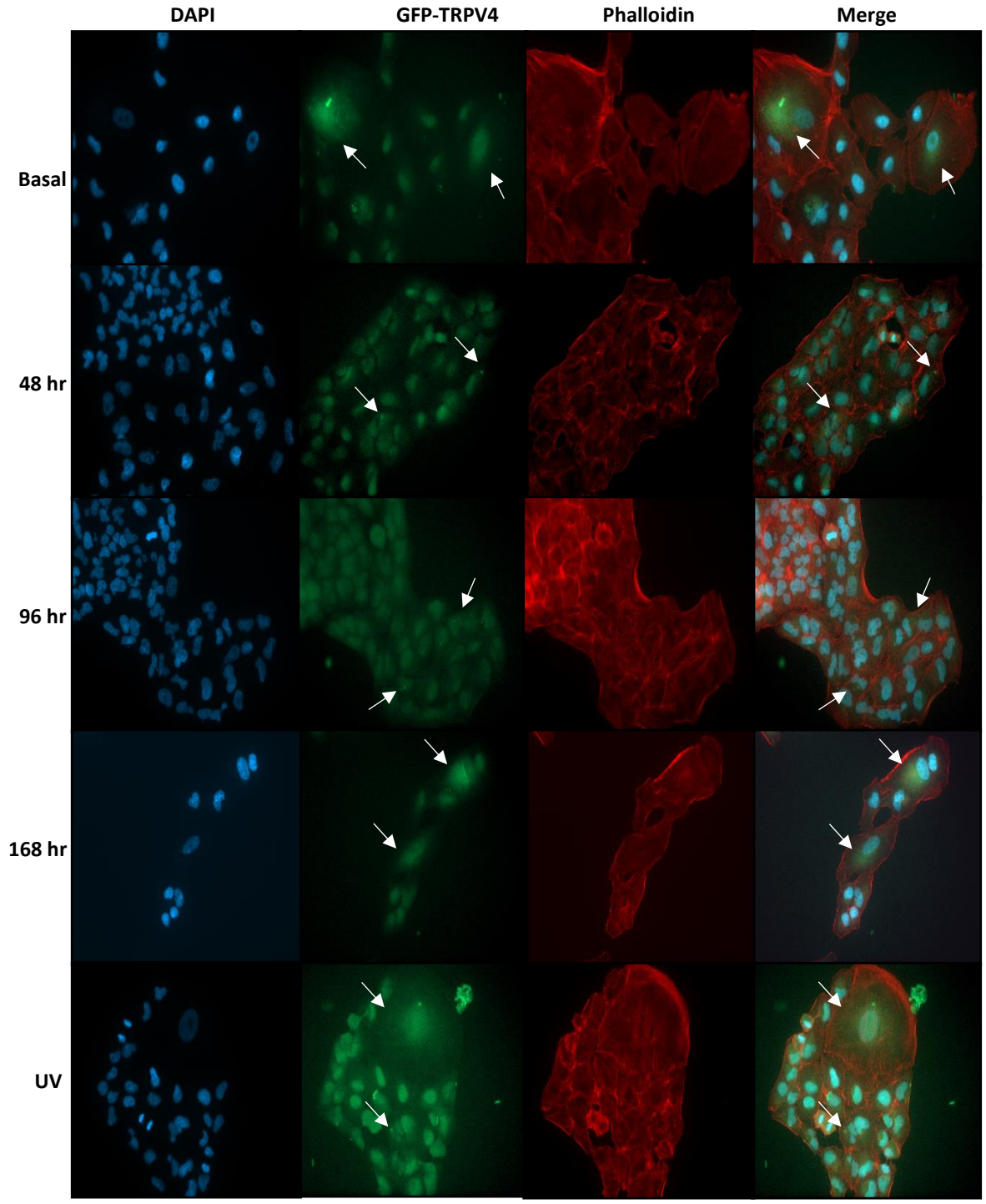

Figure 5.33. ***Immunofluorescent microscopy analysis of A549-GFP-TRPV4 cell line infected with RV-16*** *at MOI 1 for up to 168 hours with UV inactivated viral sham control. Cells stained for nuclei with DAPI (blue), GFP tagged TRPV4 expression (green) and actin cytoskeleton with phalloidin conjugate 594 (red). Three targets overlaid and merged (merge). Images representative from minimum of 10 images taken from n=1. White arrows indicate areas of interest of dense highly fluorescent granules.*

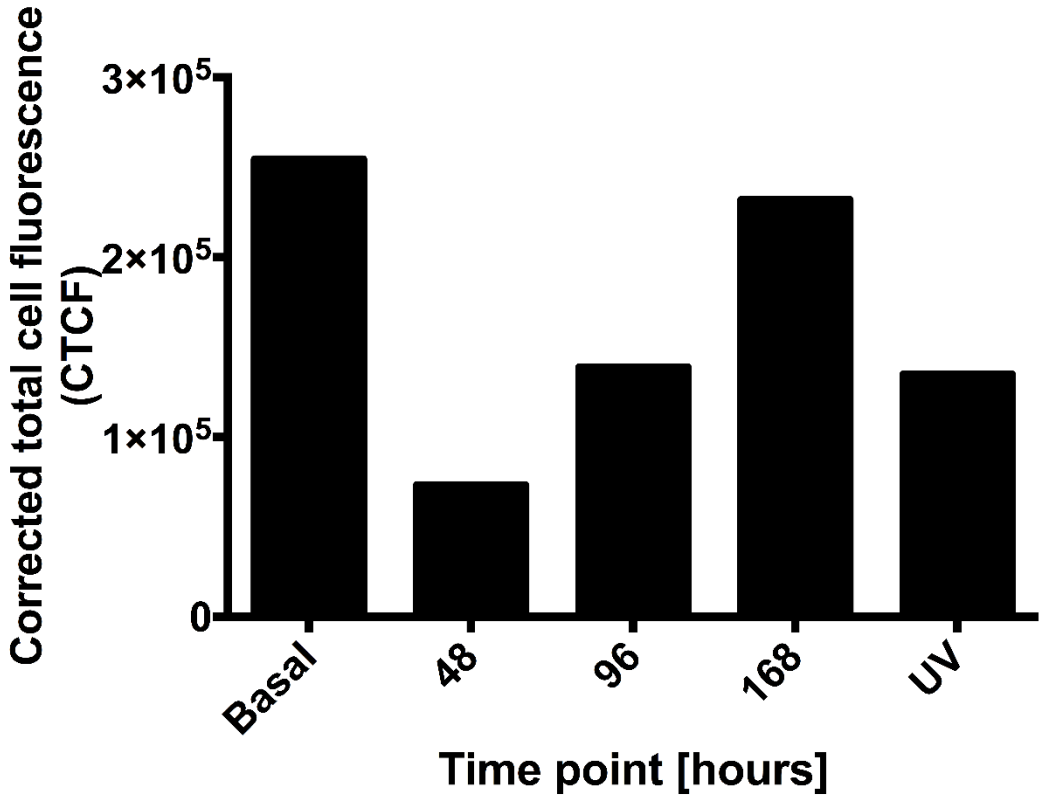

Figure 5.34. ***CTCF of GFP-tagged TRPV4 in A549 cells infected with RV-16.*** *Corrected total cell fluorescence (CTCF) measurements of GFP-tagged TRPV4 vector expression in transfected A549 cell line infected with RV-16 at MOI 1 for up to 168 hours including UV inactivated viral sham control. Measurements accompany fluorescent images Figure 5.33. N=1. Analysed using ImageJ with FIJI add-on.*

5.4 Discussion

In order the gain a better understanding the common cold virus (RV-16) has on ATP release, we used airway epithelial A549 alveolar cells infected with RV-16 for up to 168 hours (7 days). Analysis of global protein expression, ATP release, mitochondrial function and TRP channel function was undertaken to determine the role RV-16 exerts on these essential cellular mechanisms. We have shown through the course of this research that RV-16 causes increased ATP release basally, following stimulation with hypotonic solution and after the addition of non-stimulating isotonic control. This maybe because RV-16 infected A549 cells become more mechanosensitive under innocuous stimulation the longer infection continues with the largest impact between 96-168 hours (4-7 days). These findings fit with the time frame of a common cold infection becoming symptomatic and the development of a viral cough.

Here we show for the first time that RV-16 infection causes an early increase (24 hours post infection) in intracellular ATP levels, followed by a significant drop (48-72 hours) and recovery to basal levels from 96 hours. We also show this effect is mimicked by ICAM-1 receptor binding. Furthermore, we identified a novel finding that RV-16 infection causes increased ATP release both during stimulation and without.

Our data also revealed, when we carried out ratiometic analysis between intracellular ATP concentration to extracellular ATP release accounting for non-stimulated and stimulated release, we found a significantly larger ratio at 72 hours under all conditions, a trend which continued throughout the 168-hour time course.

Despite these findings we found no significant change in pannexin-1 protein expression at any point in the infection, furthermore, there was no increase in mitochondrial derived ATP production. Therefore, we hypothesise that at 48 and 72 hours, a reduction in total intracellular ATP concentration, and an increase in ATP release without concurrent increased production is caused by a metabolic pressure elsewhere in the cell, likely a result of viral replication and early immune signalling pathways.

Finally, our data acquired from seahorse metabolic analysis identified a minor glycolytic phenotypic switch during RV-16 infection following mitochondrial stress. This data is in line

with previously published data which found RV-14 caused a host cell reprogramming phenotype dependent on glycolysis (Gualdoni *et al.*, 2018).

We decided to generate a TRPV4 overexpressing cell line to study protein expression and distribution during RV-16 infection despite the limitation of using a transfected cell line where we cannot distinguish any changes as a response to a direct viral effect on our cell or an independent effect on our pCMV plasmid. Our need to use a transfected cell line outweighed this limitation as airway epithelial A549 cells possess low TRPV4 expression and only polyclonal antibodies were available with a lot of non-specific binding. We were only able to confirm positive banding through the use of another transfected cell line (HEK-TRPV4) with banding at the correct size which was not present in a wild type (parental HEK) (data shown in Chapter 4). We decided to circumvent this problem by generating a stably expressing GFP-tagged TRPV4 cell line to study the expression of TRPV4 during RV-16 infection. We utilised FACS, intracellular calcium signalling and fluorescent microscopy to assess the expression levels and the cellular distribution of TRPV4. Unfortunately, as part of our series of transfection confirmations immunofluorescent analysis of the transfected cell line identified imaging issues with the GFP tag. Images of cells appeared 'fluffy' and we were unable to achieve a clear crisp image as we had previously. As a result, we could only carry out a single experiment using select time points (48, 96 and 168 hours) instead of our standard time course (3-168 hours) to investigate the effect of RV-16 on TRPV4 expression and distribution. Unfortunately, we later determined that the previous issues with imaging the immunofluorescent stained cells were due to a mounting media problem as imaging the transfected time course cells with new mounting media eliminated those issues we faced. Given more time these experiments would have been repeated.

Investigation into the effect of RV-16 on TRPV4 expression in A549 cells using immunofluorescent microscopy revealed an interesting pattern following CTCF analysis. The reduction in CTCF identified in cells treated with UV-inactivated viral sham control (stimulated for 48 hours) was smaller than that identified in cells infected with live RV-16 at MOI 1 which suggests the decline seen at 48 hours was not solely a result of ICAM-1 receptor binding alone. The assumption is that any decline seen in CTCF correlates with a reduction in presence of GFP-tagged TRPV4, therefore, the decline seen at 48 hours following RV-16 infection suggests a reduction in expression of TRPV4, however, FACS

analysis would need to be carried out to confirm this. CTCF returned to basal levels by 168 hours. These data correspond with those findings from intracellular calcium signalling (see section 3.3.3 and 3.3.4). Together these suggest that whilst no change in global protein expression of TRPV4 was found through western blot analysis, the initial reduction in function of TRPV4 (see section 3.3.3) combined with its return in function by late infection (see section 3.3.4) suggests RV-16 may not downregulate expression of TRPV4 but may cause either non-functional translation or a post-translational modification, therefore, no or reduced GFP fluorescence seen. Further experiments to assess glycosylation of TRPV4 would need to be carried out to confirm this hypothesis.

We are aware of the limitations of our work carried out here including our choice of cell line, airway alveolar epithelial cells A549. The common cold, in particular rhinovirus, causes symptoms predominately in the upper respiratory tract whilst our cell line is from the lower respiratory tract, furthermore, cough is precipitated through innervation of the upper airway. The use of primary cells would have been optimal, however, due to costs and availably this was not possible. Part of our rationale for using A549 cells, as explained previously, is that RV infections are associated with frequent acute exacerbation of asthma and COPD, furthermore, other research has found the presence of pathogens including RV within the upper and lower respiratory tract (Mitchell *et al.*, 2016, 2018). We also believe, any effect RV infection exerts in the airway would not be localised to the upper or lower respiratory tract. A prime example is our data identified on ATP release. This ATP would move freely through the respiratory tract and likely cause hypersensitive airways precipitating a cough reflex, further spreading ATP throughout the airway.

Another limitation we are aware of is studying the effect of RV-16 infection long term without the presence of an aiding immune system to clear the infection which makes our *in vitro* infection model not entirely physiological. As a result, we decided not to investigate infection post 7 days despite our viability assays showing minimal cytotoxicity up to 9 days of infection. We would have ideally liked to have used a human tissue model, which we would hope to peruse further.

Finally, we are aware our method of assaying ATP from cell supernatants was not ideal however, this method has been used and published (Seminario-Vidal, Lazarowski & Okada, 2009). We aimed to minimise any negative effect of our sampling method by chilling plates,

dark adapting and freezing until read as soon as possible to minimise ATP degradation. Sampling ATP from supernatants produces a less sensitive method than online reading, however, we did not manage to fully optimise our online method despite months of optimisation work. Lastly, our experimental set-up here (Chapter 5) differs from that used in Chapter 3 where we made one measurement of extracellular ATP concentration in cell culture medium from cells infected with RV-16 at MOI 1 without any other stimulus (such as hypotonicity). So, despite no significant change in ATP concentration at any time point (<72 hours) in experiments from section 3.3.3.3, those experiments carried out in this chapter had significantly more measurements taken over a longer duration of time.

So, in conclusion, we have shown for the first time that RV-16 causes increased ATP release in non-stimulated and stimulated A549 cells. RV-16 causes no effect on pannexin-1 global protein expression, and finally, RV-16 infection causes a glycolytic phenotypic shift in A549 cellular metabolism.

Chapter 6

General Discussion

Evidence has been provided in this thesis which adds to the current understanding of cough during *in vitro* human rhinovirus-16 infection. RV-16 was found to cause no significant difference in TRPA1, V1 and V4 or P2X3R expression and function in either A549 airway epithelial or 1321N1-P2X3 neuronal cell lines. We found that synthetic dsRNA poly(I:C) also caused no observable difference in TRPA1, V1 and V4 or P2X3R mRNA or protein expression of function in either A549 or 1321N1-P2X3 cell lines. We further delineated the hypotonic mediated ATP release pathway and identified an integral role of calcium-calmodulin kinase along with other important mediators of the intracellular signalling pathway. We identified a novel distribution pattern of pannexin-1 channel expression during hypotonic stimulation in A549 cell line which could be effectively reduced or inhibited with pathway specific inhibitors. Finally, we reported for the first time that RV-16 infection causes increased intracellular ATP concentration during an early point in infection, that extracellular ATP release was significantly increased as duration of infection increase and that the A549 cell line became more responsive to hypotonic stimulation.

Taken together, our major findings suggest that RV-16 infection leads to excessive ATP release causing a hypersensitive environment within the airway. These findings may provide hope to treating viral, post-viral and chronic cough conditions.

6.1 TRP Channel and P2XR Expression in Response to Synthetic Viral Stimuli Poly(I:C) and RV-16

It is well documented that thermo-TRP channels, TRPA1, TRPV1 and TRPV4 play central roles in cough (Grace *et al.*, 2012; O'Connell *et al.*, 1996, 1994; Zhu *et al.*, 2009a; Bonvini *et al.*, 2016; Smit *et al.*, 2012; Birrell *et al.*, 2009; Grace *et al.*, 2014). They have important physiological roles in the sensation of temperature and irritants and the regulation of cell volume and mucociliary clearance (Lorenzo *et al.*, 2008; Liu *et al.*, 2006; Sidhaye *et al.*, 2006, 2008; Story *et al.*, 2003; Caterina *et al.*, 1997, 2000). In a first of its kind paper, RV-16 was found to massively upregulate expression of TRPA1 and TRPV1 in a neuronal cell line (Abdullah *et al.*, 2014). However, in Chapter 3 we have shown that RV-16 did not cause any discernible change in expression of TRPA1 or TRPV1 despite using the same MOI of RV-16 (MOI 1). Furthermore, we expanded our approach to that previously published, and

investigated the effect of RV-16 on the airway using A549 cell line, and also investigated the function of TRPA1 and TRPV1. We also investigated the expression and function of TRPV4, not previously studied before in an infection model with rhinovirus.

This concept was further expanded to include investigation of poly(I:C) stimulation of airway and neuronal cell lines to study TRPA1, TRPV1, TRPV4 and P2X3R expression and function. Poly(I:C) stimulation provided a good control to distinguish any potential changes in TRP channel or P2XR expression or function from that induced from RV-16 infection as poly(I:C) is a synthetic dsRNA analogue, whereas, RV-16 is a ssRNA virus. Previously published findings have identified that poly(I:C) stimulation of neuronal cell line models (tooth pulp and DRG neurons) causes hyperresponsiveness of TRPA1 and TRPV1 channels in response to specific agonists, cinnamaldehyde and capsaicin, respectively (Clarke *et al.*, 2017; Qi *et al.*, 2011). However, we found no change in mRNA, protein expression or specific receptor function when stimulated with poly(I:C) at any time point in either our airway or neuronal cell line. Although in this thesis we used a difference concentration of poly(I:C) (10 µg ml^{-1}) to those published (25µg ml^{-1}). These data led us to believe that the dsRNA stage of a viral life cycle, as mimicked by poly(I:C), was unlikely to be involved in virally induced cough. However, RV-16 infection alone only led to inhibition of TRPA1 and P2X3 signalling during early infection which was not seen when longer term infection was investigated. This suggests that ssRNA alone is also unlikely to cause cough and is likely part of a larger overall mechanism causing viral cough.

It is important to note that use of immortalised A549 cell line does not completely mimic an *in vivo* RV-16 infection as A549 cells are from the lower airway. Whilst RV-16 generally causes upper respiratory tract infection it has been shown to infect and replicate in the lower airway (Papadopoulos *et al.*, 2000). Furthermore, the cell line is of adenocarcinoma origin so their endogenous protein expression and response to inflammatory stimulation may be different from that of primary origin, such as primary bronchial epithelial cells (HBE) or primary lung endothelial cells (HMVEC). Another important consideration is our use of transfected 1321N1-P2X3 cell line. The transfection used an exogenous vector containing P2X3R and controlled independently of the nucleus, therefore, any expression change caused by RV-16 may not be representative of a physiological response.

An interesting avenue to pursue further would be to expand this approach and investigate the effects of other respiratory tract infection pathogens which cause cough, such as respiratory syncytial virus (RSV), parainfluenza virus and adenovirus. These have briefly been touched upon by others who found increased expression of TRPA1 and TRPV1 on airway bronchial cells (Omar *et al.*, 2017) and heightened cough sensitivity (Ye *et al.*, 2011) . However, no published data currently exists investigating TRPV4 during infection with other respiratory tract pathogens.

6.2 The Effect of Hypotonic TRPV4 Activation on Downstream Signalling and ATP Release

The work carried out in Chapter 4 further characterised the pathway of hypotonic induced ATP release. Previous studies exploring this pathway identified the role of TRPV4 following hypotonic stimulation, and that ATP release following this was facilitated by pannexin-1 channel opening (Ransford *et al.*, 2009; Seminario-Vidal *et al.*, 2011; Ohbuchi *et al.*, 2014). We identified that we could eliminate hypotonic induced ATP release through inhibition of pannexin-1 with carbenoxolone, and in combination with actin, PKC, or most importantly, calcium-calmodulin kinase inhibition. These data suggest that pannexin-1 and calcium-calmodulin kinase play integral roles in the hypotonic induced ATP release pathway. Most interestingly, from that line of investigation we identified that inhibition of TRPV4 did not affect peak ATP release as we initially hypothesised as TRPV4 is the primary sensor to hypotonic stimulation, of which is a potent agonist of TRPV4. Instead inhibition of TRPV4 with HC067047 caused a significant delay in ATP release. We hypothesised that this was a result of a redundancy system by-passing TRPV4 signal transduction, therefore, delaying downstream signalling and the end point of ATP release. In order to conclusively establish this role, we would have ideally carried out sampling experiments to measure ATP release, as previously established, with a combination of TRPV4 inhibitor HC067047 and either pannexin-1 inhibitor carbenoxolone or calcium-calmodulin kinase inhibitor KN93.

Our findings that TRPV4 activation via hypotonic stimulation led to pannexin-1 activation and subsequent ATP release are in line with previously published literature (Rahman *et al.*, 2018; Seminario-Vidal *et al.*, 2011), and that inhibition of TRPV4 caused less ATP release.

The hypothesis raised by Rahman *et al.* (2018) and Weilinger, Tang & Thompson (2012), that Src family kinases may regulate pannexin-1 activation, poses important and interesting questions. With the knowledge that Src family kinases regulate the phosphorylation and subsequent activation of pannexin-1, it raises the possibly that Src family kinases play a more pivotal role in hypotonic induced ATP release than initially thought as RhoA activation (via GEF activity) and MLC phosphorylation are regulated by Src family kinase activity (Garcia *et al.*, 1999). Further work should be carried out to investigate the hypothesis that Src family kinases play a pivotal role in regulation of pannexin-1 activation using both pan and specific inhibitors of Src family kinases such as PP 2 (Lck and Fyn), SU6656 (Src, Fyn, Lyn and c-Yes) and KX2-391 (Src) and site directed mutagenesis of Src family kinases binding sites in RhoA and pannexin-1 sequences for use in a hypotonic stimulation model.

An important consideration to mention here is that our sampling method was not as sensitive as others have used (Seminario-Vidal, Lazarowski & Okada, 2009). However, all our controls worked where they should have so we are confident in the reliability of our findings.

Previous studies have shown that hypotonic stimulation, and the cellular swelling as a result, cause intracellular calcium elevations (Tatur *et al.*, 2007; Missiaen *et al.*, 1996) which in turn regulates exocytosis of ATP during hypotonic stimulation (Boudreault & Grygorczyk, 2004; Tatur *et al.*, 2008). Therefore, we expected to see elevations in intracellular calcium concentration following hypotonic stimulus, however we did not. Without further investigation using other fluorescent calcium dyes we cannot definitively say if our model of hypotonic stimulation caused calcium elevations or not. We would have ideally carried out Fura-2 ratiometric calcium assays utilising an alternative plate reader format used previously in Chapter 3.

The data within this thesis provide the first evidence that hypotonic stimulation of A549 cells cause a distinct distribution pattern of pannexin-1 channel through the cell which could be prevented or altered with the application of inhibitors to the 'hypotonic pathway'. Having determined that hypotonic induced ATP release could be inhibited or reduced, and that global expression of pannexin-1 remained consistent throughout experiments we hypothesised that hypotonic stimulation causes pannexin-1 insertion in to the plasma membrane to facilitate ATP release. The physical appearance of A549 cells possessed a

distinct compartmentalisation of pannexin-1 staining following hypotonic stimulation that was abolished with pannexin-1 inhibitor carbenoxolone, and severely reduced with inhibition of TRPV4, MLC, ROCKII and calcium-calmodulin kinase. A similar phenotype has previously been published on mechanically stimulated astrocytes and primary epithelial airway cultures (Ransford *et al.*, 2009; Albalawi *et al.*, 2017), but not previously seen in our cell line or stimulus. However, in line with that published data were our findings in isotonic stimulated cells, which was used as a control for mechanical stimulation. We identified that pannexin-1 staining became highly granular, distinct from basal or hypotonic stimulated cells, with a large degree of overlap with the actin cytoskeleton. This data strongly suggests that our mechanical stimulation control was insufficient to cause ATP release, but strong enough to stimulate mechanical induced changes within the cells.

We believe these data support our hypothesis that hypotonic and mechanical stimulation cause movement of endosomal compartments through the cell to transport pannexin-1 channel to the plasma membrane, especially since previous data has shown that extracellular ATP is able to cause pannexin-1 internalisation to endosomal compartments (Boyce *et al.*, 2015). However, to conclusively confirm this we would have carried out further experiments including sub-cellular fractionation and carry out western blot analysis on endosomal, cytosol and membrane fractions for pannexin-1 expression, tracking SNAREs and other endosomal markers, such as EEA or Rabs, and blocking endosomal components to monitor changes in pannexin-1 whole cell distribution.

Furthermore, we would have repeated experiments we had attempted previously (data not shown, problem with reagents) of RV-16 infected A549 cells exposed to hypotonic stimulation and isotonic controls to investigate if RV-16 causes increased membrane expression of pannexin-1, thereby leading to increased ATP release, as shown in Chapter 5.

We feel the physiological relevance of this work carried out provide a potential therapeutic benefit for treating viral and, in particular, post-viral cough. Elucidation of this mechanism we hypothesise is taking place would mean a potential therapeutic target to block or reduce ATP release following insult to the airway, allowing recovery time without a hypersensitive airway precipitating further cough and damage.

6.3 Exploring the Effect of Human Rhinovirus-16 on the Hypotonic Pathway, ATP release and TRPV4 Expression

It is now emerging that ATP may be a major component in causing cough during an URTI, unlike previously thought that thermo-TRP channels TRPA1 and TRPV1 were behind the airway hypersensitivity seen with infection (Atkinson *et al.,* 2016*;* Bonvini *et al.,* 2016; Fowles *et al.,* 2017). Clinical trials have failed to show the importance of TRPA1 and TRPV1 in causing cough, particularly in chronic cough conditions (Khalid *et al.*, 2014). However, other more recent clinical trials that have shifted focus to ATP have shown potentially life changing results through inhibition ATP sensitive P2X3 receptor (Abdulqawi *et al.*, 2015). However, despite these advancements we are still no closer to defining the mechanism of cough during URTI and related chronic cough conditions. We and others also believe that TRPV4 may also underpin the mechanism of viral cough during URTI. Here we have shown that in response to common cold virus, RV-16, airway cell line A549 significantly increased ATP output both basally and following stimulation. Furthermore, that at early stages in infection with RV-16 total intracellular ATP concentration was increased, followed by a large significant reduction coinciding with increased extracellular release. This supports previous studies that ATP and P2X3 signalling are at the cruces of viral and chronic cough.

Previous studies have shown that RV-B14 is able to directly influence the cellular metabolism of HeLa and fibroblast cells causing an anabolic reprogramming of host metabolism (Gualdoni *et al.*, 2018). However, the use of non-airway cells and a non-physiological MOI (3.5-5) means we cannot assume this same reprogramming response occurs in the airway during an URTI *in vivo*. Therefore, we carried out mitochondrial stress tests on A549 cell line infected with RV-16. Consistent with published literature (Gualdoni *et al.*, 2018), we identified a minor non-significant glycolytic shift in phenotype. However, we had expected to see a larger shift in phenotype and increased ATP production from basal as indicated by our extracellular ATP sampling and intracellular ATP concentration experiments. However, there was no discernible difference from basal at any infection point for OCR, ECAR, ATP linked respiration, or proton leak. Although, we did identify a general trend of increased proton leak during early infection, not seen by late infection. Furthermore, there was increased non-mitochondrial respiration in cells stimulated with UV inactivated viral sham control. These data suggest that either indirect ICAM-1

stimulation leading to the downstream activation of inflammatory pathways, such as MAP kinase and NFκB pathways, or as a result of direct TLR2 activation from protomers within the RV protein coat (Triantafilou *et al.*, 2011), were enough to increase cellular metabolism. Further work would be required to confirm this hypothesis by investigating the activity and expression of glycogen synthase kinase-3 (GSK3) and the mammalian target of rapamycin (mTOR) pathway.

These data, along with those collected in Chapter 4, lead us to conclude that infection with RV-16 does not lead to increased ATP production but is likely a result of a pannexin-1 mediated effect and that hypotonic stimulation of the airway which causes pannexin-1 membrane insertion, and increased ATP as a consequence, without any energy burden on the cell. But this hypothesis would require further investigation to prove as stated above section 6.2.

In order to study the effect of RV-16 on TRPV4 cellular distribution during infection, we permanently overexpressed a GFP-tagged TRPV4 construct in wild type A549 cell line (section 5.3.2), previously endogenously expressing very low levels of TRPV4. Characterisation of this generated cell line showed that transfection was stable, albeit with lower overall levels of expression than cell lines we have previously generated. However, stimulation with receptor specific agonist GSK1016790A (Thorneloe *et al.*, 2008) induced a potent response significantly stronger than that induced in wild type, as shown thorough intracellular calcium signalling assay. Through further characterisation we identified that transfection caused diffuse granularity of the GFP tag throughout the cell which suggested to us that transfection was intracellular and present of the plasma membrane.

The stably transfected cell line generated was infected with RV-16 and subject to immunofluorescent analysis. RV-16 infection caused a reduction in GFP fluorescence during early infection, including UV inactivated viral sham control, which was restored by 7 days, this was consistent in all field of view despite our preliminary findings. RV-16 has previously been shown to cause Golgi fragmentation without affecting protein secretion (Mousnier *et al.*, 2014), however, specific proteins have not been investigated so we can't definitively confirm if post-translational modification still occur unaffected by the viral effects. Therefore, we hypothesise that this reduction in GFP signal was a result of altered glycosylation (Xu *et al.*, 2006) of the TRPV4 receptor during translation leading to an altered

protein structure, thereby dampening or preventing the GFP fluorescence. Further investigation into this would require utilising tunicamycin to block N-linked glycosylation, the use of glycoprotein stains for western blot detection of O-GlcNAc and lectins for enrichment and identification of glycoproteins.

The results of this thesis demonstrate that RV-16 infection causes a reduction in TRPV4 signalling at early infection with restoration to basal levels by 72 hours onwards (up to 168 hours). Furthermore, global expression using whole cell lysates was unaffected, in conjunction with our immunofluorescent images using our transfected cell line suggest that RV-16 infection may alter post-translational modifications of TRPV4. The importance of this is yet unknown, however, our findings that RV-16 infection leads to increased ATP release basally, following hypotonic and mechanical stimulation suggest a modification resulting in a gain in function. Once again further work to assess the status of other post-translational modifications such as N-linked glycosylation and phosphorylation, as listed above.

6.4 Final conclusions

In conclusion, we have shown in our investigation that poly(I:C) stimulation of A549 airway cells and 1321N1-P2X3 cell line cause no significant changes in mRNA, protein expression or function of TRPA1, TRPV1, TRPV4 or P2X3 receptor. Furthermore, that RV-16 infection causes no change to protein expression in either cell line but does lead to reduced response of TRPA1 and P2X3 in A549 and 1321N1-P2X3, respectively, which is quickly restored during early infection. Collectively, these suggest that viral cough is not mediated by a virally induced effect on either thermo-TRP or P2X3R expression or function in the airway or underlying nerves during a common cold infection.

We have shown that hypotonic induced ATP release can be significantly reduced following inhibition of pannexin-1 and in combination with calcium-calmodulin kinase inhibition, and that these proteins are integral to hypotonic induced ATP release. The hypothesised redundancy in hypotonic induced ATP release suggests inhibition of a component of this pathway may reduce stimulated ATP release without significant interference and off target effects seen with other pharmacological interventions (Abdulqawi *et al.*, 2015). However, our findings that suggest pannexin-1 is not constitutively expressed at the cell membrane

where cells displayed a distinct phenotype of pannexin-1 distribution following hypotonic stimulation pose an interesting target to reduce ATP release following insult in the airway. Blockade or inhibition of this ATP release would allow recovery time without a hypersensitive environment in the airway, which would be of great importance during a URTI.

Finally, we have also shown that RV-16 infection causes increased ATP release basally from 72 hours through 168 hours, which coincides with the time at which a viral cough is produced (3-5 days) (Eccles, 2005). This increased ATP release occurs independent of a confounding stimulus, such as hypotonicity, which reflects the cough hypersensitivity seen with a viral cough and URTI. Simply, less of a stimulus is required to cause a cough.

We identified a RV-16 driven shift in host glycolytic metabolism which suggested to us that RV-16 infection causes a cellular stress which requires increased glucose uptake. This change in cellular phenotype supports our findings that RV-16 infected cells release more ATP basally likely in response to virally driven cellular stress without causing cell death.

The data and investigation presented in this thesis could provide attractive pharmacological targets for intervention in treatment of viral cough during URTI.

References

Abdullah, H., Heaney, L.G., Cosby, S.L. & McGarvey, L.P. a (2014) Rhinovirus upregulates transient receptor potential channels in a human neuronal cell line: implications for respiratory virus-induced cough reflex sensitivity. *Thorax*. **69** (1), pp. 46–54.

Abdulqawi, R., Dockry, R., Holt, K., Layton, G., McCarthy, B.G., Ford, A.P. & Smith, J.A. (2015) P2X3 receptor antagonist (AF-219) in refractory chronic cough: a randomised, double-blind, placebo-controlled phase 2 study. *Lancet*. **385** (9974), pp. 1198–1205.

Acuña-Castillo, C., Coddou, C., Bull, P., Brito, J. & Huidobro-Toro, J.P. (2007) Differential role of extracellular histidines in copper, zinc, magnesium and proton modulation of the P2X7 purinergic receptor. *Journal of neurochemistry*. **101** (1), pp. 17–26.

Agopyan, N., Head, J., Yu, S. & Simon, S.A. (2004) TRPV1 receptors mediate particulate matter-induced apoptosis. *American Journal of Physiology-Lung Cellular and Molecular Physiology*. **286** (3), pp. L563–L572.

Aizawa, N., Wyndaele, J.-J., Homma, Y. & Igawa, Y. (2012) Effects of TRPV4 cation channel activation on the primary bladder afferent activities of the rat. *Neurourology and urodynamics*. **31** (1), pp. 148–155.

Akopova, I., Tatur, S., Grygorczyk, M., Luchowski, R., Gryczynski, I., Gryczynski, Z., Borejdo, J. & Grygorczyk, R. (2012) Imaging exocytosis of ATP-containing vesicles with TIRF microscopy in lung epithelial A549 cells. *Purinergic signalling*. **8** (1), pp. 59–70.

Albalawi, F., Lu, W., Beckel, J.M., Lim, J.C., McCaughey, S.A. & Mitchell, C.H. (2017) The P2X7 Receptor Primes IL-1β and the NLRP3 Inflammasome in Astrocytes Exposed to Mechanical Strain. *Frontiers in cellular neuroscience*. **11**pp. 227.

Alenmyr, L., Uller, L., Greiff, L., Högestätt, E.D. & Zygmunt, P.M. (2014) TRPV4-mediated calcium influx and ciliary activity in human native airway epithelial cells. *Basic & clinical pharmacology & toxicology*. **114** (2), pp. 210–216.

Alper, C.M., Doyle, W.J., Winther, B. & Hendley, J.O. (2008) Upper respiratory virus detection without parent-reported illness in children is virus-specific. *Journal of clinical virology : the official publication of the Pan American Society for Clinical Virology*. **43** (1), pp. 120–122.

Amano, M., Ito, M., Kimura, K., Fukata, Y., Chihara, K., Nakano, T., Matsuura, Y. & Kaibuchi, K. (1996a) Phosphorylation and activation of myosin by Rho-associated kinase (Rho-kinase). *The Journal of biological chemistry*. **271** (34), pp. 20246–20249.

Amano, M., Mukai, H., Ono, Y., Chihara, K., Matsui, T., Hamajima, Y., Okawa, K., Iwamatsu, A. & Kaibuchi, K. (1996b) Identification of a putative target for Rho as the serine-threonine kinase protein kinase N. *Science (New York, N.Y.)*. **271** (5249), pp. 648–650.

Andersson, D.A., Gentry, C., Moss, S. & Bevan, S. (2008) Transient receptor potential A1 is a sensory receptor for multiple products of oxidative stress. *The Journal of neuroscience : the official journal of the Society for Neuroscience*. **28** (10), pp. 2485–

2494.

Andersson, K.-E., Gratzke, C. & Hedlund, P. (2010) The role of the transient receptor potential (TRP) superfamily of cation-selective channels in the management of the overactive bladder. *BJU international*. **106** (8), pp. 1114–1127.

Andrade, Y.N., Fernandes, J., Vázquez, E., Fernández-Fernández, J.M., Arniges, M., Sánchez, T.M., Villalón, M. & Valverde, M.A. (2005) TRPV4 channel is involved in the coupling of fluid viscosity changes to epithelial ciliary activity. *The Journal of cell biology*. **168** (6), pp. 869–874.

Andrè, E., Campi, B., Materazzi, S., Trevisani, M., Amadesi, S., Massi, D., Creminon, C., Vaksman, N., Nassini, R., Civelli, M., Baraldi, P.G., Poole, D.P., Bunnett, N.W., Geppetti, P., et al. (2008) Cigarette smoke-induced neurogenic inflammation is mediated by alpha,beta-unsaturated aldehydes and the TRPA1 receptor in rodents. *The Journal of clinical investigation*. **118** (7), pp. 2574–2582.

Appelgren, A., Appelgren, B., Kopp, S., Lundeberg, T. & Theodorsson, E. (1998) Substance P-associated increase of intra-articular temperature and pain threshold in the arthritic TMJ. *Journal of orofacial pain*. **12** (2), pp. 101–107.

Araki, I. (2011) TRP channels in urinary bladder mechanosensation. In: Shahidul Islam (ed.). *Transient Receptor Potential Channels: Advances in experimental medicine and biology*. pp. pp. 861–879.

Arniges, M., Vázquez, E., Fernández-Fernández, J.M. & Valverde, M.A. (2004) Swelling-activated Ca2+ entry via TRPV4 channel is defective in cystic fibrosis airway epithelia. *The Journal of biological chemistry*. **279** (52), pp. 54062–54068.

Arnoult, D., Soares, F., Tattoli, I., Castanier, C., Philpott, D.J. & Girardin, S.E. (2009) An N-terminal addressing sequence targets NLRX1 to the mitochondrial matrix. *Journal of Cell Science*. **122** (17), pp. 3161–3168.

Arruda, E., Pitkäranta, A., Witek, T.J., Doyle, C.A., Hayden, F.G. & Hayden, F.G. (1997) Frequency and natural history of rhinovirus infections in adults during autumn. *Journal of clinical microbiology*. **35** (11), pp. 2864–2868.

Atkinson, S.K., Sadofsky, L.R. & Morice, A.H. (2016) How does rhinovirus cause the common cold cough? *BMJ open respiratory research*. **3** (1), pp. e000118.

Bae, Y.-J., Moon, K.A., Kim, T.-B., Jang, Y.J., Lee, Y.S., Park, C.S., Lee, K.-Y., Moon, H.-B. & Cho, Y.S. (2012) The role of nitrosative stress in the pathogenesis of unexplained chronic cough with cough hypersensitivity. *American journal of rhinology & allergy*. **26** (1), pp. e10-4.

Bai, J., Miao, B., Wu, X., Luo, X., Ma, R., Zhang, J., Li, L., Shi, J. & Li, H. (2015) Enhanced expression of SAM-pointed domain-containing Ets-like factor in chronic rhinosinusitis with nasal polyps. *The Laryngoscope*. **125** (3), pp. E97-103.

Baltimore, D. (1971) Expression of animal virus genomes. *Bacteriological reviews*. **35** (3), pp. 235–241.

Bandell, M., Story, G.M., Hwang, S.W., Viswanath, V., Eid, S.R., Petrus, M.J., Earley, T.J. &

Patapoutian, A. (2004) Noxious cold ion channel TRPA1 is activated by pungent compounds and bradykinin. *Neuron*. **41** (6), pp. 849–857.

Bao, B.A., Lai, C.P., Naus, C.C. & Morgan, J.R. (2012) Pannexin1 Drives Multicellular Aggregate Compaction via a Signaling Cascade That Remodels the Actin Cytoskeleton. *Journal of Biological Chemistry*. **287** (11), pp. 8407–8416.

Bao, L., Locovei, S. & Dahl, G. (2004) Pannexin membrane channels are mechanosensitive conduits for ATP. *FEBS letters*. **572** (1–3), pp. 65–68.

Barco, A., Feduchi, E. & Carrasco, L. (2000) A stable HeLa cell line that inducibly expresses poliovirus 2A(pro): effects on cellular and viral gene expression. *Journal of virology*. **74** (5), pp. 2383–2392.

Bardin, P.G., Johnston, S.L., Sanderson, G., Robinson, B.S., Pickett, M.A., Fraenkel, D.J. & Holgate, S.T. (1994) Detection of rhinovirus infection of the nasal mucosa by oligonucleotide in situ hybridization. *American Journal of Respiratory Cell and Molecular Biology*. **10** (2), pp. 207–213.

Barnes, P.J. (2001) Neurogenic inflammation in the airways. *Respiration Physiology*. **125** (1–2), pp. 145–154.

Barrera, N.P., Ormond, S.J., Henderson, R.M., Murrell-Lagnado, R.D. & Edwardson, J.M. (2005) Atomic force microscopy imaging demonstrates that P2X2 receptors are trimers but that P2X6 receptor subunits do not oligomerize. *The Journal of biological chemistry*. **280** (11), pp. 10759–10765.

Basavappa, R., Syed, R., Flore, O., Icenogle, J.P., Filman, D.J. & Hogle, J.M. (1994) Role and mechanism of the maturation cleavage of VP0 in poliovirus assembly: structure of the empty capsid assembly intermediate at 2.9 A resolution. *Protein science : a publication of the Protein Society*. **3** (10), pp. 1651–1669.

Basavappa, S., Pedersen, S.F., Jørgensen, N.K., Ellory, J.C. & Hoffmann, E.K. (1998) Swelling-Induced Arachidonic Acid Release via the 85-kDa cPLA $_2$ in Human Neuroblastoma Cells. *Journal of Neurophysiology*. **79** (3), pp. 1441–1449.

Basoglu, O.K., Barnes, P.J., Kharitonov, S.A. & Pelleg, A. (2015) Effects of Aerosolized Adenosine 5'-Triphosphate in Smokers and Patients with Chronic Obstructive Pulmonary Disease. *Chest*. **148** (2), pp. 430–435.

Basoglu, O.K., Pelleg, A., Essilfie-Quaye, S., Brindicci, C., Barnes, P.J. & Kharitonov, S.A. (2005) Effects of aerosolized adenosine 5'-triphosphate vs adenosine 5'-monophosphate on dyspnea and airway caliber in healthy nonsmokers and patients with asthma. *Chest*. **128** (4), pp. 1905–1909.

Baumgarten, C.R., Lehmkuhl, B., Henning, R., Brunnee, T., Dorow, P., Schilling, W. & Kunkel, G. (1992) Bradykinin and other inflammatory mediators in BAL-fluid from patients with active pulmonary inflammation. *Agents and actions. Supplements*. **38 (Pt 3)**pp. 475–481.

Bautista, D.M., Jordt, S.-E.E., Nikai, T., Tsuruda, P.R., Read, A.J., Poblete, J., Yamoah, E.N., Basbaum, A.I. & Julius, D. (2006) TRPA1 mediates the inflammatory actions of environmental irritants and proalgesic agents. *Cell*. **124** (6), pp. 1269–1282.

Bautista, D.M., Movahed, P., Hinman, A., Axelsson, H.E., Sterner, O., Högestätt, E.D., Julius, D., Jordt, S.-E. & Zygmunt, P.M. (2005) Pungent products from garlic activate the sensory ion channel TRPA1. *Proceedings of the National Academy of Sciences of the United States of America*. **102** (34), pp. 12248–12252.

Bayer, N., Schober, D., Hüttinger, M., Blaas, D. & Fuchs, R. (2001) Inhibition of clathrin-dependent endocytosis has multiple effects on human rhinovirus serotype 2 cell entry. *The Journal of biological chemistry*. **276** (6), pp. 3952–3962.

Becker, D., Bereiter-Hahn, J. & Jendrach, M. (2009) Functional interaction of the cation channel transient receptor potential vanilloid 4 (TRPV4) and actin in volume regulation. *European Journal of Cell Biology*. **88** (3), pp. 141–152.

Becker, D., Blase, C., Bereiter-Hahn, J. & Jendrach, M. (2005) TRPV4 exhibits a functional role in cell-volume regulation. *Journal of cell science*. **118** (Pt 11), pp. 2435–2440.

Belsham, G.J. & Sonenberg, N. (2000) Picornavirus RNA translation: Roles for cellular proteins. *Trends in Microbiology*. **8** (0), pp. 330–335.

Belvisi, M.G., Birrell, M.A., Khalid, S., Wortley, M.A., Dockry, R., Coote, J., Holt, K., Dubuis, E., Kelsall, A., Maher, S.A., Bonvini, S., Woodcock, A. & Smith, J.A. (2016) Neurophenotypes in Airway Diseases. Insights from Translational Cough Studies. *American journal of respiratory and critical care medicine*. **193** (12), pp. 1364–1372.

Benemei, S., Patacchini, R., Trevisani, M. & Geppetti, P. (2015) TRP channels. *Current opinion in pharmacology*. **22C**pp. 18–23.

Bessac, B.F. & Jordt, S.-E. (2008) Breathtaking TRP channels: TRPA1 and TRPV1 in airway chemosensation and reflex control. *Physiology (Bethesda, Md.)*. **23**pp. 360–370.

Bhave, G., Hu, H.-J., Glauner, K.S., Zhu, W., Wang, H., Brasier, D.J., Oxford, G.S. & Gereau, R.W. (2003) Protein kinase C phosphorylation sensitizes but does not activate the capsaicin receptor transient receptor potential vanilloid 1 (TRPV1). *Proceedings of the National Academy of Sciences*. **100** (21), pp. 12480–12485.

Bhave, G., Zhu, W., Wang, H., Brasier, D.J., Oxford, G.S. & Gereau, R.W. (2002) cAMP-dependent protein kinase regulates desensitization of the capsaicin receptor (VR1) by direct phosphorylation. *Neuron*. **35** (4), pp. 721–731.

Bhowmick, N.A., Ghiassi, M., Bakin, A., Aakre, M., Lundquist, C.A., Engel, M.E., Arteaga, C.L. & Moses, H.L. (2001) Transforming Growth Factor-β1 Mediates Epithelial to Mesenchymal Transdifferentiation through a RhoA-dependent Mechanism Carl-Henrik Heldin (ed.). *Molecular Biology of the Cell*. **12** (1), pp. 27–36.

Biagioli, M.C., Kaul, P., Singh, I. & Turner, R.B. (1999) The role of oxidative stress in rhinovirus induced elaboration of IL-8 by respiratory epithelial cells. *Free radical biology & medicine*. **26** (3–4), pp. 454–462.

Binshtok, A.M., Wang, H., Zimmermann, K., Amaya, F., Vardeh, D., Shi, L., Brenner, G.J., Ji, R.-R., Bean, B.P., Woolf, C.J. & Samad, T.A. (2008) Nociceptors are interleukin-1beta sensors. *The Journal of neuroscience : the official journal of the Society for Neuroscience*. **28** (52), pp. 14062–14073.

Birder, L., Kullmann, F.A., Lee, H., Barrick, S., de Groat, W., Kanai, A. & Caterina, M. (2007) Activation of Urothelial Transient Receptor Potential Vanilloid 4 by 4 -Phorbol 12,13-Didecanoate Contributes to Altered Bladder Reflexes in the Rat. *Journal of Pharmacology and Experimental Therapeutics*. **323** (1), pp. 227–235.

Birrell, M.A., Belvisi, M.G., Grace, M., Sadofsky, L., Faruqi, S., Hele, D.J., Maher, S.A., Freund-Michel, V. & Morice, A.H. (2009) TRPA1 agonists evoke coughing in guinea pig and human volunteers. *American journal of respiratory and critical care medicine*. **180** (11), pp. 1042–1047.

Birring, S.S., Brew, J., Kilbourn, A., Edwards, V., Wilson, R. & Morice, A.H. (2017) Rococo study: a real-world evaluation of an over-the-counter medicine in acute cough (a multicentre, randomised, controlled study). *BMJ Open*. **7** (1), pp. e014112.

Bizzintino, J., Lee, W.-M., Laing, I.A., Vang, F., Pappas, T., Zhang, G., Martin, A.C., Khoo, S.-K., Cox, D.W., Geelhoed, G.C., McMinn, P.C., Goldblatt, J., Gern, J.E. & Le Souëf, P.N. (2011) Association between human rhinovirus C and severity of acute asthma in children. *The European respiratory journal*. **37** (5), pp. 1037–1042.

Blaas, D. & Fuchs, R. (2016) Mechanism of human rhinovirus infections. *Molecular and Cellular Pediatrics*. **3** (1), pp. 21.

Bo, X., Jiang, L.-H., Wilson, H.L., Kim, M., Burnstock, G., Surprenant, A. & North, R.A. (2003) Pharmacological and biophysical properties of the human P2X5 receptor. *Molecular pharmacology*. **63** (6), pp. 1407–1416.

Bochkov, Y.A., Palmenberg, A.C., Lee, W.-M., Rathe, J.A., Amineva, S.P., Sun, X., Pasic, T.R., Jarjour, N.N., Liggett, S.B. & Gern, J.E. (2011) Molecular modeling, organ culture and reverse genetics for a newly identified human rhinovirus C. *Nature medicine*. **17** (5), pp. 627–632.

Bochkov, Y.A., Watters, K., Ashraf, S., Griggs, T.F., Devries, M.K., Jackson, D.J., Palmenberg, A.C. & Gern, J.E. (2015) Cadherin-related family member 3, a childhood asthma susceptibility gene product, mediates rhinovirus C binding and replication. *Proceedings of the National Academy of Sciences of the United States of America*. **112** (17), pp. 5485–5490.

Bonham, A.C., Kott, K.S., Ravi, K., Kappagoda, C.T. & Joad, J.P. (1996) Substance P contributes to rapidly adapting receptor responses to pulmonary venous congestion in rabbits. *The Journal of physiology*. **493 (Pt 1**pp. 229–238.

Bønnelykke, K., Sleiman, P., Nielsen, K., Kreiner-Møller, E., Mercader, J.M., Belgrave, D., den Dekker, H.T., Husby, A., Sevelsted, A., Faura-Tellez, G., Mortensen, L.J., Paternoster, L., Flaaten, R., Mølgaard, A., et al. (2014) A genome-wide association study identifies CDHR3 as a susceptibility locus for early childhood asthma with severe exacerbations. *Nature Genetics*. **46** (1), pp. 51–55.

Bonvini, S.J., Birrell, M.A., Grace, M.S., Maher, S.A., Adcock, J.J., Wortley, M.A., Dubuis, E., Ching, Y.-M., Ford, A.P., Shala, F., Miralpeix, M., Tarrason, G., Smith, J.A. & Belvisi, M.G. (2016) Transient receptor potential cation channel, subfamily V, member 4 and airway sensory afferent activation: Role of adenosine triphosphate. *Journal of Allergy and Clinical Immunology*. **138** (1), pp. 249–261.e12.

Bossios, A., Psarras, S., Gourgiotis, D., Skevaki, C.L., Constantopoulos, A.G., Saxoni-Papageorgiou, P. & Papadopoulos, N.G. (2005) Rhinovirus infection induces cytotoxicity and delays wound healing in bronchial epithelial cells. *Respiratory research*. **6**pp. 114.

Boudreault, F. & Grygorczyk, R. (2004) Cell swelling-induced ATP release is tightly dependent on intracellular calcium elevations. *The Journal of Physiology*. **561** (2), pp. 499–513.

Bourne, H.R., Sanders, D.A. & McCormick, F. (1990) The GTPase superfamily: a conserved switch for diverse cell functions. *Nature*. **348** (6297), pp. 125–132.

Bowerfind, W.M.L., Fryer, A.D. & Jacoby, D.B. (2002) Double-stranded RNA causes airway hyperreactivity and neuronal M2 muscarinic receptor dysfunction. *Journal of applied physiology (Bethesda, Md. : 1985)*. **92** (4), pp. 1417–1422.

Boyce, A.K.J., Kim, M.S., Wicki-Stordeur, L.E. & Swayne, L.A. (2015) ATP stimulates pannexin 1 internalization to endosomal compartments. *Biochemical Journal*. **470** (3), pp. 319–330.

Brabec, M., Schober, D., Wagner, E., Bayer, N., Murphy, R.F., Blaas, D. & Fuchs, R. (2005) Opening of size-selective pores in endosomes during human rhinovirus serotype 2 in vivo uncoating monitored by single-organelle flow analysis. *Journal of virology*. **79** (2), pp. 1008–1016.

Brake, A.J., Wagenbach, M.J. & Julius, D. (1994) New structural motif for ligand-gated ion channels defined by an ionotropic ATP receptor. *Nature*. **371** (6497), pp. 519–523.

Braman, S.S. (2006) Postinfectious cough: ACCP evidence-based clinical practice guidelines. *Chest*. **129** (1 Suppl), pp. 138S–146S.

Bruewer, M., Luegering, A., Kucharzik, T., Parkos, C.A., Madara, J.L., Hopkins, A.M. & Nusrat, A. (2003) Proinflammatory cytokines disrupt epithelial barrier function by apoptosis-independent mechanisms. *Journal of immunology (Baltimore, Md. : 1950)*. **171** (11), pp. 6164–6172.

Büch, T.R.H., Schäfer, E.A.M., Demmel, M.T., Boekhoff, I., Thiermann, H., Gudermann, T., Steinritz, D. & Schmidt, A. (2013) Functional expression of the transient receptor potential channel TRPA1, a sensor for toxic lung inhalants, in pulmonary epithelial cells. *Chemico-Biological Interactions*. **206**pp. 462–471.

Burbelo, P.D., Miyamoto, S., Utani, A., Brill, S., Yamada, K.M., Hall, A. & Yamada, Y. (1995) p190-B, a new member of the Rho GAP family, and Rho are induced to cluster after integrin cross-linking. *The Journal of biological chemistry*. **270** (52), pp. 30919–30926.

Cadieux, A., Monast, N.P., Pomerleau, F., Fournier, A. & Lanoue, C. (1999) Bronchoprotector properties of calcitonin gene-related peptide in guinea pig and human airways. Effect of pulmonary inflammation. *American journal of respiratory and critical care medicine*. **159** (1), pp. 235–243.

Callahan, P.L., Mizutani, S. & Colonno, R.J. (1985) Molecular cloning and complete sequence determination of RNA genome of human rhinovirus type 14. *Proceedings of the National Academy of Sciences of the United States of America*. **82** (3), pp. 732–

736.

Canning, B.J. & Mori, N. (2011) Encoding of the cough reflex in anesthetized guinea pigs. *American journal of physiology. Regulatory, integrative and comparative physiology*. **300** (2), pp. R369-77.

Canning, B.J., Mori, N. & Mazzone, S.B. (2006) Vagal afferent nerves regulating the cough reflex. *Respiratory physiology & neurobiology*. **152** (3), pp. 223–242.

Carr, M.J., Kollarik, M., Meeker, S.N. & Undem, B.J. (2003) A role for TRPV1 in bradykinin-induced excitation of vagal airway afferent nerve terminals. *The Journal of pharmacology and experimental therapeutics*. **304** (3), pp. 1275–1279.

Casalino-Matsuda, S.M., Monzón, M.E. & Forteza, R.M. (2006) Epidermal Growth Factor Receptor Activation by Epidermal Growth Factor Mediates Oxidant-Induced Goblet Cell Metaplasia in Human Airway Epithelium. *American Journal of Respiratory Cell and Molecular Biology*. **34** (5), pp. 581–591.

Caterina, M.J., Leffler, A., Malmberg, A.B., Martin, W.J., Trafton, J., Petersen-Zeitz, K.R., Koltzenburg, M., Basbaum, A.I. & Julius, D. (2000) Impaired nociception and pain sensation in mice lacking the capsaicin receptor. *Science (New York, N.Y.)*. **288** (5464), pp. 306–313.

Caterina, M.J., Rosen, T.A., Tominaga, M., Brake, A.J. & Julius, D. (1999) A capsaicin-receptor homologue with a high threshold for noxious heat. *Nature*. **398** (6726), pp. 436–441.

Caterina, M.J., Schumacher, M.A., Tominaga, M., Rosen, T.A., Levine, J.D. & Julius, D. (1997) The capsaicin receptor: a heat-activated ion channel in the pain pathway. *Nature*. **389** (6653), pp. 816–824.

Chang, A.B., Gibson, P.G., Ardill, J. & McGarvey, L.P.A. (2007) Calcitonin gene-related peptide relates to cough sensitivity in children with chronic cough. *The European respiratory journal*. **30** (1), pp. 66–72.

Chapados, R., Abe, K., Ihida-Stansbury, K., McKean, D., Gates, A.T., Kern, M., Merklinger, S., Elliott, J., Plant, A., Shimokawa, H. & Jones, P.L. (2006) ROCK controls matrix synthesis in vascular smooth muscle cells: coupling vasoconstriction to vascular remodeling. *Circulation research*. **99** (8), pp. 837–844.

Chen, C.-C., Akopian, A.N., Sivilottit, L., Colquhoun, D., Burnstock, G. & Wood, J.N. (1995) A P2X purinoceptor expressed by a subset of sensory neurons. *Nature*. **377** (6548), pp. 428–431.

Chen, G., Korfhagen, T.R., Xu, Y., Kitzmiller, J., Wert, S.E., Maeda, Y., Gregorieff, A., Clevers, H. & Whitsett, J.A. (2009) SPDEF is required for mouse pulmonary goblet cell differentiation and regulates a network of genes associated with mucus production. *The Journal of clinical investigation*. **119** (10), pp. 2914–2924.

Chen, J., Kang, D., Xu, J., Lake, M., Hogan, J.O., Sun, C., Walter, K., Yao, B. & Kim, D. (2013) Species differences and molecular determinant of TRPA1 cold sensitivity. *Nature communications*. **4**pp. 2501.

Chen, Y., Hamati, E., Lee, P.-K., Lee, W.-M., Wachi, S., Schnurr, D., Yagi, S., Dolganov, G., Boushey, H., Avila, P. & Wu, R. (2006) Rhinovirus Induces Airway Epithelial Gene Expression through Double-Stranded RNA and IFN-Dependent Pathways. *American Journal of Respiratory Cell and Molecular Biology*. **34** (2), pp. 192–203.

Cherfils-Vicini, J., Platonova, S., Gillard, M., Laurans, L., Validire, P., Caliandro, R., Magdeleinat, P., Mami-Chouaib, F., Dieu-Nosjean, M.-C., Fridman, W.-H., Damotte, D., Sautès-Fridman, C. & Cremer, I. (2010) Triggering of TLR7 and TLR8 expressed by human lung cancer cells induces cell survival and chemoresistance. *The Journal of clinical investigation*. **120** (4), pp. 1285–1297.

Chessell, I.P., Hatcher, J.P., Bountra, C., Michel, A.D., Hughes, J.P., Green, P., Egerton, J., Murfin, M., Richardson, J., Peck, W.L., Grahames, C.B.A., Casula, M.A., Yiangou, Y., Birch, R., et al. (2005) Disruption of the P2X7 purinoceptor gene abolishes chronic inflammatory and neuropathic pain. *Pain*. **114** (3), pp. 386–396.

Chiba, Y. & Misawa, M. (2004) The role of RhoA-mediated Ca2+ sensitization of bronchial smooth muscle contraction in airway hyperresponsiveness. *Journal of smooth muscle research = Nihon Heikatsukin Gakkai kikanshi*. **40** (4–5), pp. 155–167.

Chiba, Y., Takada, Y., Miyamoto, S., MitsuiSaito, M., Karaki, H. & Misawa, M. (1999) Augmented acetylcholine-induced, Rho-mediated Ca2+ sensitization of bronchial smooth muscle contraction in antigen-induced airway hyperresponsive rats. *British journal of pharmacology*. **127** (3), pp. 597–600.

Chiba, Y., Ueno, A., Shinozaki, K., Takeyama, H., Nakazawa, S., Sakai, H. & Misawa, M. (2005) Involvement of RhoA-mediated Ca2+ sensitization in antigen-induced bronchial smooth muscle hyperresponsiveness in mice. *Respiratory Research*. **6** (1), pp. 4.

Chiozzi, P., Sanz, J.M., Ferrari, D., Falzoni, S., Aleotti, A., Buell, G.N., Collo, G. & Di Virgilio, F. (1997) Spontaneous cell fusion in macrophage cultures expressing high levels of the P2Z/P2X7 receptor. *The Journal of cell biology*. **138** (3), pp. 697–706.

Chiu, I.M., von Hehn, C.A. & Woolf, C.J. (2012) Neurogenic inflammation and the peripheral nervous system in host defense and immunopathology. *Nature neuroscience*. **15** (8), pp. 1063–1067.

Cho, Y., Park, S.., Lee, C.K., Yoo, B. & Moon, H.B. (2003) Elevated substance P levels in nasal lavage fluids from patients with chronic nonproductive cough and increased cough sensitivity to inhaled capsaicin. *Journal of Allergy and Clinical Immunology*. **112** (4), pp. 695–701.

Choudry, N.B., Fuller, R.W. & Pride, N.B. (1989) Sensitivity of the human cough reflex: effect of inflammatory mediators prostaglandin E2, bradykinin, and histamine. *The American review of respiratory disease*. **140** (1), pp. 137–141.

Chrzanowska-Wodnicka, M. & Burridge, K. (1996) Rho-stimulated contractility drives the formation of stress fibers and focal adhesions. *The Journal of cell biology*. **133** (6), pp. 1403–1415.

Chuang, H.H., Prescott, E.D., Kong, H., Shields, S., Jordt, S.E., Basbaum, A.I., Chao, M. V &

Julius, D. (2001) Bradykinin and nerve growth factor release the capsaicin receptor from PtdIns(4,5)P2-mediated inhibition. *Nature*. **411** (6840), pp. 957–962.

Chun, Y.H., Park, J.Y., Lee, H., Kim, H.S., Won, S., Joe, H.J., Chung, W.J., Yoon, J., Kim, H.H., Kim, J.T. & Lee, J.S. (2013) Rhinovirus-Infected Epithelial Cells Produce More IL-8 and RANTES Compared With Other Respiratory Viruses. *Allergy, Asthma & Immunology Research*. **5** (4), pp. 216.

Clapham, D.E. (2003) TRP channels as cellular sensors. *Nature*. **426** (December), pp. 517–524.

Clarke, R., Monaghan, K., About, I., Griffin, C.S., Sergeant, G.P., El Karim, I., McGeown, J.G., Cosby, S.L., Curtis, T.M., McGarvey, L.P. & Lundy, F.T. (2017) TRPA1 activation in a human sensory neuronal model: relevance to cough hypersensitivity? *The European respiratory journal*. **50** (3), pp. 1700995.

Cockayne, D.A., Hamilton, S.G., Zhu, Q.M., Dunn, P.M., Zhong, Y., Novakovic, S., Malmberg, A.B., Cain, G., Berson, A., Kassotakis, L., Hedley, L., Lachnit, W.G., Burnstock, G., McMahon, S.B., et al. (2000) Urinary bladder hyporeflexia and reduced pain-related behaviour in P2X3-deficient mice. *Nature*. **407** (6807), pp. 1011–1015.

Colbert, H.A., Smith, T.L. & Bargmann, C.I. (1997) OSM-9, a novel protein with structural similarity to channels, is required for olfaction, mechanosensation, and olfactory adaptation in Caenorhabditis elegans. *The Journal of neuroscience : the official journal of the Society for Neuroscience*. **17** (21), pp. 8259–8269.

Collier, J.G. & Fuller, R.W. (1984) Capsaicin inhalation in man and the effects of sodium cromoglycate. *British journal of pharmacology*. **81** (1), pp. 113–117.

Collo, G., North, R.A., Kawashima, E., Merlo-Pich, E., Neidhart, S., Surprenant, A. & Buell, G. (1996) Cloning OF P2X5 and P2X6 receptors and the distribution and properties of an extended family of ATP-gated ion channels. *The Journal of neuroscience : the official journal of the Society for Neuroscience*. **16** (8), pp. 2495–2507.

Colonno, R.J., Condra, J.H., Mizutani, S., Callahan, P.L., Davies, M.E. & Murcko, M.A. (1988) Evidence for the direct involvement of the rhinovirus canyon in receptor binding. *Proceedings of the National Academy of Sciences of the United States of America*. **85** (15), pp. 5449–5453.

Comstock, A.T., Ganesan, S., Chattoraj, A., Faris, A.N., Margolis, B.L., Hershenson, M.B. & Sajjan, U.S. (2011) Rhinovirus-induced barrier dysfunction in polarized airway epithelial cells is mediated by NADPH oxidase 1. *Journal of virology*. **85** (13), pp. 6795–6808.

Corey, D.P., García-Añoveros, J., Holt, J.R., Kwan, K.Y., Lin, S.-Y., Vollrath, M.A., Amalfitano, A., Cheung, E.L.-M., Derfler, B.H., Duggan, A., Géléoc, G.S.G., Gray, P.A., Hoffman, M.P., Rehm, H.L., et al. (2004) TRPA1 is a candidate for the mechanosensitive transduction channel of vertebrate hair cells. *Nature*. **432** (7018), pp. 723–730.

Cosens, D.J. & Manning, A. (1969) Abnormal electroretinogram from a Drosophila mutant.

Nature. **224** (5216), pp. 285–287.

Curley, F.J., Irwin, R.S., Pratter, M.R., Stivers, D.H., Doern, G. V, Vernaglia, P.A., Larkin, A.B. & Baker, S.P. (1988) Cough and the common cold. *The American review of respiratory disease*. **138** (2), pp. 305–311.

Cvetkov, T.L., Huynh, K.W., Cohen, M.R. & Moiseenkova-Bell, V.Y. (2011) Molecular architecture and subunit organization of TRPA1 ion channel revealed by electron microscopy. *The Journal of biological chemistry*. **286** (44), pp. 38168–38176.

Dakhama, A., Kanehiro, A., Mäkelä, M.J., Loader, J.E., Larsen, G.L. & Gelfand, E.W. (2002) Regulation of airway hyperresponsiveness by calcitonin gene-related peptide in allergen sensitized and challenged mice. *American journal of respiratory and critical care medicine*. **165** (8), pp. 1137–1144.

Dakhama, A., Park, J.-W., Taube, C., El Gazzar, M., Kodama, T., Miyahara, N., Takeda, K., Kanehiro, A., Balhorn, A., Joetham, A., Loader, J.E., Larsen, G.L. & Gelfand, E.W. (2005) Alteration of airway neuropeptide expression and development of airway hyperresponsiveness following respiratory syncytial virus infection. *American journal of physiology. Lung cellular and molecular physiology*. **288** (4), pp. L761-70.

Danthi, P., Tosteson, M., Li, Q.-H. & Chow, M. (2003) Genome delivery and ion channel properties are altered in VP4 mutants of poliovirus. *Journal of virology*. **77** (9), pp. 5266–5274.

Dauletbaev, N., Cammisano, M., Herscovitch, K. & Lands, L.C. (2015) Stimulation of the RIG-I/MAVS Pathway by Polyinosinic:Polycytidylic Acid Upregulates IFN-β in Airway Epithelial Cells with Minimal Costimulation of IL-8. *Journal of immunology (Baltimore, Md. : 1950)*. **195** (6), pp. 2829–2841.

Davis, M.P., Bottley, G., Beales, L.P., Killington, R.A., Rowlands, D.J. & Tuthill, T.J. (2008) Recombinant VP4 of human rhinovirus induces permeability in model membranes. *Journal of virology*. **82** (8), pp. 4169–4174.

Deering-Rice, C.E., Johansen, M.E., Roberts, J.K., Thomas, K.C., Romero, E.G., Lee, J., Yost, G.S., Veranth, J.M. & Reilly, C.A. (2012) Transient Receptor Potential Vanilloid-1 (TRPV1) Is a Mediator of Lung Toxicity for Coal Fly Ash Particulate Material. *Molecular Pharmacology*. **81** (3), pp. 411–419.

Delany, N.S., Hurle, M., Facer, P., Alndaf, T., Plumpton, C., Kinghorn, I., See, C.G., Costigan, M., Anand, P., Woolf, C.J., Crowther, D., Sanseau, P. & Tate, S.N. (2001) Identification and characterization of a novel human vanilloid receptor-like protein, VRL-2. *Physiological Genomics*. **4** (3), pp. 165–174.

Dicpinigaitis, P. V., Tibb, A.S., Ramsey, D.L., Carr, A.N. & Poore, C.L. (2014) Stability of cough reflex sensitivity during viral upper respiratory tract infection (common cold). *Pulmonary Pharmacology & Therapeutics*. **28** (2), pp. 154–157.

Dicpinigaitis, P. V & Alva, R. V (2005) Safety of capsaicin cough challenge testing. *Chest*. **128** (1), pp. 196–202.

Dicpinigaitis, P. V, Bhat, R., Rhoton, W.A., Tibb, A.S. & Negassa, A. (2011) Effect of viral upper respiratory tract infection on the urge-to-cough sensation. *Respiratory*

medicine. **105** (4), pp. 615–618.

Dicpinigaitis, P. V, Spinner, L., Santhyadka, G. & Negassa, A. (2008) Effect of tiotropium on cough reflex sensitivity in acute viral cough. *Lung*. **186** (6), pp. 369–374.

Diekmann, D., Brill, S., Garrett, M.D., Totty, N., Hsuan, J., Monfries, C., Hall, C., Lim, L. & Hall, A. (1991) Bcr encodes a GTPase-activating protein for p21rac. *Nature*. **351** (6325), pp. 400–402.

Ding, S. & Sachs, F. (1999) Ion permeation and block of P2X2 purinoceptors: Single channel recordings. *Journal of Membrane Biology*. **172**pp. 215–223.

Diogenes, A., Ferraz, C.C.R., Akopian, A.N., Henry, M.A. & Hargreaves, K.M. (2011) LPS sensitizes TRPV1 via activation of TLR4 in trigeminal sensory neurons. *Journal of dental research*. **90** (6), pp. 759–764.

Doerner, J.F., Gisselmann, G., Hatt, H. & Wetzel, C.H. (2007) Transient receptor potential channel A1 is directly gated by calcium ions. *The Journal of biological chemistry*. **282** (18), pp. 13180–13189.

Dunham, J.P., Kelly, S. & Donaldson, L.F. (2008) Inflammation reduces mechanical thresholds in a population of transient receptor potential channel A1-expressing nociceptors in the rat. *The European journal of neuroscience*. **27** (12), pp. 3151–3160.

Durham, P.L. (2006) Calcitonin gene-related peptide (CGRP) and migraine. *Headache*. **46 Suppl 1**pp. S3-8.

Eccles, R. (2005) Understanding the symptoms of the common cold and influenza. *The Lancet. Infectious diseases*. **5** (11), pp. 718–725.

Eccles, R. & Lee, P.C.L. (2004) Cough induced by airway vibration as a model of airway hyperreactivity in patients with acute upper respiratory tract infection. *Pulmonary Pharmacology & Therapeutics*. **17** (6), pp. 337–342.

Eccles, R., Loose, I., Jawad, M. & Nyman, L. (2003) Effects of acetylsalicylic acid on sore throat pain and other pain symptoms associated with acute upper respiratory tract infection. *Pain medicine (Malden, Mass.)*. **4** (2), pp. 118–124.

Eccles, R., Morris, S. & Jawad, M. (1992) Lack of effect of codeine in the treatment of cough associated with acute upper respiratory tract infection. *Journal of clinical pharmacy and therapeutics*. **17** (3), pp. 175–180.

Egan, T.M. & Khakh, B.S. (2004) Contribution of calcium ions to P2X channel responses. *The Journal of neuroscience : the official journal of the Society for Neuroscience*. **24** (13), pp. 3413–3420.

El-Hashim, A.Z. & Amine, S.A. (2005) The role of substance P and bradykinin in the cough reflex and bronchoconstriction in guinea-pigs. *European journal of pharmacology*. **513** (1–2), pp. 125–133.

El-Hashim, A.Z. & Jaffal, S.M. (2009) Nerve growth factor enhances cough and airway obstruction via TrkA receptor- and TRPV1-dependent mechanisms. *Thorax*. **64** (9), pp. 791–797.

El-Hashim, A.Z., Jaffal, S.M., Al-Rashidi, F.T., Luqmani, Y.A. & Akhtar, S. (2013) Nerve growth factor enhances cough via a central mechanism of action. *Pharmacological research : the official journal of the Italian Pharmacological Society*. **74**pp. 68–77.

Empey, D.W., Laitinen, L.A., Jacobs, L., Gold, W.M. & Nadel, J.A. (1976) Mechanisms of bronchial hyperreactivity in normal subjects after upper respiratory tract infection. *The American review of respiratory disease*. **113** (2), pp. 131–139.

Etienne-Manneville, S. & Hall, A. (2002) Rho GTPases in cell biology. *Nature*. **420** (6916), pp. 629–635.

Evans, C.M., Fryer, A.D., Jacoby, D.B., Gleich, G.J. & Costello, R.W. (1997) Pretreatment with antibody to eosinophil major basic protein prevents hyperresponsiveness by protecting neuronal M2 muscarinic receptors in antigen-challenged guinea pigs. *The Journal of clinical investigation*. **100** (9), pp. 2254–2262.

Evengard, B., Nilsson, C.G., Lindh, G., Lindquist, L., Eneroth, P., Fredrikson, S., Terenius, L. & Henriksson, K.G. (1998) Chronic fatigue syndrome differs from fibromyalgia. No evidence for elevated substance P levels in cerebrospinal fluid of patients with chronic fatigue syndrome. *Pain*. **78** (2), pp. 153–155.

Van Eyk, J.E., Arrell, D.K., Foster, D.B., Strauss, J.D., Heinonen, T.Y.K., Furmaniak-Kazmierczak, E., Côté, G.P. & Mak, A.S. (1998) Different Molecular Mechanisms for Rho Family GTPase-dependent, Ca2+-independent Contraction of Smooth Muscle. *Journal of Biological Chemistry*. **273** (36), pp. 23433–23439.

Falzoni, S., Munerati, M., Ferrari, D., Spisani, S., Moretti, S. & Di Virgilio, F. (1995) The purinergic P2Z receptor of human macrophage cells. Characterization and possible physiological role. *Journal of Clinical Investigation*. **95** (3), pp. 1207–1216.

Farina, C., Krumbholz, M., Giese, T., Hartmann, G., Aloisi, F. & Meinl, E. (2005) Preferential expression and function of Toll-like receptor 3 in human astrocytes. *Journal of Neuroimmunology*. **159** (1–2), pp. 12–19.

Fernandes, E.S., Vong, C.T., Quek, S., Cheong, J., Awal, S., Gentry, C., Aubdool, A.A., Liang, L., Bodkin, J. V., Bevan, S., Heads, R. & Brain, S.D. (2013) Superoxide generation and leukocyte accumulation: key elements in the mediation of leukotriene B_4 -induced itch by transient receptor potential ankyrin 1 and transient receptor potential vanilloid 1. *The FASEB Journal*. **27** (4), pp. 1664–1673.

Fernandes, J., Lorenzo, I.M., Andrade, Y.N., Garcia-Elias, A., Serra, S.A., Fernández-Fernández, J.M. & Valverde, M.A. (2008) IP3 sensitizes TRPV4 channel to the mechano- and osmotransducing messenger 5'-6'-epoxyeicosatrienoic acid. *The Journal of general physiology*. **131** (5), pp. i2.

Fernández-Fernández, J.M., Andrade, Y.N., Arniges, M., Fernandes, J., Plata, C., Rubio-Moscardo, F., Vázquez, E. & Valverde, M.A. (2008) Functional coupling of TRPV4 cationic channel and large conductance, calcium-dependent potassium channel in human bronchial epithelial cell lines. *Pflügers Archiv : European journal of physiology*. **457** (1), pp. 149–159.

Ferrandiz-Huertas, C., Mathivanan, S., Wolf, C.J., Devesa, I. & Ferrer-Montiel, A. (2014)

Trafficking of ThermoTRP Channels. *Membranes*. **4** (3), pp. 525–564.

Flynn, P., Mellor, H., Casamassima, A. & Parker, P.J. (2000) Rho GTPase control of protein kinase C-related protein kinase activation by 3-phosphoinositide-dependent protein kinase. *The Journal of biological chemistry*. **275** (15), pp. 11064–11070.

Foster, R., Hu, K.Q., Lu, Y., Nolan, K.M., Thissen, J. & Settleman, J. (1996) Identification of a novel human Rho protein with unusual properties: GTPase deficiency and in vivo farnesylation. *Molecular and cellular biology*. **16** (6), pp. 2689–2699.

Fowles, H.E., Rowland, T., Wright, C. & Morice, A. (2017) Tussive challenge with ATP and AMP: does it reveal cough hypersensitivity? *European Respiratory Journal*. **49** (2), pp. 1601452.

Fox, A.J., Lalloo, U.G., Belvisi, M.G., Bernareggi, M., Chung, K.F. & Barnes, P.J. (1996) Bradykinin-evoked sensitization of airway sensory nerves: a mechanism for ACE-inhibitor cough. *Nature medicine*. **2** (7), pp. 814–817.

Fryer, A.D. & Maclagan, J. (1984) Muscarinic inhibitory receptors in pulmonary parasympathetic nerves in the guinea-pig. *British journal of pharmacology*. **83** (4), pp. 973–978.

Gamarnik, A. V & Andino, R. (1998) Switch from translation to RNA replication in a positive-stranded RNA virus. *Genes & development*. **12** (15), pp. 2293–2304.

Ganju, P., O'Bryan, J.P., Der, C., Winter, J. & James, I.F. (1998) Differential regulation of SHC proteins by nerve growth factor in sensory neurons and PC12 cells. *The European journal of neuroscience*. **10** (6), pp. 1995–2008.

Gao, X., Wu, L. & O'Neil, R.G. (2003) Temperature-modulated diversity of TRPV4 channel gating: activation by physical stresses and phorbol ester derivatives through protein kinase C-dependent and -independent pathways. *The Journal of biological chemistry*. **278** (29), pp. 27129–27137.

García-Martínez, C., Morenilla-Palao, C., Planells-Cases, R., Merino, J.M. & Ferrer-Montiel, A. (2000) Identification of an aspartic residue in the P-loop of the vanilloid receptor that modulates pore properties. *The Journal of biological chemistry*. **275** (42), pp. 32552–32558.

Garcia-Sanz, N., Fernández-Carvajal, A., Morenilla-Palao, C., Planells-Cases, R., Fajardo-Sánchez, E., Fernández-Ballester, G. & Ferrer-Montiel, A. (2004) Identification of a Tetramerization Domain in the C Terminus of the Vanilloid Receptor. *Journal of Neuroscience*. **24** (23), pp. 5307–5314.

Garcia, J.G.N., Verin, A.D., Schaphorst, K., Siddiqui, R., Patterson, C.E., Csortos, C. & Natarajan, V. (1999) Regulation of endothelial cell myosin light chain kinase by Rho, cortactin, and p60 ^{src}. *American Journal of Physiology-Lung Cellular and Molecular Physiology*. **276** (6), pp. L989–L998.

Garrett, M.D., Self, A.J., van Oers, C. & Hall, A. (1989) Identification of distinct cytoplasmic targets for ras/R-ras and rho regulatory proteins. *The Journal of biological chemistry*. **264** (1), pp. 10–13.

Gavett, S.H. & Wills-Karp, M. (1993) Elevated lung G protein levels and muscarinic receptor affinity in a mouse model of airway hyperreactivity. *The American journal of physiology*. **265** (5 Pt 1), pp. L493-500.

Gentile, D.A. & Skoner, D.P. (2001) Viral rhinitis. *Current Allergy and Asthma Reports*. **1** (3), pp. 227–234.

Gerrard, J.W., Cockcroft, D.W., Mink, J.T., Cotton, D.J., Poonawala, R. & Dosman, J.A. (1980) Increased nonspecific bronchial reactivity in cigarette smokers with normal lung function. *The American review of respiratory disease*. **122** (4), pp. 577–581.

Gever, J.R., Soto, R., Henningsen, R. a., Martin, R.S., Hackos, D.H., Panicker, S., Rubas, W., Oglesby, I.B., Dillon, M.P., Milla, M.E., Burnstock, G. & Ford, A.P.D.W. (2010) AF-353, a novel, potent and orally bioavailable P2X3/P2X2/3 receptor antagonist. *British Journal of Pharmacology*. **160** (March 2009), pp. 1387–1398.

Gombedza, F., Kondeti, V., Al-Azzam, N., Koppes, S., Duah, E., Patil, P., Hexter, M., Phillips, D., Thodeti, C.K. & Paruchuri, S. (2017) Mechanosensitive transient receptor potential vanilloid 4 regulates *Dermatophagoides farinae* –induced airway remodeling *via* 2 distinct pathways modulating matrix synthesis and degradation. *The FASEB Journal*. **31** (4), pp. 1556–1570.

Gorina, S. & Pavletich, N.P. (1996) Structure of the p53 tumor suppressor bound to the ankyrin and SH3 domains of 53BP2. *Science (New York, N.Y.)*. **274** (5289), pp. 1001–1005.

Gosens, R., Zaagsma, J., Meurs, H. & Halayko, A.J. (2006) Muscarinic receptor signaling in the pathophysiology of asthma and COPD. *Respiratory research*. **7** (1), pp. 73.

Grace, M., Birrell, M.A., Dubuis, E., Maher, S.A. & Belvisi, M.G. (2012) Transient receptor potential channels mediate the tussive response to prostaglandin E2 and bradykinin. *Thorax*. **67** (10), pp. 891–900.

Grace, M.S., Baxter, M., Dubuis, E., Birrell, M. a. & Belvisi, M.G. (2014) Transient receptor potential (TRP) channels in the airway: Role in airway disease. *British Journal of Pharmacology*. **171**pp. 2593–2607.

Grace, M.S., Dubuis, E., Birrell, M.A. & Belvisi, M.G. (2013) Pre-clinical studies in cough research: role of Transient Receptor Potential (TRP) channels. *Pulmonary pharmacology & therapeutics*. **26** (5), pp. 498–507.

Greiller, C.L., Suri, R., Jolliffe, D.A., Kebadze, T., Hirsman, A.G., Griffiths, C.J., Johnston, S.L. & Martineau, A.R. (2018) Vitamin D attenuates rhinovirus-induced expression of intercellular adhesion molecule-1 (ICAM-1) and platelet-activating factor receptor (PAFR) in respiratory epithelial cells. *The Journal of Steroid Biochemistry and Molecular Biology*.

Groneberg, D.A., Niimi, A., Dinh, Q.T., Cosio, B., Hew, M., Fischer, A. & Chung, K.F. (2004) Increased expression of transient receptor potential vanilloid-1 in airway nerves of chronic cough. *American journal of respiratory and critical care medicine*. **170** (12), pp. 1276–1280.

Grünberg, K., Timmers, M.C., Smits, H.H., de Klerk, E.P., Dick, E.C., Spaan, W.J., Hiemstra,

P.S. & Sterk, P.J. (1997) Effect of experimental rhinovirus 16 colds on airway hyperresponsiveness to histamine and interleukin-8 in nasal lavage in asthmatic subjects in vivo. *Clinical and experimental allergy : journal of the British Society for Allergy and Clinical Immunology*. **27** (1), pp. 36–45.

Grunert, H.P., Wolf, K.U., Langner, K.D., Sawitzky, D., Habermehl, K.O. & Zeichhardt, H. (1997) Internalization of human rhinovirus 14 into HeLa and ICAM-1-transfected BHK cells. *Medical microbiology and immunology*. **186** (1), pp. 1–9.

Grygorczyk, R., Furuya, K. & Sokabe, M. (2013) Imaging and characterization of stretch-induced ATP release from alveolar A549 cells. *The Journal of physiology*. **591** (5), pp. 1195–1215.

Gualdoni, G.A., Mayer, K.A., Kapsch, A.-M., Kreuzberg, K., Puck, A., Kienzl, P., Oberndorfer, F., Frühwirth, K., Winkler, S., Blaas, D., Zlabinger, G.J. & Stöckl, J. (2018) Rhinovirus induces an anabolic reprogramming in host cell metabolism essential for viral replication. *Proceedings of the National Academy of Sciences of the United States of America*. **115** (30), pp. E7158–E7165.

Gum, R.J., Wakefield, B. & Jarvis, M.F. (2012) P2X receptor antagonists for pain management: examination of binding and physicochemical properties. *Purinergic signalling*. **8** (Suppl 1), pp. 41–56.

Guo, A., Vulchanova, L., Wang, J., Li, X. & Elde, R. (1999) Immunocytochemical localization of the vanilloid receptor 1 (VR1): relationship to neuropeptides, the P2X3 purinoceptor and IB4 binding sites. *The European journal of neuroscience*. **11** (3), pp. 946–958.

Gwaltney, Jr., J.M., Hendley, J.O. & Patrie, J.T. (2003) Symptom Severity Patterns in Experimental Common Colds and Their Usefulness in Timing Onset of Illness in Natural Colds. *Clinical Infectious Diseases*. **36** (6), pp. 714–723.

Gwaltney, J.M., Hendley, J.O., Simon, G. & Jordan, W.S. (1966) Rhinovirus Infections in an Industrial Population. *New England Journal of Medicine*. **275** (23), pp. 1261–1268.

Gwaltney, J.M., Hendley, J.O., Simon, G. & Jordan, W.S. (1967) Rhinovirus Infections in an Industrial Population. *JAMA*. **202** (6), pp. 494.

Hadfield, a T., Lee, W.M., Zhao, R., Oliveira, M. a, Minor, I., Rueckert, R.R. & Rossmann, M.G. (1997) The refined structure of human rhinovirus 16 at 2.15 A resolution: implications for the viral life cycle. *Structure (London, England : 1993)*. **5**pp. 427–441.

Hamel, B., Monaghan-Benson, E., Rojas, R.J., Temple, B.R.S., Marston, D.J., Burridge, K. & Sondek, J. (2011) SmgGDS Is a Guanine Nucleotide Exchange Factor That Specifically Activates RhoA and RhoC. *Journal of Biological Chemistry*. **286** (14), pp. 12141–12148.

Hammarström, S. (1983) Leukotrienes. *Annual review of biochemistry*. **52**pp. 355–377.

Hanácek, J., Davies, A. & Widdicombe, J.G. (1984) Influence of lung stretch receptors on the cough reflex in rabbits. *Respiration; international review of thoracic diseases*. **45** (3), pp. 161–168.

Hayes, P., Meadows, H.J., Gunthorpe, M.J., Harries, M.H., Duckworth, D.M., Cairns, W., Harrison, D.C., Clarke, C.E., Ellington, K., Prinjha, R.K., Barton, A.J.L., Medhurst, A.D., Smith, G.D., Topp, S., et al. (2000) Cloning and functional expression of a human orthologue of rat vanilloid receptor-1. *Pain*. **88** (2), pp. 205–215.

Hazama, A., Hayashi, S. & Okada, Y. (1998) Cell surface measurements of ATP release from single pancreatic beta cells using a novel biosensor technique. *Pflugers Archiv : European journal of physiology*. **437** (1), pp. 31–35.

Hede, S.E., Amstrup, J., Christoffersen, B.C. & Novak, I. (1999) Purinoceptors evoke different electrophysiological responses in pancreatic ducts. P2Y inhibits K(+) conductance, and P2X stimulates cation conductance. *The Journal of biological chemistry*. **274** (45), pp. 31784–31791.

Heikkinen, T. & Järvinen, A. (2003) The common cold. *The Lancet*. **361** (9351), pp. 51–59.

Hellwig, N., Albrecht, N., Harteneck, C., Schultz, G. & Schaefer, M. (2005) Homo- and heteromeric assembly of TRPV channel subunits. *Journal of cell science*. **118** (Pt 5), pp. 917–928.

Hermes, S.M., Andresen, M.C. & Aicher, S.A. (2016) Localization of TRPV1 and P2X3 in unmyelinated and myelinated vagal afferents in the rat. *Journal of chemical neuroanatomy*. **72**pp. 1–7.

Herold, J. & Andino, R. (2001) Poliovirus RNA replication requires genome circularization through a protein-protein bridge. *Molecular cell*. **7** (3), pp. 581–591.

Hewat, E.A. & Blaas, D. (2004) Cryoelectron microscopy analysis of the structural changes associated with human rhinovirus type 14 uncoating. *Journal of virology*. **78** (6), pp. 2935–2942.

Hewat, E.A., Neumann, E., Conway, J.F., Moser, R., Ronacher, B., Marlovits, T.C. & Blaas, D. (2000) The cellular receptor to human rhinovirus 2 binds around the 5-fold axis and not in the canyon: a structural view. *The EMBO journal*. **19** (23), pp. 6317–6325.

Hewson, C.A., Haas, J.J., Bartlett, N.W., Message, S.D., Laza-Stanca, V., Kebadze, T., Caramori, G., Zhu, J., Edbrooke, M.R., Stanciu, L.A., Kon, O.M., Papi, A., Jeffery, P.K., Edwards, M.R., et al. (2010) Rhinovirus induces MUC5AC in a human infection model and in vitro via NF-κB and EGFR pathways. *The European respiratory journal*. **36** (6), pp. 1425–1435.

Hewson, C.A., Jardine, A., Edwards, M.R., Laza-Stanca, V. & Johnston, S.L. (2005) Toll-like receptor 3 is induced by and mediates antiviral activity against rhinovirus infection of human bronchial epithelial cells. *Journal of virology*. **79** (19), pp. 12273–12279.

Hinman, A., Chuang, H.-H., Bautista, D.M. & Julius, D. (2006) TRP channel activation by reversible covalent modification. *Proceedings of the National Academy of Sciences of the United States of America*. **103** (51), pp. 19564–19568.

Hiraoka, K., Kaibuchi, K., Ando, S., Musha, T., Takaishi, K., Mizuno, T., Asada, M., Ménard, L., Tomhave, E. & Didsbury, J. (1992) Both stimulatory and inhibitory GDP/GTP exchange proteins, smg GDS and rho GDI, are active on multiple small GTP-binding proteins. *Biochemical and biophysical research communications*. **182** (2), pp. 921–

930.

Hisamatsu, K., Ganbo, T., Nakazawa, T., Murakami, Y., Gleich, G.J., Makiyama, K. & Koyama, H. (1990) Cytotoxicity of human eosinophil granule major basic protein to human nasal sinus mucosa in vitro. *The Journal of allergy and clinical immunology*. **86** (1), pp. 52–63.

Hofer, F., Gruenberger, M., Kowalski, H., Machat, H., Huettinger, M., Kuechler, E. & Blaas, D. (1994) Members of the low density lipoprotein receptor family mediate cell entry of a minor-group common cold virus. *Proceedings of the National Academy of Sciences of the United States of America*. **91** (5), pp. 1839–1842.

Hogan, S.P., Rosenberg, H.F., Moqbel, R., Phipps, S., Foster, P.S., Lacy, P., Kay, A.B. & Rothenberg, M.E. (2008) Eosinophils: biological properties and role in health and disease. *Clinical and experimental allergy : journal of the British Society for Allergy and Clinical Immunology*. **38** (5), pp. 709–750.

Holzer, P. (1998) Neurogenic vasodilatation and plasma leakage in the skin. *General pharmacology*. **30** (1), pp. 5–11.

Howard, J. & Bechstedt, S. (2004) Hypothesis: A helix of ankyrin repeats of the NOMPC-TRP ion channel is the gating spring of mechanoreceptors. *Current Biology*. **14** (6), pp. R224–R226.

Hu, H., Tian, J., Zhu, Y., Wang, C., Xiao, R., Herz, J.M., Wood, J.D. & Zhu, M.X. (2010) Activation of TRPA1 channels by fenamate nonsteroidal anti-inflammatory drugs. *Pflugers Archiv European Journal of Physiology*. **459**pp. 579–592.

Hua, X.-Y., Chen, P., Fox, A. & Myers, R.R. (1996) Involvement of Cytokines in Lipopolysaccharide-Induced Facilitation of CGRP Release from Capsaicin-Sensitive Nerves in the Trachea: Studies with Interleukin-1beta and Tumor Necrosis Factor-alpha. *J. Neurosci.* **16** (15), pp. 4742–4748.

Huber, M., Brabec, M., Bayer, N., Blaas, D. & Fuchs, R. (2001) Elevated endosomal pH in HeLa cells overexpressing mutant dynamin can affect infection by pH-sensitive viruses. *Traffic (Copenhagen, Denmark)*. **2** (10), pp. 727–736.

Hughes, J.H., Thomas, D.C., Hamparian, V. V & Cramblett, H.G. (1973) Acid liability of rhinovirus type 14: effect of pH, time, and temperature. *Proceedings of the Society for Experimental Biology and Medicine. Society for Experimental Biology and Medicine (New York, N.Y.)*. **144** (2), pp. 555–560.

Hunter, D.D., Myers, A.C. & Undem, B.J. (2000) Nerve growth factor-induced phenotypic switch in guinea pig airway sensory neurons. *American journal of respiratory and critical care medicine*. **161** (6), pp. 1985–1990.

Hunter, I., Cobban, H.J., Vandenabeele, P., MacEwan, D.J. & Nixon, G.F. (2003) Tumor necrosis factor-alpha-induced activation of RhoA in airway smooth muscle cells: role in the Ca2+ sensitization of myosin light chain20 phosphorylation. *Molecular pharmacology*. **63** (3), pp. 714–721.

Iglesias, R., Locovei, S., Roque, A., Alberto, A.P., Dahl, G., Spray, D.C. & Scemes, E. (2008) P2X7 receptor-Pannexin1 complex: pharmacology and signaling. *American journal of*

physiology. Cell physiology. **295** (3), pp. C752-60.

Iizuka, K., Yoshii, A., Samizo, K., Tsukagoshi, H., Ishizuka, T., Dobashi, K., Nakazawa, T. & Mori, M. (1999) A major role for the Rho-associated coiled coil forming protein kinase in G-protein-mediated Ca $^{2+}$ sensitization through inhibition of myosin phosphatase in rabbit trachea. *British Journal of Pharmacology*. **128** (4), pp. 925–933.

Inoue, D., Yamaya, M., Kubo, H., Sasaki, T., Hosoda, M., Numasaki, M., Tomioka, Y., Yasuda, H., Sekizawa, K., Nishimura, H. & Sasaki, H. (2006) Mechanisms of mucin production by rhinovirus infection in cultured human airway epithelial cells. *Respiratory physiology & neurobiology*. **154** (3), pp. 484–499.

Inoue, K., Koizumi, S., Fuziwara, S., Denda, S., Inoue, K. & Denda, M. (2002) Functional Vanilloid Receptors in Cultured Normal Human Epidermal Keratinocytes. *Biochemical and Biophysical Research Communications*. **291** (1), pp. 124–129.

Irwin, R.S., Baumann, M.H., Bolser, D.C., Boulet, L.-P., Braman, S.S., Brightling, C.E., Brown, K.K., Canning, B.J., Chang, A.B., Dicpinigaitis, P. V, Eccles, R., Glomb, W.B., Goldstein, L.B., Graham, L.M., et al. (2006) Diagnosis and management of cough executive summary: ACCP evidence-based clinical practice guidelines. *Chest*. **129** (1 Suppl), pp. 1S–23S.

Irwin, R.S., French, C.L., Chang, A.B., Altman, K.W., Adams, T.M., Altman, K.W., Azoulay, E., Barker, A.F., Birring, S.S., Blackhall, F., Bolser, D.C., Boulet, L.-P., Brightling, C., Callahan-Lyon, P., et al. (2018) Classification of Cough as a Symptom in Adults and Management Algorithms. *Chest*. **153** (1), pp. 196–209.

Irwin, R.S., Madison, J.M. & Fraire, A.E. (2000) The cough reflex and its relation to gastroesophageal reflux. *The American journal of medicine*. **108 Suppl 4a**pp. 73S–78S.

Ishihara, H., Shimura, S., Satoh, M., Masuda, T., Nonaka, H., Kase, H., Sasaki, T., Sasaki, H., Takishima, T. & Tamura, K. (1992) Muscarinic receptor subtypes in feline tracheal submucosal gland secretion. *The American journal of physiology*. **262** (2 Pt 1), pp. L223-8.

Iwase, N., Sasaki, T., Oshiro, T., Tamada, T., Nara, M., Sasamori, K., Hattori, T., Shirato, K. & Maruyama, Y. (2002) Differential effect of epidermal growth factor on serous and mucous cells in porcine airway submucosal gland. *Respiratory physiology & neurobiology*. **132** (3), pp. 307–319.

Jacoby, D.B. (2004) Pathophysiology of airway viral infections. *Pulmonary pharmacology & therapeutics*. **17** (6), pp. 333–336.

Jacoby, D.B., Xiao, H.Q., Lee, N.H., Chan-Li, Y. & Fryer, A.D. (1998) Virus- and interferon-induced loss of inhibitory M2 muscarinic receptor function and gene expression in cultured airway parasympathetic neurons. *The Journal of clinical investigation*. **102** (1), pp. 242–248.

Jacoby, D.B., Yost, B.L., Kumaravel, B., Chan-Li, Y., Xiao, H.Q., Kawashima, K. & Fryer, A.D. (2001) Glucocorticoid treatment increases inhibitory m(2) muscarinic receptor

expression and function in the airways. *American journal of respiratory cell and molecular biology*. **24** (4), pp. 485–491.

Jancsó, N., Jancsó-Gábor, A. & Szolcsányi, J. (1967) Direct evidence for neurogenic inflammation and its prevention by denervation and by pretreatment with capsaicin. *British journal of pharmacology and chemotherapy*. **31** (1), pp. 138–151.

Jang, S.K., Kräusslich, H.G., Nicklin, M.J., Duke, G.M., Palmenberg, A.C. & Wimmer, E. (1988) A segment of the 5' nontranslated region of encephalomyocarditis virus RNA directs internal entry of ribosomes during in vitro translation. *Journal of virology*. **62** (8), pp. 2636–2643.

Jang, Y.J., Kwon, H.-J. & Lee, B.-J. (2006) Effect of clarithromycin on rhinovirus-16 infection in A549 cells. *The European respiratory journal*. **27** (1), pp. 12–19.

Jardín, I., López, J.J., Diez, R., Sánchez-Collado, J., Cantonero, C., Albarrán, L., Woodard, G.E., Redondo, P.C., Salido, G.M., Smani, T. & Rosado, J.A. (2017) TRPs in Pain Sensation. *Frontiers in Physiology*. **8**pp. 392.

Jartti, T., Lee, W.-M., Pappas, T., Evans, M., Lemanske, R.F. & Gern, J.E. (2008) Serial viral infections in infants with recurrent respiratory illnesses. *The European respiratory journal*. **32** (2), pp. 314–320.

Jia, Y., Wang, X., Varty, L., Rizzo, C.A., Yang, R., Correll, C.C., Phelps, P.T., Egan, R.W. & Hey, J.A. (2004) Functional TRPV4 channels are expressed in human airway smooth muscle cells. *American journal of physiology. Lung cellular and molecular physiology*. **287** (2), pp. L272-8.

Jiang, L.-H., Kim, M., Spelta, V., Bo, X., Surprenant, A. & North, R.A. (2003) Subunit arrangement in P2X receptors. *The Journal of neuroscience : the official journal of the Society for Neuroscience*. **23** (26), pp. 8903–8910.

Jiang, L.-H., Rassendren, F., Mackenzie, A., Zhang, Y.-H., Surprenant, A. & North, R.A. (2005) N-methyl-D-glucamine and propidium dyes utilize different permeation pathways at rat P2X(7) receptors. *American journal of physiology. Cell physiology*. **289** (5), pp. C1295-302.

Jo, A.O., Ryskamp, D.A., Phuong, T.T.T., Verkman, A.S., Yarishkin, O., MacAulay, N. & Križaj, D. (2015) TRPV4 and AQP4 Channels Synergistically Regulate Cell Volume and Calcium Homeostasis in Retinal Müller Glia. *The Journal of neuroscience : the official journal of the Society for Neuroscience*. **35** (39), pp. 13525–13537.

Johnston, S.L. (2007) Innate immunity in the pathogenesis of virus-induced asthma exacerbations. *Proceedings of the American Thoracic Society*. **4** (3), pp. 267–270.

Johnston, S.L. (2005) Overview of virus-induced airway disease. *Proceedings of the American Thoracic Society*. **2** (2), pp. 150–156.

Johnston, S.L., Papi, a, Bates, P.J., Mastronarde, J.G., Monick, M.M. & Hunninghake, G.W. (1998) Low grade rhinovirus infection induces a prolonged release of IL-8 in pulmonary epithelium. *Journal of immunology (Baltimore, Md. : 1950)*. **160**pp. 6172–6181.

Johnston, S.L., Pattemore, P.K., Sanderson, G., Smith, S., Lampe, F., Josephs, L., Symington, P., O'Toole, S., Myint, S.H. & Tyrrell, D.A. (1995) Community study of role of viral infections in exacerbations of asthma in 9-11 year old children. *BMJ (Clinical research ed.)*. **310** (6989), pp. 1225–1229.

Jones, B.F. & Stewart, M.A. (2002) Duration of cough in acute upper respiratory tract infections. *Australian family physician*. **31** (10), pp. 971–973.

Joos, G.F., Germonpre, P.R., Kips, J.C., Peleman, R.A. & Pauwels, R.A. (1994) Sensory neuropeptides and the human lower airways: present state and future directions. *The European respiratory journal*. **7** (6), pp. 1161–1171.

Jordt, S.-E., Bautista, D.M., Chuang, H.-H., McKemy, D.D., Zygmunt, P.M., Högestätt, E.D., Meng, I.D. & Julius, D. (2004) Mustard oils and cannabinoids excite sensory nerve fibres through the TRP channel ANKTM1. *Nature*. **427** (January), pp. 260–265.

Jordt, S.E., Tominaga, M. & Julius, D. (2000) Acid potentiation of the capsaicin receptor determined by a key extracellular site. *Proceedings of the National Academy of Sciences of the United States of America*. **97** (14), pp. 8134–8139.

Julius, D. (2013) TRP channels and pain. *Annual review of cell and developmental biology*. **29**pp. 355–384.

Jung, J., Hwang, S.W., Kwak, J., Lee, S.Y., Kang, C.J., Kim, W.B., Kim, D. & Oh, U. (1999) Capsaicin binds to the intracellular domain of the capsaicin-activated ion channel. *The Journal of neuroscience : the official journal of the Society for Neuroscience*. **19** (2), pp. 529–538.

Jung, J., Shin, J.S., Lee, S.-Y., Hwang, S.W., Koo, J., Cho, H. & Oh, U. (2004) Phosphorylation of Vanilloid Receptor 1 by Ca^{2+} /Calmodulin-dependent Kinase II Regulates Its Vanilloid Binding. *Journal of Biological Chemistry*. **279** (8), pp. 7048–7054.

Kaan, T.K.Y., Yip, P.K., Grist, J., Cefalu, J.S., Nunn, P.A., Ford, A.P.D.W., Zhong, Y. & McMahon, S.B. (2010) Endogenous purinergic control of bladder activity via presynaptic P2X3 and P2X2/3 receptors in the spinal cord. *The Journal of neuroscience : the official journal of the Society for Neuroscience*. **30** (12), pp. 4503–4507.

Kahn, R.A., Kern, F.G., Clark, J., Gelmann, E.P. & Rulka, C. (1991) Human ADP-ribosylation factors. A functionally conserved family of GTP-binding proteins. *The Journal of biological chemistry*. **266** (4), pp. 2606–2614.

Kainulainen, L., Vuorinen, T., Rantakokko-Jalava, K., Osterback, R. & Ruuskanen, O. (2010) Recurrent and persistent respiratory tract viral infections in patients with primary hypogammaglobulinemia. *The Journal of allergy and clinical immunology*. **126** (1), pp. 120–126.

Kaiser, L., Aubert, J.-D., Pache, J.-C., Deffernez, C., Rochat, T., Garbino, J., Wunderli, W., Meylan, P., Yerly, S., Perrin, L., Letovanec, I., Nicod, L., Tapparel, C. & Soccal, P.M. (2006) Chronic Rhinoviral Infection in Lung Transplant Recipients. *American Journal of Respiratory and Critical Care Medicine*. **174** (12), pp. 1392–1399.

Kamei, J. & Takahashi, Y. (2006) Involvement of ionotropic purinergic receptors in the

histamine-induced enhancement of the cough reflex sensitivity in guinea pigs. *European journal of pharmacology*. **547** (1–3), pp. 160–164.

Kamei, J., Takahashi, Y., Yoshikawa, Y. & Saitoh, A. (2005) Involvement of P2X receptor subtypes in ATP-induced enhancement of the cough reflex sensitivity. *European journal of pharmacology*. **528** (1–3), pp. 158–161.

Kanno, H., Horikawa, Y., Hodges, R.R., Zoukhri, D., Shatos, M.A., Rios, J.D. & Dartt, D.A. (2002) Cholinergic agonists transactivate EGFR and stimulate MAPK to induce goblet cell secretion. *AJP: Cell Physiology*. **284** (4), pp. C988–C998.

Karashima, Y., Damann, N., Prenen, J., Talavera, K., Segal, A., Voets, T. & Nilius, B. (2007) Bimodal action of menthol on the transient receptor potential channel TRPA1. *The Journal of neuroscience : the official journal of the Society for Neuroscience*. **27** (37), pp. 9874–9884.

Karashima, Y., Prenen, J., Meseguer, V., Owsianik, G., Voets, T. & Nilius, B. (2008) Modulation of the transient receptor potential channel TRPA1 by phosphatidylinositol 4,5-biphosphate manipulators. *Pflugers Archiv European Journal of Physiology*. **457**pp. 77–89.

Karlsson, J.A. & Fuller, R.W. (1999) Pharmacological regulation of the cough reflex--from experimental models to antitussive effects in Man. *Pulmonary pharmacology & therapeutics*. **12** (4), pp. 215–228.

Katsumata, U., Sekizawa, K., Inoue, H., Sasaki, H. & Takishima, T. (1989) Inhibitory actions of procaterol, a beta-2 stimulant, on substance P-induced cough in normal subjects during upper respiratory tract infection. *The Tohoku journal of experimental medicine*. **158** (1), pp. 105–106.

Kaul, P., Biagioli, M.C., Singh, I. & Turner, R.B. (2000) Rhinovirus-induced oxidative stress and interleukin-8 elaboration involves p47-phox but is independent of attachment to intercellular adhesion molecule-1 and viral replication. *The Journal of infectious diseases*. **181** (6), pp. 1885–1890.

Kawai, T., Takahashi, K., Sato, S., Coban, C., Kumar, H., Kato, H., Ishii, K.J., Takeuchi, O. & Akira, S. (2005) IPS-1, an adaptor triggering RIG-I- and Mda5-mediated type I interferon induction. *Nature immunology*. **6** (10), pp. 981–988.

Kedei, N., Szabo, T., Lile, J.D., Treanor, J.J., Olah, Z., Iadarola, M.J. & Blumberg, P.M. (2001) Analysis of the native quaternary structure of vanilloid receptor 1. *The Journal of biological chemistry*. **276** (30), pp. 28613–28619.

Keller, J., Schmidt, M., Hussein, B., Rümenapp, U. & Jakobs, K.H. (1997) Muscarinic receptor-stimulated cytosol-membrane translocation of RhoA. *FEBS letters*. **403** (3), pp. 299–302.

Kerstein, P.C., del Camino, D., Moran, M.M. & Stucky, C.L. (2009) Pharmacological blockade of TRPA1 inhibits mechanical firing in nociceptors. *Molecular pain*. **5**pp. 19.

Khakh, B.S., Bao, X.R., Labarca, C. & Lester, H. a (1999) Neuronal P2X transmitter-gated cation channels change their ion selectivity in seconds. *Nature neuroscience*. **2** (4), pp. 322–330.

Khalid, S., Murdoch, R., Newlands, A., Smart, K., Kelsall, A., Holt, K., Dockry, R., Woodcock, A. & Smith, J.A. (2014) Transient receptor potential vanilloid 1 (TRPV1) antagonism in patients with refractory chronic cough: a double-blind randomized controlled trial. *The Journal of allergy and clinical immunology*. **134** (1), pp. 56–62.

Khan, A.G., Pichler, J., Rosemann, A. & Blaas, D. (2007) Human rhinovirus type 54 infection via heparan sulfate is less efficient and strictly dependent on low endosomal pH. *Journal of virology*. **81** (9), pp. 4625–4632.

Khan, A.G., Pickl-Herk, A., Gajdzik, L., Marlovits, T.C., Fuchs, R. & Blaas, D. (2011) Entry of a heparan sulphate-binding HRV8 variant strictly depends on dynamin but not on clathrin, caveolin, and flotillin. *Virology*. **412** (1), pp. 55–67.

Khan, A.G., Pickl-Herk, A., Gajdzik, L., Marlovits, T.C., Fuchs, R. & Blaas, D. (2010) Human rhinovirus 14 enters rhabdomyosarcoma cells expressing icam-1 by a clathrin-, caveolin-, and flotillin-independent pathway. *Journal of virology*. **84** (8), pp. 3984–3992.

Kichko, T.I. & Reeh, P.W. (2009) TRPV1 controls acid- and heat-induced calcitonin gene-related peptide release and sensitization by bradykinin in the isolated mouse trachea. *The European journal of neuroscience*. **29** (9), pp. 1896–1904.

Kim, D., Cavanaugh, E.J. & Simkin, D. (2008) Inhibition of transient receptor potential A1 channel by phosphatidylinositol-4,5-bisphosphate. *American journal of physiology. Cell physiology*. **295**pp. C92–C99.

Kimura, K., Ito, M., Amano, M., Chihara, K., Fukata, Y., Nakafuku, M., Yamamori, B., Feng, J., Nakano, T., Okawa, K., Iwamatsu, A. & Kaibuchi, K. (1996) Regulation of myosin phosphatase by Rho and Rho-associated kinase (Rho-kinase). *Science (New York, N.Y.)*. **273** (5272), pp. 245–248.

Kindt, K.S., Viswanath, V., Macpherson, L., Quast, K., Hu, H., Patapoutian, A. & Schafer, W.R. (2007) Caenorhabditis elegans TRPA-1 functions in mechanosensation. *Nature neuroscience*. **10** (5), pp. 568–577.

Konno, S., Grindle, K.A., Lee, W.-M., Schroth, M.K., Mosser, A.G., Brockman-Schneider, R.A., Busse, W.W. & Gern, J.E. (2002) Interferon-gamma enhances rhinovirus-induced RANTES secretion by airway epithelial cells. *American journal of respiratory cell and molecular biology*. **26** (5), pp. 594–601.

Korfhagen, T.R., Kitzmiller, J., Chen, G., Sridharan, A., Haitchi, H.-M., Hegde, R.S., Divanovic, S., Karp, C.L. & Whitsett, J.A. (2012) SAM-pointed domain ETS factor mediates epithelial cell-intrinsic innate immune signaling during airway mucous metaplasia. *Proceedings of the National Academy of Sciences of the United States of America*. **109** (41), pp. 16630–16635.

Korngreen, A. & Priel, Z. (1996) Purinergic stimulation of rabbit ciliated airway epithelia: control by multiple calcium sources. *The Journal of physiology*. **497 (Pt 1**pp. 53–66.

Koshimizu, T., Koshimizu, M. & Stojilkovic, S.S. (1999) Contributions of the C-terminal domain to the control of P2X receptor desensitization. *The Journal of biological chemistry*. **274** (53), pp. 37651–37657.

Koyama, T., Oike, M. & Ito, Y. (2001) Involvement of Rho-kinase and tyrosine kinase in hypotonic stress-induced ATP release in bovine aortic endothelial cells. *The Journal of physiology*. **532** (Pt 3), pp. 759–769.

Kreda, S.M., Seminario-Vidal, L., van Heusden, C.A., O'Neal, W., Jones, L., Boucher, R.C. & Lazarowski, E.R. (2010) Receptor-promoted exocytosis of airway epithelial mucin granules containing a spectrum of adenine nucleotides. *The Journal of physiology*. **588** (Pt 12), pp. 2255–2267.

Kronenberger, P., Schober, D., Prchla, E., Blaas, D. & Fuchs, R. (1997) Use of free-flow electrophoresis for the analysis of cellular uptake of picornaviruses. *Electrophoresis*. **18** (14), pp. 2531–2536.

Kumar, A., Zhang, J. & Yu, F.-S.X. (2006) Toll-like receptor 3 agonist poly(I:C)-induced antiviral response in human corneal epithelial cells. *Immunology*. **117**pp. 11–21.

Kusama, T., Mukai, M., Iwasaki, T., Tatsuta, M., Matsumoto, Y., Akedo, H. & Nakamura, H. (2001) Inhibition of epidermal growth factor-induced RhoA translocation and invasion of human pancreatic cancer cells by 3-hydroxy-3-methylglutaryl-coenzyme a reductase inhibitors. *Cancer research*. **61** (12), pp. 4885–4891.

Kuzhikandathil, E. V, Wang, H., Szabo, T., Morozova, N., Blumberg, P.M. & Oxford, G.S. (2001) Functional analysis of capsaicin receptor (vanilloid receptor subtype 1) multimerization and agonist responsiveness using a dominant negative mutation. *The Journal of neuroscience : the official journal of the Society for Neuroscience*. **21** (22), pp. 8697–8706.

Kwan, K.Y., Allchorne, A.J., Vollrath, M.A., Christensen, A.P., Zhang, D.-S., Woolf, C.J. & Corey, D.P. (2006) TRPA1 contributes to cold, mechanical, and chemical nociception but is not essential for hair-cell transduction. *Neuron*. **50** (2), pp. 277–289.

Kwan, K.Y. & Corey, D.P. (2009) Burning Cold: Involvement of TRPA1 in Noxious Cold Sensation. *The Journal of General Physiology*. **133** (3), pp. 251–256.

Laing, R.J. & Dhaka, A. (2015) ThermoTRPs and Pain. *The Neuroscientist : a review journal bringing neurobiology, neurology and psychiatry*.

Lakshmi, S. & Joshi, P.G. (2005) Co-activation of P2Y2 receptor and TRPV channel by ATP: implications for ATP induced pain. *Cellular and molecular neurobiology*. **25** (5), pp. 819–832.

Lamson, D., Renwick, N., Kapoor, V., Liu, Z., Palacios, G., Ju, J., Dean, A., St George, K., Briese, T. & Lipkin, W.I. (2006) MassTag polymerase-chain-reaction detection of respiratory pathogens, including a new rhinovirus genotype, that caused influenza-like illness in New York State during 2004-2005. *The Journal of infectious diseases*. **194** (10), pp. 1398–1402.

Larsen, G.L., Fame, T.M., Renz, H., Loader, J.E., Graves, J., Hill, M. & Gelfand, E.W. (1994) Increased acetylcholine release in tracheas from allergen-exposed IgE-immune mice. *The American journal of physiology*. **266** (3 Pt 1), pp. L263-70.

Lartey, J. & López Bernal, A. (2009) RHO protein regulation of contraction in the human uterus. *Reproduction (Cambridge, England)*. **138** (3), pp. 407–424.

Lassen, L., Haderslev, P., Jacobsen, V., Iversen, H., Sperling, B. & Olesen, J. (2002) CGRP may play a causative role in migraine. *Cephalalgia*. **22** (1), pp. 54–61.

Latorre, R., Zaelzer, C. & Brauchi, S. (2009) Structure-functional intimacies of transient receptor potential channels. *Quarterly reviews of biophysics*. **42**pp. 201–246.

Laude, E.A., Higgins, K.S. & Morice, A.H. (1993) A comparative study of the effects of citric acid, capsaicin and resiniferatoxin on the cough challenge in guinea-pig and man. *Pulmonary pharmacology*. **6** (3), pp. 171–175.

Lee, H., Iida, T., Mizuno, A., Suzuki, M. & Caterina, M.J. (2005a) Altered thermal selection behavior in mice lacking transient receptor potential vanilloid 4. *The Journal of neuroscience : the official journal of the Society for Neuroscience*. **25** (5), pp. 1304–1310.

Lee, J., Cha, S.-K., Sun, T.-J. & Huang, C.-L. (2005b) PIP $_2$ Activates TRPV5 and Releases Its Inhibition by Intracellular Mg $^{2+}$. *The Journal of General Physiology*. **126** (5), pp. 439–451.

Lee, W.M., Monroe, S.S. & Rueckert, R.R. (1993) Role of maturation cleavage in infectivity of picornaviruses: activation of an infectosome. *Journal of virology*. **67** (4), pp. 2110–2122.

Lee, Y.F., Nomoto, A., Detjen, B.M. & Wimmer, E. (1977) A protein covalently linked to poliovirus genome RNA. *Proceedings of the National Academy of Sciences of the United States of America*. **74** (1), pp. 59–63.

Leigh, R., Oyelusi, W., Wiehler, S., Koetzler, R., Zaheer, R.S., Newton, R. & Proud, D. (2008) Human rhinovirus infection enhances airway epithelial cell production of growth factors involved in airway remodeling. *The Journal of allergy and clinical immunology*. **121** (5), pp. 1238–1245.e4.

Lessler, J., Reich, N.G., Brookmeyer, R., Perl, T.M., Nelson, K.E. & Cummings, D.A. (2009) Incubation periods of acute respiratory viral infections: a systematic review. *The Lancet Infectious Diseases*. **9** (5), pp. 291–300.

Li, G.D., Milani, D., Dunne, M.J., Pralong, W.F., Theler, J.M., Petersen, O.H. & Wollheim, C.B. (1991) Extracellular ATP causes Ca2(+)-dependent and -independent insulin secretion in RINm5F cells. Phospholipase C mediates Ca2+ mobilization but not Ca2+ influx and membrane depolarization. *The Journal of biological chemistry*. **266** (6), pp. 3449–3457.

Liao, M., Cao, E., Julius, D. & Cheng, Y. (2013) Structure of the TRPV1 ion channel determined by electron cryo-microscopy. *Nature*. **504** (7478), pp. 107–112.

Lieb, T., Frei, C.W., Frohock, J.I., Bookman, R.J. & Salathe, M. (2002) Prolonged increase in ciliary beat frequency after short-term purinergic stimulation in human airway epithelial cells. *The Journal of physiology*. **538** (Pt 2), pp. 633–646.

Liedtke, W., Choe, Y., Martí-Renom, M.A., Bell, A.M., Denis, C.S., AndrejŠali, Hudspeth, A.J., Friedman, J.M. & Heller, S. (2000) Vanilloid Receptor–Related Osmotically Activated Channel (VR-OAC), a Candidate Vertebrate Osmoreceptor. *Cell*. **103** (3), pp. 525–535.

Liedtke, W., Tobin, D.M., Bargmann, C.I. & Friedman, J.M. (2003) Mammalian TRPV4 (VR-OAC) directs behavioral responses to osmotic and mechanical stimuli in Caenorhabditis elegans. *Proceedings of the National Academy of Sciences*. **100** (Supplement 2), pp. 14531–14536.

Lieu, T., Kollarik, M., Myers, A.C. & Undem, B.J. (2011) Neurotrophin and GDNF family ligand receptor expression in vagal sensory nerve subtypes innervating the adult guinea pig respiratory tract. *American journal of physiology. Lung cellular and molecular physiology*. **300** (5), pp. L790-8.

Lieu, T.M., Myers, A.C., Meeker, S. & Undem, B.J. (2012) TRPV1 induction in airway vagal low-threshold mechanosensory neurons by allergen challenge and neurotrophic factors. *American journal of physiology. Lung cellular and molecular physiology*. **302** (9), pp. L941-8.

Liu, B. & Qin, F. (2005) Functional Control of Cold- and Menthol-Sensitive TRPM8 Ion Channels by Phosphatidylinositol 4,5-Bisphosphate. *Journal of Neuroscience*. **25** (7), pp. 1674–1681.

Liu, T., Xu, Z.-Z., Park, C.-K., Berta, T. & Ji, R.-R. (2010) Toll-like receptor 7 mediates pruritus. *Nature neuroscience*. **13** (12), pp. 1460–1462.

Liu, X., Bandyopadhyay, B.C., Bandyopadhyay, B., Nakamoto, T., Singh, B., Liedtke, W., Melvin, J.E. & Ambudkar, I. (2006) A role for AQP5 in activation of TRPV4 by hypotonicity: concerted involvement of AQP5 and TRPV4 in regulation of cell volume recovery. *The Journal of biological chemistry*. **281** (22), pp. 15485–15495.

Locovei, S., Scemes, E., Qiu, F., Spray, D.C. & Dahl, G. (2007) Pannexin1 is part of the pore forming unit of the P2X(7) receptor death complex. *FEBS letters*. **581** (3), pp. 483–488.

Locovei, S., Wang, J. & Dahl, G. (2006) Activation of pannexin 1 channels by ATP through P2Y receptors and by cytoplasmic calcium. *FEBS letters*. **580** (1), pp. 239–244.

Lommatzsch, M., Cicko, S., Müller, T., Lucattelli, M., Bratke, K., Stoll, P., Grimm, M., Dürk, T., Zissel, G., Ferrari, D., Di Virgilio, F., Sorichter, S., Lungarella, G., Virchow, J.C., et al. (2010) Extracellular adenosine triphosphate and chronic obstructive pulmonary disease. *American journal of respiratory and critical care medicine*. **181** (9), pp. 928–934.

Lorenzo, I.M., Liedtke, W., Sanderson, M.J. & Valverde, M.A. (2008) TRPV4 channel participates in receptor-operated calcium entry and ciliary beat frequency regulation in mouse airway epithelial cells. *Proceedings of the National Academy of Sciences of the United States of America*. **105** (34), pp. 12611–12616.

Lotz, M., Vaughan, J.H. & Carson, D.A. (1988) Effect of neuropeptides on production of inflammatory cytokines by human monocytes. *Science (New York, N.Y.)*. **241** (4870), pp. 1218–1221.

Louie, J.K., Roy-Burman, A., Guardia-LaBar, L., Boston, E.J., Kiang, D., Padilla, T., Yagi, S., Messenger, S., Petru, A.M., Glaser, C.A. & Schnurr, D.P. (2009) Rhinovirus Associated With Severe Lower Respiratory Tract Infections in Children. *The Pediatric Infectious*

Disease Journal. **28** (4), pp. 337–339.

Lowry, R., Wood, A. & Higenbottam, T. (1994) The effect of anticholinergic bronchodilator therapy on cough during upper respiratory tract infections. *British journal of clinical pharmacology*. **37** (2), pp. 187–191.

Lundberg, J.M., Brodin, E., Hua, X. & Saria, A. (1984) Vascular permeability changes and smooth muscle contraction in relation to capsaicin-sensitive substance P afferents in the guinea-pig. *Acta physiologica Scandinavica*. **120** (2), pp. 217–227.

Ma, W., Korngreen, A., Uzlaner, N., Priel, Z. & Silberberg, S.D. (1999) Extracellular sodium regulates airway ciliary motility by inhibiting a P2X receptor. *Nature*. **400** (6747), pp. 894–897.

Ma, W., Korngreen, A., Weil, S., Cohen, E.B.-T., Priel, A., Kuzin, L. & Silberberg, S.D. (2006) Pore properties and pharmacological features of the P2X receptor channel in airway ciliated cells. *The Journal of Physiology*. **571** (3), pp. 503–517.

Machesky, L.M. & Hall, A. (1997) Role of actin polymerization and adhesion to extracellular matrix in Rac- and Rho-induced cytoskeletal reorganization. *The Journal of cell biology*. **138** (4), pp. 913–926.

Macpherson, L.J., Dubin, A.E., Evans, M.J., Marr, F., Schultz, P.G., Cravatt, B.F. & Patapoutian, A. (2007) Noxious compounds activate TRPA1 ion channels through covalent modification of cysteines. *Nature*. **445** (7127), pp. 541–545.

Macpherson, L.J., Geierstanger, B.H., Viswanath, V., Bandell, M., Eid, S.R., Hwang, S. & Patapoutian, A. (2005) The pungency of garlic: activation of TRPA1 and TRPV1 in response to allicin. *Current biology : CB*. **15** (10), pp. 929–934.

Madaule, P. & Axel, R. (1985) A novel ras-related gene family. *Cell*. **41** (1), pp. 31–40.

Madaule, P., Eda, M., Watanabe, N., Fujisawa, K., Matsuoka, T., Bito, H., Ishizaki, T. & Narumiya, S. (1998) Role of citron kinase as a target of the small GTPase Rho in cytokinesis. *Nature*. **394** (6692), pp. 491–494.

Madison, J.M. & Irwin, R.S. (2003) Pharmacotherapy of chronic cough in adults. *Expert Opinion on Pharmacotherapy*. **4** (7), pp. 1039–1048.

Maher, S.A., Birrell, M.A. & Belvisi, M.G. (2009) Prostaglandin E_2 Mediates Cough via the EP_3 Receptor. *American Journal of Respiratory and Critical Care Medicine*. **180** (10), pp. 923–928.

Mak, J.C. & Barnes, P.J. (1990) Autoradiographic visualization of muscarinic receptor subtypes in human and guinea pig lung. *The American review of respiratory disease*. **141** (6), pp. 1559–1568.

Mak, J.C.W. & Barnes, P.J. (1988) Autoradiographic localization of calcitonin gene-related peptide (CGRP) binding sites in human and guinea pig lung. *Peptides*. **9** (5), pp. 957–963.

Mansoor, S.E., Lü, W., Oosterheert, W., Shekhar, M., Tajkhorshid, E. & Gouaux, E. (2016) X-ray structures define human P2X3 receptor gating cycle and antagonist action.

Nature. **538** (7623), pp. 66–71.

Maruo, K., Yamamoto, H., Yamamoto, S., Nagata, T., Fujikawa, H., Kanno, T., Yaguchi, T., Maruo, S., Yoshiya, S. & Nishizaki, T. (2006) Modulation of P2X receptors via adrenergic pathways in rat dorsal root ganglion neurons after sciatic nerve injury. *Pain*. **120** (1–2), pp. 106–112.

Mazzone, S.B., Mori, N. & Canning, B.J. (2005) Synergistic interactions between airway afferent nerve subtypes regulating the cough reflex in guinea-pigs. *The Journal of physiology*. **569** (Pt 2), pp. 559–573.

Mbikou, P., Fajmut, A., Brumen, M. & Roux, E. (2011) Contribution of Rho kinase to the early phase of the calcium-contraction coupling in airway smooth muscle. *Experimental physiology*. **96** (2), pp. 240–258.

McAlexander, M.A. & Taylor-Clark, T. (2011) The role of transient receptor potential channels in respiratory symptoms and pathophysiology. *Advances in experimental medicine and biology*. **704**pp. 969–986.

McGaraughty, S., Wismer, C.T., Zhu, C.Z., Mikusa, J., Honore, P., Chu, K.L., Lee, C.-H., Faltynek, C.R. & Jarvis, M.F. (2003) Effects of A-317491, a novel and selective P2X3/P2X2/3 receptor antagonist, on neuropathic, inflammatory and chemogenic nociception following intrathecal and intraplantar administration. *British journal of pharmacology*. **140** (8), pp. 1381–1388.

McGarvey, L.P.A. & Morice, A.H. (2006) Clinical cough and its mechanisms. *Respiratory physiology & neurobiology*. **152** (3), pp. 363–371.

McGarvey, L.P., Butler, C.A., Stokesberry, S., Polley, L., McQuaid, S., Abdullah, H., Ashraf, S., McGahon, M.K., Curtis, T.M., Arron, J., Choy, D., Warke, T.J., Bradding, P., Ennis, M., et al. (2014) Increased expression of bronchial epithelial transient receptor potential vanilloid 1 channels in patients with severe asthma. *The Journal of allergy and clinical immunology*. **133** (3), pp. 704–12.e4.

McGregor, S. & Mayor, H.D. (1971) Biophysical and biochemical studies on rhinovirus and poliovirus. II. Chemical and hydrodynamic analysis of the rhinovirion. *Journal of virology*. **7** (1), pp. 41–46.

McIntyre, C.L., Knowles, N.J. & Simmonds, P. (2013) Proposals for the classification of human rhinovirus species A, B and C into genotypically assigned types. *The Journal of general virology*. **94** (Pt 8), pp. 1791–1806.

McKemy, D.D., Neuhausser, W.M. & Julius, D. (2002) Identification of a cold receptor reveals a general role for TRP channels in thermosensation. *Nature*. **416** (6876), pp. 52–58.

McNamara, C.R., Mandel-Brehm, J., Bautista, D.M., Siemens, J., Deranian, K.L., Zhao, M., Hayward, N.J., Chong, J. a, Julius, D., Moran, M.M. & Fanger, C.M. (2007) TRPA1 mediates formalin-induced pain. *Proceedings of the National Academy of Sciences of the United States of America*. **104** (33), pp. 13525–13530.

Meents, J.E., Fischer, M.J.M. & McNaughton, P.A. (2017) Sensitization of TRPA1 by Protein Kinase A Alexander G. Obukhov (ed.). *PLOS ONE*. **12** (1), pp. e0170097.

Meylan, E., Curran, J., Hofmann, K., Moradpour, D., Binder, M., Bartenschlager, R. & Tschopp, J. (2005) Cardif is an adaptor protein in the RIG-I antiviral pathway and is targeted by hepatitis C virus. *Nature*. **437** (7062), pp. 1167–1172.

Miller, E.K., Lu, X., Erdman, D.D., Poehling, K.A., Zhu, Y., Griffin, M.R., Hartert, T.V., Anderson, L.J., Weinberg, G.A., Hall, C.B., Iwane, M.K., Edwards, K.M. & New Vaccine Surveillance Network (2007) Rhinovirus-Associated Hospitalizations in Young Children. *The Journal of Infectious Diseases*. **195** (6), pp. 773–781.

Minke, B. (2006) TRP channels and Ca2+ signaling. *Cell Calcium*. **40**pp. 261–275.

Minke, B., Wu, C. & Pak, W.L. (1975) Induction of photoreceptor voltage noise in the dark in Drosophila mutant. *Nature*. **258** (5530), pp. 84–87.

Missiaen, L., De Smedt, H., Parys, J.B., Sienaert, I., Vanlingen, S., Droogmans, G., Nilius, B. & Casteels, R. (1996) Hypotonically induced calcium release from intracellular calcium stores. *The Journal of biological chemistry*. **271** (9), pp. 4601–4604.

Mitchell, A.B., Mourad, B., Tovey, E., Buddle, L., Peters, M., Morgan, L. & Oliver, B.G. (2016) Spirometry filters can be used to detect exhaled respiratory viruses. *Journal of Breath Research*. **10** (4), pp. 46002.

Mitchell, A.B., Tang, B., Shojaei, M., Barnes, L.S., Nalos, M., Oliver, B.G. & McLean, A.S. (2018) A novel sampling method to detect airborne influenza and other respiratory viruses in mechanically ventilated patients: a feasibility study. *Annals of Intensive Care*. **8** (1), pp. 45.

Mitchell, J.E., Campbell, A.P., New, N.E., Sadofsky, L.R., Kastelik, J. a, Mulrennan, S. a, Compton, S.J. & Morice, A.H. (2005) Expression and characterization of the intracellular vanilloid receptor (TRPV1) in bronchi from patients with chronic cough. *Experimental lung research*. **31** (March 2004), pp. 295–306.

Mohapatra, D.P. & Nau, C. (2003) Desensitization of Capsaicin-activated Currents in the Vanilloid Receptor TRPV1 Is Decreased by the Cyclic AMP-dependent Protein Kinase Pathway. *Journal of Biological Chemistry*. **278** (50), pp. 50080–50090.

Moiseenkova-Bell, V.Y., Stanciu, L.A., Serysheva, I.I., Tobe, B.J. & Wensel, T.G. (2008) Structure of TRPV1 channel revealed by electron cryomicroscopy. *Proceedings of the National Academy of Sciences of the United States of America*. **105** (21), pp. 7451–7455.

Montell, C. (2005) The TRP superfamily of cation channels. *Science's STKE : signal transduction knowledge environment*. **2005** (February), pp. re3.

Montell, C. & Rubin, G.M. (1989) Molecular characterization of the Drosophila trp locus: a putative integral membrane protein required for phototransduction. *Neuron*. **2** (4), pp. 1313–1323.

Monto, A.S., Gravenstein, S., Elliott, M., Colopy, M. & Schweinle, J. (2000) Clinical signs and symptoms predicting influenza infection. *Archives of internal medicine*. **160** (21), pp. 3243–3247.

Moore, K.A., Undem, B.J. & Weinreich, D. (2000) Antigen inhalation unmasks NK-2

tachykinin receptor-mediated responses in vagal afferents. *American journal of respiratory and critical care medicine*. **161** (1), pp. 232–236.

Moparthi, L., Survery, S., Kreir, M., Simonsen, C., Kjellbom, P., Högestätt, E.D., Johanson, U. & Zygmunt, P.M. (2014) Human TRPA1 is intrinsically cold- and chemosensitive with and without its N-terminal ankyrin repeat domain. *Proceedings of the National Academy of Sciences of the United States of America*. **111** (47), pp. 16901–16906.

Moqrich, A., Hwang, S.W., Earley, T.J., Petrus, M.J., Murray, A.N., Spencer, K.S.R., Andahazy, M., Story, G.M. & Patapoutian, A. (2005) Impaired thermosensation in mice lacking TRPV3, a heat and camphor sensor in the skin. *Science (New York, N.Y.)*. **307** (5714), pp. 1468–1472.

Morice, A.H. (2014) Developing antitussives the clinician's pipeline—what do we need? *Journal of Thoracic Disease*. 6 (7) p.pp. S735–S738.

Morice, A.H. (2010) The cough hypersensitivity syndrome: a novel paradigm for understanding cough. *Lung*. **188 Suppl**pp. S87-90.

Morice, A.H., Fontana, G.A., Belvisi, M.G., Birring, S.S., Chung, K.F., Dicpinigaitis, P. V, Kastelik, J.A., McGarvey, L.P., Smith, J.A., Tatar, M. & Widdicombe, J. (2007) ERS guidelines on the assessment of cough. *The European respiratory journal*. **29** (6), pp. 1256–1276.

Morice, A.H., Kastelik, J.A. & Thompson, R. (2001) Cough challenge in the assessment of cough reflex. *British journal of clinical pharmacology*. **52** (4), pp. 365–375.

Morice, A.H., Lowry, R., Brown, M.J. & Higenbottam, T. (1987) Angiotensin-converting enzyme and the cough reflex. *Lancet (London, England)*. **2** (8568), pp. 1116–1118.

Morice, A.H., McGarvey, L., Pavord, I. & British Thoracic Society Cough Guideline Group (2006) Recommendations for the management of cough in adults. *Thorax*. **61 Suppl 1**pp. i1-24.

Mosavi, L.K., Cammett, T.J., Desrosiers, D.C. & Peng, Z. (2004) The ankyrin repeat as molecular architecture for protein recognition. *Protein Science*. **13** (6), pp. 1435–1448.

Mousnier, a., Swieboda, D., Pinto, a., Guedan, a., Rogers, a. V., Walton, R., Johnston, S.L. & Solari, R. (2014) Human Rhinovirus 16 Causes Golgi Apparatus Fragmentation without Blocking Protein Secretion. *Journal of Virology*. **88**pp. 11671–11685.

Mukhopadhyay, I., Gomes, P., Aranake, S., Shetty, M., Karnik, P., Damle, M., Kuruganti, S., Thorat, S. & Khairatkar-Joshi, N. (2011) Expression of functional TRPA1 receptor on human lung fibroblast and epithelial cells. *Journal of receptor and signal transduction research*. **31** (5), pp. 350–358.

Murakami, M., Xu, F., Miyoshi, I., Sato, E., Ono, K. & Iijima, T. (2003) Identification and characterization of the murine TRPM4 channel. *Biochemical and biophysical research communications*. **307** (3), pp. 522–528.

Myers, A.C., Kajekar, R. & Undem, B.J. (2002) Allergic inflammation-induced neuropeptide production in rapidly adapting afferent nerves in guinea pig airways. *American*

journal of physiology. Lung cellular and molecular physiology. **282** (4), pp. L775-81.

Nagata, K., Duggan, A., Kumar, G. & García-Añoveros, J. (2005) Nociceptor and hair cell transducer properties of TRPA1, a channel for pain and hearing. *The Journal of neuroscience : the official journal of the Society for Neuroscience*. **25** (16), pp. 4052–4061.

Nagaya, N., Tittle, R.K., Saar, N., Dellal, S.S. & Hume, R.I. (2005) An intersubunit zinc binding site in rat P2X2 receptors. *The Journal of biological chemistry*. **280** (28), pp. 25982–25993.

Nairn, A.C. & Perry, S. V (1979) Calmodulin and myosin light-chain kinase of rabbit fast skeletal muscle. *Biochemical Journal*. **179** (1), pp. 89.

Nakazawa, K., Yamakoshi, Y., Tsuchiya, T. & Ohno, Y. (2005) Purification and aqueous phase atomic force microscopic observation of recombinant P2X2 receptor. *European journal of pharmacology*. **518** (2–3), pp. 107–110.

Nassini, R., Pedretti, P., Moretto, N., Fusi, C., Carnini, C., Facchinetti, F., Viscomi, A.R., Pisano, A.R., Stokesberry, S., Brunmark, C., Svitacheva, N., McGarvey, L., Patacchini, R., Damholt, A.B., et al. (2012) Transient receptor potential ankyrin 1 channel localized to non-neuronal airway cells promotes non-neurogenic inflammation. *PloS one*. **7** (8), pp. e42454.

Neelands, T.R., Burgard, E.C., Uchic, M.E., McDonald, H.A., Niforatos, W., Faltynek, C.R., Lynch, K.J. & Jarvis, M.F. (2003) 2', 3'-O-(2,4,6,trinitrophenyl)-ATP and A-317491 are competitive antagonists at a slowly desensitizing chimeric human P2X3 receptor. *British journal of pharmacology*. **140** (1), pp. 202–210.

Neumann, S., Doubell, T.P., Leslie, T. & Woolf, C.J. (1996) Inflammatory pain hypersensitivity mediated by phenotypic switch in myelinated primary sensory neurons. *Nature*. **384** (6607), pp. 360–364.

Newcomb, D.C., Sajjan, U.S., Nagarkar, D.R., Wang, Q., Nanua, S., Zhou, Y., McHenry, C.L., Hennrick, K.T., Tsai, W.C., Bentley, J.K., Lukacs, N.W., Johnston, S.L. & Hershenson, M.B. (2008) Human rhinovirus 1B exposure induces phosphatidylinositol 3-kinase-dependent airway inflammation in mice. *American journal of respiratory and critical care medicine*. **177** (10), pp. 1111–1121.

Nicke, A., Bäumert, H.G., Rettinger, J., Eichele, A., Lambrecht, G., Mutschler, E. & Schmalzing, G. (1998) P2X1 and P2X3 receptors form stable trimers: a novel structural motif of ligand-gated ion channels. *The EMBO journal*. **17** (11), pp. 3016–3028.

Nicol, G.D., Lopshire, J.C. & Pafford, C.M. (1997) Tumor necrosis factor enhances the capsaicin sensitivity of rat sensory neurons. *The Journal of neuroscience : the official journal of the Society for Neuroscience*. **17** (3), pp. 975–982.

Nilius, B., Appendino, G. & Owsianik, G. (2012) The transient receptor potential channel TRPA1: From gene to pathophysiology. *Pflugers Archiv European Journal of Physiology*. **464**pp. 425–458.

Nilius, B., Owsianik, G., Voets, T. & Peters, J. a J. a. (2007) *Transient receptor potential*

cation channels in disease.

Nilius, B., Prenen, J., Wissenbach, U., Bödding, M. & Droogmans, G. (2001) Differential activation of the volume-sensitive cation channel TRP12 (OTRPC4) and volume-regulated anion currents in HEK-293 cells. *Pflügers Archiv*. **443** (2), pp. 227–233.

Nilius, B., Vriens, J., Prenen, J., Droogmans, G. & Voets, T. (2004) TRPV4 calcium entry channel: a paradigm for gating diversity. *American Journal of Physiology-Cell Physiology*. **286** (2), pp. C195–C205.

Nishio, N., Taniguchi, W., Sugimura, Y.K., Takiguchi, N., Yamanaka, M., Kiyoyuki, Y., Yamada, H., Miyazaki, N., Yoshida, M. & Nakatsuka, T. (2013) Reactive oxygen species enhance excitatory synaptic transmission in rat spinal dorsal horn neurons by activating TRPA1 and TRPV1 channels. *Neuroscience*. **247**pp. 201–212.

Nobes, C.D. & Hall, A. (1995) Rho, rac, and cdc42 GTPases regulate the assembly of multimolecular focal complexes associated with actin stress fibers, lamellipodia, and filopodia. *Cell*. **81** (1), pp. 53–62.

North, R.A. (2002) Molecular Physiology of P2X Receptors. *Physiological Reviews*. **82** (4), pp. 1013–1067.

Novak, J.E. & Kirkegaard, K. (1991) Improved method for detecting poliovirus negative strands used to demonstrate specificity of positive-strand encapsidation and the ratio of positive to negative strands in infected cells. *Journal of virology*. **65** (6), pp. 3384–3387.

Nugent, C.I. & Kirkegaard, K. (1995) RNA binding properties of poliovirus subviral particles. *Journal of virology*. **69** (1), pp. 13–22.

Numao, T. & Agrawal, D.K. (1992) Neuropeptides modulate human eosinophil chemotaxis. *Journal of immunology (Baltimore, Md. : 1950)*. **149** (10), pp. 3309–3315.

Numazaki, M., Tominaga, T., Takeuchi, K., Murayama, N., Toyooka, H. & Tominaga, M. (2003) Structural determinant of TRPV1 desensitization interacts with calmodulin. *Proceedings of the National Academy of Sciences*. **100** (13), pp. 8002–8006.

Numazaki, M., Tominaga, T., Toyooka, H. & Tominaga, M. (2002) Direct phosphorylation of capsaicin receptor VR1 by protein kinase Cepsilon and identification of two target serine residues. *The Journal of biological chemistry*. **277** (16), pp. 13375–13378.

O'Connell, F., Springall, D.R., Moradoghli-Haftvani, A., Krausz, T., Price, D., Fuller, R.W., Polak, J.M. & Pride, N.B. (1995) Abnormal intraepithelial airway nerves in persistent unexplained cough? *American journal of respiratory and critical care medicine*. **152** (6 Pt 1), pp. 2068–2075.

O'Connell, F., Thomas, V.E., Pride, N.B. & Fuller, R.W. (1994) Capsaicin cough sensitivity decreases with successful treatment of chronic cough. *American Journal of Respiratory and Critical Care Medicine*. **150** (2), pp. 374–380.

O'Connell, F., Thomas, V.E., Studham, J.M., Pride, N.B. & Fuller, R.W. (1996) Capsaicin cough sensitivity increases during upper respiratory infection. *Respiratory medicine*.

90 (5), pp. 279–286.

Oettgen, P., Finger, E., Sun, Z., Akbarali, Y., Thamrongsak, U., Boltax, J., Grall, F., Dube, A., Weiss, A., Brown, L., Quinn, G., Kas, K., Endress, G., Kunsch, C., et al. (2000) PDEF, a novel prostate epithelium-specific ets transcription factor, interacts with the androgen receptor and activates prostate-specific antigen gene expression. *The Journal of biological chemistry*. **275** (2), pp. 1216–1225.

Oh, J.J., Razfar, A., Delgado, I., Reed, R.A., Malkina, A., Boctor, B. & Slamon, D.J. (2006) 3p21.3 tumor suppressor gene H37/Luca15/RBM5 inhibits growth of human lung cancer cells through cell cycle arrest and apoptosis. *Cancer research*. **66** (7), pp. 3419–3427.

Ohbuchi, T., Takenaga, F., Hohchi, N., Wakasugi, T., Ueta, Y. & Suzuki, H. (2014) Possible contribution of pannexin-1 to ATP release in human upper airway epithelia. *Physiological reports*. **2** (2), pp. e00227.

Ohga, N., Kikuchi, A., Ueda, T., Yamamoto, J. & Takai, Y. (1989) Rabbit intestine contains a protein that inhibits the dissociation of GDP from and the subsequent binding of GTP to rhoB p20, a ras p21-like GTP-binding protein. *Biochemical and biophysical research communications*. **163** (3), pp. 1523–1533.

Okada, S.F., Nicholas, R.A., Kreda, S.M., Lazarowski, E.R. & Boucher, R.C. (2006) Physiological Regulation of ATP Release at the Apical Surface of Human Airway Epithelia. *Journal of Biological Chemistry*. **281** (32), pp. 22992–23002.

Okada, S.F., Ribeiro, C.M.P., Sesma, J.I., Seminario-Vidal, L., Abdullah, L.H., van Heusden, C., Lazarowski, E.R. & Boucher, R.C. (2013) Inflammation Promotes Airway Epithelial ATP Release via Calcium-Dependent Vesicular Pathways. *American Journal of Respiratory Cell and Molecular Biology*. **49** (5), pp. 814–820.

Okada, T., Inoue, R., Yamazaki, K., Maeda, A., Kurosaki, T., Yamakuni, T., Tanaka, I., Shimizu, S., Ikenaka, K., Imoto, K. & Mori, Y. (1999) Molecular and functional characterization of a novel mouse transient receptor potential protein homologue TRP7. Ca(2+)-permeable cation channel that is constitutively activated and enhanced by stimulation of G protein-coupled receptor. *The Journal of biological chemistry*. **274** (39), pp. 27359–27370.

Oliveira, M., Zhao, R., Lee, W., Kremer, M., Minor, I., Rueckert, R., Diana, G., Pevear, D., Dutko, F. & Mckinlay, M. (1993) The structure of human rhinovirus 16. *Structure*. **1**pp. 51–68.

Oliver, B.G.G., Lim, S., Wark, P., Laza-Stanca, V., King, N., Black, J.L., Burgess, J.K., Roth, M. & Johnston, S.L. (2008) Rhinovirus exposure impairs immune responses to bacterial products in human alveolar macrophages. *Thorax*. **63** (6), pp. 519–525.

Olson, J.K. & Miller, S.D. (2004) Microglia Initiate Central Nervous System Innate and Adaptive Immune Responses through Multiple TLRs. *The Journal of Immunology*. **173** (6), pp. 3916–3924.

Omar, S., Clarke, R., Abdullah, H., Brady, C., Corry, J., Winter, H., Touzelet, O., Power, U.F., Lundy, F., McGarvey, L.P.A. & Cosby, S.L. (2017) Respiratory virus infection up-

regulates TRPV1, TRPA1 and ASICS3 receptors on airway cells. Ralph Tripp (ed.). *PloS one*. **12** (2), pp. e0171681.

Othumpangat, S., Regier, M. & Piedimonte, G. (2012) Nerve growth factor modulates human rhinovirus infection in airway epithelial cells by controlling ICAM-1 expression. *American journal of physiology. Lung cellular and molecular physiology*. **302** (10), pp. L1057-66.

Otsuka, K., Niimi, A., Matsumoto, H., Ito, I., Yamaguchi, M., Matsuoka, H., Jinnai, M., Oguma, T., Takeda, T., Nakaji, H., Chin, K., Sasaki, K., Aoyama, N. & Mishima, M. (2011) Plasma substance P levels in patients with persistent cough. *Respiration; international review of thoracic diseases*. **82** (5), pp. 431–438.

Palmenberg, A.C., Rathe, J. a. & Liggett, S.B. (2010) Analysis of the complete genome sequences of human rhinovirus. *Journal of Allergy and Clinical Immunology*. **125** (6), pp. 1190–1199.

Palmenberg, A.C., Spiro, D., Kuzmickas, R., Wang, S., Djikeng, A., Rathe, J.A., Fraser-Liggett, C.M. & Liggett, S.B. (2009) Sequencing and analyses of all known human rhinovirus genomes reveal structure and evolution. *Science (New York, N.Y.)*. **324** (5923), pp. 55–59.

Palombini, B.C., Villanova, C.A., Araújo, E., Gastal, O.L., Alt, D.C., Stolz, D.P. & Palombini, C.O. (1999) A pathogenic triad in chronic cough: asthma, postnasal drip syndrome, and gastroesophageal reflux disease. *Chest*. **116** (2), pp. 279–284.

Panjwani, A., Strauss, M., Gold, S., Wenham, H., Jackson, T., Chou, J.J., Rowlands, D.J., Stonehouse, N.J., Hogle, J.M. & Tuthill, T.J. (2014) Capsid protein VP4 of human rhinovirus induces membrane permeability by the formation of a size-selective multimeric pore. *PLoS pathogens*. **10** (8), pp. e1004294.

Papadopoulos, N.G., Bates, P.J., Bardin, P.G., Papi, A., Leir, S.H., Fraenkel, D.J., Meyer, J., Lackie, P.M., Sanderson, G., Holgate, S.T. & Johnston, S.L. (2000) Rhinoviruses infect the lower airways. *The Journal of infectious diseases*. **181** (6), pp. 1875–1884.

Papadopoulos, N.G. & Johnston, S.L. (2000) Rhinoviruses as pathogens of the lower respiratory tract. *Canadian Respiratory Journal*. **7** (5), pp. 409–414.

Papadopoulos, N.G., Sanderson, G., Hunter, J. & Johnston, S.L. (1999) Rhinoviruses replicate effectively at lower airway temperatures. *Journal of medical virology*. **58** (1), pp. 100–104.

Papi, A., Contoli, M., Adcock, I.M., Bellettato, C., Padovani, A., Casolari, P., Stanciu, L.A., Barnes, P.J., Johnston, S.L., Ito, K. & Caramori, G. (2013) Rhinovirus infection causes steroid resistance in airway epithelium through nuclear factor κB and c-Jun N-terminal kinase activation. *Journal of Allergy and Clinical Immunology*. **132** (5), pp. 1075–1085.e6.

Papi, A. & Johnston, S.L. (1999) Rhinovirus Infection Induces Expression of Its Own Receptor Intercellular Adhesion Molecule 1 (ICAM-1) via Increased NF- B-mediated Transcription. *Journal of Biological Chemistry*. **274** (14), pp. 9707–9720.

Pappas, D.E., Hendley, J.O., Hayden, F.G. & Winther, B. (2008) Symptom profile of

common colds in school-aged children. *The Pediatric infectious disease journal*. **27** (1), pp. 8–11.

Park, C.-K., Xu, Z.-Z., Berta, T., Han, Q., Chen, G., Liu, X.-J. & Ji, R.-R. (2014) Extracellular microRNAs activate nociceptor neurons to elicit pain via TLR7 and TRPA1. *Neuron*. **82** (1), pp. 47–54.

Park, K.-S., Korfhagen, T.R., Bruno, M.D., Kitzmiller, J.A., Wan, H., Wert, S.E., Khurana Hershey, G.K., Chen, G. & Whitsett, J.A. (2007) SPDEF regulates goblet cell hyperplasia in the airway epithelium. *The Journal of clinical investigation*. **117** (4), pp. 978–988.

Passariello, C., Schippa, S., Conti, C., Russo, P., Poggiali, F., Garaci, E. & Palamara, A.T. (2006) Rhinoviruses promote internalisation of Staphylococcus aureus into non-fully permissive cultured pneumocytes. *Microbes and infection*. **8** (3), pp. 758–766.

Paulsen, C.E., Armache, J.-P., Gao, Y., Cheng, Y. & Julius, D. (2015) Structure of the TRPA1 ion channel suggests regulatory mechanisms. *Nature*. **520** (7548), pp. 511–517.

Pégorier, S., Wagner, L.A., Gleich, G.J. & Pretolani, M. (2006) Eosinophil-derived cationic proteins activate the synthesis of remodeling factors by airway epithelial cells. *Journal of immunology (Baltimore, Md. : 1950)*. **177** (7), pp. 4861–4869.

Peier, A.M., Moqrich, A., Hergarden, A.C., Reeve, A.J., Andersson, D.A., Story, G.M., Earley, T.J., Dragoni, I., McIntyre, P., Bevan, S. & Patapoutian, A. (2002) A TRP channel that senses cold stimuli and menthol. *Cell*. **108** (5), pp. 705–715.

Pelegrin, P. & Surprenant, A. (2006) Pannexin-1 mediates large pore formation and interleukin-1beta release by the ATP-gated P2X7 receptor. *The EMBO journal*. **25** (21), pp. 5071–5082.

Pelletier, J. & Sonenberg, N. (1988) Internal initiation of translation of eukaryotic mRNA directed by a sequence derived from poliovirus RNA. *Nature*. **334** (6180), pp. 320–325.

Petersen, C.C., Berridge, M.J., Borgese, M.F. & Bennett, D.L. (1995) Putative capacitative calcium entry channels: expression of Drosophila trp and evidence for the existence of vertebrate homologues. *The Biochemical journal*. **311 (Pt 1**pp. 41–44.

Phipps, R.J. & Richardson, P.S. (1976) The effects of irritation at various levels of the airway upon tracheal mucus secretion in the cat. *The Journal of Physiology*. **261** (3), pp. 563–581.

Placido, R., Auricchio, G., Falzoni, S., Battistini, L., Colizzi, V., Brunetti, E., Di Virgilio, F. & Mancino, G. (2006) P2X(7) purinergic receptors and extracellular ATP mediate apoptosis of human monocytes/macrophages infected with Mycobacterium tuberculosis reducing the intracellular bacterial viability. *Cellular immunology*. **244** (1), pp. 10–18.

Poole, D.P., Castelucci, P., Robbins, H.L., Chiocchetti, R. & Furness, J.B. (2002) The distribution of P2X3 purine receptor subunits in the guinea pig enteric nervous system. *Autonomic neuroscience : basic & clinical*. **101** (1–2), pp. 39–47.

Pratter, M.R. (2006) Cough and the common cold: ACCP evidence-based clinical practice guidelines. *Chest*. **129** (1 Suppl), pp. 72S–74S.

Prescott, E.D. & Julius, D. (2003) A Modular PIP2 Binding Site as a Determinant of Capsaicin Receptor Sensitivity. *Science*. **300** (5623), pp. 1284–1288.

Profita, M., Giorgi, R. Di, Sala, A., Bonanno, A., Riccobono, L., Mirabella, F., Gjomarkaj, M., Bonsignore, G., Bousquet, J. & Vignola, A.M. (2005) Muscarinic receptors, leukotriene B4 production and neutrophilic inflammation in COPD patients. *Allergy*. **60** (11), pp. 1361–1369.

Proud, D., Reynolds, C.J., Lacapra, S., Kagey-Sobotka, A., Lichtenstein, L.M. & Naclerio, R.M. (1988) Nasal Provocation with Bradykinin Induces Symptoms of Rhinitis and a Sore Throat. *American Review of Respiratory Disease*. **137** (3), pp. 613–616.

Psarras, S., Volonaki, E., Skevaki, C.L., Xatzipsalti, M., Bossios, A., Pratsinis, H., Tsigkos, S., Gourgiotis, D., Constantopoulos, A.G., Papapetropoulos, A., Saxoni-Papageorgiou, P. & Papadopoulos, N.G. (2006) Vascular endothelial growth factor-mediated induction of angiogenesis by human rhinoviruses. *The Journal of allergy and clinical immunology*. **117** (2), pp. 291–297.

Puhakka, T., Mäkelä, M.J., Malmström, K., Uhari, M., Savolainen, J., Terho, E.O., Pulkkinen, M. & Ruuskanen, O. (1998) The common cold: effects of intranasal fluticasone propionate treatment. *The Journal of allergy and clinical immunology*. **101** (6 Pt 1), pp. 726–731.

Putney, J.W. & Tomita, T. (2012) Phospholipase C signaling and calcium influx. *Advances in biological regulation*. **52** (1), pp. 152–164.

Qi, J., Buzas, K., Fan, H., Cohen, J.I., Wang, K., Mont, E., Klinman, D., Oppenheim, J.J. & Howard, O.M.Z. (2011) Painful pathways induced by TLR stimulation of dorsal root ganglion neurons. *Journal of immunology (Baltimore, Md. : 1950)*. **186** (11), pp. 6417–6426.

Racaniello, V.R. (2001) Picornaviridae: The Viruses and Their Replication. In: B. N; Fields, D. M; Knipe, P. M; Howelet, D. E; Griffin, R. A; Lamb, M. A; Martin, B; Roizman, & S. E; Straus (eds.). *Fields Virology*. 4th Ed. Philadelphia: Lippincott Willaims & Wilkins. pp. pp. 685–722.

Rahman, M., Sun, R., Mukherjee, S., Nilius, B. & Janssen, L.J. (2018) TRPV4-stimulation releases ATP via pannexin channels in human pulmonary fibroblasts. *American Journal of Respiratory Cells and Molecular Biology*. (C), pp. 1–40.

Rajan, D., Gaston, K.A., McCracken, C.E., Erdman, D.D. & Anderson, L.J. (2013) Response to Rhinovirus Infection by Human Airway Epithelial Cells and Peripheral Blood Mononuclear Cells in an In Vitro Two-Chamber Tissue Culture System Gernot Zissel (ed.). *PLoS ONE*. **8** (6), pp. e66600.

Ramachandran, R., Morice, A.H. & Compton, S.J. (2006) Proteinase-Activated Receptor $_2$ Agonists Upregulate Granulocyte Colony-Stimulating Factor, IL-8, and VCAM-1 Expression in Human Bronchial Fibroblasts. *American Journal of Respiratory Cell and Molecular Biology*. **35** (1), pp. 133–141.

Ramnarine, S.I., Haddad, E.B., Khawaja, A.M., Mak, J.C. & Rogers, D.F. (1996) On muscarinic control of neurogenic mucus secretion in ferret trachea. *The Journal of physiology*. **494 (Pt 2**pp. 577–586.

Ramsey, I.S., Delling, M. & Clapham, D.E. (2006) AN INTRODUCTION TO TRP CHANNELS doi:10.1146/annurev.physiol.68.040204.100431. *Annual Review of Physiology*. **68** (2), pp. 619–647.

Ramsingh, R., Grygorczyk, A., Solecki, A., Cherkaoui, L.S., Berthiaume, Y. & Grygorczyk, R. (2011) Cell deformation at the air-liquid interface induces Ca^{2+} -dependent ATP release from lung epithelial cells. *American Journal of Physiology-Lung Cellular and Molecular Physiology*. **300** (4), pp. L587–L595.

Ransford, G.A., Fregien, N., Qiu, F., Dahl, G., Conner, G.E. & Salathe, M. (2009) Pannexin 1 contributes to ATP release in airway epithelia. *American journal of respiratory cell and molecular biology*. **41** (5), pp. 525–534.

Rassendren, F., Buell, G., Newbolt, A., North, R.A. & Surprenant, A. (1997) Identification of amino acid residues contributing to the pore of a P2X receptor. *The EMBO Journal*. **16** (12), pp. 3446–3454.

Reid, D.D., Williams, R.E. & Hirch, A. (1953) Colds among office workers, an epidemiological study. *Lancet (London, England)*. **265** (6799), pp. 1303–1306.

Reilly, C.A., Taylor, J.L., Lanza, D.L., Carr, B.A., Crouch, D.J. & Yost, G.S. (2003) Capsaicinoids cause inflammation and epithelial cell death through activation of vanilloid receptors. *Toxicological sciences : an official journal of the Society of Toxicology*. **73** (1), pp. 170–181.

Reiter, B., Kraft, R., Günzel, D., Zeissig, S., Schulzke, J.-D., Fromm, M. & Harteneck, C. (2006) TRPV4-mediated regulation of epithelial permeability. *FASEB journal : official publication of the Federation of American Societies for Experimental Biology*. **20** (11), pp. 1802–1812.

Reza Etemadi, M., Ling, K.-H., Zainal Abidin, S., Chee, H.-Y. & Sekawi, Z. (2017) Gene expression patterns induced at different stages of rhinovirus infection in human alveolar epithelial cells Kok Keng Tee (ed.). *PLOS ONE*. **12** (5), pp. e0176947.

Rezaee, F., Meednu, N., Emo, J.A., Saatian, B., Chapman, T.J., Naydenov, N.G., De Benedetto, A., Beck, L.A., Ivanov, A.I. & Georas, S.N. (2011) Polyinosinic:polycytidylic acid induces protein kinase D-dependent disassembly of apical junctions and barrier dysfunction in airway epithelial cells. *The Journal of allergy and clinical immunology*. **128** (6), pp. 1216–1224.e11.

Ridley, A.J. & Hall, A. (1994) Signal transduction pathways regulating Rho-mediated stress fibre formation: requirement for a tyrosine kinase. *The EMBO journal*. **13** (11), pp. 2600–2610.

Ridley, A.J. & Hall, A. (1992) The small GTP-binding protein rho regulates the assembly of focal adhesions and actin stress fibers in response to growth factors. *Cell*. **70** (3), pp. 389–399.

Ridley, A.J., Paterson, H.F., Johnston, C.L., Diekmann, D. & Hall, A. (1992) The small GTP-

binding protein rac regulates growth factor-induced membrane ruffling. *Cell*. **70** (3), pp. 401–410.

Roberts, J.A., Raeburn, D., Rodger, I.W. & Thomson, N.C. (1984) Comparison of in vivo airway responsiveness and in vitro smooth muscle sensitivity to methacholine in man. *Thorax*. **39** (11), pp. 837–843.

Rogers, D.F. (2001) Motor control of airway goblet cells and glands. *Respiration physiology*. **125** (1–2), pp. 129–144.

Rogers, D.F., Aursudkij, B. & Barnes, P.J. (1989) Effects of tachykinins on mucus secretion in human bronchi in vitro. *European journal of pharmacology*. **174** (2–3), pp. 283–286.

Rohács, T., Lopes, C.M.B., Michailidis, I. & Logothetis, D.E. (2005) PI(4,5)P2 regulates the activation and desensitization of TRPM8 channels through the TRP domain. *Nature Neuroscience*. **8** (5), pp. 626–634.

Rojas, A.M., Fuentes, G., Rausell, A. & Valencia, A. (2012) The Ras protein superfamily: evolutionary tree and role of conserved amino acids. *The Journal of cell biology*. **196** (2), pp. 189–201.

Rosenbaum, T., Gordon-Shaag, A., Munari, M. & Gordon, S.E. (2004) Ca^{2+} /Calmodulin Modulates TRPV1 Activation by Capsaicin. *The Journal of General Physiology*. **123** (1), pp. 53–62.

Rossmann, M.G., Arnold, E., Erickson, J.W., Frankenberger, E.A., Griffith, J.P., Hecht, H.-J., Johnson, J.E., Kamer, G., Luo, M., Mosser, A.G., Rueckert, R.R., Sherry, B. & Vriend, G. (1985) Structure of a human common cold virus and functional relationship to other picornaviruses. *Nature*. **317** (6033), pp. 145–153.

Rubio, M.E. & Soto, F. (2001) Distinct Localization of P2X receptors at excitatory postsynaptic specializations. *The Journal of neuroscience : the official journal of the Society for Neuroscience*. **21** (2), pp. 641–653.

Rueden, C.T., Schindelin, J., Hiner, M.C., DeZonia, B.E., Walter, A.E., Arena, E.T. & Eliceiri, K.W. (2017) ImageJ2: ImageJ for the next generation of scientific image data. *BMC Bioinformatics*. **18** (1), pp. 529.

Sadofsky, L.R., Boa, A.N., Maher, S. a., Birrell, M. a., Belvisi, M.G. & Morice, A.H. (2011) TRPA1 is activated by direct addition of cysteine residues to the N-hydroxysuccinyl esters of acrylic and cinnamic acids. *Pharmacological Research*. **63** (1), pp. 30–36.

Sajjan, U., Wang, Q., Zhao, Y., Gruenert, D.C. & Hershenson, M.B. (2008) Rhinovirus disrupts the barrier function of polarized airway epithelial cells. *American journal of respiratory and critical care medicine*. **178** (12), pp. 1271–1281.

Samad, A., Sura, L., Benedikt, J., Ettrich, R., Minofar, B., Teisinger, J. & Vlachova, V. (2011) The C-terminal basic residues contribute to the chemical- and voltage-dependent activation of TRPA1. *The Biochemical journal*. **433** (1), pp. 197–204.

Schaafsma, D., Bos, I.S.T., Zuidhof, A.B., Zaagsma, J. & Meurs, H. (2006a) Inhalation of the Rho-kinase inhibitor Y-27632 reverses allergen-induced airway hyperresponsiveness

after the early and late asthmatic reaction. *Respiratory Research*. **7** (1), pp. 121.

Schaafsma, D., Zuidhof, A.B., Nelemans, S.A., Zaagsma, J. & Meurs, H. (2006b) Inhibition of Rho-kinase normalizes nonspecific hyperresponsiveness in passively sensitized airway smooth muscle preparations. *European Journal of Pharmacology*. **531** (1–3), pp. 145–150.

Schaefer, A., Reinhard, N.R. & Hordijk, P.L. (2014) Toward understanding RhoGTPase specificity: structure, function and local activation. *Small GTPases*. **5** (2), pp. e968004.

Schindelin, J., Arganda-Carreras, I., Frise, E., Kaynig, V., Longair, M., Pietzsch, T., Preibisch, S., Rueden, C., Saalfeld, S., Schmid, B., Tinevez, J.-Y., White, D.J., Hartenstein, V., Eliceiri, K., et al. (2012) Fiji: an open-source platform for biological-image analysis. *Nature Methods*. **9** (7), pp. 676–682.

Schober, D., Kronenberger, P., Prchla, E., Blaas, D. & Fuchs, R. (1998) Major and minor receptor group human rhinoviruses penetrate from endosomes by different mechanisms. *Journal of virology*. **72** (2), pp. 1354–1364.

Schroeder, K. & Fahey, T. (2002) Systematic review of randomised controlled trials of over the counter cough medicines for acute cough in adults. *BMJ (Clinical research ed.)*. **324** (7333), pp. 329–331.

Schuler, B. a., Schreiber, M.T., Li, L., Mokry, M., Kingdon, M.L., Raugi, D.N., Smith, C., Hameister, C., Racaniello, V.R. & Hall, D.J. (2014) Major and minor group rhinoviruses elicit differential signaling and cytokine responses as a function of receptor-mediated signal transduction. *PLoS ONE*. **9** (4), pp. e93897.

Schwartz, M. (2004) Rho signalling at a glance. *Journal of cell science*. **117** (Pt 23), pp. 5457–5458.

Seemungal, T., Harper-Owen, R., Bhowmik, A., Moric, I., Sanderson, G., Message, S., MacCallum, P., Meade, T.W., Jefferies, D.J., Johnston, S.L. & Wedzicha, J.A. (2001) Respiratory Viruses, Symptoms, and Inflammatory Markers in Acute Exacerbations and Stable Chronic Obstructive Pulmonary Disease. *American Journal of Respiratory and Critical Care Medicine*. **164** (9), pp. 1618–1623.

Seminario-Vidal, L., Kreda, S., Jones, L., O'Neal, W., Trejo, J., Boucher, R.C. & Lazarowski, E.R. (2009) Thrombin promotes release of ATP from lung epithelial cells through coordinated activation of rho- and Ca2+-dependent signaling pathways. *The Journal of biological chemistry*. **284** (31), pp. 20638–20648.

Seminario-Vidal, L., Lazarowski, E.R. & Okada, S.F. (2009) Assessment of Extracellular ATP Concentrations. In: *Methods in molecular biology (Clifton, N.J.)*. pp. pp. 25–36.

Seminario-Vidal, L., Okada, S.F., Sesma, J.I., Kreda, S.M., van Heusden, C.A., Zhu, Y., Jones, L.C., O'Neal, W.K., Penuela, S., Laird, D.W., Boucher, R.C. & Lazarowski, E.R. (2011) Rho signaling regulates pannexin 1-mediated ATP release from airway epithelia. *The Journal of biological chemistry*. **286** (30), pp. 26277–26286.

Sénatore, S., Reddy, V.R., Sémériva, M., Perrin, L. & Lalevée, N. (2010) Response to mechanical stress is mediated by the TRPA channel painless in the Drosophila heart.

PLoS Genetics. **6** (9), .

Sequeira, P.C., Senaratne, R.H. & Riley, L.W. (2014) Inhibition of toll-like receptor 2 (TLR-2)-mediated response in human alveolar epithelial cells by mycolic acids and *Mycobacterium tuberculosis mce1* operon mutant. *Pathogens and Disease*. **70** (2), pp. 132–140.

Serafini, T., Orci, L., Amherdt, M., Brunner, M., Kahn, R.A. & Rothman, J.E. (1991) ADP-ribosylation factor is a subunit of the coat of Golgi-derived COP-coated vesicles: a novel role for a GTP-binding protein. *Cell*. **67** (2), pp. 239–253.

Seth, R.B., Sun, L., Ea, C.-K. & Chen, Z.J. (2005) Identification and characterization of MAVS, a mitochondrial antiviral signaling protein that activates NF-kappaB and IRF 3. *Cell*. **122** (5), pp. 669–682.

Seymour, M.L., Gilby, N., Bardin, P.G., Fraenkel, D.J., Sanderson, G., Penrose, J.F., Holgate, S.T., Johnston, S.L. & Sampson, A.P. (2002) Rhinovirus infection increases 5-lipoxygenase and cyclooxygenase-2 in bronchial biopsy specimens from nonatopic subjects. *The Journal of infectious diseases*. **185** (4), pp. 540–544.

Shao, F., Vacratsis, P.O., Bao, Z., Bowers, K.E., Fierke, C.A. & Dixon, J.E. (2003) Biochemical characterization of the Yersinia YopT protease: cleavage site and recognition elements in Rho GTPases. *Proceedings of the National Academy of Sciences of the United States of America*. **100** (3), pp. 904–909.

Shapiro, D., Deering-Rice, C.E., Romero, E.G., Hughen, R.W., Light, A.R., Veranth, J.M. & Reilly, C.A. (2013) Activation of transient receptor potential ankyrin-1 (TRPA1) in lung cells by wood smoke particulate material. *Chemical research in toxicology*. **26** (5), pp. 750–758.

Shigematsu, H., Sokabe, T., Danev, R., Tominaga, M. & Nagayama, K. (2010) A 3.5-nm structure of rat TRPV4 cation channel revealed by Zernike phase-contrast cryoelectron microscopy. *The Journal of biological chemistry*. **285** (15), pp. 11210–11218.

Shin, S.H., Lee, E.J., Hyun, S., Chun, J., Kim, Y. & Kang, S.S. (2012) Phosphorylation on the Ser 824 residue of TRPV4 prefers to bind with F-actin than with microtubules to expand the cell surface area. *Cellular Signalling*. **24** (3), pp. 641–651.

Shin, Y.-H., Namkoong, E., Choi, S., Bae, J.-S., Jin, M., Hwang, S.-M., Arote, R., Choi, S.-Y. & Park, K. (2013) Capsaicin regulates the NF-κB pathway in salivary gland inflammation. *Journal of dental research*. **92** (6), pp. 547–552.

Sidhaye, V.K., Güler, A.D., Schweitzer, K.S., D'Alessio, F., Caterina, M.J. & King, L.S. (2006) Transient receptor potential vanilloid 4 regulates aquaporin-5 abundance under hypotonic conditions. *Proceedings of the National Academy of Sciences of the United States of America*. **103** (12), pp. 4747–4752.

Sidhaye, V.K., Schweitzer, K.S., Caterina, M.J., Shimoda, L. & King, L.S. (2008) Shear stress regulates aquaporin-5 and airway epithelial barrier function. *Proceedings of the National Academy of Sciences*. **105** (9), pp. 3345–3350.

Skern, T., Sommergruber, W., Blaas, D., Gruendler, P., Fraundorfer, F., Pieler, C., Fogy, I. &

Kuechler, E. (1985) Human rhinovirus 2: complete nucleotide sequence and proteolytic processing signals in the capsid protein region. *Nucleic acids research*. **13** (6), pp. 2111–2126.

Smit, L.A., Kogevinas, M., Antó, J.M., Bouzigon, E., González, J., Le Moual, N., Kromhout, H., Carsin, A.-E., Pin, I., Jarvis, D., Vermeulen, R., Janson, C., Heinrich, J., Gut, I., et al. (2012) Transient receptor potential genes, smoking, occupational exposures and cough in adults. *Respiratory Research*. **13** (1), pp. 26.

Smith, G.D., Gunthorpe, M.J., Kelsell, R.E., Hayes, P.D., Reilly, P., Facer, P., Wright, J.E., Jerman, J.C., Walhin, J.-P., Ooi, L., Egerton, J., Charles, K.J., Smart, D., Randall, A.D., et al. (2002) TRPV3 is a temperature-sensitive vanilloid receptor-like protein. *Nature*. **418** (6894), pp. 186–190.

Smith, T.J., Kremer, M.J., Luo, M., Vriend, G., Arnold, E., Kamer, G., Rossmann, M.G., McKinlay, M.A., Diana, G.D. & Otto, M.J. (1986) The site of attachment in human rhinovirus 14 for antiviral agents that inhibit uncoating. *Science (New York, N.Y.)*. **233** (4770), pp. 1286–1293.

Somlyo, A.P. & Somolyo, A. V. (2003) Ca 2+ Sensitivity of Smooth Muscle and Nonmuscle Myosin II: Modulated by G Proteins, Kinases, and Myosin Phosphatase. *Physiological Reviews*. **83** (4), pp. 1325–1358.

Sotomayor, M., Corey, D.P. & Schulten, K. (2005) In Search of the Hair-Cell Gating Spring. *Structure*. **13** (4), pp. 669–682.

Souslova, V., Cesare, P., Ding, Y., Akopian, A.N., Stanfa, L., Suzuki, R., Carpenter, K., Dickenson, A., Boyce, S., Hill, R., Nebenuis-Oosthuizen, D., Smith, A.J., Kidd, E.J. & Wood, J.N. (2000) Warm-coding deficits and aberrant inflammatory pain in mice lacking P2X3 receptors. *Nature*. **407** (6807), pp. 1015–1017.

Southall, M.D., Li, T., Gharibova, L.S., Pei, Y., Nicol, G.D. & Travers, J.B. (2003) Activation of Epidermal Vanilloid Receptor-1 Induces Release of Proinflammatory Mediators in Human Keratinocytes. *Journal of Pharmacology and Experimental Therapeutics*. **304** (1), pp. 217–222.

Soyka, M.B., Wawrzyniak, P., Eiwegger, T., Holzmann, D., Treis, A., Wanke, K., Kast, J.I. & Akdis, C.A. (2012) Defective epithelial barrier in chronic rhinosinusitis: the regulation of tight junctions by IFN-γ and IL-4. *The Journal of allergy and clinical immunology*. **130** (5), pp. 1087–1096.e10.

Spector, D.H. & Baltimore, D. (1974) Requirement of 3’-terminal poly(adenylic acid) for the infectivity of poliovirus RNA. *Proceedings of the National Academy of Sciences of the United States of America*. **71** (8), pp. 2983–2987.

Stöckl, J., Vetr, H., Majdic, O., Zlabinger, G., Kuechler, E. & Knapp, W. (1999) Human major group rhinoviruses downmodulate the accessory function of monocytes by inducing IL-10. *The Journal of clinical investigation*. **104** (7), pp. 957–965.

Story, G.M., Peier, A.M., Reeve, A.J., Eid, S.R., Mosbacher, J., Hricik, T.R., Earley, T.J., Hergarden, A.C., Andersson, D.A., Hwang, S.W., McIntyre, P., Jegla, T., Bevan, S. & Patapoutian, A. (2003) ANKTM1, a TRP-like channel expressed in nociceptive

neurons, is activated by cold temperatures. *Cell*. **112** (6), pp. 819–829.

Strotmann, R., Harteneck, C., Nunnenmacher, K., Schultz, G. & Plant, T.D. (2000) OTRPC4, a nonselective cation channel that confers sensitivity to extracellular osmolarity. *Nature Cell Biology*. **2** (10), pp. 695–702.

Strübing, C., Krapivinsky, G., Krapivinsky, L. & Clapham, D.E. (2003) Formation of Novel TRPC Channels by Complex Subunit Interactions in Embryonic Brain. *Journal of Biological Chemistry*. **278** (40), pp. 39014–39019.

Sun, Y. & Chai, T.C. (2004) Up-Regulation of P2X3 Receptor During Stretch of Bladder Urothelial Cells From Patients With Interstitial Cystitis. *The Journal of Urology*. **171** (1), pp. 448–452.

Sura, L., Zíma, V., Marsakova, L., Hynkova, A., Barvík, I. & Vlachova, V. (2012) C-terminal acidic cluster is involved in Ca2+-induced regulation of human transient receptor potential ankyrin 1 channel. *Journal of Biological Chemistry*. **287**pp. 18067–18077.

Surprenant, A., Buell, G. & North, R.A. (1995) P2X receptors bring new structure to ligand-gated ion channels. *Trends in neurosciences*. **18** (5), pp. 224–229.

Suzuki, M., Hirao, A. & Mizuno, A. (2003) Microtubule-associated [corrected] protein 7 increases the membrane expression of transient receptor potential vanilloid 4 (TRPV4). *The Journal of biological chemistry*. **278** (51), pp. 51448–51453.

Suzuki, M., Mizuno, A., Kodaira, K. & Imai, M. (2003) Impaired pressure sensation in mice lacking TRPV4. *The Journal of biological chemistry*. **278** (25), pp. 22664–22668.

Svitkin, Y. V, Gradi, A., Imataka, H., Morino, S. & Sonenberg, N. (1999) Eukaryotic initiation factor 4GII (eIF4GII), but not eIF4GI, cleavage correlates with inhibition of host cell protein synthesis after human rhinovirus infection. *Journal of virology*. **73** (4), pp. 3467–3472.

Takahashi, N., Hamada-Nakahara, S., Itoh, Y., Takemura, K., Shimada, A., Ueda, Y., Kitamata, M., Matsuoka, R., Hanawa-Suetsugu, K., Senju, Y., Mori, M.X., Kiyonaka, S., Kohda, D., Kitao, A., et al. (2014) TRPV4 channel activity is modulated by direct interaction of the ankyrin domain to PI(4,5)P2. *Nature Communications*. **5**pp. 4994.

Takemura, M., Niimi, A., Matsumoto, H., Ueda, T., Matsuoka, H., Yamaguchi, M., Jinnai, M., Chin, K. & Mishima, M. (2012) Clinical, physiological and anti-inflammatory effect of montelukast in patients with cough variant asthma. *Respiration; international review of thoracic diseases*. **83** (4), pp. 308–315.

Tattoli, I., Carneiro, L.A., Jéhanno, M., Magalhaes, J.G., Shu, Y., Philpott, D.J., Arnoult, D. & Girardin, S.E. (2008) NLRX1 is a mitochondrial NOD-like receptor that amplifies NF-κB and JNK pathways by inducing reactive oxygen species production. *EMBO reports*. **9** (3), pp. 293–300.

Tatur, S., Groulx, N., Orlov, S.N. & Grygorczyk, R. (2007) Ca2+-dependent ATP release from A549 cells involves synergistic autocrine stimulation by coreleased uridine nucleotides. *The Journal of physiology*. **584** (Pt 2), pp. 419–435.

Tatur, S., Kreda, S., Lazarowski, E. & Grygorczyk, R. (2008) Calcium-dependent release of

adenosine and uridine nucleotides from A549 cells. *Purinergic signalling*. **4** (2), pp. 139–146.

Taylor-Clark, T.E. & Undem, B.J. (2011) Sensing pulmonary oxidative stress by lung vagal afferents. *Respiratory physiology & neurobiology*. **178** (3), pp. 406–413.

Teran, L.M., Seminario, M.C., Shute, J.K., Papi, A., Compton, S.J., Low, J.L., Gleich, G.J. & Johnston, S.L. (1999) RANTES, macrophage-inhibitory protein 1alpha, and the eosinophil product major basic protein are released into upper respiratory secretions during virus-induced asthma exacerbations in children. *The Journal of infectious diseases*. **179** (3), pp. 677–681.

Thorneloe, K.S., Sulpizio, A.C., Lin, Z., Figueroa, D.J., Clouse, A.K., McCafferty, G.P., Chendrimada, T.P., Lashinger, E.S.R., Gordon, E., Evans, L., Misajet, B.A., DeMarini, D.J., Nation, J.H., Casillas, L.N., et al. (2008) N-((1S)-1- -3-hydroxypropanoyl)-1-piperazinyl]carbonyl}-3-methylbutyl)-1-benzothiophene-2-carboxamide (GSK1016790A), a Novel and Potent Transient Receptor Potential Vanilloid 4 Channel Agonist Induces Urinary Bladder Contraction and Hyperactivity: Part I. *Journal of Pharmacology and Experimental Therapeutics*. **326** (2), pp. 432–442.

Todaka, H., Taniguchi, J., Satoh, J., Mizuno, A. & Suzuki, M. (2004) Warm temperature-sensitive transient receptor potential vanilloid 4 (TRPV4) plays an essential role in thermal hyperalgesia. *The Journal of biological chemistry*. **279** (34), pp. 35133–35138.

Tomassini, J.E., Graham, D., DeWitt, C.M., Lineberger, D.W., Rodkey, J.A. & Colonno, R.J. (1989) cDNA cloning reveals that the major group rhinovirus receptor on HeLa cells is intercellular adhesion molecule 1. *Proceedings of the National Academy of Sciences of the United States of America*. **86** (13), pp. 4907–4911.

Trahey, M. & McCormick, F. (1987) A cytoplasmic protein stimulates normal N-ras p21 GTPase, but does not affect oncogenic mutants. *Science (New York, N.Y.)*. **238** (4826), pp. 542–545.

Triantafilou, K., Vakakis, E., Richer, E.A.J., Evans, G.L., Villiers, J.P. & Triantafilou, M. (2011) Human rhinovirus recognition in non-immune cells is mediated by Toll-like receptors and MDA-5, which trigger a synergetic pro-inflammatory immune response. *Virulence*. **2** (1), pp. 22–29.

Tritsch, N.X., Yi, E., Gale, J.E., Glowatzki, E. & Bergles, D.E. (2007) The origin of spontaneous activity in the developing auditory system. *Nature*. **450** (7166), pp. 50–55.

Tsang, S.K., McDermott, B.M., Racaniello, V.R. & Hogle, J.M. (2001) Kinetic analysis of the effect of poliovirus receptor on viral uncoating: the receptor as a catalyst. *Journal of virology*. **75** (11), pp. 4984–4989.

Uehata, M., Ishizaki, T., Satoh, H., Ono, T., Kawahara, T., Morishita, T., Tamakawa, H., Yamagami, K., Inui, J., Maekawa, M. & Narumiya, S. (1997) Calcium sensitization of smooth muscle mediated by a Rho-associated protein kinase in hypertension. *Nature*. **389** (6654), pp. 990–994.

Ulmann, L., Hatcher, J.P., Hughes, J.P., Chaumont, S., Green, P.J., Conquet, F., Buell, G.N., Reeve, A.J., Chessell, I.P. & Rassendren, F. (2008) Up-regulation of P2X4 receptors in spinal microglia after peripheral nerve injury mediates BDNF release and neuropathic pain. *The Journal of neuroscience : the official journal of the Society for Neuroscience*. **28** (44), pp. 11263–11268.

Unger, B.L., Ganesan, S., Comstock, A.T., Faris, A.N., Hershenson, M.B. & Sajjan, U.S. (2014) Nod-like receptor X-1 is required for rhinovirus-induced barrier dysfunction in airway epithelial cells. *Journal of virology*. **88** (7), pp. 3705–3718.

Valera, S., Hussy, N., Evans, R.J., Adami, N., North, R.A., Surprenant, A. & Buell, G. (1994) A new class of ligand-gated ion channel defined by P2X receptor for extracellular ATP. *Nature*. 371 (6497) p.pp. 516–519.

Vannier, B., Peyton, M., Boulay, G., Brown, D., Qin, N., Jiang, M., Zhu, X. & Birnbaumer, L. (1999) Mouse trp2, the homologue of the human trpc2 pseudogene, encodes mTrp2, a store depletion-activated capacitative Ca2+ entry channel. *Proceedings of the National Academy of Sciences of the United States of America*. **96** (5), pp. 2060–2064.

Verkman, A.S. (2013) Aquaporins. *Current biology : CB*. **23** (2), pp. R52-5.

Virgen-Slane, R., Rozovics, J.M., Fitzgerald, K.D., Ngo, T., Chou, W., van der Heden van Noort, G.J., Filippov, D. V, Gershon, P.D. & Semler, B.L. (2012) An RNA virus hijacks an incognito function of a DNA repair enzyme. *Proceedings of the National Academy of Sciences of the United States of America*. **109** (36), pp. 14634–14639.

Virginio, C., MacKenzie, A., Rassendren, F.A., North, R.A. & Surprenant, A. (1999) Pore dilation of neuronal P2X receptor channels. *Nature neuroscience*. **2** (4), pp. 315–321.

Virginio, C., North, R.A. & Surprenant, A. (1998) Calcium permeability and block at homomeric and heteromeric P2X2 and P2X3 receptors, and P2X receptors in rat nodose neurones. *The Journal of physiology*. **510 (Pt 1)**pp. 27–35.

Voets, T., Prenen, J., Vriens, J., Watanabe, H., Janssens, A., Wissenbach, U., Bödding, M., Droogmans, G. & Nilius, B. (2002) Molecular determinants of permeation through the cation channel TRPV4. *The Journal of biological chemistry*. **277** (37), pp. 33704–33710.

Vriens, J., Watanabe, H., Janssens, A., Droogmans, G., Voets, T. & Nilius, B. (2004) Cell swelling, heat, and chemical agonists use distinct pathways for the activation of the cation channel TRPV4. *Proceedings of the National Academy of Sciences of the United States of America*. **101** (1), pp. 396–401.

Wang, J.H., Kim, H. & Jang, Y.J. (2009) Cigarette smoke extract enhances rhinovirus-induced toll-like receptor 3 expression and interleukin-8 secretion in A549 cells. *American journal of rhinology & allergy*. **23** (6), pp. e5-9.

Wang, J.H., Kwon, H.J. & Jang, Y.J. (2009) Rhinovirus upregulates matrix metalloproteinase-2, matrix metalloproteinase-9, and vascular endothelial growth factor expression in nasal polyp fibroblasts. *The Laryngoscope*. **119** (9), pp. 1834–1838.

Wang, K., Birring, S.S., Taylor, K., Fry, N.K., Hay, A.D., Moore, M., Jin, J., Perera, R., Farmer, A., Little, P., Harrison, T.G., Mant, D. & Harnden, A. (2014) Montelukast for postinfectious cough in adults: a double-blind randomised placebo-controlled trial. *The Lancet. Respiratory medicine*. **2** (1), pp. 35–43.

Wang, Y.Y., Chang, R.B., Waters, H.N., McKemy, D.D. & Liman, E.R. (2008) The nociceptor ion channel TRPA1 is potentiated and inactivated by permeating calcium ions. *The Journal of biological chemistry*. **283** (47), pp. 32691–32703.

Watanabe, H., Davis, J.B., Smart, D., Jerman, J.C., Smith, G.D., Hayes, P., Vriens, J., Cairns, W., Wissenbach, U., Prenen, J., Flockerzi, V., Droogmans, G., Benham, C.D. & Nilius, B. (2002a) Activation of TRPV4 channels (hVRL-2/mTRP12) by phorbol derivatives. *The Journal of biological chemistry*. **277** (16), pp. 13569–13577.

Watanabe, H., Vriens, J., Prenen, J., Droogmans, G., Voets, T. & Nilius, B. (2003) Anandamide and arachidonic acid use epoxyeicosatrienoic acids to activate TRPV4 channels. *Nature*. **424** (6947), pp. 434–438.

Watanabe, H., Vriens, J., Suh, S.H., Benham, C.D., Droogmans, G. & Nilius, B. (2002b) Heat-evoked activation of TRPV4 channels in a HEK293 cell expression system and in native mouse aorta endothelial cells. *Journal of Biological Chemistry*. **277** (49), pp. 47044–47051.

Watanabe, H., Vriens, J., Suh, S.H., Benham, C.D., Droogmans, G. & Nilius, B. (2002c) Heat-evoked activation of TRPV4 channels in a HEK293 cell expression system and in native mouse aorta endothelial cells. *The Journal of biological chemistry*. **277** (49), pp. 47044–47051.

Watanabe, N., Horie, S., Michael, G.J., Keir, S., Spina, D., Page, C.P. & Priestley, J.V. (2006) Immunohistochemical co-localization of transient receptor potential vanilloid (TRPV)1 and sensory neuropeptides in the guinea-pig respiratory system. *Neuroscience*. **141** (3), pp. 1533–1543.

Watanabe, N., Kato, T., Fujita, A., Ishizaki, T. & Narumiya, S. (1999) Cooperation between mDia1 and ROCK in Rho-induced actin reorganization. *Nature Cell Biology*. **1** (3), pp. 136–143.

Webb, T.E., Simon, J., Krishek, B.J., Bateson, A.N., Smart, T.G., King, B.F., Burnstock, G. & Barnard, E.A. (1993) Cloning and functional expression of a brain G-protein-coupled ATP receptor. *FEBS letters*. **324** (2), pp. 219–225.

Webber, S.E., Lim, J.C. & Widdicombe, J.G. (1991) The effects of calcitonin gene-related peptide on submucosal gland secretion and epithelial albumin transport in the ferret trachea in vitro. *British journal of pharmacology*. **102** (1), pp. 79–84.

Wei, L., Zhou, W., Wang, L. & Schwartz, R.J. (2000) β_1-Integrin and PI 3-kinase regulate RhoA-dependent activation of skeletal α-actin promoter in myoblasts. *American Journal of Physiology-Heart and Circulatory Physiology*. **278** (6), pp. H1736–H1743.

Weilinger, N.L., Tang, P.L. & Thompson, R.J. (2012) Anoxia-Induced NMDA Receptor Activation Opens Pannexin Channels via Src Family Kinases. *Journal of Neuroscience*. **32** (36), pp. 12579–12588.

Wes, P.D., Chevesich, J., Jeromin, A., Rosenberg, C., Stetten, G. & Montell, C. (1995) TRPC1, a human homolog of a Drosophila store-operated channel. *Proceedings of the National Academy of Sciences of the United States of America*. **92** (21), pp. 9652–9656.

Widdicombe, J.G. (1995) Neurophysiology of the cough reflex. *European Respiratory Journal*. **8**pp. 1193–1202.

Widdicombe, J.G. (1954) Respiratory reflexes from the trachea and bronchi of the cat. *The Journal of physiology*. **123** (1), pp. 55–70.

Wilkinson, T.M.A., Hurst, J.R., Perera, W.R., Wilks, M., Donaldson, G.C. & Wedzicha, J.A. (2006) Effect of interactions between lower airway bacterial and rhinoviral infection in exacerbations of COPD. *Chest*. **129** (2), pp. 317–324.

Winkler, C.W., Taylor, K.G. & Peterson, K.E. (2014) Location is everything: let-7b microRNA and TLR7 signaling results in a painful TRP. *Science signaling*. **7** (327), pp. pe14.

Winning, A.J., Hamilton, R.D., Shea, S.A. & Guz, A. (1986) Respiratory and cardiovascular effects of central and peripheral intravenous injections of capsaicin in man: evidence for pulmonary chemosensitivity. *Clinical science (London, England : 1979)*. **71** (5), pp. 519–526.

Winther, B., Gwaltney, J.M. & Hendley, J.O. (1990) Respiratory virus infection of monolayer cultures of human nasal epithelial cells. *The American review of respiratory disease*. **141** (4 Pt 1), pp. 839–845.

Winther, B., Hayden, F.G. & Hendley, J.O. (2006) Picornavirus infections in children diagnosed by RT-PCR during longitudinal surveillance with weekly sampling: Association with symptomatic illness and effect of season. *Journal of medical virology*. **78** (5), pp. 644–650.

Wissenbach, U., Bödding, M., Freichel, M. & Flockerzi, V. (2000) Trp12, a novel Trp related protein from kidney. *FEBS letters*. **485** (2–3), pp. 127–134.

Witek, T.J., Ramsey, D.L., Carr, A.N. & Riker, D.K. (2015) The natural history of community-acquired common colds symptoms assessed over 4-years. *Rhinology*. **53** (1), pp. 81–88.

Woolf, C.J. (1996) Phenotypic Modification of Primary Sensory Neurons: The Role of Nerve Growth Factor in the Production of Persistent Pain. *Philosophical Transactions of the Royal Society B: Biological Sciences*. **351** (1338), pp. 441–448.

Wuichet, K. & Søgaard-Andersen, L. (2014) Evolution and diversity of the Ras superfamily of small GTPases in prokaryotes. *Genome biology and evolution*. **7** (1), pp. 57–70.

Xu, F., Satoh, E. & Iijima, T. (2003) Protein kinase C-mediated Ca2+ entry in HEK 293 cells transiently expressing human TRPV4. *British journal of pharmacology*. **140** (2), pp. 413–421.

Xu, H., Fu, Y., Tian, W. & Cohen, D.M. (2006) Glycosylation of the osmoresponsive transient receptor potential channel TRPV4 on Asn-651 influences membrane

trafficking. *American Journal of Physiology-Renal Physiology*. **290** (5), pp. F1103–F1109.

Xu, H., Zhao, H., Tian, W., Yoshida, K., Roullet, J.-B. & Cohen, D.M. (2003) Regulation of a Transient Receptor Potential (TRP) Channel by Tyrosine Phosphorylation. *Journal of Biological Chemistry*. **278** (13), pp. 11520–11527.

Yamaya, M., Sekizawa, K., Masuda, T., Morikawa, M., Sawai, T. & Sasaki, H. (1995) Oxidants affect permeability and repair of the cultured human tracheal epithelium. *The American journal of physiology*. **268** (2 Pt 1), pp. L284-93.

Yan, Z., Khadra, A., Li, S., Tomic, M., Sherman, A. & Stojilkovic, S.S. (2010) Experimental characterization and mathematical modeling of P2X7 receptor channel gating. *The Journal of neuroscience : the official journal of the Society for Neuroscience*. **30** (42), pp. 14213–14224.

Ye, X.M., Zhong, N.S., Liu, C.L. & Chen, R.C. (2011) Cough reflex sensitivity is increased in guinea pigs with parainfluenza virus infection. *Experimental lung research*. **37** (3), pp. 186–194.

Yeo, N.-K. & Jang, Y.J. (2010) Rhinovirus infection-induced alteration of tight junction and adherens junction components in human nasal epithelial cells. *The Laryngoscope*. **120** (2), pp. 346–352.

Yeo, W.W., Foster, G. & Ramsay, L.E. (1991) Prevalence of persistent cough during long-term enalapril treatment: controlled study versus nifedipine. *The Quarterly journal of medicine*. **80** (293), pp. 763–770.

Yoshii, A., Iizuka, K., Dobashi, K., Horie, T., Harada, T., Nakazawa, T. & Mori, M. (1999) Relaxation of Contracted Rabbit Tracheal and Human Bronchial Smooth Muscle by Y-27632 through Inhibition of Ca^{2+} Sensitization. *American Journal of Respiratory Cell and Molecular Biology*. **20** (6), pp. 1190–1200.

Yuta, A., Doyle, W.J., Gaumond, E., Ali, M., Tamarkin, L., Baraniuk, J.N., Van Deusen, M., Cohen, S. & Skoner, D.P. (1998) Rhinovirus infection induces mucus hypersecretion. *Am J Physiol Lung Cell Mol Physiol*. **274** (6), pp. L1017-1023.

Zhang, X., Li, L. & McNaughton, P.A. (2008) Proinflammatory mediators modulate the heat-activated ion channel TRPV1 via the scaffolding protein AKAP79/150. *Neuron*. **59** (3), pp. 450–461.

Zhao, X.-H., Laschinger, C., Arora, P., Szászi, K., Kapus, A. & McCulloch, C.A. (2007) Force activates smooth muscle alpha-actin promoter activity through the Rho signaling pathway. *Journal of cell science*. **120** (Pt 10), pp. 1801–1809.

Zhu, G., Gulsvik, a, Bakke, P., Ghatta, S., Anderson, W., Lomas, D. a, Silverman, E.K. & Pillai, S.G. (2009a) Association of TRPV4 gene polymorphisms with chronic obstructive pulmonary disease. *Hum Mol Genet*. **18** (11), pp. 2053–2062.

Zhu, L., Lee, P.-K., Lee, W.-M., Zhao, Y., Yu, D. & Chen, Y. (2009b) Rhinovirus-induced major airway mucin production involves a novel TLR3-EGFR-dependent pathway. *American journal of respiratory cell and molecular biology*. **40** (5), pp. 610–619.

Zhu, Z., Tang, W., Gwaltney, J.M., Wu, Y. & Elias, J.A. (1997) Rhinovirus stimulation of interleukin-8 in vivo and in vitro: role of NF-kappaB. *The American journal of physiology*. **273** (4 Pt 1), pp. L814-24.

Zhu, Z., Tang, W., Ray, A., Wu, Y., Einarsson, O., Landry, M.L., Gwaltney, J. & Elias, J.A. (1996) Rhinovirus stimulation of interleukin-6 in vivo and in vitro. Evidence for nuclear factor kappa B-dependent transcriptional activation. *The Journal of clinical investigation*. **97** (2), pp. 421–430.

Zurborg, S., Yurgionas, B., Jira, J. a, Caspani, O. & Heppenstall, P. a (2007) Direct activation of the ion channel TRPA1 by Ca2+. *Nature neuroscience*. **10** (3), pp. 277–279.